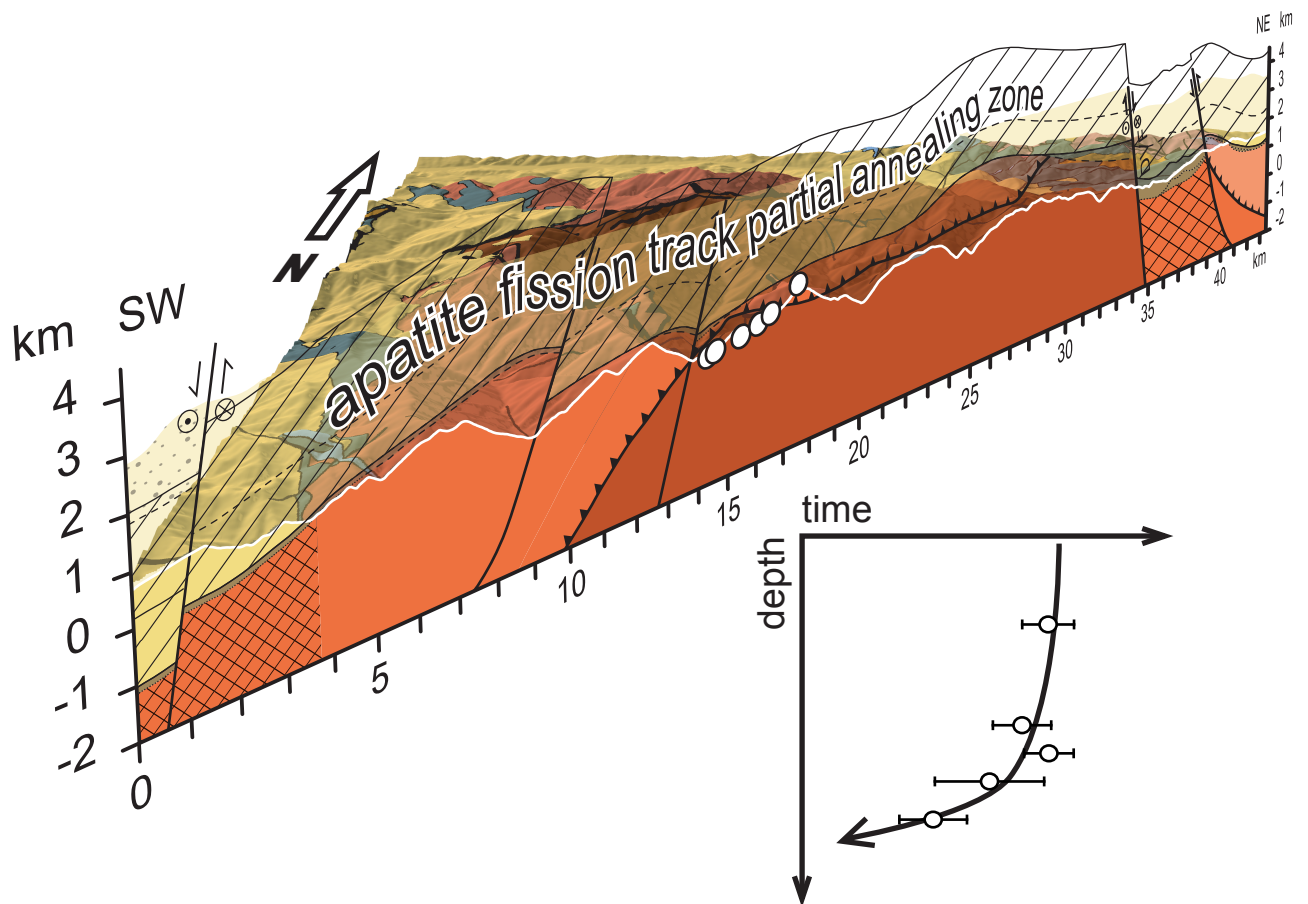


Habe nun, ach! Philosophie,  
Juristerei und Medizin  
Und leider auch Theologie  
Durchaus studiert, mit heißem Bemühn.  
Da steh ich nun, ich armer Tor!  
Und bin so klug als wie zuvor

(Johann Wolfgang von Goethe)



# Thermal and structural evolution of the East Carpathians in northern Romania: from Cretaceous orogeny to final exhumation during Miocene collision



von  
Heike R. Gröger  
aus  
Northeim (Deutschland)

Basel, 2006



**Thermal and structural evolution  
of the East Carpathians in northern Romania:  
from Cretaceous orogeny  
to final exhumation during Miocene collision**

**Inauguraldissertation**

zur

Erlangung der Würde eines Doktors der Philosophie

vorgelegt der

Philosophisch-Naturwissenschaftlichen Fakultät

der Universität Basel

von

Heike R. Gröger

aus

Northeim (Deutschland)

Basel, 2006

Genemigt von der Philosophisch-Naturwissenschaftlichen Fakultät  
auf Antrag von:

PD. Dr. Liviu Matenco  
Faculty of Earth and Life Sciences  
Vrije Universiteit Amsterdam

Prof. Bernhard Fügenschuh  
Institut für Geologie und Paläontologie  
Universität Innsbruck

Prof. Andreas Wetzel  
Institut für Geologie und Paläontologie  
Universität Basel

Prof. Stefan M. Schmid  
Institut für Geologie und Paläontologie  
Universität Basel

(Fakultätsverantwortlicher)  
Basel, den 06. Juni 2006

Prof. Hans-Jakob Wirz  
(Dekan der Philosophisch-Naturwissenschaftlichen Fakultät)

## Abstract

Combining thermochronological methods with structural field data, this study aims to reconstruct the Tertiary burial and exhumation history of the northeastern part of the Tisza-Dacia block during its invasion in the Carpathian embayment and final soft collision with the European margin. Zircon fission track data additionally provide information about the last metamorphic overprint during the Cretaceous.

Within the basement units of the northern Central East Carpathians (Bucovinian nappe stack) and the Preluca massif (Biharia unit) zircon fission tracks are largely reset during the last (Cretaceous) orogeny. Temperatures during this Alpine metamorphic overprint increase from external to internal within the northern East Carpathians from sub-greenschist facies conditions to at least greenschist facies conditions. Greenschist facies conditions are also observed in the Preluca massif. The close neighbourhood of Coniacian to Campanian zircon FT cooling ages with Cenomanian sediments suggests Late Cretaceous tectonic exhumation in the northern East Carpathians. The most likely explanation for this tectonic exhumation is a - so far undocumented - Late Cretaceous extension related to orogenic collapse (Gosau type basins).

The Tertiary evolution is characterised by the invasion of the previously amalgamated Tisza-Dacia and ALCAPA blocks into the Carpathian embayment and Miocene soft collision of both these blocks with the European margin. The juxtaposition of the ALCAPA and Tisza-Dacia blocks, with Tisza-Dacia in a lower plate position, is announced by the onset of Oligocene turbiditic sedimentation. The Burdigalian SE-directed over-thrusting of the Pienides (non-metamorphic flysch units) is interpreted to express the final stages of this juxtaposition. Burial heating caused full annealing of fission tracks in apatite (i.e.  $>120^{\circ}\text{C}$ ) in the Central East Carpathian basement in the NE of the study area, while in the basement of the Preluca massif in the SW of the study area temperatures related to Paleogene to Early Miocene burial did not exceed  $80^{\circ}\text{C}$ .

The post-Burdigalian (post-16 Ma) soft collision of Tisza-Dacia with the European margin occurred in two stages expressed by predominantly sinistral strike-slip deformation during constant NE-SW shortening. During and following soft collision, combined uplift and erosion caused exhumation of the buried rocks along the European margin. Uplift reaches up to 9 km in the Rodna horst

The first post-Burdigalian transpressional stage (16-12 Ma) is related to perpendicular convergence of Tisza-Dacia with the NW-SE striking European margin. Minor exhumation during this stage resulted in Middle Miocene apatite fission track cooling ages (15-13 Ma) in the west of the study area.

The transtensional stage (12-10 Ma) led to the formation of the Bogdan-Drăgăș-Voda fault system. Sinistral transtension allowed for the docking and fitting of Tisza-Dacia with the NW-SE striking European margin. Oblique E-W convergence led to strain partitioning with thrusting in the external thrust belt and internal strike-slip deformation. Differential lateral movements are distributed and deformation is accommodated by E-W striking sinistral strike slip faults and SW-NE striking normal faults, which led to fragmentation into SW-tilted blocks. Fragmentation and differential offset along the bounding faults resulted in the formation of triangular-shaped graben and corresponding horst structures. Enhanced exhumation during transtensional activity led to advective heat transport and resulted in Middle to Late Miocene apatite fission track cooling ages (13-7) in the east of the study area.

## Organisation of this thesis

This thesis is organised into six Chapters, two of which are published as articles in international journals. An outline of each chapter as well as the contribution of the various authors, are provided below.

### Chapter 1:

#### Introduction

Besides providing a general introduction to the study area and the geological frame, this chapter outlines the scope and the aims of this study. Additionally, a short introduction to the history and culture of the study area is given.

### Chapter 2:

#### **Thermal history of the Maramures area (Northern Romania) constrained by zircon fission track analysis: Cretaceous metamorphism and Late Cretaceous to Paleocene exhumation**

This chapter aims to constrain the thermal development of the basement units of the northern East Carpathians. Temperatures during late Early Cretaceous orogeny and the following Paleogene stages of exhumation are reconstructed on the basis of zircon fission track data.

H.R. Gröger performed sampling, preparation and dating of the fission track samples. She also wrote a first draft of the manuscript. M. Tischler participated during sampling and the development of the manuscript. B. Fügenschuh introduced H.R. Gröger to the fission track method and helped with interpretation of the data. He also significantly improved the quality of the resulting manuscript. S.M. Schmid significantly improved the interpretation of the data and the quality of the final manuscript.

### Chapter 3:

#### **Miocene tectonics of the Maramures area (Northern Romania): implications for the Mid-Hungarian fault zone**

Tischler, M., Gröger, H.R., Fügenschuh, B., Schmid, S.M.

published 2006: *International Journal of Earth Sciences*

This study focuses on the Late Tertiary tectonic history of the study area. It is mainly based on structural fieldwork and a kinematic analysis of mesoscale structures, but it also incorporates fission track ages.

In close collaboration with H.R. Gröger, M. Tischler performed the fieldwork and the collection of structural and fault slip data for the kinematic analysis. He wrote a first draft of the manuscript, which was significantly improved in collaboration with H.R. Gröger. H.R. Gröger provided the fission track data which critically improve the constraints for the exhumation history. B. Fügenschuh contributed during fieldwork, structural and fission track data analysis and by correction of the manuscript. S.M. Schmid also contributed by providing guidance during field work as well as during structural data analysis and significantly improved the quality of the final manuscript.



## Chapter 4:

### **Tertiary cooling and exhumation history in the Maramures area (internal eastern Carpathians, northern Romania): thermochronology and structural data.**

Gröger, H.R., Fügenschuh, B., Tischler, M., Schmid, S.M., Foeken, J.P.T.

published 2008: *Geological Society, London, Special Publications*

This chapter aims at reconstructing the Tertiary burial and exhumation history of the study area. Based mainly on fission track data the thermochronological history is elaborated and exhumation is quantified. (U-Th)/He data, as well as the kinematic analysis of mesoscale structures, provide additional information.

H.R. Gröger has performed sampling, preparation and dating of the fission track samples. She wrote a first draft of the manuscript. B. Fügenschuh introduced H.R. Gröger to the fission track method and supported the interpretation of the data. He also provided valuable help in preparation of the manuscript. M. Tischler contributed during fieldwork and provided the kinematic data. S.M Schmid also contributed by providing guidance during field work and significantly improved the quality of the final manuscript. J. Foeken (SUERC, Glasgow), in collaboration with H.R. Gröger, provided the (U-Th)/He data.

## Chapter 5:

### **Paleogene burial followed by Middle Miocene exhumation during soft collision of Tisza-Dacia with the European margin**

Based on the exhumation data elaborated in Chapter 4, this chapter reconstructs the Tertiary burial and exhumation history in the study area within the framework of a palinspastic reconstruction by Tischler (2005). Uplift during and following Miocene soft collision of Tisza-Dacia with the European margin is quantified.

H.R. Gröger provided the uplift data inferred from apatite fission track data. M. Tischler involved uplift data based of stratigraphical information and performed the contouring of the uplift map. H.R. Gröger wrote a first version of the manuscript, in collaboration with M. Tischler. B. Fügenschuh considerably improved the interpretation of the data and the resulting manuscript.

## Chapter 6:

### **Summary**

This chapter summarizes the results of the presented thesis

### **Appendices**

Appendix A: Stratigraphic ages and correlations

Appendix B: Fission track analysis- methodology

Appendix C: Fission track analysis- analytical procedure

Appendix D: Statistical problems of single grain ages at low track densities

Appendix E: Fission track data

## Acknowledgements

First of all I would like to thank my supervisors, Bernhard Fügenschuh, Stefan Schmid and Andreas Wetzel for initiating a project in a region of Europe I fell in love with during my time as a PhD student: The Maramures in Northern Romania.

Bernhard Fügenschuh familiarized me with the fission track dating method. His always positive perspective on any kind of problem (and there are numerous) did not always help in finding solutions, but made at first sight insurmountable problems appear significantly smaller. His efficient work on numerous manuscripts significantly improved whatever I wrote. A 3-pages-mixture of disarranged results would return within two days transformed into a smashing abstract, which featured fascinating geology I never dreamt of. This efficiency proved extremely helpful during the last half year, while my thesis was rapidly developing.

During fieldwork and discussions here in Basel I profited a lot from the Schmid/Fügenschuh team. The combination of Stefans constant and very active interest in any geological question (even at one o'clock in the morning) together with Fügis never ending effort in making me understand, helped me to profit from Stefans enormous experience in Alpine geology (in a very large scale). Among many other things, my skills regarding the "traditional" work of a geologist (field-work, reading of maps and profiles) were vastly improved here in Basel.

Apart from the structural understanding of the field geology I profited a lot from field-work with Andreas Wetzel, who introduced me to the sedimentological aspects of the geology we were working in.

In Basel the interaction in the Alpine-Carpathian-Dinaride working group was very fruitful for the interpretation of the data. Mihai Marin is thanked for his effort to make me understand the Romanian ways. He organised much that would have been impossible for me. I thank Kamil Ustaszewski for his open ear, especially at the end of my thesis.

The work in the Maramures led to many contacts with Romanian as well as Hungarian colleagues. I send special thanks to M. Sandulescu and D. Badescu for the introduction into the geology of the Maramures and fruitful discussions. For sharing their data as well as many discussions Ion Balintoni, Alexandru Voda, Carol Strutinski, Daniel Radu, Lazlo Fodor and Lazlo Csontos are gratefully acknowledged. Without these people, this thesis would not have been possible.

Apart from the above mentioned I have to send my special thanks to Liviu Matenco for his fast and constructive help in almost any aspect. Moreover I am indebted, since he accepted the role as an external reviewer of this thesis, a great and time-consuming effort.

I would like to stress the very inspiring atmosphere during my years here in Basel. The group of PhD students and Post Docs is somehow a small version of Europe condensed into one house. The interaction with all these colleagues, especially besides the scientific work, made my time in Basel very colourful and there is only one thing left to say: I already miss you all!

For their scientific support I especially thank my colleagues in the fission-track-group, namely Zoltan Timar-Geng, Horst Dresmann and Katy Waite. They always already had the literature I was still searching for. Especially the endless discussions with Katy Waite improved my understanding about fission tracks. Even better was the fact that a 30 min discussion about

the usefulness of a Chi-Square test could easily end in a three hour chat about.... (you know, what women talk about).

What a fission tracker - as everybody dependant on a lot of sample preparation- should never forget is to thank the people running the labs. My thank goes especially to the student helpers Christian Seiler and Richy Waite and our technical staff Willy Tschudin, Hans-Ruedi Ruegg and Heinz Hürlimann. Christian proved to be an invaluable student helper, working even cleaner than I did. The personal interest and involvement in sample preparation by Richy Waite and Willy Tschudin led to great improvements, resulting in speeding up the preparation process, as well as reaching better results (I know, Fügen, you still prefer hand polishing). Hans-Ruedi Ruegg always kept an open mind for whatever technical problem one could have (and he always had the necessary spare parts).

Apart from the lab work other people in Basel are gratefully acknowledged, who keep the system running. Joelle Glanzmann provided support in all questions of administration. Verena Scheuring helped me very efficiently, especially in the last few month of the thesis. A good library is utterly worthless without somebody who knows where the books are. In all questions of computers Konrad Leu always had an open ear, and he answered even the most stupid questions.

Finlay Stuart and Jürgen Foeken introduced me to the (U-Th)/He method during two nice weeks in Glasgow. I thank them for their effort and for leading me to run their machine. To Jürgen Foeken I am especially grateful for doing the handpicking of apatite.

I think very friendly of Mioara and Luci Lungulescu and Man Ludovica. They provided a "home" in Romania for Matthias and me, making it sometimes hard to distinguish if going to the field or going back to Basel was "coming home". Their constant hospitality and the family-like atmosphere, including the wonderful food, kept our strength during the excessive field work.

I also thank my family, who had the patience to wait so long and who always motivated me to go on in my work and after all: Came to celebrate with me the successful finish!

Last, and most definitely not least, I would like to thank my closest colleague during this PhD project: Matthias Tischler. Our interaction, especially during common field work, was very productive and inspiring. He is my most critical co-author, computer-specialist, sample pack donkey, the great love of my life,...-to make it short: The best man of all! His calmness and nerves, especially during the final phase, made finishing (and printing) of this thesis possible.

## Table of contents

Abstract .....	I
Organisation of this thesis .....	II
Acknowledgements .....	IV
Table of contents .....	VI
<b>Chapter 1: Introduction.....</b>	<b>1</b>
1.1 Geological overview .....	2
1.2 Outline of the projects incorporating this thesis.....	4
1.3 Aims and approach of this thesis.....	4
1.4 History and culture of the study area- a personal perspective.....	4
<b>Chapter 2: Mesozoic thermal history of the Maramures area (Northern Romania) constrained by zircon fission track analysis: Cretaceous metamorphism and Late Cretaceous to Paleocene exhumation.....</b>	<b>7</b>
2.1 Abstract.....	7
2.2 Introduction .....	8
2.3 Geological setting .....	9
2.4 Methods: Zircon fission track analysis.....	12
2.5 Results.....	12
2.5.1 Sampling approach .....	12
2.5.2 Zircon fission track data.....	12
2.5.3 Constraints regarding Alpine metamorphism in the Bucovinian nappe stack.....	16
2.6 Interpretation and Discussion .....	18
2.6.1 Late Early Cretaceous nappe-stacking ("Austrian" phase) .....	18
2.6.2 Albian-Early Cenomanian ? nappe folding and thrusting (Late "Austrian" phase).....	19
2.6.3 Late Cretaceous exhumation .....	19
2.6.4 Latest Cretaceous thrusting ("Laramian" phase) and Paleocene exhumation.....	20
2.6.5 Eocene burial to second exhumation during Miocene .....	20
2.7 Conclusions .....	20
2.8 Acknowledgements .....	20
<b>Chapter 3: Miocene tectonics of the Maramures area (Northern Romania): implications for the Mid-Hungarian fault zone.....</b>	<b>23</b>
Tischler, M., Gröger, H.R., Fügenschuh, B., Schmid, S.M. <i>International Journal of Earth Sciences 2006</i>	
3.1 Abstract.....	23
3.2 Introduction .....	24
3.3 Geological Setting.....	26
3.4 Methods .....	27
3.4.1 Derivation of kinematic axes .....	27
3.4.2 Fission Track Analysis.....	28
3.5 Structural analysis.....	29
3.5.1 Early Burdigalian top-SE thrusting of the Pienides .....	29
3.5.2 Late Burdigalian NE-SW extension .....	30
3.5.3 Post-Burdigalian structures .....	30

3.5.4	Stratigraphical timing constraints regarding post-Burdigalian deformation .....	30
3.6	Constraints from fission track data .....	32
3.7	Synthesis of data .....	32
3.7.1	Burdigalian thrusting of the Pienides followed by NE-SW extension.....	32
3.7.2	Post-Burdigalian faulting along the Bogdan- and Dragos-Voda faults .....	33
3.7.3	Estimates of horizontal and vertical components of displacement across the Bogdan-Voda and Dragos-Voda faults .....	34
3.8	Discussion of earlier work and large-scale correlations .....	35
3.8.1	Comparison with previous data from the working area .....	35
3.8.2	Burdigalian top-SE thrusting of the Pienides followed by NE-SW extension in the larger scale context .....	35
3.8.3	Post-Burdigalian activity along the Bogdan-Dragos-Voda fault system in the larger scale context .....	35
3.9	Conclusions.....	36
3.10	Acknowledgements.....	37
3.11	Appendix.....	37
<b>Chapter 4: Tertiary cooling and exhumation history in the Maramures area (internal eastern Carpathians, northern Romania): thermochronology and structural data..... 45</b>		
Gröger, H.R., Fügenschuh, B., Tischler, M., Schmid, S.M., Foeken, J.P.T.		
<i>Geological Society, London, Special Publications 2008</i>		
4.1	Abstract .....	45
4.2	Geological setting.....	47
4.3	Methods.....	49
4.3.1	Fission track analysis: methodology and analytical procedure .....	49
4.3.2	Apatite (U-Th)/He dating: methodology and analytical procedure.....	49
4.4	Results of kinematic analyses.....	49
4.5	Results of the thermochronological analysis .....	51
4.5.1	Sampling approach.....	51
4.5.2	Zircon FT data .....	52
4.5.3	Apatite FT data.....	52
4.5.4	Apatite (U-Th)/He data.....	54
4.6	Thermal modelling of the apatite FT data.....	55
4.7	Revealing the Miocene exhumation history of the Rodna horst .....	58
4.7.1	Summary of the Miocene exhumation history deduced for the Rodna horst.....	62
4.8	Revealing the total amount of Miocene exhumation for the entire study area.....	62
4.9	Recapitulation of results .....	64
4.10	Discussion .....	64
4.10.1	Hydrothermal overprint.....	64
4.10.2	Burial and exhumation in the study area .....	64
4.10.3	Relation between uplift and cooling .....	65
4.10.4	Uplift and exhumation at a regional scale .....	65
4.11	Conclusions.....	66
4.12	Appendix.....	67

<b>Chapter 5: Paleogene burial followed by Middle Miocene exhumation during soft collision of Tisza-Dacia with the European margin.....</b>	<b>69</b>
5.1 Introduction .....	70
5.2 Constraints of the post 16 Ma uplift .....	71
5.3 Reconstruction of the Paleogene burial and Miocene exhumation.....	76
5.3.1 Paleogene to Early Miocene: Sedimentation burial (Interval 65-20 Ma).....	76
5.3.2 Burdigalian: Syn- and post emplacement of the Pienides (Interval 20-16 Ma) .....	76
5.3.3 Middle Miocene to present day: Soft collision (Interval 16-0 Ma) .....	79
5.4 Uplift during and following soft collision .....	81
5.5 Conclusions .....	83
<b>Chapter 6: Summary.....</b>	<b>85</b>
6.1 Cretaceous orogeny and Late Cretaceous to Paleocene exhumation .....	86
6.2 Paleogene to Early Miocene burial .....	86
6.3 Post-Burdigalian soft collision of Tisza-Dacia with the European margin.....	86
6.4 Possible further fields of investigation.....	88
<b>References .....</b>	<b>89</b>
<b>Appendices .....</b>	<b>99</b>
Appendix A: Stratigraphic ages and correlations .....	99
Appendix B: Fission track analysis- methodology .....	100
Appendix C: Fission track analysis- analytical procedure.....	102
Appendix D: Statistical problems of single grain ages at low track densities .....	109
Appendix E: Fission track data.....	on CD

---

# **Chapter 1:**

# **Introduction**

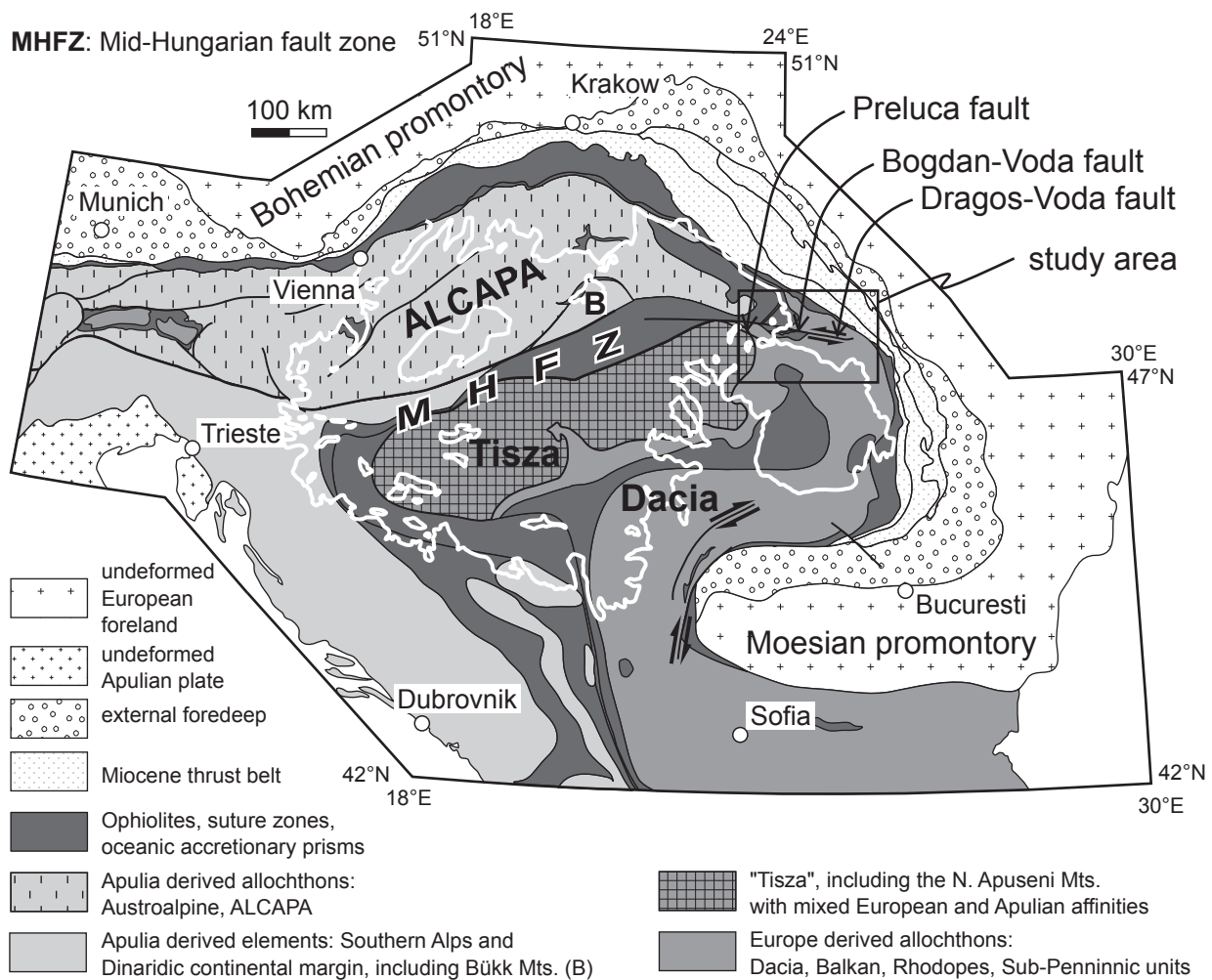


**Fig. 1.1.** Major tectonic units of the Alps, Carpathians and Dinarides (simplified after Schmid et al. 2008). Located within the Carpathian embayment are three major continental blocks: ALCAPA, Tisza and Dacia. During emplacement in Tertiary times a zone of repeated tectonic activity developed between ALCAPA and the already consolidated Tisza-Dacia block: the Mid-Hungarian fault zone. Large areas of the Mid-Hungarian fault zone are buried below the sediments of the Pannonian basin. The Neogene Transylvanian and Pannonian basin sediments are outlined by the white line.

## 1.1 Geological overview

One of the key parts in understanding the formation of the Carpathian orogen is the Tertiary tectonic history of crustal blocks, juxtaposed against the highly irregular European continental margin (e.g. Royden 1988). The European continental margin features a large-scale bight ("Carpathian embayment") between the Bohemian and Moesian promontories (Fig. 1.1), thought to have been formerly occupied by (partly?) oceanic crust by many authors (e.g. Balla 1982).

The continental units found within this embayment show marked differences in their contrasting Triassic and Jurassic sedimentary facies (e.g. Csontos and Vörös 2004 and references

therein). ALCAPA ("Alpine North Pannonian" Csontos et al. 1992; "North Pannonian block", Sperner et al. 2002) shows Apulian affinities. Dacia ("Rhodopia", Burchfiel 1980; "Median/Marginal Dacides", Sandulescu 1988; "Dacides", Csontos et al. 1992; "Getic Craton", Balintoni 1995) shows European affinities. Tisza ("Tisia", Balintoni 1995) shows mixed Apulian and European affinities. After amalgamation of Tisza and Dacia during the Cretaceous, they are considered to represent one single block, the Tisza-Dacia block (Csontos 1995, Csontos and Vörös 2004), regarding the Tertiary development.

While the definition of the eastern block, Dacia, as an independent continental block during pre-Cretaceous times is commonly agreed upon, the definition and affinities of Tisza is a



matter of debate. Some authors consider Tisza to represent a part of ALCAPA, postulating a pre-Cretaceous single western block ("Apulia", Burchfiel 1980; "Preapulia", Balintoni 1995; "Inner Dacides (Austroalpine)", Sandulescu 1988, Sandulescu 1994). This interpretation implies, that after Cretaceous times all mentioned blocks were amalgamated, i.e. that deformations during Tertiary collision with the European margin have to be considered as block-internal. However, a post-Cretaceous subdivision in two blocks- ALCAPA and Tisza-Dacia is corroborated by paleomagnetic data, which indicates opposed rotations of both blocks (e.g. Patrascu et al. 1994, Marton et al. 2002, Marton and Fodor 2003).

In this thesis the subdivision into three continental blocks termed ALCAPA, Tisza and Dacia is used. The study area is located where these three continental blocks meet (Fig. 1.1). Most of the basement units outcropping in the study area belong to the northern East Carpathians (e.g. Sandulescu et al. 1981), representing the northernmost part of Dacia. The Preluca massif, south of the Preluca fault, forms the northeasternmost outcrop of the Tisza block (e.g. Haas and Pero 2004), which is in large parts buried below the Neogene fill of the Pannonian basin. Further outcrops of Tisza include the Apuseni mountains as well as some inselbergs in Hungary and Croatia (Fig. 1.1). ALCAPA sensu strictu is not outcropping in the study area, but an accretionary prism which developed between ALCAPA and Tisza-Dacia, the Pienides (e.g. Aroldi 2001).

During the Tertiary, space problems and corner effects at the promontories led to extensive deformation accompanied by opposed rotations of the invading blocks (e.g. Fodor et al. 1999). The major tectonic lineament along which the ALCAPA and Tisza-Dacia blocks are juxtaposed is a broad zone of deformation, termed the Mid-Hungarian fault zone. Unravelling of the tectonic history of this fault zone, dividing the major blocks which constitute the present day Carpathian embayment, can provide crucial constraints for the tectonic development of the intra-Carpathian area.

Unfortunately, most of the Mid-Hungarian fault zone is covered by the Neogene sediments of the Pannonian basin, restricting field-work to small areas at the basin borders. The study area of this thesis is located in one of these areas, in northern Romania, where structures related to the Mid-Hungarian fault zone, can be studied in outcrop.

The main driving force during emplacement

of these continental blocks is thought to have been the eastward translation of parts of the Eastern Alps by lateral escape (e.g. Ratschbacher et al. 1991a, b), coupled with slab retreat of the subducting partly(?) oceanic fill of the Carpathian embayment (e.g. Royden 1988; Wortel and Spakman 2000; Sperner et al. 2005). The Tertiary final emplacement of ALCAPA and Tisza-Dacia along the European margin is the result of soft collision of both these blocks with the European margin (Royden 1993, Morley 2002). Several studies address emplacement mechanisms of ALCAPA (Sperner et al. 2002) and Tisza-Dacia along the European margin (Linzer et al. 1998; Schmid et al. 1998; Zweigel et al. 1998). Emplacement mechanisms for Tisza-Dacia address mostly the southern East Carpathians (Morley 1996; Zweigel et al. 1998) and South Carpathians (Schmid et al. 1998; Fügenschuh and Schmid 2005). This study focuses on the northern East Carpathians.

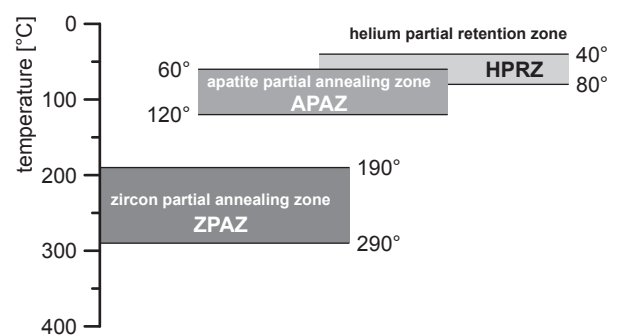


**Fig. 1.2.** Partial annealing zones for fission tracks in zircon (ZPAZ) and apatite (APAZ) and the helium partial retention zone in apatite (HPRZ). Temperature intervals are after Hurford 1986 (ZPAZ), Gleadow and Duddy 1981, Green et al. 1989 (APAZ) and Wolf et al. 1998 (HPRZ).

The combination of structural and sedimentological field observations with thermochronological data is very useful to quantify and date tectonic uplift and exhumation (e.g. Sobel and Dumitru 1997; Fügenschuh et al. 2000; Fügenschuh and Schmid 2003, 2005; Foeken et al. 2003; Reiners et al. 2003, Persano et al. 2004). Using three different thermochronological systems- zircon fission track, apatite fission track and apatite (U-Th)/He analyses- a large temperature range is constrained (290-40°C; Fig. 1.2). Low-temperature thermochronology on apatite (apatite fission track analyses, (U-Th)/He analyses) is a useful tool for constraining exhumation in soft collisional regimes, where major uplift and exposure of high grade metamorphic rocks is inhibited (Royden 1993; Morley 1996).

## 1.2 Outline of the projects incorporating this thesis

The project providing the framework for the presented study are mainly NF-project “The Dragos Voda fault in northern Romania – the eastern termination of the Mid-Hungarian Line fault system?” (Nr. 21-64979.01), and its follow-up project (Nr. 200020-105136/1). Initiated by Bernhard Fügenschuh and supported by Andreas Wetzel and Stefan Schmid, this project is designed to obtain field-based and geochronological evidence to augment the existing geophysical dataset concerning the tectonic history of the Mid-Hungarian fault zone.

Since most of the Mid-Hungarian fault zone is covered by the young sediments of the Pannonian basin, the focus of this project lies on the basin border (Northern Romania), where outcrops permit field-based studies. Within the study area, several map scale faults are first order candidates for representing the continuation of the Mid-Hungarian fault zone (Fig. 1.1): The Bogdan-Voda fault, the Dragos-Voda fault and the Preluca fault.

Another NF-project granted to Stefan Schmid (Nr. 200021-101882/1) aims at continuing the work and expanding the scope towards the Dinarides. The long term aim of all of the above-mentioned projects is the improvement of the general tectonic map presented (Schmid et al. 2008), together with the better understanding of the Late Tertiary emplacement of the crustal blocks into the Carpathian embayment. Another goal is the palinspastic restoration of the Late Tertiary tectonic history of the Carpathian embayment.

- In order to reconstruct the Late Tertiary tectonic history of the study area, the following approach was chosen:

- Detailed structural fieldwork focussing on Miocene structures in basement as well as sedimentary units of the study area.

- Extensive geochronology utilising fission track dating on apatite and zircon in combination with (U-Th)/He dating on apatite in order to constrain the exhumation history of the study area.

- Detailed sedimentological fieldwork on Late Tertiary strata, in order to reconstruct their depositional setting and thus obtain constraints for synsedimentary tectonics.

- Paleomagnetic analysis of selected sites within the study area in order to provide the link to already existing paleomagnetic databases.

Two complementary PhD-theses are situated

within the larger framework of the original project, each concentrating on different aspects of the approaches mentioned above. While the PhD thesis of Matthias Tischler (Tischler 2005) concentrates on structural and sedimentological field-work, including paleomagnetic data, this thesis focussed on thermochronological analyses, integrated with the results from structural and sedimentological field work.

## 1.3 Aims and approach of this thesis

Combining different thermo-chronometers, focussing on zircon and apatite fission track analysis, the main goal of this study is to quantify Tertiary burial and Miocene final exhumation of Tisza-Dacia during collision with the European margin. In combination with the analysis of brittle Late Tertiary structures, the emplacement mechanisms are discussed. The zircon fission track data additionally provide constraints for the last metamorphic overprint during Cretaceous orogeny.

Due to the different approaches taken, each chapter includes an individual introduction into the general and regional geological frame – focussing on the information relevant to the respective chapter. This thesis has significantly profited from the integration into the aforementioned larger project. Most notably, close collaboration with the author of the parallel thesis, Matthias Tischler, especially during common field-work and final interpretation of the results, proved very fruitful. A brief description of the aim and approach of each chapter, including the various authors' contributions, is presented in the section “Organisation of this thesis” above.

## 1.4 History and culture of the study area – a personal perspective

Most of the study area is located in a historical region called Maramures, within the Romanian administrative district of the same name, while extending into parts of the neighbouring administrative districts. Main geographic features of the Romanian part of the Maramures are the Viseu and Iza rivers. In the north the Tisa river forms the frontier to the Ukraine. To the east and south the Maramures is delimited by mountains. The area is characterised by a continental climate with hot and humid summers and very cold winters. It is one of the rainiest regions in Romania. Hence during fieldwork umbrellas and rubber boots proved to be

pieces of equipment as important as hammers and hand lenses.

The first settlers in the present day region of the Maramures and Transylvania have been the so-called Dacians. In the first centuries A.C. most of Transylvania was part of the Roman empire, while the Maramures remained unoccupied, constituting "free Dacia". The two most important faults in this study are named after two Dacian rulers (lord="Voda") born in the Maramures - Bogdan und Dragos. During medieval times, until the beginning of the 20<sup>th</sup> century, the Maramures was mostly part of the Hungarian and later the Austrian-Hungarian empire (Verseck 2002). Even today, Hungarian and German minorities still live in the region. Since the First World War the Maramures is divided into a Ukrainian and Romanian part.

The special geographical layout of the area, a natural fortress ringed by mountains, kept the Maramures largely untouched by the blessings of the 20<sup>th</sup> century. The everyday-life in a small Maramures village revolves around agriculture. The idyllic scenery is characterised by people cutting hay, stacking it in the traditional cone-shaped heaps, and horse-carts passing by. After field work, we had the opportunity to enjoy the beneficiaries of such a non-industrial agriculture, most notably the very delicious homemade food as well as the fruit brandy (Horinca, Tuica) the region is famous for. The hospitality of the people, which invited us several times to drink with them, led to a real "spiritual" understanding of the geology. The region is famous for its textiles production (cloths, tablecloths, carpets). The people still

wear traditional folk costumes (Fig. 1.3) on many occasions. The most traditional atmosphere can be found in the villages along the Iza valley.

Another important economical factor in the area is lumber industry. The Vaser valley, for example, is only accessible by an old narrow-track steam train, which is still in use by the woodcutters. Using this train allowed us for sampling 40 km up the valley (sample series Maramures mountains). The area has a long tradition of wood building. Still most of the buildings in smaller villages are made of wood (Fig. 1.3). The ornaments, especially on the traditional gates, as well as doorways, turn some of the houses into real pieces of art. Famous are the orthodox wooden churches, their roofs constructed out of millions of wooden chips. Some of the churches along the Iza valley are on the Unesco list of World Heritage sites (Williams and Wildmann 2001)

Apart from the traditional use of the land by woodcutting and agriculture, mining is an important economical factor. The grey atmosphere of the concrete architecture in mining towns like Baia Sprie or Căvnic is in strong contrast to the idyllic charm of the Maramures villages. The exploited ore deposits are related to the Miocene magmatism in the area. The mines of Baia Borsa and Baia Mare acquired an unpleasant famousness in the years 2000 and 2001, when accidents led to the disastrous discharge of industrial waste, containing cyanides and heavy metals, into the rivers Tisa and Danube (Verseck 2002).

The summers we spend during field-work have always been a source of enjoyment and helped

*Fig. 1.3. The picture shows the author of this thesis Heike R. Gröger (left) and the author of the parallel thesis incorporated in this project Matthias Tischler (right), presenting the traditional folk costume of the Maramures area. The photograph is taken in front of a wooden farm house, typical for the Maramures villages.*



us to relax from the laboratory and office work during the year in Basel. The picturesque landscape and the hospitality of the people make it easy to fall in love with the Maramures region.

## Chapter 2:

# Thermal history of the Maramures area (Northern Romania) constrained by zircon fission track analysis: Cretaceous metamorphism and Late Cretaceous to Paleocene exhumation.

### 2.1 Abstract

The Cretaceous Alpine nappe stacking in the northern East Carpathians is generally considered to have taken place under sub-greenschist facies conditions. The samples described derive from the Bucovinian nappe stack (Central East Carpathians, Rodna mountains) and the Biharia nappe system (Preluca massif).

The Alpine top to the NE directed nappe stacking led to an increasing temperature gradient during deformation. Sub-greenschist facies conditions during the Alpine metamorphic overprint only caused partial annealing of fission tracks in zircon in the external main chain of the Central East Carpathians. Full annealing of zircon points to at least 350°C in the more internal elements (Rodna mountains, Preluca massif). This temperature gradient is interpreted to have resulted from increasing tectonic overburden (up to at least 20 km) towards more internal units. Late Cretaceous cooling and exhumation is well constrained by zircon fission track ages. It commences earlier in the more external main chain of the Central East Carpathians (Cenomanian) than in the Rodna mountains and the Preluca massif (Campanian).

The close neighbourhood of Coniacian to Campanian zircon fission track cooling ages to Cenomanian sediments suggests tectonic exhumation in the Rodna mountains. This tectonic exhumation may be due to a phase of Late Cretaceous extensional tectonics so far not supported by structural data. Extensional tectonics related to orogenic collapse (Gosau type basins) is the most likely process, which allows for extensional tectonics.

## 2.2 Introduction

The highly arcuate Carpathian orogen acquired its present-day geometry during its formation in Tertiary times. Crustal blocks of different provenance (ALCAPA, Tisza, Dacia; Fig. 2.1) are located within the so-called Carpathian embayment between the Bohemian and Moesian promontories. Tertiary emplacement of these blocks was driven by lateral extrusion in the Alps (Ratschbacher et al. 1991a, 1991b), combined with roll back of the subducted lithospheric slab formerly occupying the Carpathian embayment (Csontos 1995, Spermer et al. 2005). Numerous studies focussing on the invasion of these continental blocks into the Carpathian embayment (e.g. Balla 1987; Royden and Baldi 1988; Csontos et al. 1992; Fodor et al 1999) considerably improved our understanding of the Tertiary tectonic evolution, during which Tisza and Dacia are generally considered as one block, the Tisza-Dacia block (Csontos 1995; Csontos and Vorös 2004). However, their Cretaceous histories are less well constrained (e.g. Burchfiel 1980; Sandulescu 1988; Sandulescu 1994; Csontos and Vorös 2004).

The Alpine Bucovinian nappe stack, constituting part of the Central East Carpathians (Sandulescu et al. 1981), represents the northernmost part of the continental Dacia block (Fig. 2.1). This Dacia block (or Dacides, Csontos et al. 1992) comprises the Danubian nappes, the Bucovinian nappe pile of the East Carpathians (Sandulescu et

al. 1981), the Biharia nappe system, the Getic and Supragetic nappes of the South Carpathians, the Carpatho-Balkan units Sredna-Gora and Serbo-Macedonian. The Bucovinian nappe stack is build up, from bottom to top, by the Infrabucovinian nappes, correlated with the Getic nappes, followed by the Subbucovinian and Bucovinian nappes, correlated with the Supragetic nappes (Sandulescu 1994). According to a recent compilation of tectonic units by Schmid *et al.* (2006) the basement units of the Biharia nappe system are considered as the most internal part of Dacia, but classically they are attributed to Tisza (e.g. Haas and Péro 2004).

Juxtaposition of Tisza and Dacia started during the Alpine, late Early Cretaceous, orogeny of the Central East Carpathians, leading to the closure of the intervening oceanic domain (Transylvanides, Sandulescu 1988; Vardar-Mures zone, Csontos and Vorös 2004). The Transylvanides, Middle Triassic to Middle/Late Jurassic ophiolites (Sandulescu 1994), are obducted onto the Bucovinian nappe pile (Sandulescu 1988, 1994).

While the Pre-Alpine metamorphic development of the basement units in the study area is relatively well established (Bucovinian nappe stack, Kräutner 1988, 1991, Voda and Balintoni 1994; Tisza, ???), the degree of Alpine metamorphic overprint is still a matter of debate. Within the Bucovinian nappe stack late Early Cretaceous (Aptian/Albian) nappe stacking is generally considered to have occurred under sub-greenschist metamorphic conditions (Sandulescu

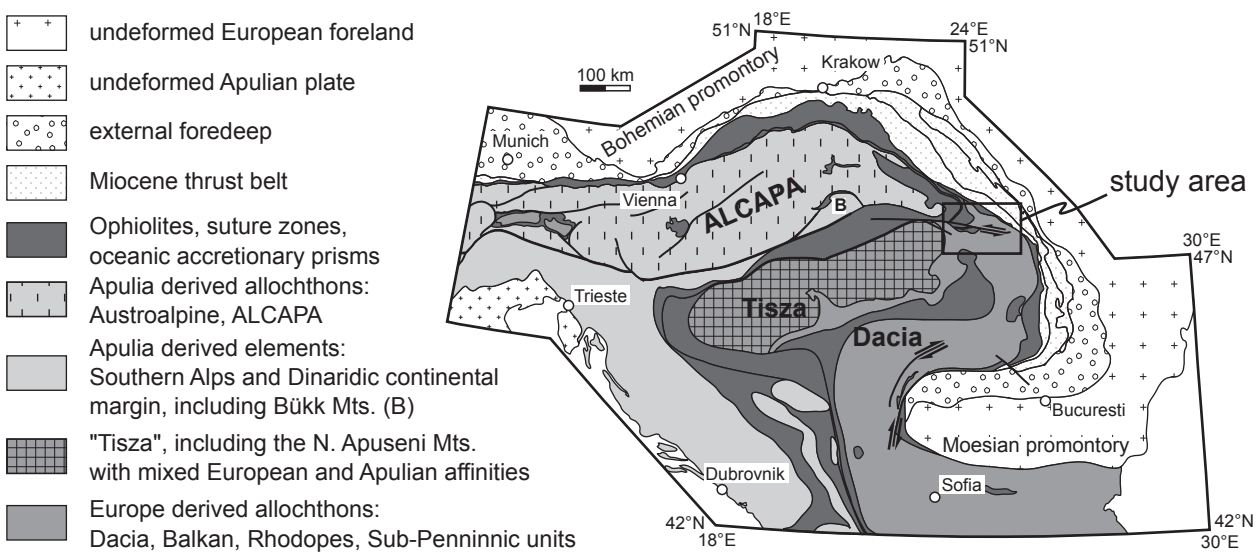


**Fig. 2.1.** Tectonic overview of the Alpine-Carpathian-Pannonian area (simplified after Schmid et al. 2008). The three major continental blocks occupying the Carpathian embayment- ALCAPA, Tisza and Dacia- have been finally emplaced during Tertiary times.

et al. 1981). This is indicated by the low degree of metamorphism of Permian to lower Cretaceous sedimentary units separating the individual nappes (Sandulescu et al. 1981). However, recent publications reveal Alpine-age metamorphic overprint, ranging from greenschist facies to locally epidote-amphibolite facies (Pană and Erdmer 1994, Balintoni et al. 1997, Dallmeyer et al. 1998). This Alpine-age overprint has been documented in the Rodna horst, a massif exhumed in a more internal location in respect of the main range of the Central East Carpathians (Fig. 2.2).

This study discusses Cretaceous metamorphism and late Cretaceous to Paleogene exhumation in the northern East Carpathians by using zircon fission track analysis. The samples derive from the external East Carpathian chain (Bucovinian nappe system), the internal Rodna horst (Bucovinian nappe system) and the even more internal Preluca massif (Biharia nappe system, Fig. 2.2). Since annealing of fission tracks in zircon occurs in a temperature range of 200-350°C (Hurford 1986, Yamada et al. 1995, Tagami et al. 1996), it largely overlaps with the assumed degree of Cretaceous metamorphism in the study area. Therefore the metamorphic and cooling history have to be discussed in the light of additional geochronological data (Ar/Ar, Dallmeyer et al. 1998) and stratigraphic constraints.

### 2.3 Geological setting

Of the Bucovinian nappe stack the tectonically deepest Infrabucovinian nappe is only exposed in a series of windows (Fig. 2.2), of which the Rodna window (Kräutner 1988) is one of the biggest. The metamorphic basement units of the Bucovinian nappe pile are predominantly composed of polymetamorphic paragneisses with rare occurrences of orthogneiss (Kräutner 1938, Kräutner 1988, 1991, Voda and Balintoni 1994).

Dominant in all three nappe systems is a Pre-Cambrian amphibolite facies basement, thought to be derived from Proterozoic sediments (Rebra, Negrișoara and Bretila series; Kräutner 1988). The Subbucovinian and Bucovinian nappes additionally feature a series composed of Cambrian sediments and eruptive rocks (Tulghes series), its greenschist facies metamorphic overprint has been dated by K-Ar methods as Caledonian (Ordovician (450-470 Ma); Kräutner 1988, 1991, and therein). According to Kräutner (1991), the Variscan and Alpine orogenies only caused a regional greenschist facies overprint.

The Infra- and Subbucovinian nappes

feature a Post-Caledonian sedimentary cover that underwent a prograde greenschist facies metamorphic overprint of uncertain age (Kräutner 1991). Palynological data indicate a Silurian to Lower Carboniferous (Sandulescu et al. 1981, Kräutner 1988, 1991, and references therein) age of these cover units, while K-Ar age data point to a late Carboniferous age (310 Ma, Kräutner 1991) of the greenschist facies overprint during the Variscan cycle. A recent study by Balintoni et al. (1997) offers a different interpretation. The stratigraphic age of these cover units in the Rodna window (Repedea, Rusaia and Cimpoiasa series, Kräutner 1991; Rodna series, Voda and Balintoni 1994), traditionally interpreted as Silurian to Carboniferous in age, is questioned by Balintoni et al. (1997). In contradiction to palynological and biostratigraphical dating, these units are interpreted as Jurassic cover, based on their similarities in structural position and lithology to metamorphosed Jurassic cover units exposed in the Vaser window (Balintoni et al. 1997). Greenschist facies overprint is inferred to be Alpine in age in the Rodna window.

A Post-Variscan Permian to Lower Cretaceous cover with highly variable facies developed in the different nappes (Sandulescu et al. 1981, Sandulescu 1994). Common to all the nappes are the Middle Triassic dolomites, an Upper Triassic hiatus and Middle Jurassic siliciclastic marls (Sandulescu 1994). While sedimentation is only documented until the end of Barremian for the Subbucovinian and Infrabucovinian nappes, a Barremian to Aptian (or even Albian, Kräutner et al. 1975) wildflysch is found on top of the Bucovinian nappes and below the Transylvanian nappes. No sub-greenschist facies Permian to lower Cretaceous sediments are preserved, however, in the Rodna horst, exhumed during the Miocene (Gröger et al. 2008).

Alpine thrusting in the Bucovinian nappe pile is of late Early Cretaceous age (former Mid-Cretaceous: Aptian/Albian, 125-99.6 Ma, "Austrian" phase). Sandulescu (1982) narrows the time span for "Austrian" tectonic activity between late Aptian and Albian. Nappe stacking during the "Austrian" phase is top E to ESE directed (Dallmeyer et al. in prep.). The nappe pile is folded along SE to SSE-striking fold axes, as suggested in map view by the strike of the windows exposing the Infrabucovinian units (Fig. 2.2) and as indicated by a related crenulation lineation (NW-SE in the Rodna horst, Balintoni et al. 1997; NNW-SSE further to the east, Balintoni and Baier 2001). Folding is probably contemporaneous with the "Austrian" juxtaposition (Sandulescu 1982)

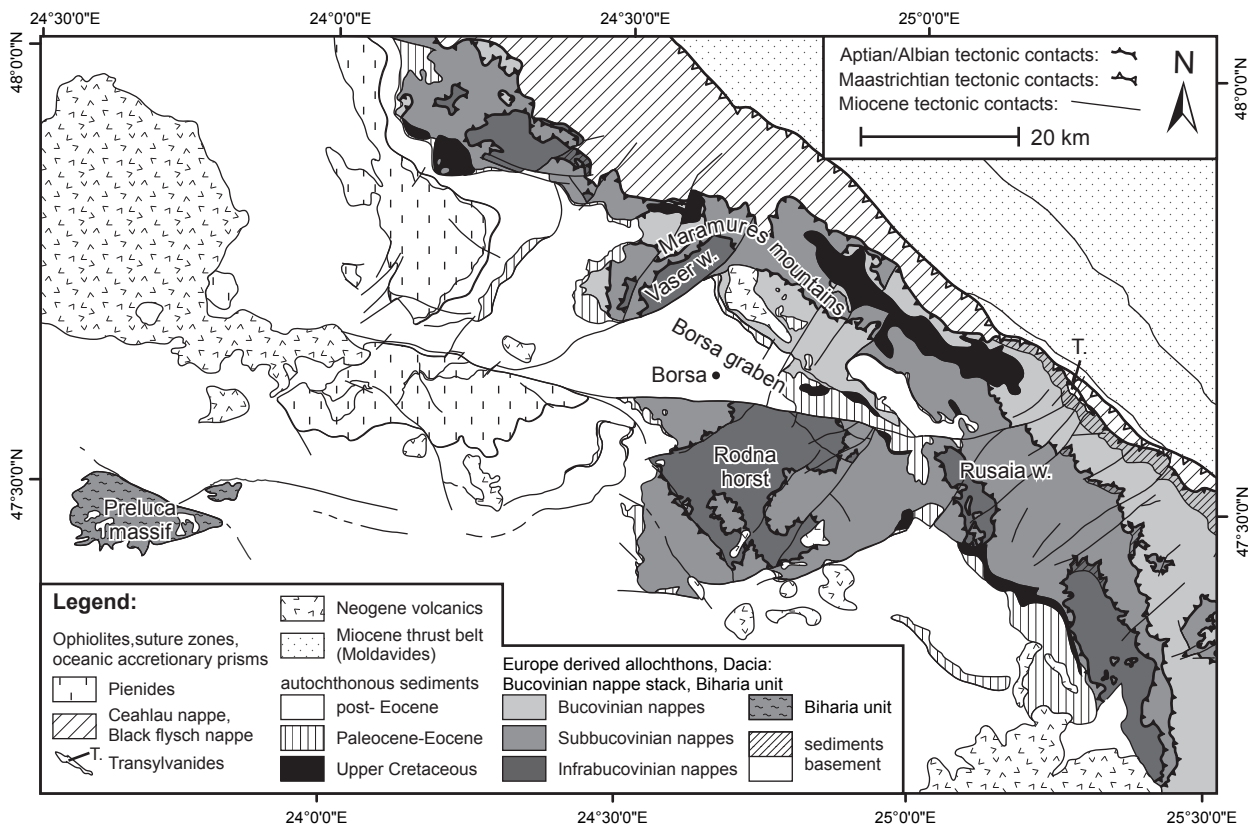


**Fig. 2.2.** Tectonic map of the study area. Late Early Cretaceous thrusting ("Austrian" phase) led to the Bucovinian nappe stack, representing allochthons derived from the European continent (Dacia, Fig. 2.1). Suturing of the Bucovinian nappe stack with the external Ceahlau and Black flysch nappes occurred during a late stage of "Austrian" thrusting. The juxtaposition of the late Early Cretaceous nappe pile against the internal Moldavides is latest Cretaceous ("Laramian" phase). Final emplacement along the Eastern European margin is the result of Miocene tectonics, documented in the external Moldavides.

The map is compiled after Giusca and Radulescu (1967), Raileanu and Radulescu (1967), Ianovici and Dessila-Codarcea (1968), Ianovici et al. (1968), Raileanu and Saulea (1968), Ianovici and Radulescu (1968), Borcos et al. (1980), Krättner et al. (1978, 1982, 1983, 1989), Dicea et al. (1980), Sandulescu (1980), Sandulescu et al. (1981), Sandulescu and Russo-Sandulescu (1981), Rusu et al. (1983), Sandulescu et al. (1991) and Aroldi (2001).

of the Bucovinian nappe stack onto the Black flysch and Ceahlau nappes. The nappe contacts are sealed by (Upper?) Cenomanian strata (Ianovici et al. 1968, Sandulescu et al. 1981). Pre-Cenomanian erosion even exposed the lowermost Infrabucovinian units, since these are also unconformably overlain by Cenomanian strata, for example in the Rusaia window (Fig. 2.2).

Generally, the "Austrian" compressional phase is considered to have taken place under sub-greenschist facies conditions, based on observations in the Permian to lower Cretaceous cover (Sandulescu et al. 1981). However, "dynamic" greenschist facies metamorphism close to the nappe contacts is locally described, especially in the Rodna horst (Krättner et al. 1978, 1982, 1983, 1989) and the Vaser window (Balintoni et al. 1997).

The post-tectonic (with respect to the "Austrian" phase) upper Cretaceous cover is still preserved as relicts along the main Central East Carpathian chain, as well as in the eastern part of the Rodna horst (Fig. 2.2, Fig. 2.3). It includes Cenomanian-Turonian conglomerates and sandstones discordantly overlain by Turonian-Coniacian (silty) marls (Sandulescu et al. 1991, Krättner et al. 1983, Krättner et al. 1978). Above a second unconformity, Santonian to Maastrichtian conglomerates are documented in the Borsa Graben (Szász 1973, Krättner et al. 1983).

The juxtaposition of the "Austrian" nappe-pile during thrusting of the Black flysch and Ceahlau nappes with the most internal flysch units of the Moldavides is of Maastrichtian age ("Laramian" phase, Sandulescu 1982; Sandulescu 1994),



contemporaneous with thrusting in the Danubian nappes in the South Carpathians (Schmid et al. 1998; Matenco and Schmid 1999). The Paleocene sediments are not preserved (possible Paleocene sedimentation is only documented west of the Borsa Graben, Sandulescu et al. 1991; see Fig. 2.3). All this points to a sound latest Cretaceous to Paleocene collisional event, again accompanied by erosion.

Sedimentation after the "Laramian" phase starts again with conglomerates of Lutetian age (suspected Ypresian in case of the Borsa graben, Krätner et al. 1983). The late Lutetian to Priabonian facies is variable (Fig. 2.3). On the Rodna horst and in the southern and eastern parts of the study

area platform carbonates develop (Dicea et al. 1980, de Brouker et al. 1998). A general deepening towards the northwest is indicated by a change from platform carbonates towards marls and distal turbidites (Sandulescu et al. 1991). The maximum thickness of the Eocene sediments in the study area (around 1000m) can be found immediately west of the Borsa graben (Fig. 2.3). The existence of an Eocene paleorelief, as indicated by the variable facies, is also reflected by Oligocene sediments directly overlying the basement units of the Rodna horst (Krätner et al. 1982).

Deposition of thick flysch sequences started in the early Oligocene (possibly latest Eocene) and

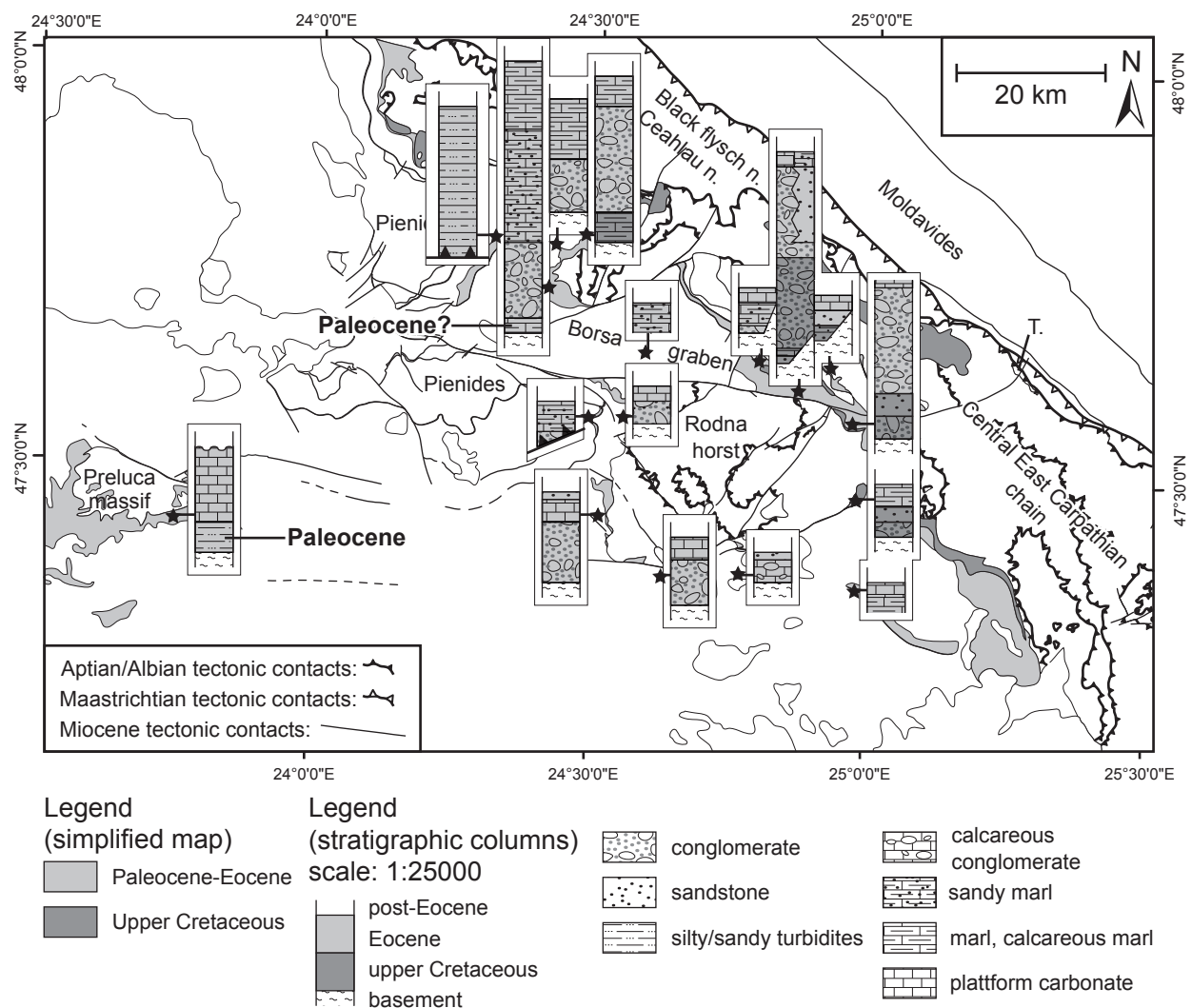


**Fig. 2.3.** Stratigraphic columns presenting the facies development during the Late Cretaceous and Eocene. Greyshade is used to discriminate between the upper Cretaceous (dark grey) and Paleocene to Eocene (light grey) sediments. The upper Cretaceous sedimentary cover is only preserved in remnants along the Central East Carpathian chain and in the easternmost part of the Rodna horst. While in the area of the Bucovinian nappes the Paleocene is largely characterised by a hiatus, Paleocene sediments are deposited at the internal Preluca massif. Stratigraphic columns after Krätner et al. (1978, 1982, 1983, 1989), Rusu et al. (1983) and Sandulescu et al. (1991).

led to burial of the underlying units (Dícea et al. 1980). Final exhumation of the basement units, induced by Miocene brittle tectonics and combined with erosion, is connected to the final stages of juxtaposition of Tisza-Dacia against the European margin (Gröger et al. 2008).

## 2.4 Method: Zircon fission track analysis

Fission track (FT) analysis (overview in Wagner und van den Haute 1992) is a radiometric dating procedure. The samples in this study are analysed using the external detector method, calculating single grain ages (Gleadow 1981). The age is calculated from the ratio between spontaneous fission tracks ( $N_s$ ), counted on a defined square on the grain, and tracks induced by thermal neutrons ( $N_i$ ), counted on the equal square on a uranium-free external detector (Fig. 2.4). The induced tracks allow to quantify the uranium content of the grain. The ages are calculated using the  $\xi$ -calibration method (Hurford and Green 1983).

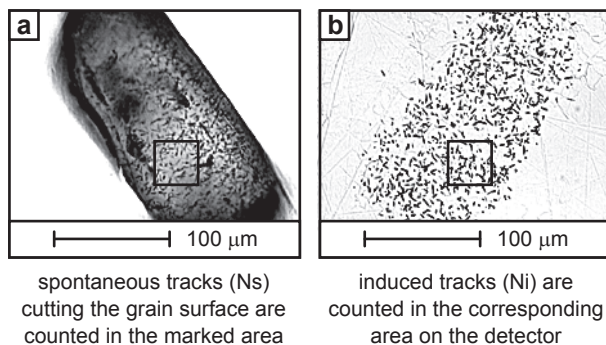


**Fig. 2.4.** Zircon fission track ages are calculated from the ratio of spontaneous tracks ( $N_s$ ) counted on the grain (a) and induced tracks ( $N_i$ ) counted on a uranium free mica detector (b).

Fission tracks are only preserved in the mineral lattice at low temperatures. At higher temperatures the tracks anneal immediately. Within a certain temperature range, called partial annealing zone they anneal slowly and at temperatures below that partial annealing zone the tracks are preserved. The zircon partial annealing zone (ZPAZ) has been addressed in experimental (e.g. Yamada et al. 1995) and empirical studies (e.g. Hurford 1986, Tagami et al. 1996, Tagami and Shimada 1996). While the lower temperature limit at  $\sim 200^\circ\text{C}$  (Tagami et al. 1996) is generally agreed, the upper temperature limit is still a matter of debate, ranging between 300 and  $400^\circ\text{C}$  (Yamada et al. 1995). The closure temperature

of zircon FT ages is estimated at  $240 \pm 50^\circ\text{C}$  (Hurford 1986), which is, within error bars, in accordance with other authors (Tagami et al. 1996, Zaun and Wagner 1985).

After conventional crushing, sieving, magnetic and heavy liquid separation zircon grains were mounted in PFA® Teflon, polished and etched for 12-24 hours in an eutectic melt of NaOH/KOH (relation 16/23 g) at  $225^\circ\text{C}$ . Irradiation was carried out at the High Flux Australian Reactor (HIFAR) with neutron fluxes monitored in CN1. Muscovite was used as an external detector and etched for 40 minutes at room temperature in 40% HF.

Fission tracks were counted on a Zeiss® microscope with a computer-controlled scanning stage ("Langstage", Dumitru 1993) at magnifications of  $\times 1600$  (dry). All ages mentioned are central ages (Galbraith and Laslett 1993). Ages were calculated using a  $\xi$  value of  $141.40 \pm 6.33$  (fish canyon tuff standard, CN1) for zircon with the aid of the windows software TrackKey (Dunkl 2002).

## 2.5 Results

### 2.5.1 Sampling approach

A profile was sampled (M01-09, M12-M14) along the main Central East Carpathian chain from the Maramures Mountains towards the SE (Fig. 2.5). Samples M01 to M05 are from the Infrabucovinian nappes, while samples M06 to M14 are from the Bucovinian and Subbucovinian nappes. The Rodna horst was sampled in more detail (Fig. 2.5). The Subbucovinian nappes were traversed by two vertical profiles, located in the southwestern (R2, 4 samples) and eastern (R4, 3 samples) parts of this basement body, respectively. An additional sample was taken in the northeastern corner (R1-1). From the Infrabucovinian window exposed in the Rodna horst, one vertical profile (R3, 6 samples) was sampled. Additionally, three samples aligned WSW-ENE (R5-1, R5-2, R5-3) were taken. 3 samples were taken from the the Preluca massif (Biharia nappe system, P1-P3). Wherever possible, samples were taken in close contact to the autochthonous sedimentary cover in order to provide independent stratigraphic and thermal control.

### 2.5.2 Zircon fission track data

Along the Central East Carpathian chain (Fig. 2.5; Table 2.1, row 1-12) central ages scatter between Cenomanian and late Jurassic (96.1-162.3 Ma). More internally located samples show Cenomanian

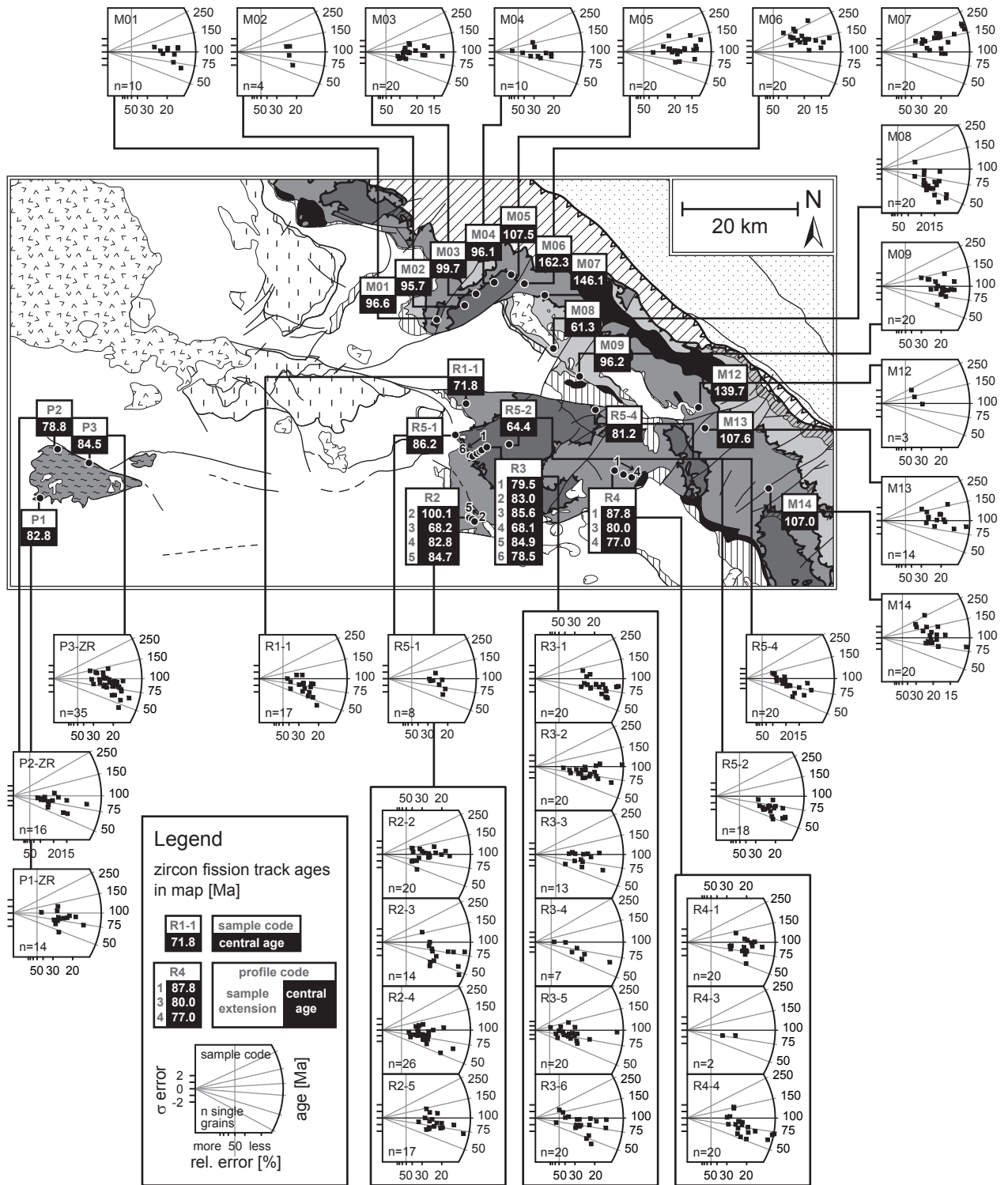


*Fig. 2.5. Results of zircon fission track analyses. The same scale is used in all the radial plots (Galbraith 1990) to allow for direct comparison. All ages in the map are central ages (Galbraith and Laslett 1993), which is a weighted mean of the single grains.*

central ages (96.1-99.7 Ma; M01-M04, M09). All these Cenomanian central ages pass the Chi-Square test ( $\chi^2 > 5$ ; Table 2.1, column 12), hence indicating Cenomanian cooling after full annealing of fission tracks in zircon. Central ages from the more

external north-easternmost samples range between late Jurassic and early Cretaceous (107.0-162.3 Ma; M05-M07, M12-M14). This spread in central ages reflects the observed scattering of single grain ages between late Cretaceous and Paleozoic (oldest

single grain: 310 Ma, M06). This large spread in single grain ages indicates that zircon has only been partially annealed in the external samples prior to Cenomanian cooling.

The Paleocene central age of M08 (61.3 Ma) forms an exception. The extraordinary young age of M08 is most likely the result of a hydrothermal overprint and related partial annealing, caused by the Miocene volcanic body nearby (Pecskay et al. 1995). Hence, sample M08 is excluded from further discussions.

In the more internally located Rodna horst (Fig. 2.5; Table 2.1, row 13-29) and the even more

internally Preluca massif (Fig. 2.5; Table 2.1, row 30-32) zircon FT central ages show a spread between 100.1-64.4 Ma, a time interval roughly covering the Late Cretaceous. Most of the zircon FT central ages from the Rodna horst spread between Coniacian and Campanian. Most central ages pass the Chi-Square test ( $\chi^2 > 5$ ; Table 2.1, column 12), thus indicating full annealing prior to late Cretaceous cooling.

Within the Central East Carpathian main chain (Fig. 2.6a-b) the observed degree of annealing correlates with the sample position within the Alpine nappe pile. While partial annealing dominates in the Bucovinian and Subbucovinian nappes (Fig.

**Table 2.1.** Zircon fission track data. All samples have been analysed using the external detector method (Gleadow 1981) with a zeta value (Hurford and Green 1983) of  $141.40 \pm 6.33$  (Fish Canyon Tuff standard, CN1).

Code	Latitude	Longitude	Alt. [m]	N Grains	Ps [ $\times 10^5 \text{ cm}^{-2}$ ]	Ns	Pi [ $\times 10^5 \text{ cm}^{-2}$ ]	Ni	Pd [ $\times 10^5 \text{ cm}^{-2}$ ]	Nd	X <sup>2</sup> [%]	Central Age $\pm 1\sigma$ [Ma]
M01	24.496670	47.729790	540	10	176.37	1291	49.32	361	3.85	3065	34	96.6 $\pm$ 7.6
M02	24.560710	47.753720	580	4	109.39	367	30.10	101	3.77	3065	13	95.7 $\pm$ 13.5
M03	24.586640	47.772540	630	20	86.88	1468	35.45	599	5.80	3605	81	99.7 $\pm$ 6.8
M04	24.628100	47.791450	680	10	70.07	436	30.54	190	5.97	3605	84	96.1 $\pm$ 9.5
M05	24.667090	47.804300	745	20	98.44	2366	37.20	894	5.86	3605	<5	107.5 $\pm$ 7.4
M06	24.698590	47.790850	790	20	129.07	2543	33.35	657	5.91	3605	<5	162.3 $\pm$ 13.0
M07	24.736840	47.773640	835	20	86.63	2193	25.01	633	6.14	3605	10	146.1 $\pm$ 10.5
M08	24.770543	47.690263	820	20	123.09	2703	52.32	1149	3.69	3065	<5	61.3 $\pm$ 4.7
M09	24.833619	47.647505	1660	20	126.15	2501	32.18	638	3.50	3065	22	96.2 $\pm$ 6.5
M12	25.112014	47.603497	985	3	134.43	164	25.41	31	3.77	3065	21	139.7 $\pm$ 29.5
M13	25.128220	47.571246	930	14	253.89	1812	58.71	419	3.54	3065	23	107.6 $\pm$ 8.5
M14	25.279510	47.478662	850	20	137.67	2830	30.60	629	3.38	3065	<5	107.0 $\pm$ 9.1
P1	23.574760	47.430957	315	14	79.60	1010	25.22	320	3.73	3065	55	82.8 $\pm$ 6.6
P2	23.628772	47.509842	215	16	155.74	1919	47.40	584	3.42	3065	38	78.8 $\pm$ 5.6
P3	23.686807	47.488712	610	35	128.38	3336	40.87	1062	3.81	3065	<5	84.5 $\pm$ 5.5
R1-1	24.559360	47.597860	1550	17	91.73	996	31.13	338	3.46	2967	25	71.8 $\pm$ 6.1
R2-2	24.597260	47.414920	1105	20	80.41	981	32.38	395	5.74	3605	78	100.1 $\pm$ 7.6
R2-3	24.595860	47.415710	885	14	98.81	1326	36.22	486	3.57	2967	<5	68.2 $\pm$ 6.4
R2-4	24.590430	47.419300	705	26	115.20	2312	34.43	691	3.52	2967	12	82.8 $\pm$ 5.9
R2-5	24.583480	47.421240	600	17	121.09	1625	33.68	452	3.35	2967	49	84.7 $\pm$ 6.1
R3-1	24.620652	47.533782	2020	20	188.30	2550	55.68	754	3.35	3065	47	79.5 $\pm$ 5.1
R3-2	24.582850	47.423290	1465	20	74.15	1642	39.02	864	6.25	3605	62	83.0 $\pm$ 5.5
R3-3	24.608990	47.528930	1310	13	76.26	842	38.77	428	6.20	3605	37	85.6 $\pm$ 6.8
R3-4	24.604450	47.526330	1155	7	94.77	607	60.11	385	6.14	3605	50	68.1 $\pm$ 5.5
R3-5	24.597630	47.523200	1005	20	114.82	1751	57.05	870	6.08	3605	14	84.9 $\pm$ 5.9
R3-6	24.587980	47.518690	945	20	92.24	934	49.77	504	6.03	3605	11	78.5 $\pm$ 6.4
R4-1	24.920150	47.500800	1638	16	75.16	1710	21.93	499	3.66	3065	28	87.8 $\pm$ 6.3
R4-3	24.941010	47.494710	980	2	116.94	107	37.16	34	3.62	3065	86	80.0 $\pm$ 16.2
R4-4	24.960230	47.490430	700	20	134.72	1923	45.89	655	3.69	3065	<5	77.0 $\pm$ 5.8
R5-1	24.546451	47.552021	1150	8	204.11	635	57.54	179	3.46	3065	47	86.2 $\pm$ 8.4
R5-2	24.449131	47.460078	1245	18	150.94	1556	53.45	551	3.24	2967	90	64.4 $\pm$ 4.5
R5-4	24.872870	47.596160	1270	20	161.18	2517	50.33	786	3.58	3065	10	81.2 $\pm$ 5.5

**Code:** sample code; **Locality X:** Latitude in WGS84; **Locality Y:** Longitude in WGS84; **Loc. Z [m]:** altitude above sea level; **N Grains:** number of grains counted; **Ps [ $\times 10^5 \text{ cm}^{-2}$ ]:** spontaneous track density; **Ns:** number of spontaneous tracks counted; **Pi [ $\times 10^5 \text{ cm}^{-2}$ ]:** induced track density; **Ni:** number of induced tracks counted; **Pd [ $\times 10^5 \text{ cm}^{-2}$ ]:** standard track density; **Nd:** number of standard tracks counted; **X<sup>2</sup> [%]:** Chi-square probability (Galbraith 1981). **Central Age  $\pm 1\sigma$  [Ma]:** zircon fission track central age (Galbraith and Laslett 1993).

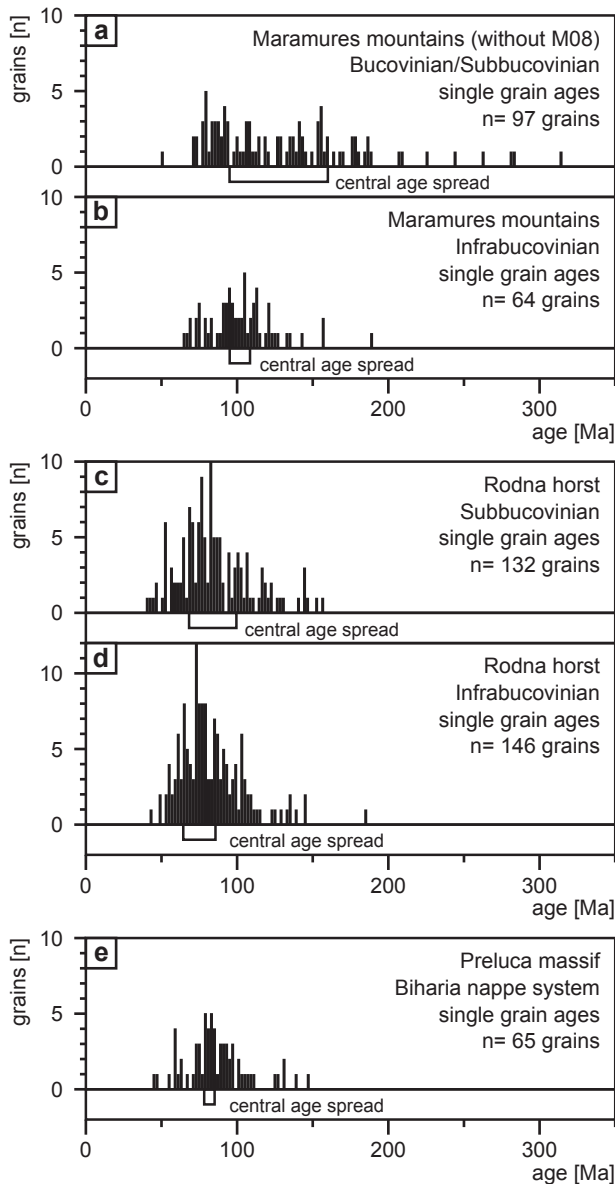


**Fig. 2.6.** Zircon FT ages from the Maramures mountains (a,b) as well as the Rodna horst (c,d), subdivided by their tectonostratigraphic position, and from the Preluca massif (e). While late Early Cretaceous nappe stacking caused full annealing of zircon in the Infrabucovinian (b,d) and internal Subbucovinian nappes (c), only partial annealing is observed in the external parts of the Bucovinian and Subbucovinian nappes (a). In the Preluca massif zircon has also been fully annealed (e) prior to Cretaceous cooling.

2.6a), samples from the tectonostratigraphically lower Infrabucovinian nappes show a relatively well defined Cenomanian cooling peak (Fig. 2.6b). Exceptions include a partially annealed sample from the top of the Infrabucovinian nappe (M05), and a Cenomanian cooling age at the base of the Bucovinian nappes (M09). In the more internally

located Rodna horst, however, no such correlation can be observed (Fig. 2.6c-d). Apart from R2-2 (100.1 Ma), which is older than all other samples, central as well as single grain ages show a similar spread in the Subbucovinian and Infrabucovinian nappes. Moreover, no age vs. altitude relation is detected in the vertical profiles (Fig. 2.5). The Preluca massif shows the same age distribution than the Rodna horst (Fig. 2.6e), even though testified by far less single grains.

In order to evaluate the geological significance of the observed large spread of central ages in the Rodna horst, vertical profile R2 is now examined in more detail (Fig. 2.7). Closely spaced samples from this profile reflect large differences in central ages (R2-2: 100.1 Ma, R2-3: 68.2 Ma). However, the overall time interval within which the single grain ages of R2-2 and R2-3 scatter (Fig. 2.7a-b), is roughly the same for both samples. The same overall range in single grain ages is observed for all Rodna samples (Fig. 2.7c). This indicates that the different central ages are merely of statistical relevance. This

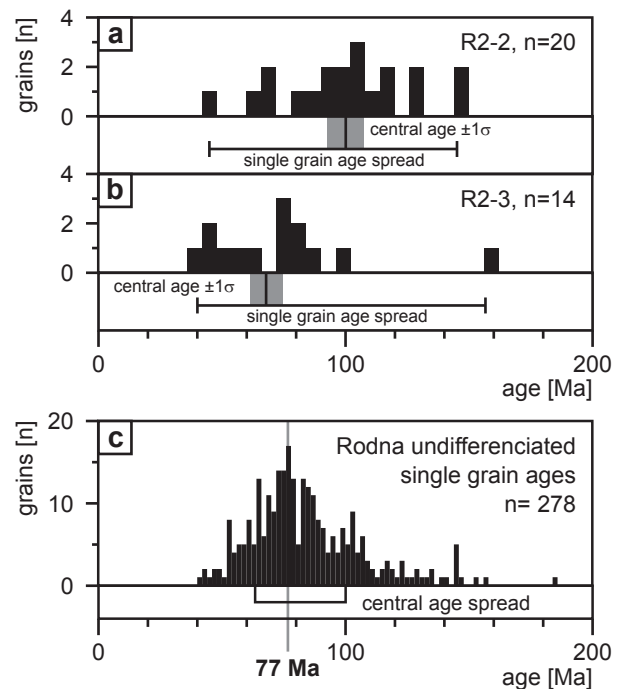


**Fig. 2.7.**

a,b: Zircon FT ages of samples R2-2 (a) and R2-3 (b, Subbucovinian nappes). Although the central ages are rather different, both samples show a similar spread in single grain ages. The central ages are merely the result of the most pronounced portion within one sample.

c: The histogram of all single grain ages from the Rodna horst indicates cooling during the late Cretaceous with a peak in Campanian times (77 Ma).

spread in single grain ages can be aggravated by inhomogeneous annealing behaviour, resulting in shifts of single grain age distributions within one sample. Apart from cooling alpha radiation damage is another important factor influencing the annealing behaviour of zircon grains (Gleadow 1981, Kasuya and Naeser 1988, Rahn et al. 2004). The alpha radiation damage accumulates in relation to entire grain age and uranium content of the grain (Gleadow 1981, Timar Geng et al. 2005). Strong reduction of alpha radiation damage requires higher temperatures than those needed for FT annealing (Rahn et al. 2004 and therein). Due to these considerations, the zircon central ages in the Rodna horst will not be interpreted individually. However, an overall mean in Campanian times (single grain age peak at 77 Ma; Fig. 2.7c) is interpreted to best document the overall time of cooling through the ZPAZ.

In summary, zircon FT data indicate a metamorphic imprint during Alpine tectogenesis, followed by late Cretaceous cooling and exhumation. Alpine metamorphic temperatures must have exceeded 300°C (upper limit of ZPAZ; Hurford 1986, Yamada et al. 1995b) in the lowermost unit (Infrabucovinian nappes) of the Central East Carpathian chain as well as in those parts of the Infrabucovinian and Subbucovinian nappes, which are exposed in the Rodna horst. Cooling and exhumation is of late Cretaceous age within the whole studied area. However, it may start earlier in the main chain of the Central East Carpathians (Cenomanian) as compared to the more internal Rodna horst (Campanian) and Preluca massif (Campanian). Since apatite fission tracks have been fully annealed during post-Cretaceous burial heating (Gröger et al. 2008), they do not provide additional information regarding the Cretaceous exhumation history.

### 2.5.3 Constraints regarding Alpine metamorphism in the Bucovinian nappe stack

By combining the zircon FT data of the Bucovinian nappe stack with Ar/Ar data from the same area (Dallmeyer et al. 1998, Dallmeyer et al. in prep.) maximum temperatures reached during Alpine metamorphism may be estimated more precisely (Fig. 2.8). The temperature intervals given in Fig. 2.8 are based on the upper limit of the ZPAZ (at least 300 °C, Hurford 1986, Yamada et al. 1995) as well as on the widely accepted temperatures for argon retention in muscovite (400±25°C; von

Blanckenburg et al. 1989, Hames and Bowring 1994) and hornblende (500±25°C; Harrison 1981, McDougall and Harrison 1999). In the Rodna horst central ages which do not represent cooling ages (R2-3 and R4-4 failed the Chi-Square test) are omitted. The data indicate metamorphic temperatures which increase from the NE to the SW.

At the north-easternmost rim of the study area sub-greenschist facies metamorphic conditions (200-300°C) during Alpine nappe stacking are indicated by (1) the partial annealing of zircon, (2) the undisturbed Ar/Ar ages and (3) the sub-greenschist facies Permian to Lower Cretaceous sedimentary cover. The neighbouring zone to the SW is characterised by fully annealed zircon and pre-Alpine Ar/Ar ages, indicating temperatures between 300-400°C. Further to the SW zircon fission tracks are fully annealed, and all muscovite Ar/Ar ages are Cretaceous, while pre-Alpine Ar/Ar ages in hornblende are still preserved. All this indicates temperatures of 400-500°C. Moreover, the widespread occurrence of prograde greenschist facies rocks in the central part of the Rodna horst excludes temperatures exceeding the greenschist facies for the last metamorphism. Cretaceous Ar/Ar ages of hornblende in the south-westernmost corner of the Rodna horst suggest temperatures exceeding 500°C and hence epidote-amphibolite metamorphic conditions (Dallmeyer et al. 1998).

Assuming an intermediate geothermal gradient of 25°C/km isotherms for Cretaceous-age peak metamorphic conditions were projected into a schematic cross section across the Rodna horst (Fig. 2.8). The contact between Infrabucovinian and Subbucovinian nappes is openly folded with NW-SE striking axes. The upright fold axial planes are tilted by 10 degrees towards the SW. This Cretaceous folding also affected the isotherms of Alpine peak metamorphic conditions, which dip at angles of about 15-20°C across the nappe contacts towards the foreland in respect to Cretaceous age thrusting, i.e. to the E or NE.

Given the assumed geothermal gradient of 25°C/km the observed temperatures along the Central East Carpathian chain (200-300°C) and in the south-westernmost corner of the Rodna horst (>500°C) correspond to overburdens of 8-12 km and >20 km, respectively. This implies a differential exhumation of some 10 km between the southwesternmost corner of the Rodna horst and the Central East Carpathian chain.

However, the position of the 400°C isotherm is relatively weakly constrained. The line is drawn

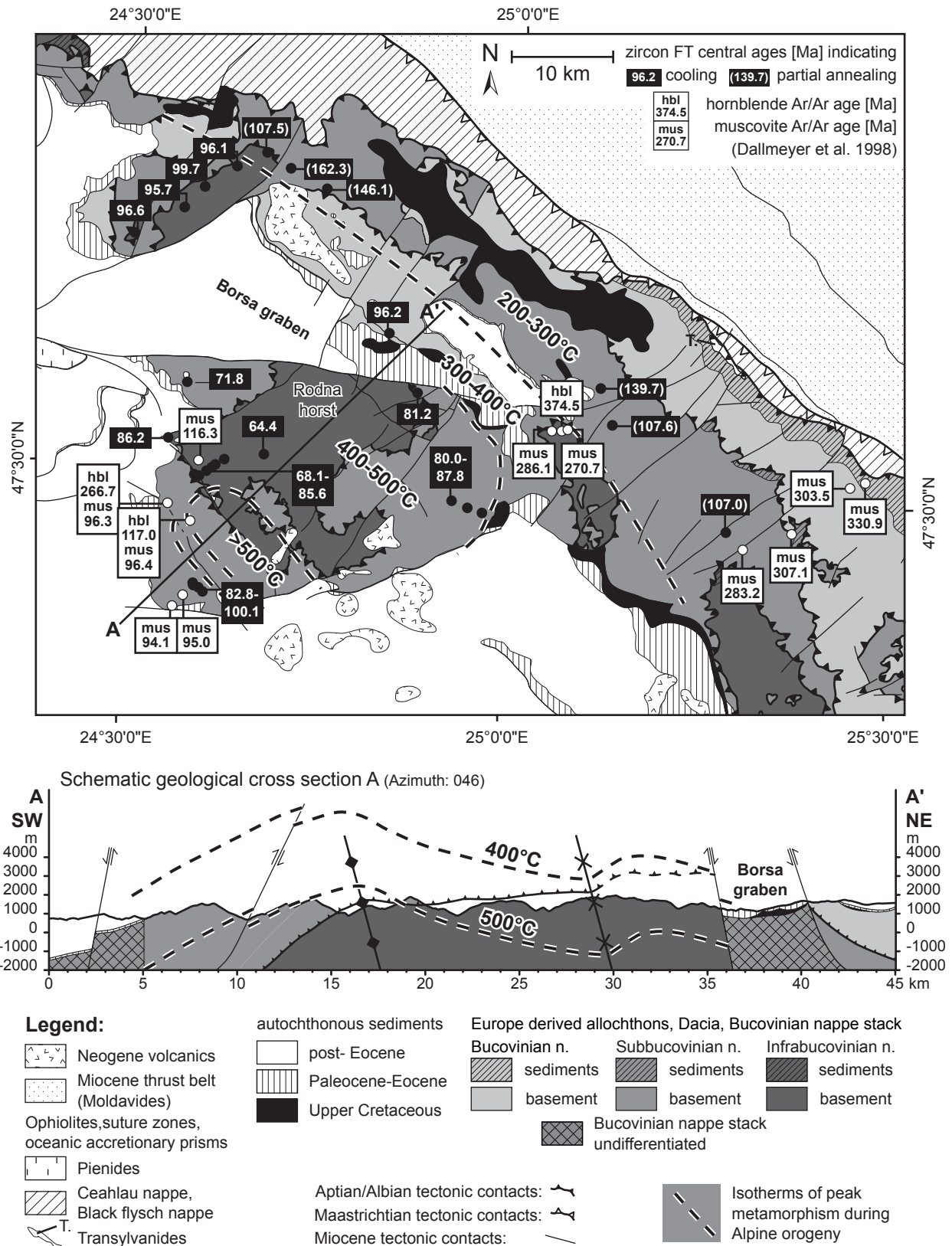


**Fig. 2.8.** Zircon fission track data of this study combined with Ar/Ar-data of Dallmeyer et al. (1998). A SW-increasing temperature is suggested. While along the Central East Carpathians chain sub-greenschist facies conditions are indicated by partial annealing of zircon, Cretaceous hornblende Ar/Ar ages indicate epidote-amphibolite facies in the SW corner of the Rodna horst.

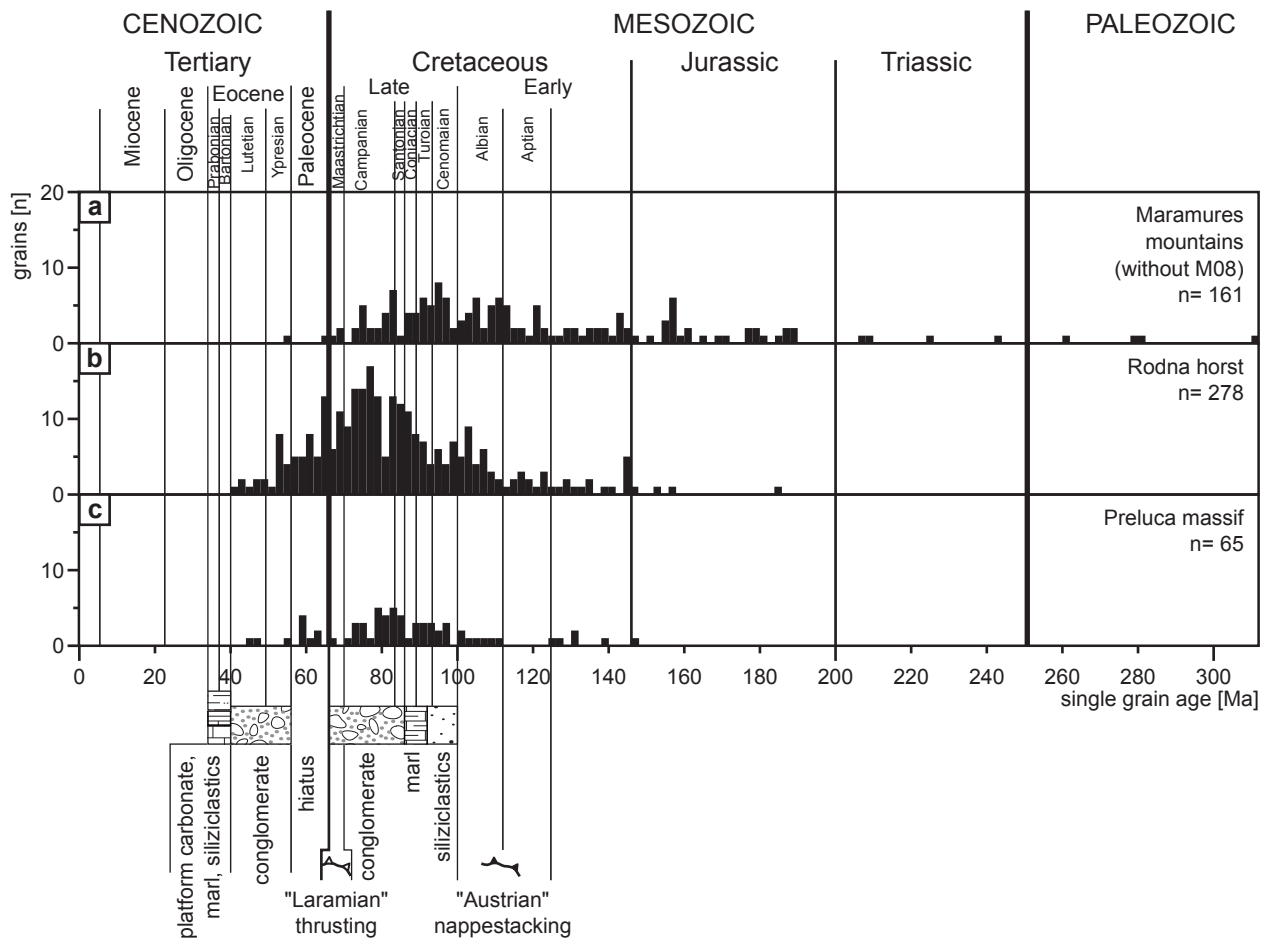


**Fig. 2.9.** Diagram comparing the observed zircon fission track single grain ages with tectonic events and the stratigraphic development. The single grain ages indicate partial annealing and Cenomanian cooling in the Central East Carpathian chain (Maramures mountains, a). Cooling and exhumation in the Rodna horst (b) and the Preluca massif (c) is contemporaneous with the deposition of Late Cretaceous conglomerates.

under the assumption that peak temperatures exceeded 400°C within most of the Rodna horst, as is suggested by the schematic cross section and the interpretation of the late Cretaceous exhumation history discussed below.

## 2.6 Interpretation and Discussion

### 2.6.1 Late Early Cretaceous nappe stacking ("Austrian" phase)

All of the analysed samples from the study area show at least partial annealing of fission tracks in zircon, followed by Late Cretaceous cooling and exhumation (Fig. 2.9). The most likely reason for this observation is burial by Alpine age nappe stacking since the degree of annealing and thus metamorphism depends on the position of the sample within the Alpine nappe stack.

This is especially clear in the more externally

located main Central East Carpathian chain, where samples in the tectonostratigraphically lowest units (Infrabucovinian nappes) show full annealing of zircon, while in the upper units (Subbucovinian/Bucovinian nappes) partial annealing is dominant. An increasing temperature from external to internal is most obvious in the Subbucovinian nappes, which display partial annealing along the external Central East Carpathian chain and full annealing in the internal Rodna horst. The even more internally situated Preluca massif (Biharia nappe system) shows also fully annealing of fission tracks in zircon (Fig. 2.9c).

This southwestward increase in temperature implies increasing tectonic overburden i.e. an increasing thickness of the overriding units in this same direction. This strongly indicates overall top NE-directed thrusting during Cretaceous nappe stacking. Top NE-thrusting contradicts the top E to ESE thrusting proposed by structural data



(Dallmeyer et al. in prep.). However, it nicely agrees with the NW-SE trending fold axes. An estimation using published geological maps (Krätner et al. 1989, Sandulescu et al. 1991) shows a decrease in thickness of the Subbucovinian nappe from at least 6.5 km in the southwestern part of the Rodna horst to about 1.5 km at the Vaser window (Fig. 2.2). The thermochronological data confirm greenschist up to epidote-amphibolite metamorphic conditions locally as suggested by other authors (Pană and Erdmer 1994, Balintoni et al. 1997, Dallmeyer et al. 1998).

### 2.6.2 Albian-early Cenomanian ? nappe folding and thrusting (Late "Austrian" phase)

In the late stage of nappe stacking the Bucovinian nappe pile is folded and juxtaposed against the external Black flysch and Ceahlau nappes. Post-collisional erosion is documented by (Upper) Cenomanian and Turonian conglomerates and sandstones, overstepping the folded nappe contacts (Ianovici and Dessila-Codarcea 1968). A possible onset of sedimentation in lower Cenomanian times is uncertain.

Juxtaposition of the Bucovinian nappe stack against the external Black flysch and Ceahlau nappes is contemporaneous to Cenomanian zircon FT central ages along the main Central East Carpathian chain and Cenomanian Ar/Ar muscovite ages (Dallmeyer et al. 1998) in the south-westernmost corner of the Rodna horst, documenting cooling below 400°C (Fig. 2.8). The Coniacian to Campanian zircon FT central ages from the Rodna horst and the Preluca massif indicate that this areas were still at temperatures above the ZPAZ (i.e. above 300°C)

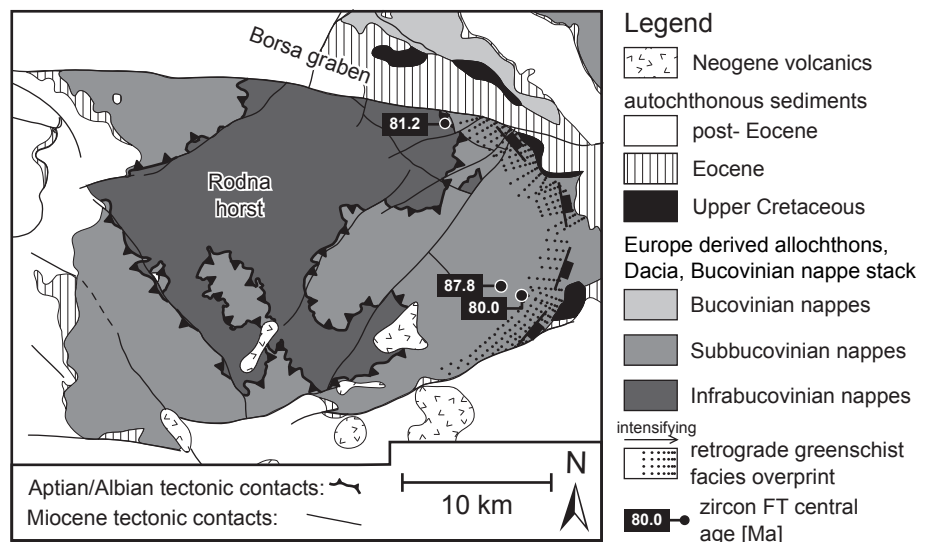
during Cenomanian times.

### 2.6.3 Late Cretaceous exhumation

The Coniacian to Campanian zircon FT central ages indicate upper Cretaceous cooling and exhumation in the Rodna horst and the Preluca massif. The close spatial neighbourhood of Coniacian to Campanian zircon FT central ages and Cenomanian sediments in the eastern part of the Rodna horst suggests fast exhumation, dominantly by extension and to a smaller extent by erosion (Fig. 2.10). However, the lack of clearly mapped structures which would document extension (major normal faulting) argues against such an interpretation at first sight. Yet a zone of greenschist facies retromorphism in the Subbucovinian basement was mapped, running parallel to the sedimentary contact (Krätner et al. 1978, 1983). This greenschist facies retromorphism possibly marks a low angle shear zone of late Cretaceous age, allowing for the exhumation of the basement units of the Rodna horst. A possible continuation of this feature into the Borsa graben could explain the deposition of syntectonic Santonian to Maastrichtian conglomerates (Szasz 1973; see Fig. 2.9).

The late Cretaceous sedimentation in the study area most likely indicates orogenic collapse (Willingshofer et al. 1999) analogous to the younger Gosau basins in the Eastern Alps (Neubauer et al. 1995) as already proposed by Dallmeyer et al. (1998). The syntectonic character of the upper Cretaceous sediments is suggested by their proximal facies (mostly conglomerates and sandstones, Sandulescu et al. 1981) and their discordant succession (Krätner et al. 1978; Krätner et al. 1983; Sandulescu et al. 1991). In spite of these indications Late Cretaceous

**Fig. 2.10.** The occurrence of zircon FT central ages (Coniacian to Campanian) younger than neighbouring upper Cenomanian sediments indicates tectonically controlled exhumation. A retrograde greenschist facies metamorphic overprint parallel to the sedimentary contact (Krätner et al. 1978, 1983) may serve as a normal fault, although it is not mapped as a shear zone.



extensional structures are not yet documented in the study area.

#### 2.6.4 Latest Cretaceous thrusting (“Laramian” phase) and Paleocene exhumation

During the “Laramian” phase the Ceahlau and Blackflysh units were thrust onto the most internal nappes of the Moldavides, carrying the Mid-Cretaceous nappe stack along “piggy-back” fashion. This stage of thrusting is accompanied by erosion and exhumation in the more external part of the study area, expressed in a depositional hiatus during the Paleocene (Fig. 2.3). In the SW of the study area at the Preluca massif sandstones and conglomerates are deposited during the Paleocene.

#### 2.6.5 Eocene burial to second exhumation during Miocene

Renewed burial starts in the Eocene by the sedimentation of conglomerates, followed by marls and platform carbonates. Burial continued in Oligocene times with flysch sedimentation, starting with fine grained siliciclastics and coarsening into sand dominated flysch units. Related burial metamorphism, however, did not reach temperatures to even allow for partial annealing of zircon fission tracks, as is indicated by the complete lack of zircon FT single grain ages younger than Eocene (Fig. 2.9).

During Miocene brittle tectonics the sampled basement units of the Preluca massif (Biharia nappe system) and the Rodna horst and Maramures mountains (Bucovinian nappe stack) are exhumed again by some 4.0 km and 5.0-7.0 km respectively (Gröger et al. 2008). Thus Miocene differential exhumation between the Central East Carpathian chain and the Rodna horst can be estimated to not exceed 2 km. While Miocene exhumation dominates the present day geometry in map view, it did not cause sufficient differential exhumation in order to explain the differences in amount of exhumation between the main East Carpathian chain and the Rodna horst at the beginning of the Early Cretaceous.

## 2.7 Conclusions

Alpine age metamorphism is documented for the Central East Carpathians and is interpreted to have resulted from Alpine (“Austrian”) top to the NE directed nappe stacking. While this Alpine metamorphic overprint only reached sub-

greenschist facies in the main chain of the Central East Carpathians, temperatures of up to at least 500°C are documented in the more internal Rodna horst and the Preluca massif. This temperature gradient is interpreted to have resulted from increasing tectonic overburden (up to at least 20 km) towards more internal units. Probably this overburden was also partly provided by the Transylvanian nappe stack and/or even higher tectonic units of unknown origin. Late Cretaceous cooling and exhumation is well constrained by zircon fission track data. It commences earlier in the more external Central East Carpathians (Cenomanian) than in the Rodna horst and the Preluca massif (Coniacian to Campanian). Cenomanian exhumation is interpreted as a result of late-stage shortening related to Austrian nappe folding.

At the beginning of the Late Cretaceous differential exhumation by around 10 km is required between the Rodna horst (>300°C) and the externally located Central East Carpathian chain. The close neighbourhood of Coniacian to Campanian zircon FT cooling ages to Cenomanian sediments suggests tectonic exhumation. Latest Cretaceous (“Laramian”) juxtaposition of the whole nappe pile against the internal Moldavides caused exhumation by erosion, indicated by an extensive Paleocene hiatus in sedimentation. However, the “piggy-back”-style transport of the nappe pile does not allow for tectonically induced differential exhumation. Differential exhumation during final Miocene emplacement only amounts to 2 km between the internal Rodna horst and the external Central East Carpathian chain.

Therefore the close neighbourhood of Coniacian to Campanian zircon FT cooling ages to Cenomanian sediments suggest a phase of Late Cretaceous tectonic exhumation so far not supported by structural data. Additional work is required to evaluate the role of Late Cretaceous extensional tectonics in the study area. Extensional tectonics related to orogenic collapse (Gosau type basins) is the most likely process, which allows for extensional tectonics.

## 2.8 Acknowledgements

We are most grateful for the excellent introduction into the study area and its geology provided by M. Săndulescu and L. Matenco and their ongoing support. Fruitful discussions with I. Balintoni, D. Radu, and C. Strutinski are also highly appreciated. F. Neubauer is gratefully

acknowledged for discussion of yet unpublished Ar/Ar data from the study area, which significantly improved the interpretation of our results. Financial support by the Swiss National Science foundation (NF-project Nr. 21-64979.01, granted to B.F) is gratefully acknowledged.



# Chapter 3:

## Miocene tectonics of the Maramures area (Northern Romania): implications for the Mid-Hungarian fault zone

M. TISCHLER<sup>1</sup>, H.R. GRÖGER<sup>1</sup>, B. FÜGENSCHUH<sup>2</sup>, S.M. SCHMID<sup>1</sup>

<sup>1</sup>*Geologisch-Paläontologisches Institut, Universität Basel, Bernoullistrasse 32, 4056 Basel, Switzerland  
(e-mail corresponding author: M.Tischler@unibas.ch)*

<sup>2</sup>*Institut für Geologie und Paläontologie, Universität Innsbruck, Innrain 52, Bruno Sander Haus, 6020  
Innsbruck, Austria*

**(International Journal of Earth Sciences: 2006)**

### 3.1 Abstract

The interplay between the emplacement of crustal blocks (e.g. "ALCAPA", "Tisza", "Dacia") and subduction retreat is a key issue for understanding the Miocene tectonic history of the Carpathians. Coeval thrusting and basin formation is linked by transfer zones, such as the Mid-Hungarian fault zone, which separates ALCAPA from Tisza-Dacia. The presented study provides new kinematic data from this transfer zone.

Early Burdigalian (20.5 to ~18.5 Ma) SE-directed thrusting of the easternmost tip of ALCAPA (Pienides), over Tisza-Dacia is linked to movements along the Mid-Hungarian fault zone and the Periadriatic line, accommodating the lateral extrusion of ALCAPA. Minor Late Burdigalian (~18.5 to 16 Ma) NE-SW extension is interpreted as related to back-arc extension.

Post Burdigalian (post-16 Ma) NE-SW shortening and NW-SE extension correlate with "soft collision" of Tisza-Dacia with the European foreland coupled with southward migration of active subduction. During this stage the Bogdan-Voda and Dragos-Voda faults were kinematically linked to the Mid-Hungarian fault zone. Sinistral transpression (16 to 12 Ma) at the Bogdan-Voda fault was followed by sinistral transtension (12 to 10 Ma) along the coupled Bogdan- Dragos-Voda fault system. During the transtensional stage left-lateral offset was reduced eastwards by SW trending normal faults, the fault system finally terminating in an extensional horse-tail splay.

**Keywords:** Kinematic analysis, Eastern Carpathians, Mid-Hungarian fault zone, Pienides, Miocene tectonics

### 3.2 Introduction

Miocene tectonics in the Carpathian region is characterised by the formation of an arcuate fold-and-thrust-belt and contemporaneous back arc extension in the Pannonian basin (e.g. Royden 1988). The European margin features a large-scale right between the Moesian and Bohemian promontories (Fig. 3.1). According to most authors (e.g. Balla 1982; Mason et al. 1998) this Carpathian "embayment" was at least partly floored by oceanic crust. Slab retreat (e.g. Royden 1988; Wortel and Spakman 2000; Sperner et al. 2005) created the necessary space that allowed for the invasion of large continental blocks (Alcapa, Tisza and Dacia; Balla 1987) and smaller displaced terranes (Fig. 3.1).

Invasion of the ALCAPA block lasted from the Late Oligocene to the Middle Miocene (Fodor et al. 1999), but initiated earlier in case of the Tisza and Dacia blocks (Fügenschuh and Schmid 2005). Emplacement was accompanied by substantial strike-slip movements, together with extension, shortening and rotations of rigid blocks (Ratschbacher et al. 1993; Fodor et al. 1999; Márton 2000; Márton and Fodor 2003; Csontos and Vörös 2004; Horváth et al. 2005). The major displaced units are, from NW to SE (Fig. 3.1):

1) Apulia-derived allochthons, such as the Austroalpine nappes of the Eastern Alps that extend into the Central and Inner West-Carpathians (ALCAPA, e.g. Plasienska et al. 1997a, b).

2) A small stripe of units situated within the intensely deformed belt of the Mid-Hungarian fault zone (Fig. 3.1), whose Upper Paleozoic and Mesozoic cover (outcropping in the Bükk Mountains) has a marked affinity to the internal Dinarides (Kovács et al. 2000; Haas et al. 2000). These Dinaridic units also contain remnants of obducted ophiolites and oceanic accretionary prisms.

3) The Tisza block, located SE of the Mid-Hungarian fault zone and largely covered by the Neogene fill of the Pannonian basin, crops out in the North Apuseni mountains, as well as in a series of Hungarian and Croatian inselbergs. The paleogeographic position of the Tisza unit is much debated (e.g. Burchfiel 1980; Săndulescu 1984, 1994; Csontos et al. 1992; Balintoni 1995; Fodor et al. 1999; Haas and Pero 2004). Its Mesozoic cover with European as well as Apulian affinities suggests that it broke off Europe along an eastern extension of the Piedmont-Liguria basin in Mid-Jurassic times (Haas and Pero 2004; Stampfli and Borel 2004).

4) The Dacia block is a Europe-derived allochthon (or "Rhodopian" allochthon, Burchfiel 1980; Schmid et al. 1998; Fügenschuh and Schmid 2005), comprising the Balkan mountains, the Getides of the Southern Carpathians, as well as the Eastern Carpathian Bucovinian nappe system (Median Dacides of Săndulescu 1981, 1994). Some authors consider Tisza and Dacia as representing one single block (e.g. "Tisza-Dacia terrane" of Csontos and Vörös 2004) since the Late Cretaceous, but it is not yet sure as to how firmly Dacia remained attached to Tisza since the Mid-Cretaceous orogeny.

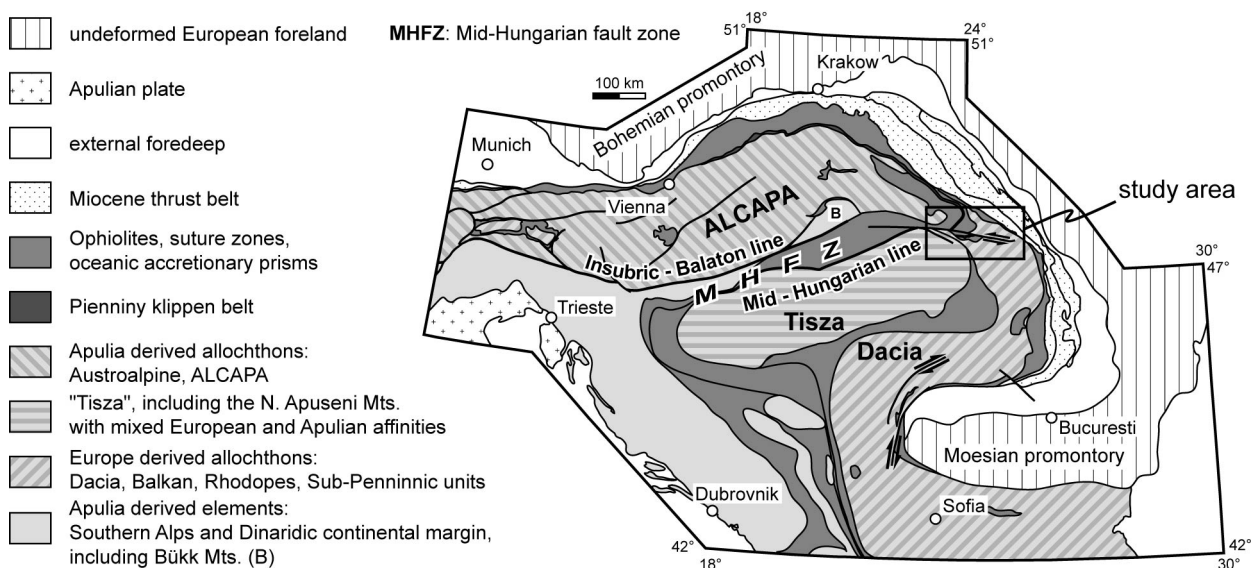


Fig. 3.1. Major tectonic units of the Alps, Carpathians and Dinarides, simplified after an unpublished compilation by S. Schmid, B. Fügenschuh K., Ustaszewski, L. Mañenco, R. Schuster and M. Tischler.

The development of the Carpathian orogen is also highly influenced by tectonic events within the Alps (Schmid et al. 2004a, b) and the Dinarides (Pamić 2000, Dimitrijević 2001). Particularly the onset of “lateral extrusion”, a mechanism defined by Ratschbacher et al. (1991a, b) in the Eastern Alps, is of major importance: Indentation by the South Alpine block, coupled to retreat of the descending European lithosphere (Royden 1988; Wortel and Spakman 2000), led to the ENE-ward translation of the ALCAPA block along the Insubric-Balaton line.

However, since the emplacement of Tisza and Dacia is unrelated to indentation in the Alps, subduction retreat is considered to provide the principal driving force for the invasion of the various blocks into the Carpathian embayment (Royden 1988; Wortel and Spakman 2000; Sperner et al. 2005). Furthermore subduction and retreat of the European plate beneath the inner Carpathians led to the formation of a back-arc-type basin: the Pannonian basin (i.e. Horváth et al. 2005; Cloetingh et al. 2005). Net east-west extension in the Pannonian basin is realized by normal faulting connected via conjugate strike-slip dominated systems. These strike-slip systems are also kinematically linked to synchronous thrusting in the external Miocene thrust belt (Royden 1988).

Field-based studies in the West Carpathians shed light on the interplay between subduction retreat and “lateral extrusion” (e.g. Nemčok 1993; Ratschbacher et al. 1993; Sperner et al. 2002). These authors documented NE-ward displacement and counter-clockwise rotation of the ALCAPA block, guided by strike-slip zones oriented sub-parallel to the collision suture. NNE-SSW shortening and ESE-WNW extension were the dominant modes of deformation during late Oligocene to mid-Miocene NE-ward movement of ALCAPA. After soft collision of ALCAPA with the European margin in the Western Carpathians at around 13 Ma ago, active subduction continued only further to the southeast, inducing NW-SE extension in the area of the Western Carpathians (Sperner et al. 2002).

The Mid-Hungarian fault zone played a key role during the emplacement of the various blocks in the Carpathian embayment. This major NE-trending strike-slip zone is thought to accommodate differential movements between ALCAPA and Tisza-Dacia. (Fig. 3.1). It is bounded to the north by the Balaton line, the NE-wards continuation of the Periadriatic line (Fodor et al. 1998). The southern boundary of the Mid-Hungarian fault zone is termed Mid-Hungarian line, defined as “a major strike-slip

fault along which the ALCAPA and Tisza-Dacia units of different provenance were juxtaposed” by Csontos and Nagymarosy (1998). ALCAPA, Tisza and Dacia feature contrasting Triassic and Jurassic sedimentary facies and fossil assemblages (Csontos and Vörös 2004, and references therein). The first important activity within the Mid-Hungarian fault zone occurred during the Oligocene (or earlier) (Csontos et al. 1992; Csontos and Nagymarosy 1998; Fodor 1999). Thereby collision led to thrusting of the ALCAPA block over Tisza and Dacia in late Oligocene times (Csontos and Nagymarosy 1998).

Corner effects at the Bohemian (Sperner et al. 2002) and Moesian (Ratschbacher et al. 1993; Schmid et al. 1998) promontories, respectively, led to opposed rotations well established by paleomagnetic studies (e.g. Márton and Fodor 1995, 2003; Márton 2000). While the timing of the emplacement of the ALCAPA block is fairly well constrained to have occurred between late Oligocene and middle Miocene times (Fodor 1999, Sperner et al. 2002), emplacement of the Dacia (and Tisza?) block commenced earlier (during the Eocene according to Fügenschuh and Schmid 2005), and ended later (in post-middle Miocene times, e.g. Mařenco et al. 2003). During mid - to late Miocene times (i.e. after 16 Ma) strike-slip deformation and extension dominated within the Mid-Hungarian fault zone, allowing for ongoing differential movements of the ALCAPA and Tisza-Dacia blocks (Csontos and Nagymarosy 1998). During this late stage the Mid-Hungarian fault zone may also have served as a transfer zone between the foreland thrust belt and the back-arc extension domain. In conclusion, diverging movement vectors as well as large opposed rotations call for important and complex tectonic movements within the Mid-Hungarian fault zone all the way from Oligocene to Miocene times.

This study covers the outcropping parts of the Mid-Hungarian fault zone at its NE termination in northern Romania (Fig. 3.1). The thrust contact of the so-called “Pienides” (Săndulescu 1981), flysch nappes situated at the contact of the easternmost tip of ALCAPA with Tisza-Dacia, represents the early Miocene Mid-Hungarian line sensu Csontos and Nagymarosy (1998) and is exposed in the study area. The Bogdan-Voda and Dragos-Voda strike-slip faults, as well as the Preluca fault near the northeastern rim of the Tisza block (Fig. 3.2), are first order candidates for representing surface exposures of the Mid-Hungarian fault zone that were active during mid- to late Miocene times.

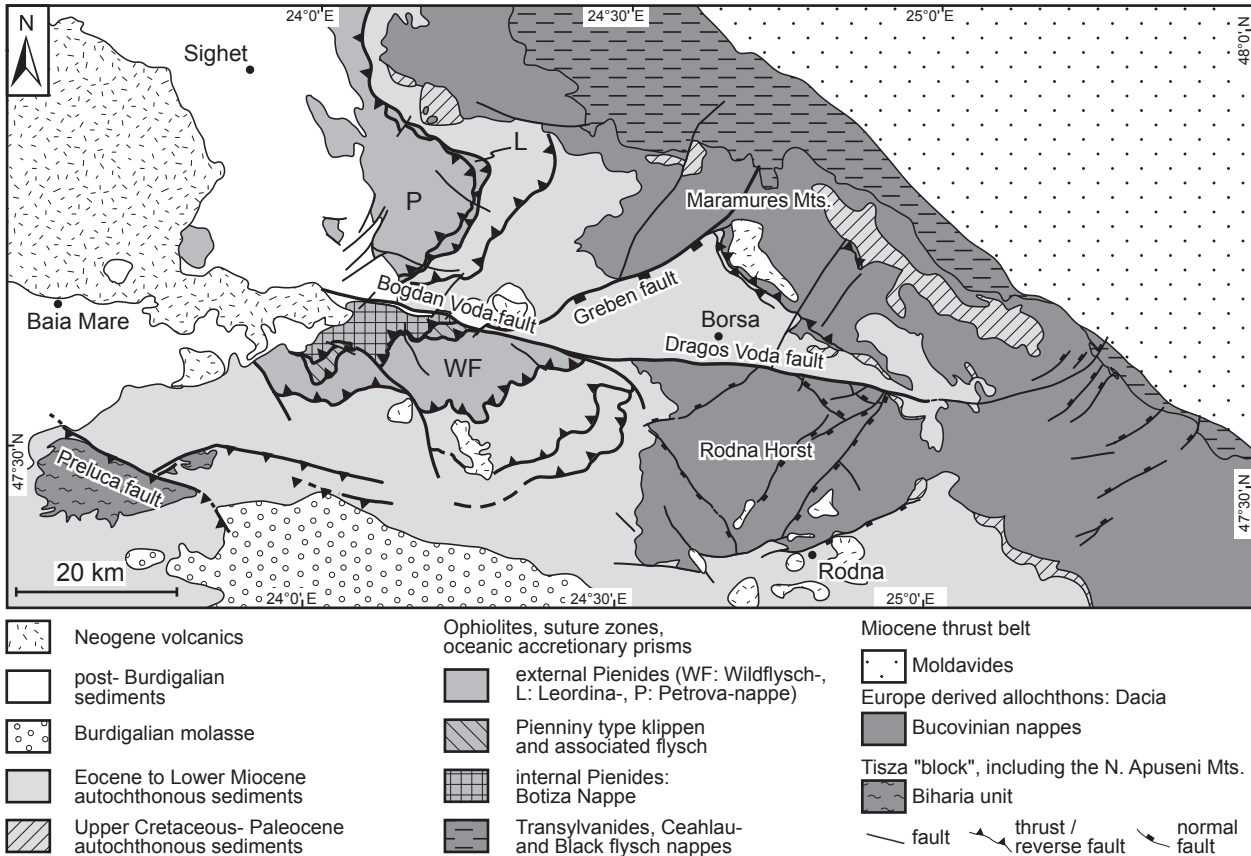


Fig. 3.2. Tectonic map of the study area based on published geological maps (1:50,000 and 1: 200,000) of the Geological Survey of Romania, Dicea et al. (1980), Săndulescu (1980), Săndulescu et al. (1981) and Aroldi (2001).

This study aims to provide further constraints on the timing and kinematics of movement along the Mid-Hungarian fault zone during back-arc extension and final emplacement of the ALCAPA, Tisza and Dacia blocks. With the aid of published and unpublished (Săndulescu pers. com.) maps of the Geological Survey of Romania, our field-work focussed on the analysis of kinematic data and was assisted by apatite fission track analyses. Stratigraphic ages are after Gradstein et al. (2004), Mediterranean and Parathetys stages are correlated according to Steiniger and Wessely (2000).

### 3.3 Geological Setting

The study area, located in the internal East Carpathians (Northern Romania) near the transition to the Western Carpathians (Fig. 3.1), comprises the northeastern tip of the Tisza block (Biharia unit) and the northernmost part of Dacia (Bucovinian nappes). Alpine-age deformation within the Bucovinian nappes and the Biharia unit started in mid-Cretaceous times ("Austrian" phase) and continued until Late Cretaceous times ("Laramide" phase, Săndulescu 1981, 1994). Upper

Cretaceous to Paleocene sediments unconformably cover these mid- and late Cretaceous tectonic contacts, as well as contacts between Tisza, Dacia and intervening oceanic remnants (Fig. 3.1). Eocene to Burdigalian strata were deposited above a second unconformity. This mainly Tertiary cover is referred to as "autochthonous cover of Tisza-Dacia" in the following. During final closure of the Carpathian embayment the Bucovinian nappes were emplaced onto Cretaceous to Miocene flysch deposits now forming the Miocene fold-and-thrust-belt of the East Carpathians.

Tisza and Dacia, together with their autochthonous cover, were overthrust by the Pienides during Burdigalian times (Săndulescu 1981). According to Săndulescu et al. (1993) the Pienides, situated at the easternmost tip of ALCAPA, comprise an external (Petrova, Leordina and Wildflysch nappes) and an internal thrust sheet (Botiza nappe). Internal and external Pienides, mainly consisting of Eocene to Oligocene non-metamorphic flysch units, can be correlated with the Ivancovce-Krichevo units and the Magura flysch of the Western Carpathians, respectively (Săndulescu 1981, 1994). Furthermore the internal Pienides



feature frontal imbricates containing phacoids of Pieniny Klippen type material embedded in Eocene flysch (Săndulescu et al. 1993). Note that these units and their equivalents form the innermost part of the Outer West Carpathians (Plasienska 1997 a, b), while they take a more internal position in our working area.

The post-Burdigalian infill of the Pannonian- and Transylvanian basins in the working area starts with the deposition of the Mid-Miocene (Badenian) Dej tuff during a period of mainly acidic volcanism (Mason et al. 1998). Subduction-related calc-alkaline magmatism (Mason et al. 1998) started during middle Miocene times in the working area (13.5 Ma, Pécskay et al. 1995). Magmatic activity led to the formation of a linear chain along the inner side of the East Carpathians decreasing in age from 12 Ma in the NW to 0.2 Ma in the SE.

From a tectonic point of view the most obvious structure is the E-striking, predominantly left-lateral, Bogdan- Dragos-Voda fault system. The Bogdan-Voda fault to the west offsets the autochthonous cover of Tisza-Dacia, as well as the nappe pile of the Pienides, and is sealed by mid-Miocene volcanics. The Dragos-Voda fault to the east delimits a horst-like crystalline body ("Rodna horst", Fig. 3.2), built up by the Bucovinian nappe stack, towards the north. Possible linkage of and mutual relationships between these two fault segments have been a point of discussion in the Romanian literature. While Săndulescu (1981) interpreted the two faults as separate, Dicea et al. (1980) mapped a single continuous fault. Other authors (e.g. Huismanns et al. 1997, Györfi et al. 1999) mapped one single fault termed "Dragos-Voda fault".

## 3.4 Methods

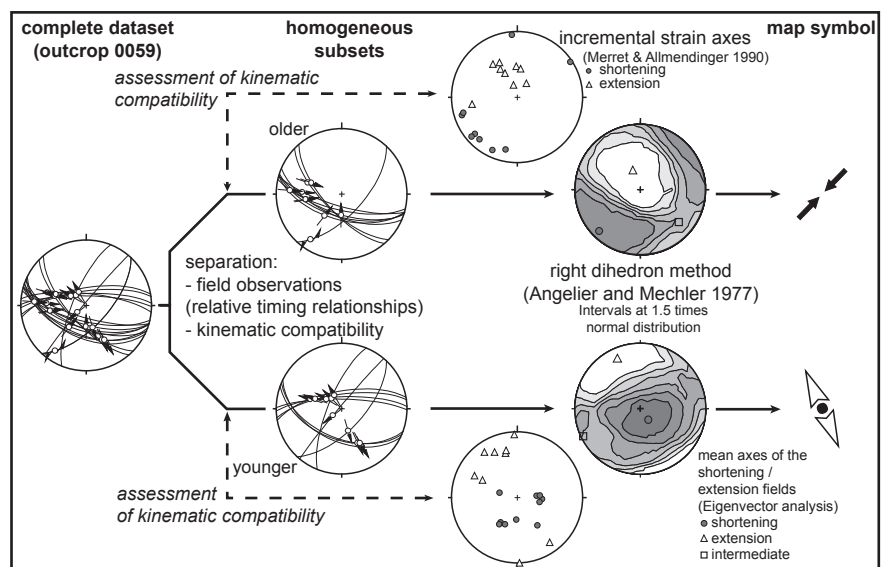
### 3.4.1 Derivation of kinematic axes

Kinematic axes (principal shortening and extension directions) were derived from meso-scale structures in order to analyse the regional tectonic history. For this purpose, fault-slip sets (orientation of fault plane, sense and direction of movement) were analysed. Fieldwork focussed on correlation of the kinematic data with large-scale structures.

The direction of movement being given by a lineation (mechanical striation or slicko-fibre orientation), the sense of movement was determined by criteria such as slicko-fibre growth direction, orientation of Riedel shears or offset of marker horizons. Inhomogeneous fault set data were separated into homogenous subsets based on field observations, and their kinematic compatibility was assessed by plotting their incremental strain axes (Fig. 3.3, Marret and Allmendinger 1990).

Kinematic axes were computed with the right dihedron method described by Angelier and Mechler (1977). Applicable to newly formed, as well as to reactivated pre-existing fractures, this simple graphical method reflects the bulk finite strain state (Pfiffner and Burkhard 1987). Eigenvectors and Eigenvalues (Bingham 1964) have been used to determine mean axes of shortening and extension (Fig. 3.3). A tabular overview on the analysed stations is found in Appendix 3.1. For calculation of kinematic axes and visualisation of fault sets we used the software TectonicsFP (Franz Reiter and Peter Acs © 1996-2000: <http://go.to/TectonicsFP>; based on TectonicVB by Hugo Ortner).

*Fig. 3.3. Flow chart for the analysis of fault-slip data. For the separation of homogenous subsets field observations as well as kinematic compatibility have been used. Kinematic compatibility has been assessed using plots of the fault sets and incremental strain axes (Marret and Almendinger 1990). For map display mean axes of shortening and extension are used. Intersection relationships in the analysed outcrop show, that transpression was followed by transtension during the post Burdigalian stages.*



### 3.4.2 Fission Track Analysis

Apatite mineral concentrates were prepared by conventional crushing, sieving, magnetic and heavy liquid separation. The grains were mounted in epoxy resin, polished and etched for 40 sec at room temperature in 6.5 % HNO<sub>3</sub>. Samples were analysed using the external detector method (Gleadow 1981), with muscovite as an external detector. Irradiation was carried out at the High

Flux Australian Reactor (HIFAR) with neutron fluxes monitored in CN5. Muscovite was etched 40 min at room temperature in 40% HF.

Fission tracks were counted on a computer-controlled Zeiss microscope at magnifications of X1250 (dry). Ages were calculated using the zeta-calibration method (Hurford and Green 1983) with a zeta-value of  $355.96 \pm 9.39$  (CN5, Durango). For data processing the windows software TRACKKEY (Dunkl 2002) was used. All ages are central ages (Galbraith and Laslett 1993), with errors quoted as

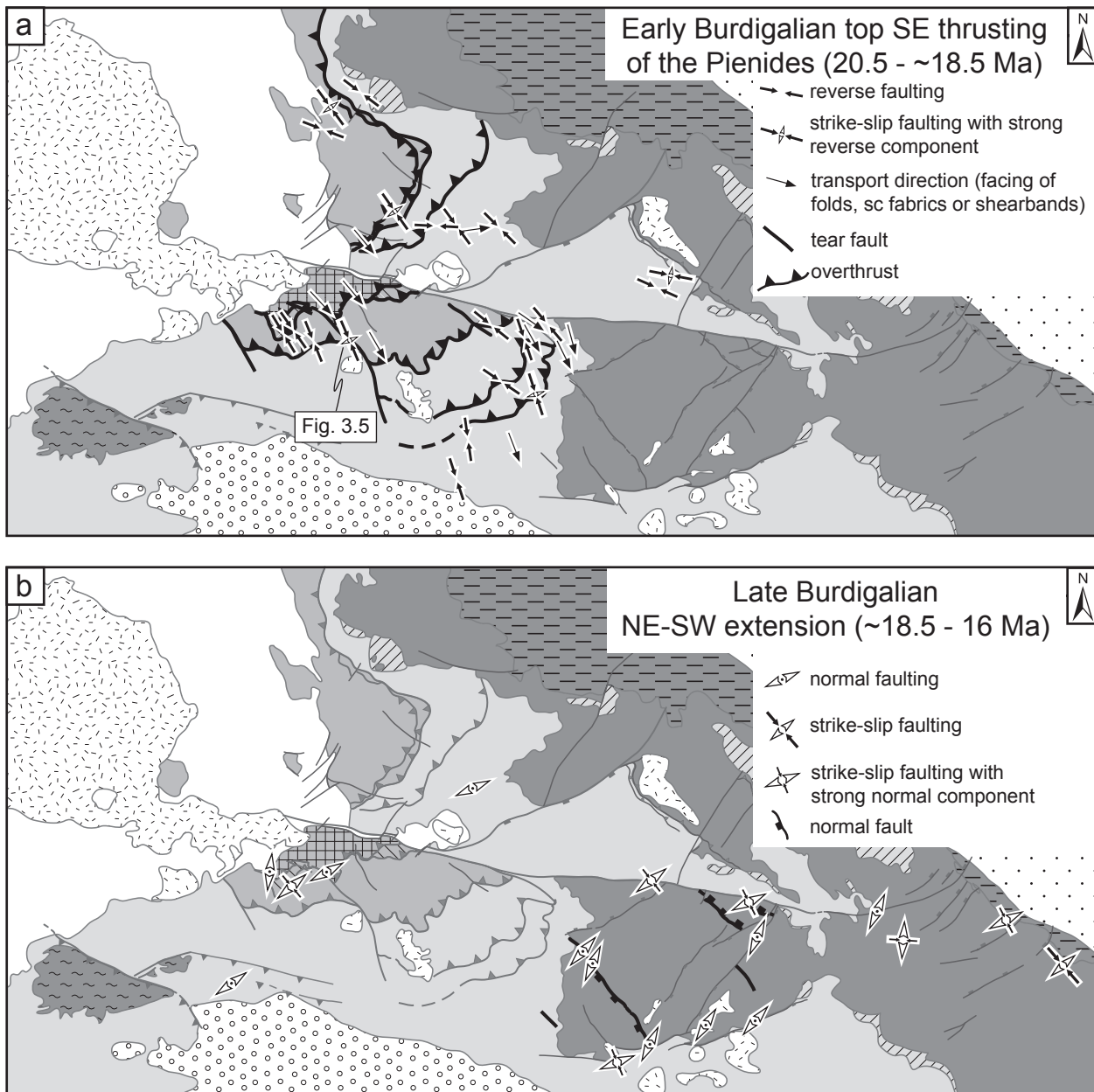


**Fig. 3.4.** Kinematics and structures related to the Burdigalian deformation phases. *a:* Early Burdigalian emplacement of the Pienides shows consistent top-SE thrusting. The pronounced bends in the nappe front are interpreted as a result of a change in thrust geometry featuring frontal and lateral ramps as well as tear faults (see text). *b:* Subordinate NE-SW extension, related to SE-striking normal faults of Late Burdigalian age.

1 $\sigma$ . Closure temperatures for apatite are  $90 \pm 30^\circ \text{C}$ , the uncertainty being given by the lower and upper limits of the apatite fission track partial annealing zone (Gleadow and Duddy 1981, Gallagher et al. 1998).

### 3.5 Structural analysis

#### 3.5.1 Early Burdigalian top-SE thrusting of the Pienides

The emplacement of the Pienides during Burdigalian times (Fig. 3.2) also led to the imbrication of the autochthonous cover of Tisza-Dacia. Deformation related to the emplacement of the Pienides is primarily controlled by the more incompetent silty-marly flysch units, which are serving as detachment horizons. The more massive sandy layers, however, only display moderate brittle deformation, even close to nappe contacts. Cataclastic shear zones related to nappe emplacement are the predominant deformation features, while folding is only locally developed. Within marly layers shear-bands and/or SC-type fabrics can locally be observed. The shortening direction related to the emplacement of the Pienides was evaluated by kinematic analysis of mesoscale faulting found near major cataclastic shear zones. Transport direction was inferred from the facing direction of outcrop-scale folds and/or SC-type fabrics and shear-bands.

The deduced kinematic directions (Fig. 3.4a) reveal a consistent displacement direction towards the SE (Appendix 3.2), both for the Pienides as well as for the imbricates of the autochthonous cover of Tisza-Dacia. The relative timing of fault sets found in two outcrops (Appendix 3.2, stations 0639, 0584) suggests a possible minor change in transport direction from top-SE towards top-ESE.

The frontal thrust of the Pienides has an extremely variable trace in map view (Fig. 3.4a), showing alternating SW- and SE-striking segments. Outcrops along the northernmost SE-striking thrust segment (Fig. 3.4a) expose SSE-striking strike-slip fault zones with a significant reverse component. The predominantly transpressional deformation encountered along this segment (see Appendix 3.2; station 0639), suggests a lateral ramp geometry. The thrust front of the Pienides south of the Bogdan-Voda fault shows three major sharp bends in map view (Fig. 3.4a). At one of the bends a steeply dipping dextral strike-slip fault zone, sub-parallel to the transport direction (Fig. 3.5), is interpreted as

a tear fault. The increase of shortening within the autochthonous cover of Tisza-Dacia, observed in front of the Pienides towards the northeast, is a map-scale argument in favour of this interpretation.

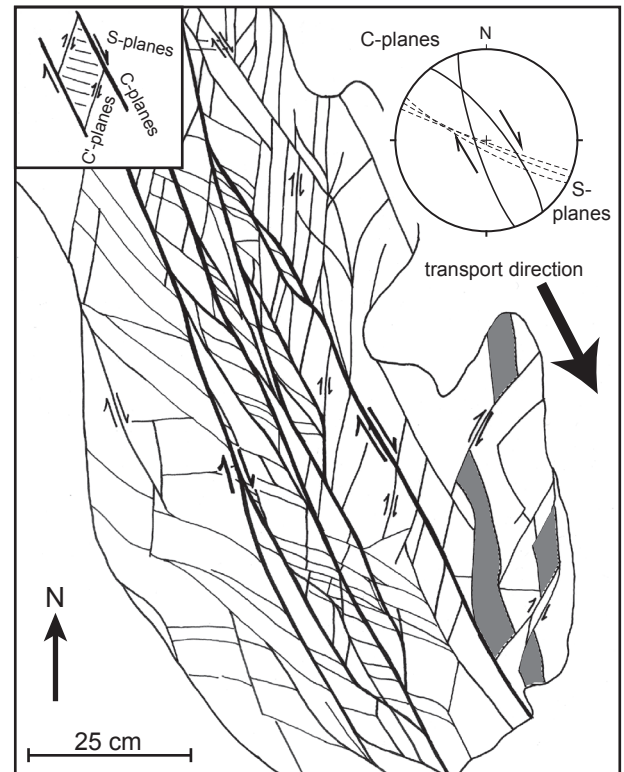


**Fig. 3.5.** Outcrop sketch (map view) of a cataclastically deformed fault zone at the NW-SE striking nappe contact of the Pienides against the autochthonous cover of Tisza-Dacia (see Fig. 3.4a). The fine-grained siliciclastics (homogenous clay rich silts) are dissected by anastomosing shear zones featuring shear band geometries. Shaded areas indicate offset of silty marker horizons. The strike-slip dominated kinematics confirm the interpretation of the NW-SE striking contacts as tear faults.

The timing of Pienide nappe emplacement and related structures is constrained by stratigraphic arguments. The youngest thrust strata are Aquitanian in age (Dicea 1980), and thrust contacts are sealed by Badenian-age (16- ~13 Ma) sediments. Hence, an intra-Burdigalian activity can be inferred. The fact, that structures related to Late Burdigalian extensional deformation (see below) overprint nappe emplacement features, allows us to suggest an Early Burdigalian (20.5~18.5 Ma) age for the emplacement of the Pienides.

### 3.5.2 Late Burdigalian NE-SW extension

While SE-trending normal faults are rarely observed in the sedimentary cover, they are more abundant within the basement units of the study area. The most prominent of these SE-striking faults are found within the SW part of the Rodna massif (Fig. 3.4b), where they offset Bucovinian-type basement as well as Oligocene strata. Kinematic analysis of these faults yielded NE-SW to NNE-SSW extension, i.e. normal faulting with a minor strike-slip component (Fig. 3.4b; Appendix 3.3).

Field evidence clearly suggests that these normal faults overprint structures related to the emplacement of the Pienides (e.g. Station 0236, Appendix 3.2, 3.3). Since structures of this phase are cut by the Dragos-Voda fault while Badenian (16 - ~13 Ma) strata are unaffected, we assume a pre-Badenian (18.5 - 16 Ma) age for this extensional deformation.

### 3.5.3 Post-Burdigalian structures

Emplacement of the Pienides was post-dated by extensive faulting. Strike-slip activity along the Bogdan-Dragos-Voda fault system can be subdivided into an earlier transpressional stage followed by transtension.

#### *Transpressional stage*

Open folds with SE- to ESE-striking fold axes (Fig. 3.6a) evidence post-Burdigalian shortening in the sedimentary units of the study area. Wavelengths of these folds range between outcrop-scale up to several hundreds of meters. While fold limbs are only weakly inclined north of the Bogdan-Voda fault, they reach dip angles of up to 50° in the south. These SE- to ESE-striking folds overprint earlier nappe emplacement structures (Fig. 3.7). Approaching the fault trace of the Bogdan-Voda fault, this late-stage folding locally intensifies, which leads to isoclinal folding around steeply inclined fold axes.

Faulting with a strong reverse component is found throughout the study area and is documented in map scale (Fig. 3.6a), as well as in outcrop scale (Appendix 3.4). The most dominant types of structures are SE-striking reverse faults (e.g. back-thrust E of Borsa; 0809, Appendix 3.4, and the Preluca fault; 0259, Appendix 3.4), as well as E-striking transpressional faults (e.g. the Bogdan-Voda fault; 0682 and 0675, Appendix 3.4). During this transpressional phase the Bogdan-Voda fault terminates at the Rodna horst in a thrust splay

geometry.

In summary, the kinematic analysis yields transpression with NE-SW and minor NW-SE extension.

#### *Transtensional stage*

E-trending strike slip faults (e.g. Bogdan-Dragos-Voda fault system) as well as SW-striking normal faults (e.g. Greben fault) can be attributed to the transtensional stage (Fig. 3.2). Deformation found along and associated with the Bogdan-Voda and Dragos-Voda faults is dominated by sinistral strike-slip faulting often featuring a normal component. Striations plunge about 5 to 15 degrees to the west along the Bogdan-Voda fault and up to 20 degrees along the Dragos-Voda fault (Appendix 3.5, 3.6). These strike-slip faults are commonly accompanied by sets of SW-striking normal faults (Appendix 3.5, 3.6).

The E-trending strike slip faults as well as SW-striking normal faults yield regionally consistent kinematic axes. The extensional axes are oriented sub-horizontally NW-SE. Shortening axes strike SW, with dip angles depending on the relative amount of the normal and strike-slip components respectively.

Near its eastern termination, the Bogdan-Dragos-Voda fault system splays into an array of SW-trending normal faults with a left-lateral component. These "horsetails", which accommodated only minor displacements, allowed for "distributed" sinistral offset. This is reflected by the lack of a map-scale discrete offset of major pre-existing tectonic boundaries, such as the front of the Bucovinian nappes (Fig. 3.2). Kinematic axes derived for these SW-NE trending normal faults are compatible with those derived for the Bogdan-Dragos-Voda fault system (Fig. 3.6b, Appendix 3.5). Sinistral transtension is further documented along the Preluca fault, where it overprints a preceding phase of top NE thrusting (Fig. 3.6b, Appendix 3.6).

### 3.5.4 Stratigraphical timing constraints regarding post-Burdigalian deformation

The formation containing the lower Badenian Dej tuff represents an ideal marker horizon in the northern part of the study area. Post-dating Burdigalian age deformation, it is affected by both the transpressive and transtensive stages along the Bogdan Voda and the Dragos-Voda fault and hence provides a lower time bracket of 16 Ma (i.e. onset of

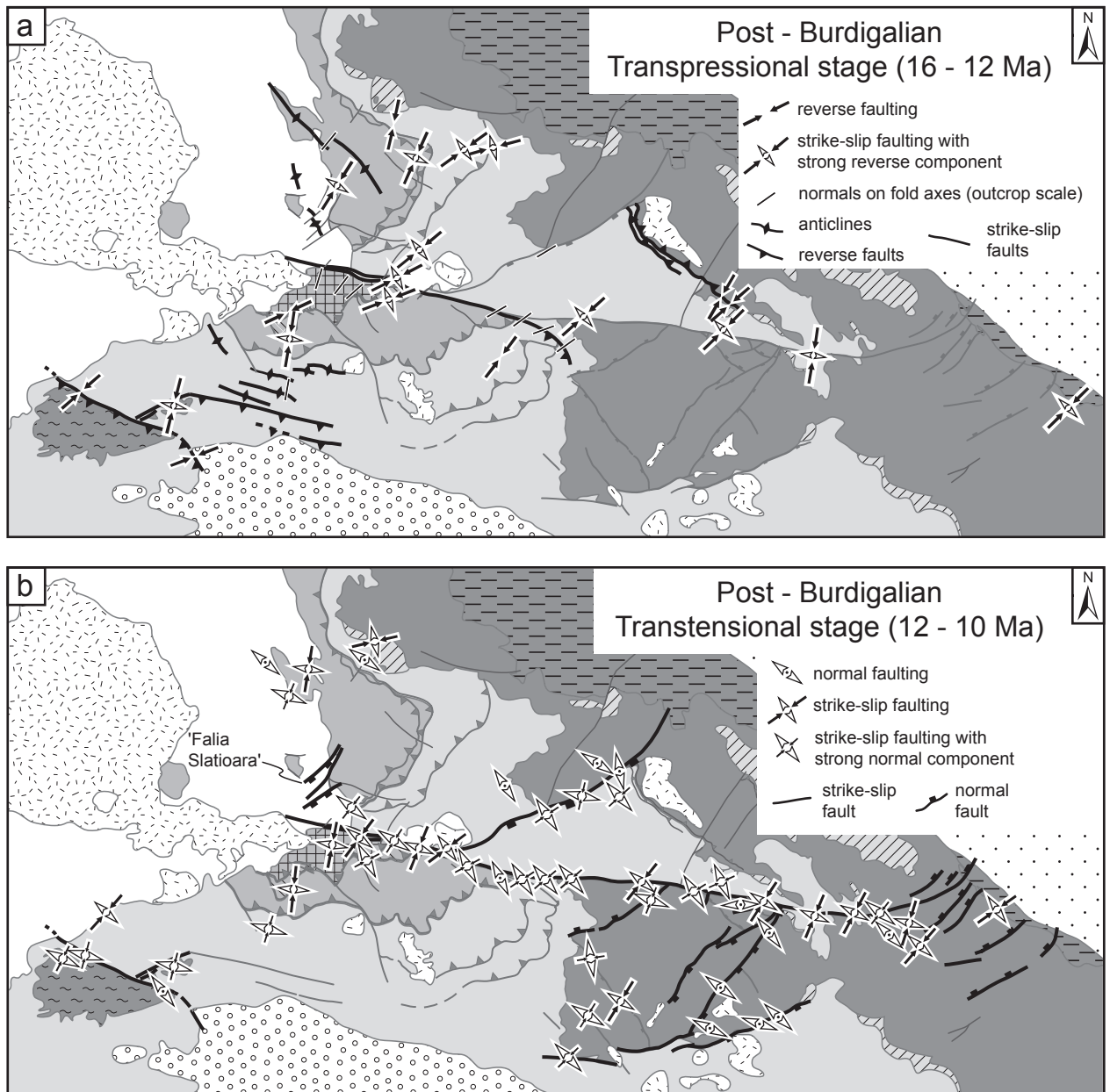


**Fig. 3.6.** Kinematics and structures related to the post-Burdigalian (16 to 10 Ma) activity of the Bogdan- and Dragos-Voda faults. Transpression (a) precedes transtension (b). Shortening is SW-NE during both phases. Note the linked Bogdan-Voda and Dragos-Voda fault activity during the transtensional stage.

the Badenian). The Preluca fault also shows post 16 Ma activity, indicated by Burdigalian strata affected by NE-SW shortening (Appendix 3.4, Station 0260).

The upper time bracket of post-Burdigalian deformation is well defined by the Neogene volcanic body near Baia Mare (Fig. 3.2). The 10 Ma old volcanics constituting the main body (Pécskay et al. 1995) seal the Bogdan-Voda fault (Fig. 3.2).

Overprinting criteria observed at outcrop and map scales indicate that transpression was followed by transtension. For example the SE-striking back-

thrust east of Borsa is cut by the younger Greben normal fault (Fig. 3.6). The timing of the change from transpression to transtension is derived from Antonescu et al. (1981). These authors map SW-trending faults (e.g. "Falia Slatioara", Fig. 3.6b) which are cutting strata younger than ~12,2 Ma (Lower Bessarabian in Antonescu et al. 1981). Since the strike of the faults mapped by Antonescu et al. (1981) is compatible with normal faults related to the transtensional stage, we infer the onset of transtension to have commenced at around 12 Ma ago.

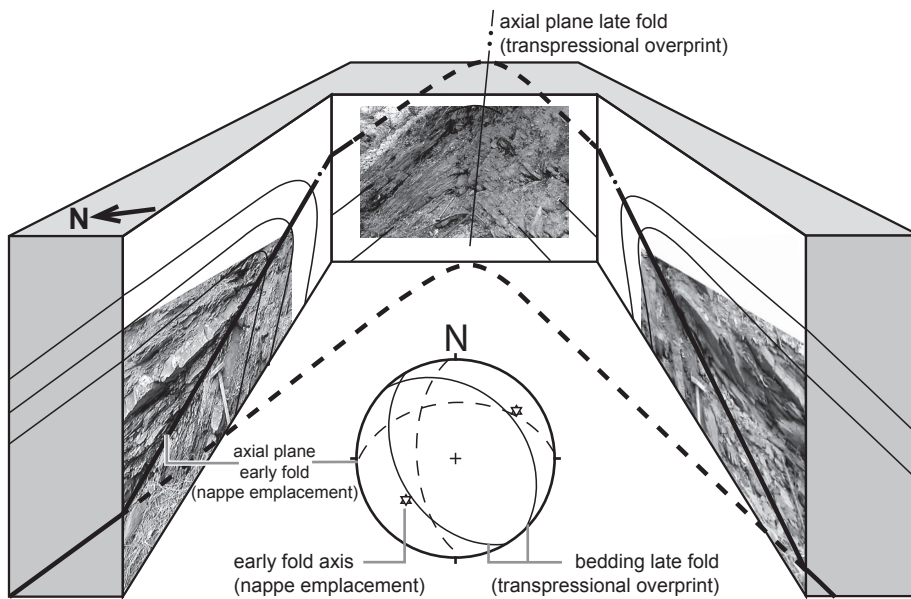


**Fig. 3.7.** Schematic block diagram of an outcrop showing the overprinting of nappe emplacement structures. The tight asymmetric folds developed during nappe emplacement (left and right) are refolded by an upright open fold with SE-trending fold axis. Such folds are related to the post Burdigalian transpressional stage and can be found throughout the study area.

### 3.6 Constraints from fission track data

Due to the lack of stratigraphical timing constraints along the Dragos-Voda fault, its activity was indirectly dated by inferences from the cooling history of the syn-kinematically exhumed Rodna horst (Fig. 3.8). A vertical profile covering about 1000 m of altitude difference has been sampled for apatite fission-track analysis (5 samples). The uppermost sample is taken close to the projected basal unconformity of the overlying Tertiary sediments. The presented samples have been selected from a larger set of data that is discussed in more detail in Gröger (2006).

Burial by Eocene to lower Miocene sediments led to total annealing of fission tracks in all samples, as evidenced by the fact that all samples passed the Chi-square test (Fig. 3.8c;  $\chi^2 > 5\%$ ). Subsequent cooling through the apatite fission-track annealing zone yielded middle to late Miocene cooling ages (11.6 to 8.6 Ma, Fig. 3.8), where the youngest ages are found at the lowest altitudes of the profile. The three uppermost samples span 710 m, but yield similar ages (11.6, 11.0 and 11.6 Ma). A significant decrease in age can only be observed in the two lowermost samples (10.2 and 8.6 Ma). The altitude vs. age relationship thus suggests enhanced exhumation between 12-11 Ma with exhumation rates of at least 1 mm/a. After 10 Ma the rate of exhumation decelerates to around 0.1 mm/a (Fig. 3.8b). Our data are in agreement with data by Sanders (1998), also depicted in Fig. 3.8a.

The enhanced cooling of the Rodna horst through the apatite partial annealing zone between

12-11 Ma is interpreted to be caused by fault-bounded exhumation in the footwall of the sinistral transtensive Dragos-Voda fault. This indirect dating of the transtensional stage based on apatite fission track analysis is consistent with stratigraphical timing constraints (12-10 Ma, see above) for transtension along the Bogdan-Voda fault. The concurrent time constraints, independently derived, support the conclusion that the Bogdan-Voda and Dragos-Voda faults acted as a single continuous fault during this second transtensional stage. Additionally, the apatite fission track data corroborate that the transtensional stage between 12-10 Ma represents the main phase of activity along the Dragos-Voda fault.

### 3.7 Synthesis of data

#### 3.7.1 Burdigalian thrusting of the Pienides followed by NE-SW extension

Analysis of the structures related to the Burdigalian-age emplacement of the Pienides consistently yielded top-SE transport (Fig. 3.4a). Thrusting of the Pienides and within the autochthonous cover of Tisza-Dacia was coeval, as indicated by stratigraphic timing criteria corroborated by our kinematic analyses. A change from top-SE to top-ESE transport, as suggested by two of the studied outcrops, could not be consistently documented for the study area.

At first sight, the constant displacement directions inferred for the thrusting of the Pienides

is in contradiction to the extremely variable trace of the frontal thrust in map view. The most likely explanation for the arcuate shape of the Pienide nappe contact is a laterally changing thrust plane geometry, with SW striking frontal ramps alternating with SE-striking tear faults and/or lateral ramps.

Although SE-striking normal faults, generated by a phase of SW-NE extension, are found throughout the study area, they are more abundant in the basement rocks of the Rodna horst (Fig. 3.4b) than in the Oligocene sediments. The age of this normal faulting is inferred as Late Burdigalian.

### 3.7.2 Post-Burdigalian faulting along the Bogdan- and Dragos-Voda faults

Our observations indicate a significant component of shortening during the earlier stage of left-lateral strike-slip movements along the Bogdan-Voda fault, which terminated towards the east along a SE striking thrust-splay, as mapped by Săndulescu (1994) and Dicea et al. (1980). Due to the scarcity of evidence for coeval transpressive deformation along the Dragos-Voda fault, we regard its role during this earlier stage of the post-Burdigalian deformation as subordinate. Hence, the

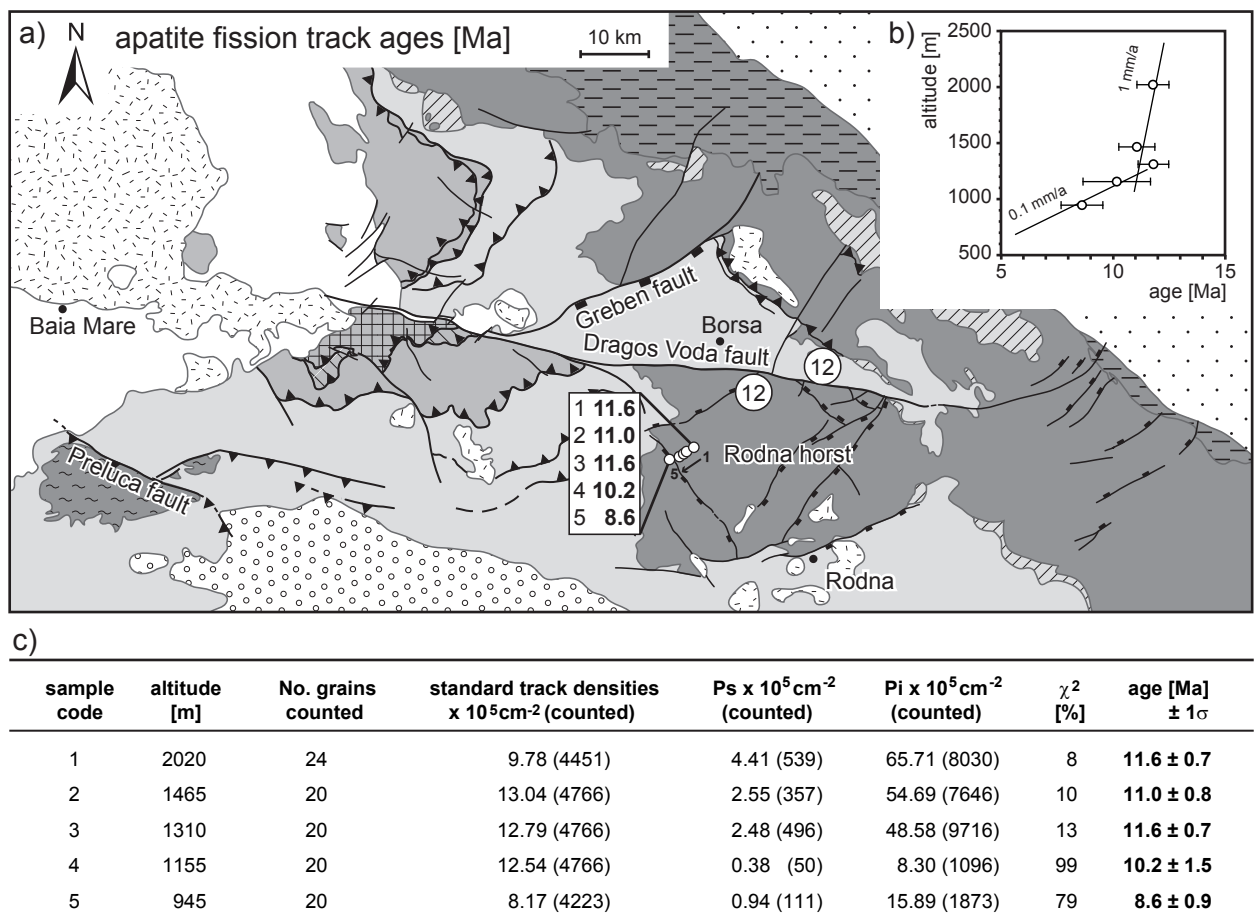


**Fig. 3.8.** Results of apatite fission track analyses. All samples were analysed using the external detector method (Gleadow 1981) and ages were calculated using the zeta-calibration method (Hurford and Green 1983) on the base of the Durango standard with a zeta value of  $355.96 \pm 9.39$ .

a: Tectonic map showing apatite fission track data. Samples labelled with circles are from Sanders (1998).

b: Altitude versus age diagram of the apatite fission track ages. The ages show relatively fast exhumation (at least 1mm/a) between 12-11 Ma followed by slow exhumation (around 0.1 mm/a) after 10 Ma.

c: Table regarding the apatite fission track data. Column 1 gives the sample code, column 2 the altitude above sea level, column 3 the number of dated grains. Columns 4, 5 and 6 show standard, spontaneous and induced track densities, respectively, and the number of counted tracks in brackets. Column 7 gives Chi-square probability (Galbraith 1981) and column 8 fission track central ages (Galbraith and Laslett 1993), which are the weighted mean of the single grain ages.

two fault segments were not yet linked, and much of the offset along the Bogdan-Voda fault was taken up by thrusting along its eastern termination. In the eastern part of the study area (near Borsa), a SE-trending back-thrust represents the major feature formed during this transpressive post-Burdigalian stage (Fig. 3.6a). The differences in deformational style between west and east may be due to earlier structures, particularly to the presence of a basement high in the area of the Rodna horst. This horst already existed during the Eocene. While the shallow marine Iza limestone formed on the Rodna horst, the pelagic sediments of the Vaser Formation were deposited north of it (Săndulescu et al. 1991, Krättner et al. 1982). During the subsequent sinistral-transtensive stage the Bogdan-Voda and Dragos-Voda faults were kinematically linked; they acted as a single Bogdan- Dragos-Voda fault system, as mapped by Dicea et al. (1980). This is confirmed by structural and kinematic data and is also very evident from map-view. Additionally, intensely faulted outcrops situated at the junction between the two segments yield similar kinematics (Appendix 3.5, 3.6, Stations 0462, 0481, 0079) further corroborate this interpretation.

Since the major SW-trending normal faults within the Rodna horst and in the Maramures Mountains (i.e. the Greben fault) are kinematically compatible with this sinistral-transtensive activity along the Bogdan- Dragos-Voda fault system, we regard their activity as contemporaneous. The transtension along the Bogdan- Dragos-Voda fault system led to final cooling and exhumation of the Rodna horst from 12 Ma onwards, as indicated by apatite fission track data. Towards the east, the net left-lateral offset along the Bogdan- Dragos-Voda fault system decreases due to the distribution of deformation into a horse-tail like array of SW-trending normal faults. At the contact of the inner East Carpathians with the Miocene thrust belt of the Moldavides the localised offset diminishes to almost zero. Transtension also affected the southeastern part of the study area, where the entire Rodna horst is affected and partly bounded by SW-striking normal faults (Fig. 3.6b, Appendix 3.6). Subordinate reactivation by transtension is also observed along the Preluca fault.

### 3.7.3 Estimates of horizontal and vertical components of displacement across the Bogdan-Voda and Dragos-Voda faults

Since movement along the Bogdan-Voda fault segment accumulated during two stages, we first evaluate the offsets along the Dragos-Voda fault, which was essentially active only during the later transtensive stage.

Based on published maps (Geological Survey of Romania) and stratigraphic logs of the sediments juxtaposed against the crystalline basement units (Dicea et al. 1980) the south-side-up vertical offset across the Dragos-Voda fault south of Borsa (Fig. 3.2) can be estimated to reach 2km. Assuming that the average measured pitch of striations at the Dragos-Voda fault of 15° (Appendix 3.5, 3.6) indicates the movement vector during transtension, the horizontal displacement had to be in the order of 7km.

Since offset along the Dragos-Voda fault continuously decreases from west to east due to coevally active SW-trending normal faults, the offset for a specific point can be estimated using a simple linear interpolation using the previously mentioned estimates for displacement together with the horizontal distance between Borsa and the point of negligible offset at the horsetail splay.

Thus the maximum offset of the Dragos-Voda fault segment, accumulated in its westernmost part, can be estimated to reach values in the order of 11km (horizontal) and 3km (vertical), respectively. For the eastern part of the Rodna horst our linear approach predicts a vertical offset in the order of 1km. Apatite fission-track ages from this region (Sanders, 1998) are identical on either side of the Dragos-Voda fault (Fig. 3.8), thus also indicating minor (i.e. <1km) vertical displacement below data resolution.

A total lateral offset of about 25km for the Bogdan-Voda fault can be deduced from the left-lateral offset of the Pienide thrust front (Fig. 3.2). The north side down component is evidenced by the relative offset of the post Burdigalian strata (Fig. 3.2). From the shallow plunge of lineations observed at the Bogdan-Voda fault (5° west), a total vertical offset of about 2.5km is obtained. Using the estimate of total lateral offset along the Dragos-Voda fault (see above), we infer that at least 11km lateral and 1km vertical offset were produced during the transtensional stage.

It should be noted that the marked difference



in vertical offsets between the Bogdan-Voda fault segment (1km) and Dragos-Voda fault segment (3km) during the transtensional stage is accommodated by the SW-trending Greben fault. Based on published geological maps (Geological Survey of Romania), the vertical offset at the Greben fault is estimated to reach about 2km.

### 3.8 Discussion of earlier work and large-scale correlations

#### 3.8.1 Comparison with previous data from the working area

Our observations and conclusions are largely comparable to a previous study in this area carried out by Györfi et al. (1999). However, we consider SW-NE shortening to be post-Burdigalian rather than Oligocene in age. Györfi et al. (1999) correlated the Late Miocene activity of the Bogdan- Dragos-Voda fault system with extensional features of Early Pannonian (~9-11.8 Ma) age described in seismic studies from the Pannonian basin. This time frame is compatible with our timing estimates for the transtensional stage (12-10 Ma).

The conclusions of Huisman et al. (1997) strongly differ from our interpretation. The major difference to our study is that we regard the early Burdigalian emplacement of the Pienides as top-SE directed rather than due to NNE-SSW compression. We partly disagree with Ciulavu (1999), who argued that extensional veins filled by hydrothermal ore deposits, dated to  $8.7 \pm 0.4$  Ma (Pécskay et al. 1994) and found within the volcanic body of Baia Mare, point towards a post-10 Ma activity of the Bogdan-Voda fault. On the available maps the pyroxene andesites (10.1 – 10.9 Ma, Pécskay et al. 1994), constituting most of the volcanic body of Baia Mare, are not crosscut by the Bogdan-Voda fault. Hence we conclude, that major activity along the Bogdan- Dragos-Voda fault system ceased at some 10 Ma ago, while the mineralized veins indicate partial reactivation of minor importance only.

#### 3.8.2 Burdigalian top-SE thrusting of the Pienides followed by NE-SW extension in the larger scale context

Based on seismic studies located in central Hungary Csontos and Nagymarosy (1998) report Oligocene to Lower Miocene-age thrusting of ALCAPA onto Tisza-Dacia along the Mid-Hungarian line. In agreement with Csontos and Nagymarosy (1998) and Csontos and Vörös

(2004) we consider the Pienide nappe contact as representing the eastward continuation of the Mid-Hungarian fault zone during Burdigalian times. Since the Pienides are correlated with parts of the Western Carpathians (Săndulescu 1981, 1994), i.e. with units that are clearly part of what is commonly referred to as “ALCAPA”, they are considered to represent the easternmost tip of ALCAPA.

Many authors postulate a significant (in the order of 90°) clockwise rotation of Tisza-Dacia during its mid-Miocene emplacement (e.g. Fodor et al. 1999, Márton and Fodor 2003). Such rotations should cause progressive reorientation of earlier formed structures (i.e. our nappe emplacement structures) as they are passively rotated together with the Tisza-Dacia block. However, we observed no regionally consistent evidence for such a change in transport directions. Thus we conclude that a major part of the rotation commenced earlier, possibly in the Early Oligocene, as is discussed in Györfi et al. (1999). This would imply that shortening across the Mid-Hungarian fault zone (Csontos and Nagymarosy 1998) and the emplacement of the Pienides in northern Romania only reflect the last stage of the juxtaposition of the ALCAPA and Tisza-Dacia blocks, a process that initiated much earlier (Csontos and Nagymarosy 1998). Comparable to the Late Burdigalian (~18.5 – 16 Ma) NE-SW extension documented in this study, Csontos and Nagymarosy (1998) report early to mid- Miocene extension within the Pannonian basin i.e. also along the Mid-Hungarian fault. Fodor et al. (1999) interpret NE-SW extension (17-15 Ma) within the Pannonian basin system as being related to back arc extension in the context of subduction roll-back in the Carpathians.

In conclusion, we regard Early Burdigalian top-SE thrusting of the Pienides, i.e. the easternmost tip of ALCAPA, to be related to transpression along the Mid-Hungarian fault zone in the context of lateral extrusion of ALCAPA. Subsequent late Burdigalian NE-SW-directed extension marks the extensional overprint of the Tisza-Dacia block due to ongoing roll-back in the northernmost East Carpathians.

#### 3.8.3 Post-Burdigalian activity along the Bogdan- Dragos-Voda fault system in the larger scale context

While subduction rollback migrates eastwards due to propagating slab detachment (Wortel and Spakman 2000) convergence in the western Carpathians comes to a halt and most likely leads to a pronounced change in deformational style along

the Mid-Hungarian fault zone (Fodor et al. 1999). Late Badenian to Sarmatian (14-11 Ma) NW-SE extension in the Pannonian basin (Fodor et al. 1999) is interpreted as a period of left lateral transtension along the Mid-Hungarian fault zone (Csontos and Nagymarosy 1998).

The left-lateral activity of the Bogdan-Voda and Dragos-Voda faults (16 – 10 Ma) coincides with this phase of sinistral transtension along the Mid-Hungarian fault zone and suggests a direct kinematic link between all these faults during this time interval. We suggest that the differing kinematics in our working area – transpression followed by transtension – may be explained by the “docking” of Tisza-Dacia with the European foreland. Starting in upper Burdigalian times, **NE-directed thrusting** of the Miocene thrust belt (Maţenco and Bertotti 2000) led to “soft collision” of Tisza-Dacia with the European foreland in the East Carpathians between some 16 to 10 Ma ago. **This scenario is comparable** to the Western Carpathians, where Sperner et al. (2002) correlate NNE-SSW compression (dated by these authors as Oligocene (?) to Mid-Miocene) with “soft collision” between ALCAPA and the European continent. Final emplacement of the northern part of Tisza-Dacia induces the change towards the transtensional activity along the Bogdan- Dragos-Voda fault system. This transtensional stage is coeval to late Sarmatian strike-slip activity in the external Miocene thrust belt of the East Carpathians (Maţenco and Bertotti, 2000).

Our data indicate a direct kinematic link between the Mid-Hungarian fault zone, the Bogdan-Voda fault and the Bogdan-Dragos-Voda fault system since post-Burdigalian times. However, since the Bogdan-Voda and Dragos-Voda faults are located within the Bucovinian basement (i.e. within the Dacia Block) they should not be considered as representing the continuation of the Mid-Hungarian Line as defined by Csontos and Nagymarosy (1998). Moreover, the amount of displacement documented for the Bogdan- Dragos-Voda fault system (~26km) rapidly diminishes towards the east. Its termination before reaching the foreland fold-and-thrust-belt, as well as the coeval activity at the Preluca fault and faulting south of the Rodna horst, suggests a rather distributed linkage of the foreland fold-and-thrust-belt with the extensional back-arc domain in post-Burdigalian times. This is in agreement with the interpretation of Maţenco and Bertotti (2000), who demonstrated that deformation caused by the final ESE-ward emplacement (Latest Sarmatian-Early Meotian, ~10 – 8 Ma) was distributed over large

parts of the East Carpathians. According to these authors the ESE movement of the central sectors of the Eastern Carpathians was accommodated by numerous E-W trending sinistral faults located east of our study area, rather than by one major strike-slip fault such as the Bogdan- Dragos-Voda fault system.

### 3.9 Conclusions

1. Early Burdigalian (20.5 - ~18.5 Ma) SE-directed emplacement of the Pienides, i.e. the eastern tip of ALCAPA, onto Tisza-Dacia is correlated with the thrusting of ALCAPA over Tisza-Dacia along the Mid-Hungarian line observed in the subsurface of the Pannonian basin (Csontos and Nagymarosy 1998). The Pienide nappe front in Maramures is kinematically linked to dextrally transpressive movements along the Mid-Hungarian fault zone that, together with the Periadriatic line, accommodates the lateral extrusion of ALCAPA.

2. Minor Late Burdigalian (18.5-16 Ma) NE-SW extension is interpreted as due to back-arc extension related to subduction roll back in the northernmost East Carpathians.

3. In post-Burdigalian (post-16 Ma) times a pronounced change in the tectonic regime led to NE-SW shortening and NW-SE extension. This change correlates with “soft collision” of Tisza-Dacia with the European foreland and the migration of active subduction from N to S along the Miocene foredeep of the Eastern Carpathians. Post-Burdigalian deformation was concentrated along the Bogdan-Voda and Dragos-Voda faults. Sinistral transpression (16 - 12 Ma) was mainly restricted to the Bogdan-Voda fault, which terminated eastwards in a thrust splay geometry. Sinistral transtension (12 – 10 Ma) was kinematically linked along the Bogdan- and Dragos-Voda fault segments (Bogdan- Dragos-Voda fault system). During this transtensional stage, coevally active SW-NE trending normal faults reduced the left-lateral offset towards the east, where the fault system terminates in an extensional horse - tail splay. The Bogdan-Dragos-Voda fault system is kinematically linked to the Mid-Hungarian fault zone during the post-Burdigalian stages, albeit deformation is distributed over large parts of the East Carpathians.

### 3.10 Acknowledgements

We are very grateful for an excellent introduction into the geology of the area by M. Săndulescu and L. Mațenco and for all the discussions we had with them and with all the other Romanian colleagues. We would also like to particularly mention the fruitful interactions with L. Csontos, L. Fodor, S. Kovács, M. Marin, E. Márton, C. Pero, D. Radu, D. Badescu and C. Krezsek during our study. M. Marin is gratefully acknowledged for providing additional data from the eastern part of the study area. The careful and constructive review by L. Ratschbacher significantly improved a first version of the text. This work was financed by NF-projects Nr. 21-64979.01, Nr. 200020-105136/1 and Nr. 200021-101882/1, granted to B.F. and S.Sch., respectively.

### 3.11 Appendix

## Appendix 3.1.

Table 3.1. Tabular overview on fault-slip data.

no.	x	y	lithology	rock age	shortening		intermediate		extension		r	regime	n data
<b>data correlated to early Burdigalian nappe emplacement</b>													
0006	24.7279	47.6816	fine flysch	Eocene	101	01	206	57	005	31	1	compressional strike slip	36
0215	24.3295	47.7339	flysch	Oligocene	324	03	233	22	062	68	3	reverse faulting	3
0236	24.0302	47.5991	flysch	Eocene	149	21	054	07	308	66	1	reverse faulting	10
0248	24.0344	47.5970	red marl	Late Cretaceous	145	12	053	08	290	75	2	reverse faulting	6
0272	24.1638	47.9015	conglomerate	L. Alb-Cenomanian	307	14	040	10	164	73	2	reverse faulting	5
0288	24.4847	47.6128	flysch	Rupelian	140	03	050	01	306	87	2	reverse faulting	8
0291	24.4334	47.5459	red marl	Late Cretaceous	124	02	034	21	219	69	2	reverse faulting	5
0314	24.2191	47.7545	flysch	Lutetian-Priabonian	145	00	236	81	055	09	3	compressional strike slip	7
0322	24.4250	47.5912	flysch	Rupelian	129	02	219	15	031	75	1	reverse faulting	6
0326	24.3450	47.4183	sandstone	Oligocene	342	16	072	01	167	74	2	reverse faulting	7
0414	24.3011	47.7350	flysch	Rupelian	093	04	185	32	357	58	1	reverse faulting	6
0453	24.4006	47.7251	flysch	Rupelian	315	02	224	28	049	62	1	reverse faulting	7
0584	24.0641	47.5791	flysch	Priabonian-?Oligocene	158	01	068	07	257	83	1	reverse faulting	18
0639	24.0950	47.8813	red marl	Late Cretaceous	137	09	233	36	035	52	1	compressional strike slip	30
0692	24.0752	47.8488	flysch	Lutetian-Priabonian	111	18	014	22	237	61	3	reverse faulting	6
0743	24.7105	47.6698	marl	Eocene	102	12	354	54	200	33	3	reverse faulting	5
0822	24.3608	47.4721	flysch	Rupelian - Aquitanian	352	05	261	14	100	76	2	reverse faulting	19
0892	24.4782	47.5418	marl	Turonian-Priabonian	162	23	331	67	070	04	1	compressional strike slip	11
1025	24.4616	47.5955	marl	Turonian-Priabonian	341	05	248	28	079	61	1	reverse faulting	14
1056	24.1420	47.5801	flysch	Priabonian-?Oligocene	157	30	037	40	271	35	2	compressional strike slip	5
<b>data correlated to late Burdigalian SW-Ne extension</b>													
0236	24.0302	47.5991	flysch	Eocene	148	36	306	51	050	11	1	extensional strike slip	29
0267	23.9266	47.4746	flysch	Chatian-Aquitainian	251	72	145	05	054	17	3	normal faulting	3
0368	24.9089	47.5638	crystalline	basement	285	73	114	17	023	03	1	normal faulting	14
0374	24.6976	47.6213	crystalline	basement	141	12	329	77	232	02	2	extensional strike slip	5
0376	24.8780	47.5983	crystalline	basement	184	58	326	26	064	17	1	extensional strike slip	11
0633	24.3596	47.7297	flysch	Rupelian	114	61	343	20	246	20	2	normal faulting	8
0765	25.1171	47.5908	crystalline	basement	144	78	293	10	024	06	3	normal faulting	5
0792	24.7005	47.4143	crystalline	basement	325	62	109	24	206	15	3	normal faulting	3
0799	24.8962	47.4492	crystalline	basement	037	68	130	01	221	21	1	normal faulting	25
0801	24.8055	47.4421	crystalline	basement	357	56	113	17	212	29	2	normal faulting	9
0802	24.5876	47.5191	crystalline	basement	087	71	297	17	204	09	1	normal faulting	43
0804	24.5811	47.5256	crystalline	basement	100	69	315	17	222	11	1	normal faulting	7
0816	24.6441	47.3919	conglomerate	Eocene	139	36	003	45	248	24	2	extensional strike slip	6
0915	24.0888	47.6218	flysch	Ypresian-Lutetian	128	81	331	08	241	03	3	normal faulting	3
0925	23.9891	47.6164	flysch	Ypresian-Lutetian	161	70	275	08	007	18	2	normal faulting	6
M 30	25.1658	47.5551	crystalline	basement	263	34	116	51	004	16	2	extensional strike slip	11
M 41	25.4644	47.5276	crystalline	basement	139	12	270	72	046	13	2	strike slip	8
M 66	25.3566	47.5826	crystalline	basement	146	19	016	63	243	19	2	extensional strike slip	7
<b>data correlated to post-Burdigalian transpressional stage</b>													
0008	24.2418	47.6984	tuff	Badenianmj	050	10	298	65	145	22	1	compressional strike slip	13
0059	24.8196	47.6257	conglomerate	Lutetian	225	12	130	23	339	63	2	compressional strike slip	9
0147	24.2452	47.8174	flysch	Lutetian-Priabonian	024	05	284	66	116	23	2	compressional strike slip	16
0237	24.0220	47.5875	flysch	Oligocene-E. Miocene	001	06	298	73	098	16	2	compressional strike slip	11
0259	23.6433	47.5093	crystalline	basement	089	01	139	24	317	66	1	reverse faulting	7
0260	23.8639	47.4366	flysch	Burdigalian	249	06	157	13	006	76	3	reverse faulting	3
0276	24.2015	47.8582	flysch	Oligocene	192	16	101	02	004	74	2	reverse faulting	6
0310	24.1013	47.7794	flysch	Priabon	212	13	321	55	114	32	1	compressional strike slip	12
0322	24.4274	47.5643	flysch	Rupelian	037	10	305	11	167	76	3	reverse faulting	2
0357	24.8414	47.6499	crystalline	basement	049	03	318	18	147	72	1	reverse faulting	6
0360	24.9921	47.5859	flysch	Lutetian	189	04	094	52	282	38	1	compressional strike slip	13
0462	24.4936	47.6215	limestone	Lutetian-Priabonian	048	05	313	45	143	45	1	compressional strike slip	6
0556	23.8153	47.4966	crystalline	basement	014	08	112	45	276	44	2	compressional strike slip	9
0631	24.3719	47.8333	flysch	Oligocene	255	00	345	61	165	29	1	compressional strike slip	5
0632	24.3395	47.8286	flysch	Oligocene	054	02	323	25	149	65	2	compressional strike slip	7
0675	24.2141	47.6546	flysch	Oligocene	249	03	351	76	159	13	1	compressional strike slip	8
0682	24.2234	47.6636	flysch	Oligocene	063	11	159	29	314	59	3	compressional strike slip	5
0809	24.8339	47.6486	marl/limestone	Lutetian-Priabonian	210	04	119	02	001	86	1	reverse faulting	12
0917	24.0219	47.6177	flysch	Ypresian-Lutetian	245	03	154	17	344	73	2	reverse faulting	13

Table 3.1. continued

no.	x	y	lithology	rock age	shortening		intermediate		extension		r	regime	n data
<b>data correlated to post-burdigalian transtensional stage</b>													
0059	24.8196	47.6257	conglomerate	Lutetian	144	72	245	03	336	17	1	extensional strike slip	9
0060	24.7894	47.6107	crystalline	basement	235	38	063	52	328	04	1	extensional strike slip	11
0079	24.4717	47.6215	limestone	Lutetian-Priabonian	223	46	069	41	327	13	1	extensional strike slip	9
0095	24.4103	47.6212	flysch	Lutetian-Priabonian	208	76	066	11	334	08	3	normal faulting	5
0152	24.1337	47.6965	tuff	Badenian	219	27	036	63	128	01	2	extensional strike slip	5
0170	24.1472	47.6656	flysch	Ypresian-Lutetian	037	16	189	72	304	08	2	strike slip	5
0180	24.3487	47.6356	flysch	Lutetian-Priabonian	245	35	058	55	152	03	2	extensional strike slip	11
0236	24.0302	47.5991	flysch/marl	Late Jur.-Eocene	186	11	072	65	281	22	1	strike slip	19
0259	23.6433	47.5093	crystalline	basement	016	44	193	46	285	02	1	extensional strike slip	7
0272	24.1638	47.9015	conglomerate	L. Albian-Cenomanian	077	09	324	67	171	21	2	strike slip	5
0275	24.1536	47.8973	limestone	Lutetian-Priabonian	156	71	038	09	305	16	2	normal faulting	7
0292	24.4926	47.7065	flysch	Rupelian	069	53	229	35	326	10	2	extensional strike slip	7
0297	24.5695	47.7276	flysch	Oligocene	196	24	359	65	103	06	2	extensional strike slip	7
0346	25.1493	47.5659	crystalline	basement	316	61	225	00	135	29	2	normal faulting	6
0360	24.9921	47.5859	sandstone	Lutetian	203	10	060	77	295	08	1	strike slip	18
0363	24.8924	47.6024	crystalline	basement	213	20	021	70	122	04	1	strike slip	14
0368	24.9089	47.5638	crystalline	basement	273	60	043	21	142	21	2	normal faulting	10
0369	24.6908	47.5981	crystalline	basement	131	68	023	07	291	21	2	extensional strike slip	11
0374	24.6976	47.6213	crystalline	basement	219	14	049	75	310	02	2	strike slip	20
0385	24.6186	47.7480	flysch	Oligocene	227	21	055	68	318	03	2	extensional strike slip	4
0386	24.6177	47.7499	crystalline	basement	248	63	080	27	348	05	1	normal faulting	12
0387	24.6069	47.7611	crystalline	basement	161	70	037	12	303	16	1	normal faulting	9
0390	24.0066	47.8386	tuff	Badenian	016	36	213	53	112	08	2	extensional strike slip	7
0413	24.8755	47.5983	crystalline	basement	298	76	178	88	088	12	2	normal faulting	8
0452	24.4124	47.7375	flysch	L. Lutetian/Bartonian	050	73	238	16	147	02	2	normal faulting	8
0462	24.4936	47.6215	limestone	Lutetian-Priabonian	224	66	051	24	320	03	1	extensional strike slip	12
0481	24.5200	47.6219	crystalline	basement	225	51	052	39	319	03	1	extensional strike slip	14
0534	23.6282	47.5041	crystalline	basement	022	45	213	44	117	06	3	extensional strike slip	4
0550	23.8101	47.4680	crystalline	basement	320	81	053	00	143	09	3	normal faulting	6
0556	23.8153	47.4966	crystalline	basement	191	14	055	70	284	13	2	extensional strike slip	9
0588	23.9867	47.5482	flysch	Early Miocene	163	50	032	29	287	25	2	extensional strike slip	11
0625	24.1412	47.6479	tuff	Ypresian-Lutetian	244	52	061	38	152	01	1	extensional strike slip	26
0681	24.2230	47.6629	sandstone	Badenian	213	37	051	51	310	09	1	strike slip	18
0712	23.9619	47.8797	sandstone	Badenian	051	64	218	26	311	05	1	normal faulting	9
0720	24.1340	47.6577	flysch	Ypresian-Lutetian	011	04	116	76	280	14	3	strike slip	8
0733	24.0414	47.8737	tuff	Badenian	009	29	202	61	102	05	1	strike slip	17
0758	25.1234	47.5824	dolomite	basement	038	01	132	82	308	08	1	extensional strike slip	23
0774	24.5453	47.4003	crystalline	basement	030	39	246	45	136	19	2	extensional strike slip	8
0797	24.9295	47.4590	conglomerate	Cretaceous	345	46	228	13	133	23	1	normal faulting	13
0799	24.8962	47.4492	crystalline	basement	021	70	198	20	289	01	2	normal faulting	9
0801	24.8055	47.4421	crystalline	basement	036	61	204	28	296	05	2	normal faulting	11
0804	24.5811	47.5256	crystalline	basement	035	54	272	21	171	27	2	extensional strike slip	8
0807	24.5791	47.4538	crystalline	basement	028	36	219	53	122	05	3	extensional strike slip	4
0814	24.6391	47.4729	crystalline	basement	032	04	203	86	302	01	3	strike slip	10
0818	24.8228	47.4932	crystalline	basement	134	82	037	01	307	08	1	normal faulting	22
0832	24.2835	47.6576	flysch	Rupelian	053	08	180	78	321	10	1	strike slip	21
0838	24.2668	47.6507	sandstone	Badenian	022	05	267	78	113	11	1	strike slip	37
0897	23.6856	47.5602	sandstone	Badenian	042	02	148	82	312	08	2	strike slip	5
M 19	25.0739	47.5916	crystalline	basement	208	03	101	79	299	10	1	strike slip	12
M 27	25.1569	47.5714	crystalline	basement	017	02	162	84	107	05	1	strike slip	9
M 32	25.1724	47.5521	crystalline	basement	041	03	139	73	310	17	1	strike slip	15
M 41	25.4644	47.5276	crystalline	basement	055	01	150	82	324	08	2	strike slip	7

**no.:** reference number of outcrop, prefix M indicated data provided by Mihai Marin

**X/Y:** coordinates of the outcrops in decimal degrees Lat/Long, WGS 84.

**shortening / intermediate / extension:** orientation of respective mean kinematic axes, derived by eigenvector analysis of the shortening/extensional fields obtained by the right dihedral method (Angelier and Mechler 1977).

**r:** data quality rating: 1: good; 2: moderate; 3: poor.

**regime:** tectonic regime of deformation assessed by the distribution of incremental strain axes (Marret and Almendinger, 1990). Reverse faulting, normal faulting, strike-slip faulting: well-clustered shortening and extension axes; compressional strike-slip: well clustered shortening axes with great circle distribution of extensional axes; extensional strike-slip: well clustered extension axes with great circle distribution of shortening axes.

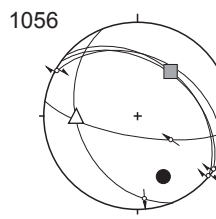
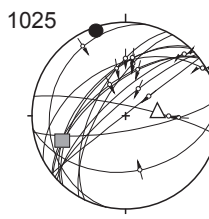
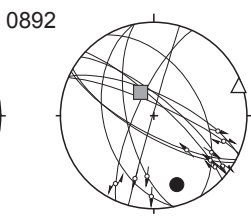
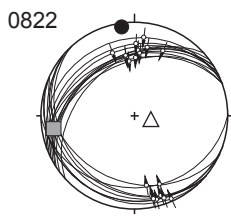
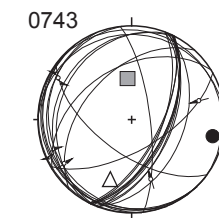
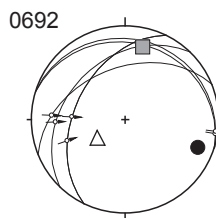
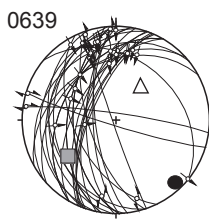
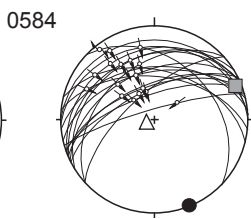
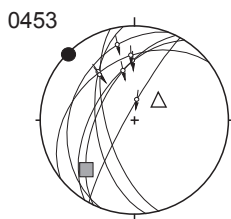
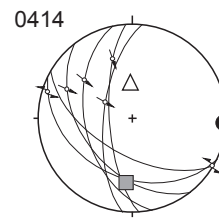
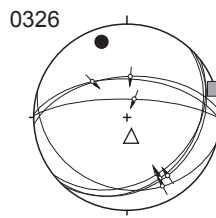
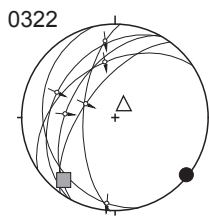
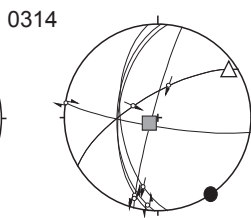
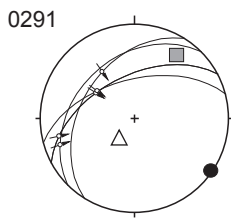
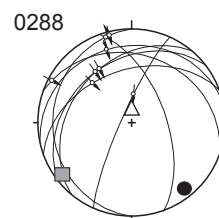
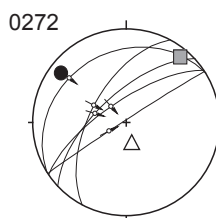
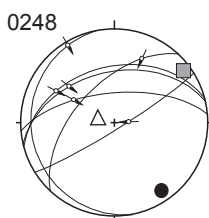
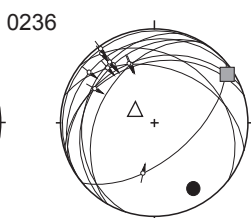
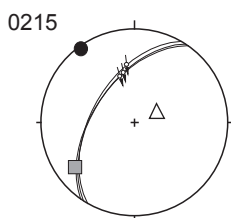
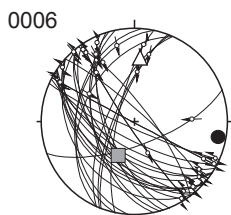
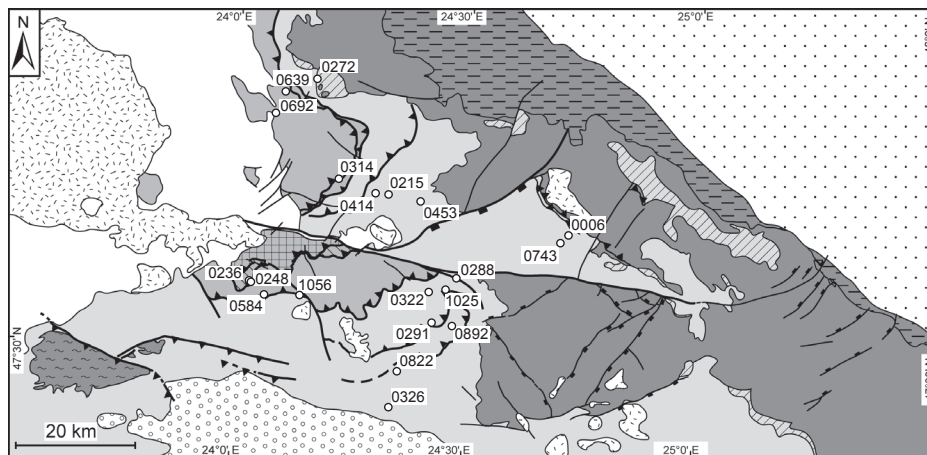
**n data:** number of fault-slip sets attributed to respective regime, only fault-slip sets with certain slip sense have been included.

Appendix 3.2.

Fig. 3.9. Fault-slip data (Early Burdigalian top SE-thrusting of the Pienides).

Legend:

- shortening
- intermediate
- △ extension



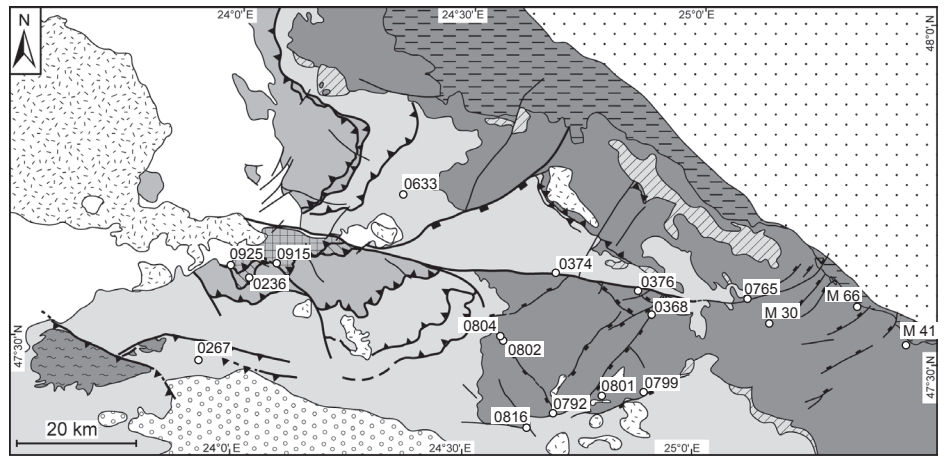
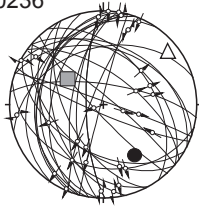
Appendix 3.3.

Fig. 3.10. Fault-slip data (Late Burdigalian NE-SW extension).

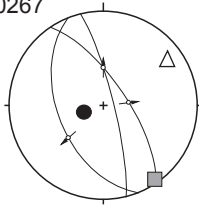
Legend:

- shortening
- intermediate
- △ extension

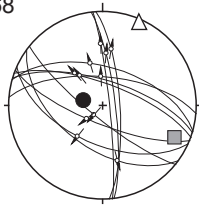
0236



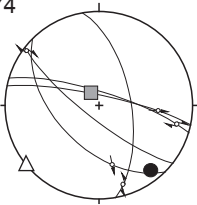
0267



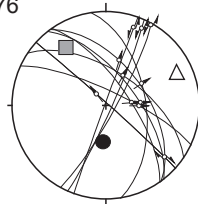
0368



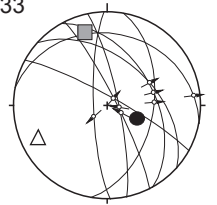
0374



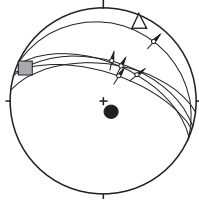
0376



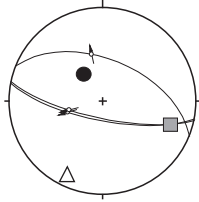
0633



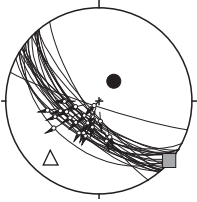
0765



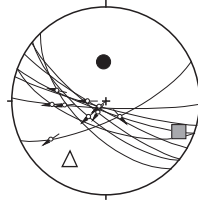
0792



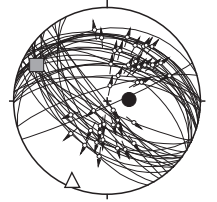
0799



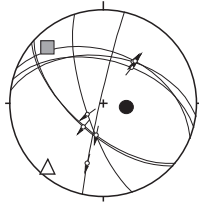
0801



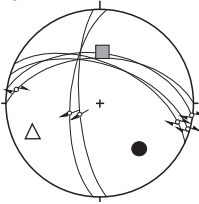
0802



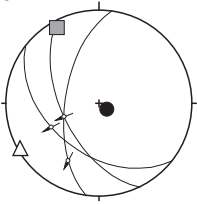
0804



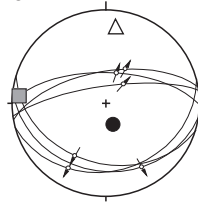
0816



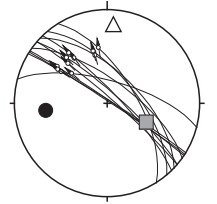
0915



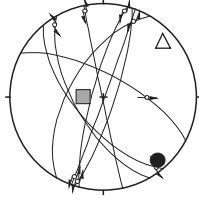
0925



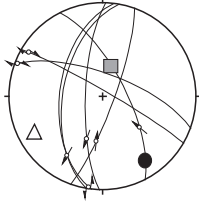
M 30



M 41



M 66

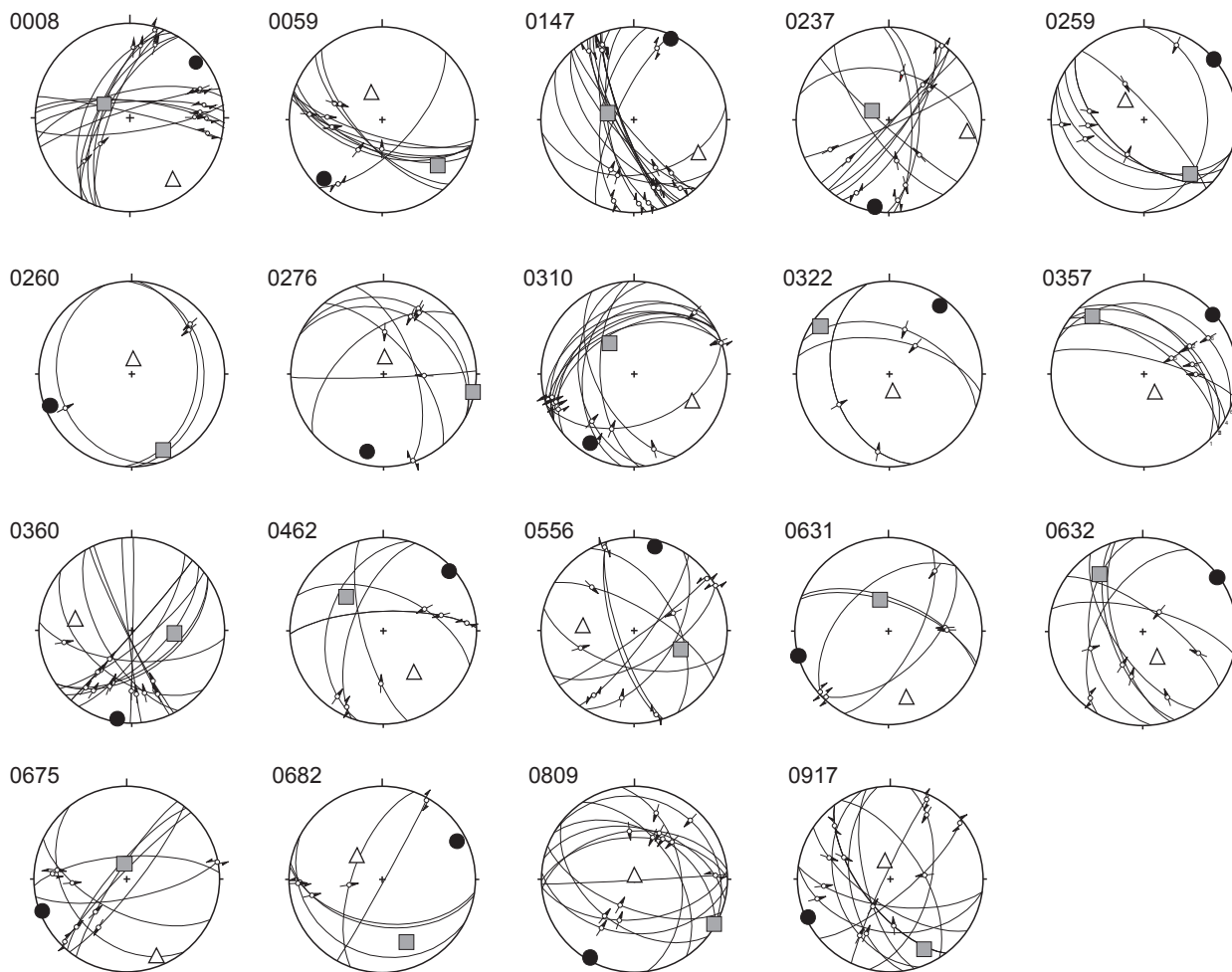
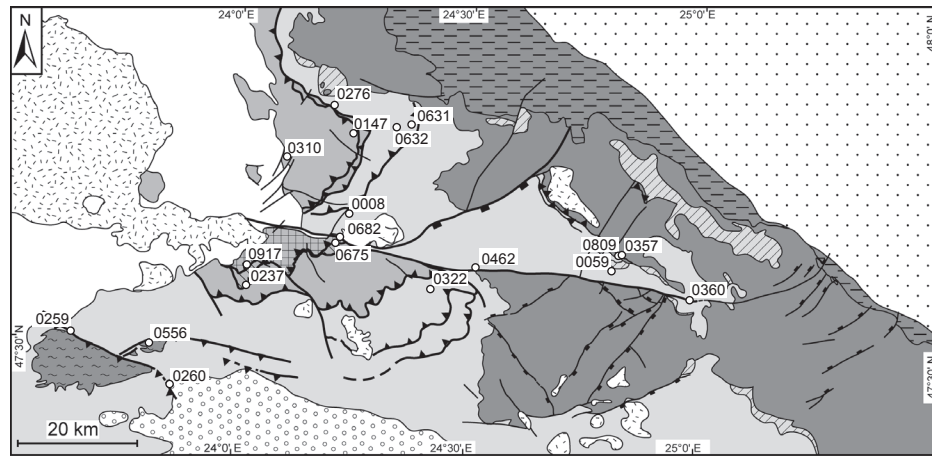


## Appendix 3.4.

Fig. 3.11. Fault-slip data (post-Burdigalian transpressional stage).

Legend:

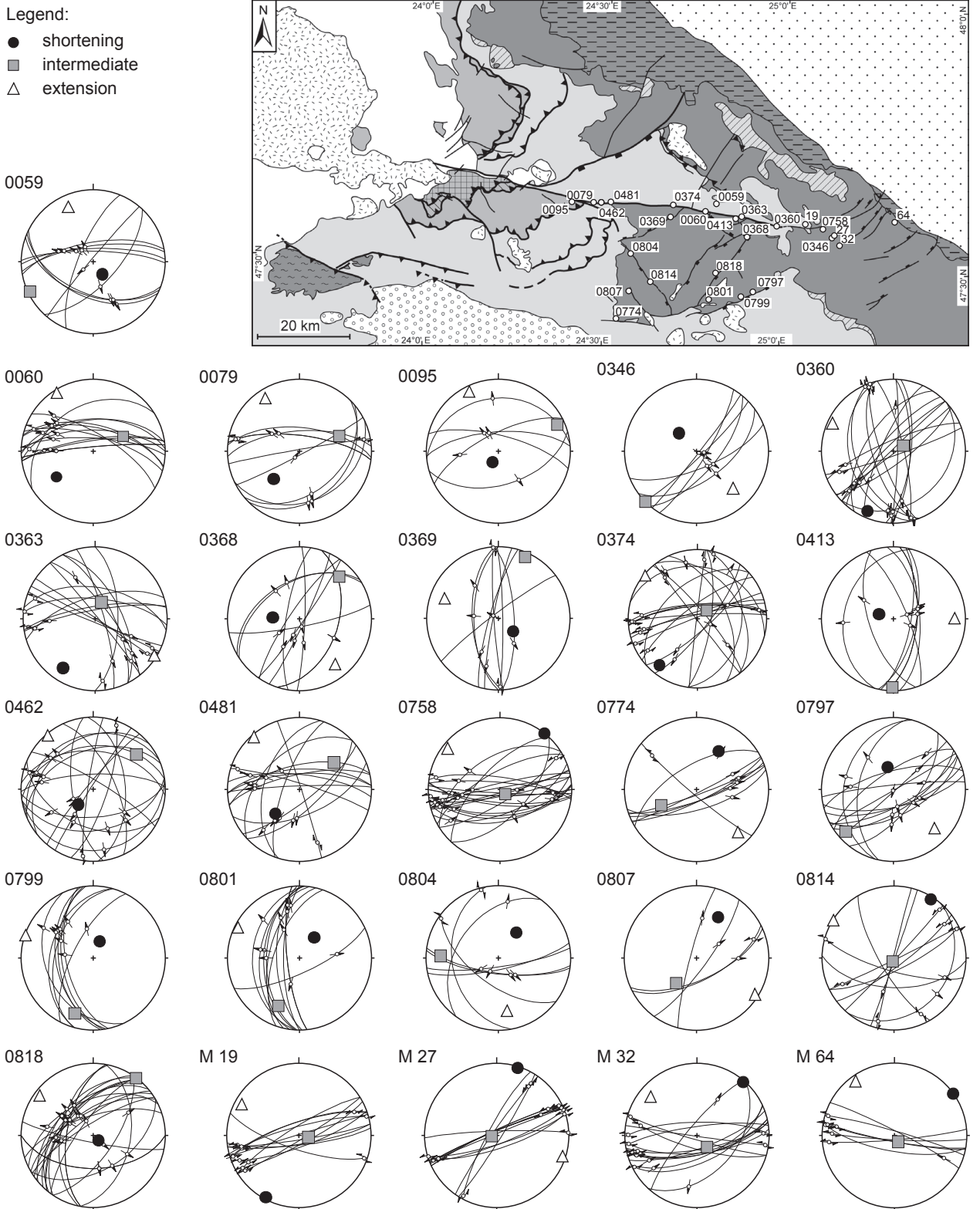
- shortening
- intermediate
- △ extension





Appendix 3.5.

Fig. 3.12. Fault-slip data (post-Burdigalian transtensional stage, eastern stations).



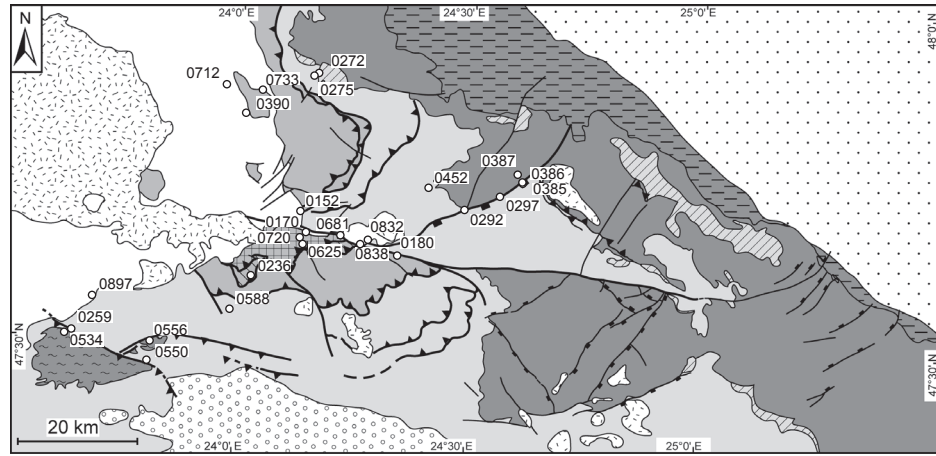
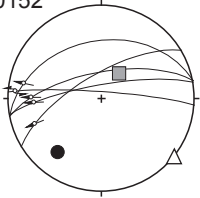
Appendix 3.6.

Fig. 3.13. Fault-slip data (post-Burdigalian transtensional stage, western stations).

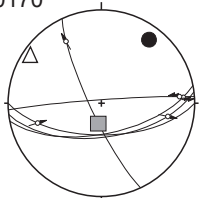
Legend:

- shortening
- intermediate
- △ extension

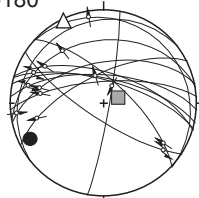
0152



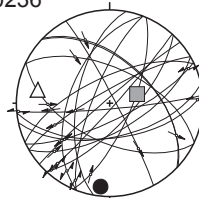
0170



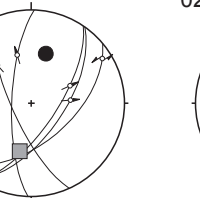
0180



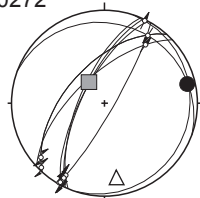
0236



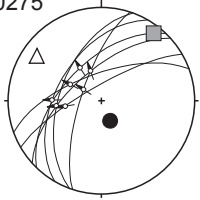
0259



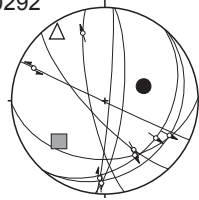
0272



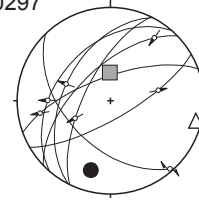
0275



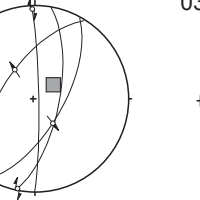
0292



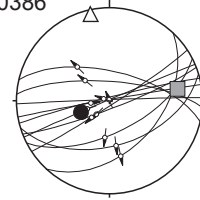
0297



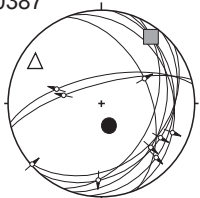
0385



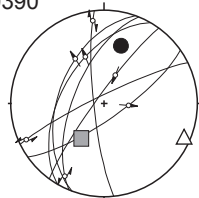
0386



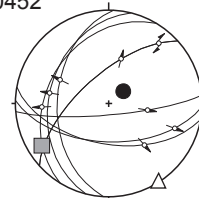
0387



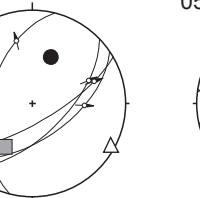
0390



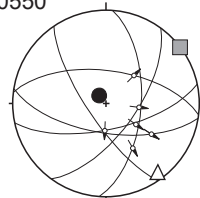
0452



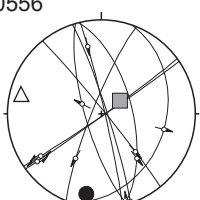
0534



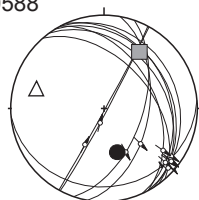
0550



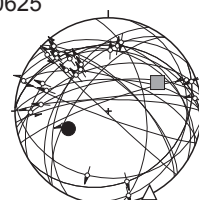
0556



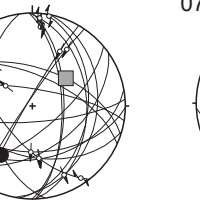
0588



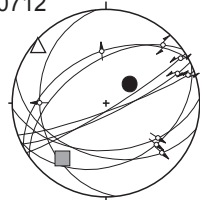
0625



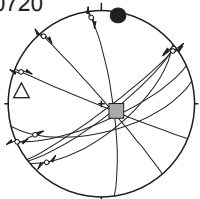
0681



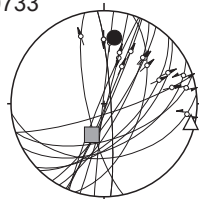
0712



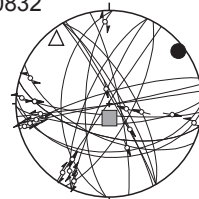
0720



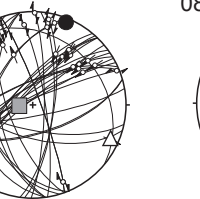
0733



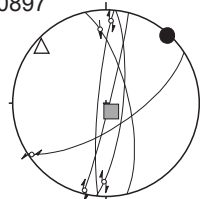
0832



0838



0897



## Chapter 4:

# Tertiary cooling and exhumation history in the Maramures area (internal eastern Carpathians, northern Romania): thermochronology and structural data

H.R. GRÖGER<sup>1,2</sup>, B. FÜGENSCHUH<sup>3</sup>, M. TISCHLER<sup>1</sup>, S.M. SCHMID<sup>1</sup>, J.P.T. FOEKEN<sup>4</sup>

<sup>1</sup>*Geologisch Paläontologisches Institut, Universität Basel, Bernoullistrasse 32, 4056 Basel, Switzerland*

<sup>2</sup>*Present address: StatoilHydro ASA, Forusbeen 50, 4035 Stavanger, Norway  
(e-mail corresponding author: heigr@statoilhydro.com)*

<sup>3</sup>*Institut für Geologie und Paläontologie, Universität Innsbruck, Innrain 52, Bruno Sander Haus, 6020 Innsbruck, Austria*

<sup>4</sup>*Scottish Universities Environmental Research Centre (SUERC), Rankine Avenue, Scottish Enterprise Technology Park, East Kilbride, G75 0QF, Scotland*

**(Geological Society, London, Special Publications: 2008)**

### 4.1 Abstract

The Tertiary kinematic history of the Maramures area is constrained by integrating thermochronological (fission track and (U-Th)/He analysis) data with field-based structural investigations. This study focuses on the tectonic evolution of the northern rim of the Tisza-Dacia block during collision with the European margin.

Cretaceous nappe stacking, related metamorphism as well as Late Cretaceous exhumation are evidenced by zircon fission track data. Subsequent Palaeogene to Early Miocene sedimentation led to burial heating and annealing of fission tracks in apatite. Final tectonic uplift was initiated during the convergence of Tisza-Dacia with the European margin, associated with transpressional deformation (16 to 12 Ma). This led to Mid-Miocene exhumation, recorded by apatite fission track cooling ages in the western part of the study area.

Transtension between 12 and 10 Ma caused brittle deformation along E-W trending strike-slip faults and SW-NE trending normal faults, delimiting blocks that were tilted towards the SW. This fragmentation of the crust led to enhanced exhumation at rates of 1 mm/a in the central part of the study area, as is documented by Middle to Late Miocene cooling ages (13 to 7 Ma). The outside estimate for the total amount of exhumation since Middle Miocene times is 7 km.

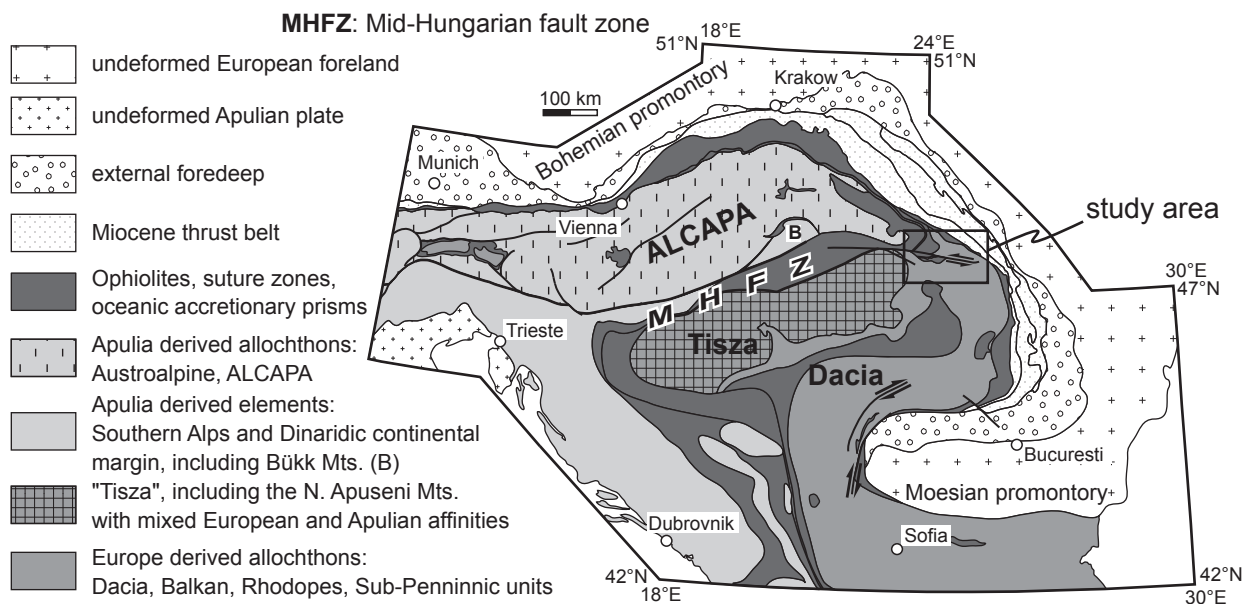


**Fig. 4.1.** Tectonic map of the Alpine-Carpathian-Pannonian area (simplified after Schmid et al. 2006). Three major continental blocks are located within the Carpathian embayment: ALCAPA, Tisza and Dacia. During emplacement in Tertiary times, a zone of repeated tectonic activity developed between ALCAPA and the already consolidated Tisza-Dacia block: the Mid-Hungarian fault zone (MHFZ).

This study addresses the cooling and exhumation history of basement units (Rodna horst and Preluca massif) in northern Romania (Maramures) by combining thermochronological analyses with structural field investigations. The study area is located in the NE prolongation of the Mid-Hungarian fault zone (Csontos & Nagymarosy 1998; Csontos & Vörös 2004), separating the ALCAPA and Tisza-Dacia mega-units (Fig. 4.1). This crustal scale boundary plays a key role during the final emplacement of these two crustal scale blocks (ALCAPA and Tisza-Dacia) in the Carpathian embayment during the Tertiary (Csontos & Nagymarosy 1998). Since the Mid-Hungarian fault zone is largely covered by Neogene sediments of the Pannonian basin, our study area represents one of the very few places where structures related to this important tectonic lineament can be studied in outcrop (Tischler et al. 2006).

Invasion of the ALCAPA and Tisza-Dacia blocks into the Carpathian embayment was triggered by a combination of lateral extrusion in the Eastern Alps (Ratschbacher et al. 1991a, b) and retreat of the European lithospheric slab (e.g. Wortel & Spakman 2000; Sperner et al. 2005). Corner effects at the Moesian and Bohemian promontories led to opposed rotations of these continental blocks during their emplacement, well established by palaeomagnetic studies (e.g. Márton 2000; Márton & Fodor 1995, 2003; Márton et al. 2006). The Mid-

Hungarian fault zone is of central importance, since it allows for differential movements between the ALCAPA and Tisza-Dacia blocks (Fodor et al. 1999; Csontos & Vörös 2004). Finally, soft collision of these blocks with the European continental margin resulted in the formation of the Miocene fold and thrust belt (Fig. 4.1; e.g. Royden 1988, Roure et al. 1993; Matenco & Bertotti 2000). A more detailed discussion of the Tertiary palaeogeographic and kinematic history of the ALCAPA and Tisza-Dacia blocks can be found in numerous earlier studies (e.g. Balla 1987; Royden & Baldi 1988; Săndulescu 1988; Csontos 1995; Csontos et al. 1992; Fodor et al. 1999; Fügenschuh and Schmid 2005).

The samples analysed in this study derive from pre-Mesozoic basement and the autochthonous sedimentary cover of the Tisza-Dacia block (Preluca massif, Rodna and Maramures mountains, respectively) and from tectonic units that are part of an accretionary prism which is situated between the ALCAPA and Tisza-Dacia blocks, the so called Pienides. According to a recent compilation of tectonic units by Schmid et al. (2006) the basement units are considered part of Dacia, but classically the Preluca massif, which is part of the Biharia nappe system, is attributed to Tisza (e.g. Haas & Péro 2004). We applied zircon fission track-, apatite fission track- and apatite (U-Th)/He thermochronological analyses. The combination of these methods constrains the thermal history

of the samples in the temperature range between 300°C and 40°C, and is well suited to elucidate the thermal evolution in soft collisional regimes, which do not feature major exhumation and exposure of high grade metamorphic rocks (Royden 1993; Morley 2002).

Numerous other studies successfully addressed cooling and exhumation histories, either based on fission track analyses alone (e.g. Sobel & Dumitru 1997; Fügenschuh et al. 2000; Dunkl & Frisch 2002; Danišík et al. 2004; Fügenschuh & Schmid 2003, 2005) or on a combination of fission track and (U-Th)/He analyses (e.g. Foeken et al. 2003; Reiners et al. 2003; Persano et al. 2005; Stöckli 2005 and references therein). Within our working area some apatite fission track data are already available from the work of Sanders (1998) and Sanders et al. 1999, who addressed the interplay between tectonics and erosion in the Southern and Eastern Carpathians and the Apuseni Mountains.

All chronostratigraphic ages will be given after Gradstein et al. (2004). Paratethys stages were correlated with Mediterranean stages according to Steininger & Wessely (2000).

## 4.2 Geological setting

The pre-Cambrian to Palaeozoic basement units of the East Carpathians (so-called Bucovinian nappe stack of the Dacia block) mainly consist of metasediments and subordinately orthogneiss (Kräutner 1991; Voda & Balintoni 1994). The Alpine-age Bucovinian nappe stack consists, from bottom to top, of the Infrabucovinian, Subbucovinian and Bucovinian nappes, occasionally separated by Permian to lower Cretaceous sediments (Săndulescu et al. 1981). Along most parts of the East Carpathians late Early Cretaceous nappe stacking is generally considered to have taken place under sub-greenschist facies metamorphic conditions. In the so-called Rodna horst (Fig. 4.2), a part of the Bucovinian nappe stack located internally of the main East Carpathian chain, greenschist facies conditions during this event were postulated by Balintoni et al. (1997). The Preluca massif, consisting of metasediments (Rusu et al. 1983), is part of the Biharia nappe system of the North Apuseni Mountains. However, in contrast to most authors (e.g. Haas & Péro 2004) the Biharia nappe system was correlated with the Bucovinian nappe system (i.e. considered as part of Dacia) by Schmid et al. (2006), based on a re-interpretation of geophysical data from the Transylvanian basin. In any case,

Tisza and Dacia became amalgamated during the Cretaceous and formed a consolidated Tisza-Dacia block ever since Early Tertiary times (Csontos 1995; Csontos & Vörös 2004).

Latest Early Cretaceous juxtaposition of the Bucovinian nappe stack against the Ceahlau and Black Flysch units (Săndulescu 1982) was followed by exhumation and erosion, leading to the sedimentation of the Late Cretaceous post-tectonic cover (Ianovici et al. 1968; Săndulescu 1994). Exhumation which followed the juxtaposition of the entire Alpine nappe pile against the internal Moldavides (Săndulescu 1982) occurred during the Latest Cretaceous (Săndulescu 1994) and led to erosion of large parts of these upper Cretaceous cover units.

The deposition of a second stack of post-tectonic sediments during the Tertiary led to renewed burial. While the sedimentation already started in Palaeocene times in the Preluca massif (Rusu et al. 1983), non-deposition and/or erosion continues in the area of the Bucovinian nappe stack, as is indicated by a Palaeocene hiatus. Eocene conglomerates (Ypresian?, Kräutner et al. 1983) are the oldest Tertiary strata preserved on the previously exhumed Bucovinian nappe stack which they stratigraphically directly overlie except for a few places where the Late Cretaceous basins remained preserved (Fig. 4.2). Late Eocene (Late Lutetian-Priabonian) sedimentation is characterized by a general deepening of the depositional environment towards the NW. While platform carbonates indicating shallow water depths are found in large parts of the study area (main East Carpathian Chain and Rodna horst: Kräutner et al. 1978, 1982, 1983, 1989; Preluca massif: Rusu et al. 1983; de Broucker et al. 1998) sandy marls and marls dominate west of the Greben fault (Fig. 4.2; Săndulescu et al. 1991). Oligocene sediments overlying the basement units of the Rodna horst in direct stratigraphic contact document the Eocene palaeorelief (Kräutner et al. 1982).

Early Oligocene to Early Miocene (Aquitanian) sedimentation is dominated by siliciclastic turbidites, which show an overall coarsening upward trend (Dicea et al. 1980; Săndulescu et al. 1991), thought to reflect the juxtaposition of ALCAPA and Tisza-Dacia (Tischler et al. this volume). A Burdigalian clastic wedge (Hida beds) testifies the overthrusting of the Pienides (Ciulavu et al. 2002), i.e. thrusting of ALCAPA onto Tisza-Dacia. The Pienides mainly consist of Eocene to Oligocene non-metamorphic flysch units (Aroldi 2001), which additionally

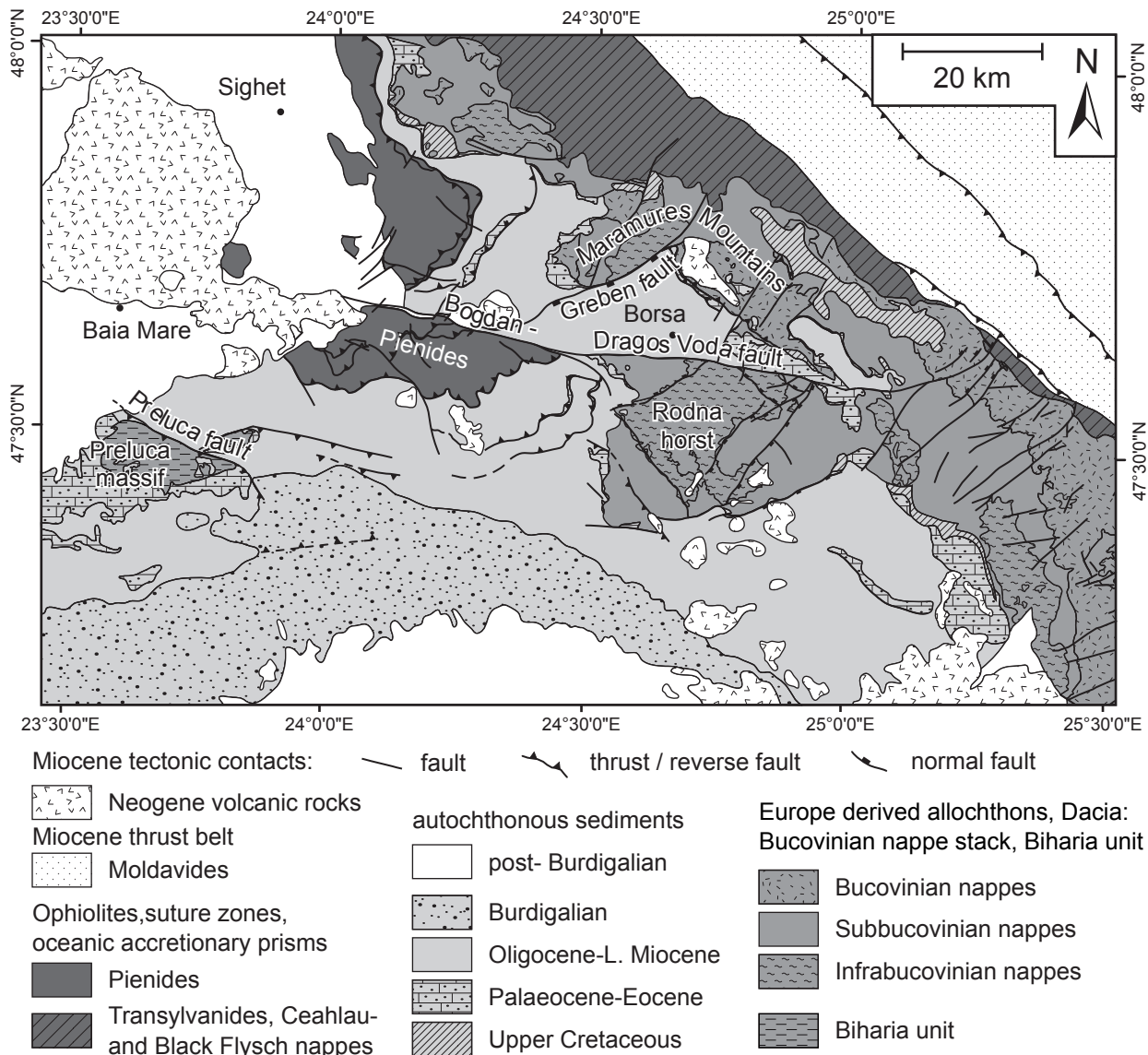


**Fig. 4.2.** Tectonic map of the study area. The Pienides, consisting of non-metamorphic flysch nappes, were emplaced in early Burdigalian times (20.5 to 18.5 Ma, Tischler et al. 2006). Middle to Late Miocene brittle tectonics (16–10 Ma) led to the exhumation of the Rodna horst and the Preluca massif (Tischler et al. 2006). The most important Middle to Late Miocene structures are the Preluca fault, the Greben fault and the Bogdan-Drăgoș-Voda fault. To the west, the Bogdan-Voda fault is sealed by Neogene volcanic rocks. The map is compiled after Giusca & Radulescu (1967), Raileanu & Radulescu (1967), Ianovici & Dessila-Codarcea (1968), Ianovici et al. (1968), Ianovici & Radulescu (1968), Raileanu & Saulea (1968), Kräutner et al. (1978, 1982, 1983, 1989), Borcos et al. (1980), Dicea et al. (1980), Sandulescu (1980), Sandulescu & Russo-Sandulescu (1981), Sandulescu et al. (1981), Rusu et al. (1983), Sandulescu et al. (1991) and Aroldi (2001).

contain phacoids of Pieniny-Klippen-type material embedded in Eocene flysch (Sandulescu 1980; Sandulescu et al. 1993).

Post-Burdigalian sedimentation starts with the deposition of the Middle Miocene (Badenian) Dej Tuff (Mason et al. 1998). Subduction-related calc-alkaline magmatism started during Middle Miocene times (13.5 Ma, Pécskay et al. 1995). Magmatic activity led to the formation of a linear

volcanic chain along the inner side of the East Carpathians, with a general trend of decreasing ages towards SE.

The most obvious structure in the study area is the E-W striking, predominantly left-lateral Bogdan-Drăgoș-Voda fault system (Tischler et al. 2006). The Bogdan-Voda fault to the west offsets the Palaeogene to Early Miocene cover of Tisza-Dacia, as well as the nappe pile of the Pienides. It

is essentially sealed by Mid-Miocene volcanic rocks (Fig. 4.2). The Dragos-Voda fault delimits the Rodna horst to the north.

### 4.3 Methods

#### 4.3.1 Fission track analysis: methodology and analytical procedure

For an overview of the methodology and applications of fission track (FT) analysis the reader is referred to Wagner and van den Haute (1992), Andriessen (1995), Gallagher et al. (1998) and Reiners & Ehlers (2005). Regarding the fission track partial annealing zones we used the temperature brackets given by Gleadow & Duddy (1981) and Green et al. (1989) for apatite (APAZ, 60 to 120 °C) and Hurford (1986) for zircon (ZPAZ, 190 to 290 °C), respectively.

After conventional crushing, sieving, magnetic and heavy liquid separation apatite grains were mounted in epoxy resin, polished and etched for 40 seconds at room temperature in 6.5% HNO<sub>3</sub>. Zircon grains were mounted in PFA® Teflon, polished and etched for 12 to 24 hours in a NaOH/KOH eutectic melt at about 225 °C. Irradiation was carried out at the High Flux Australian Reactor (HIFAR) with neutron fluxes monitored in CN5 for apatite and CN1 for zircon. All samples were analysed using the external detector method (Gleadow 1981) with muscovite as an external detector. Muscovite was etched for 40 minutes at room temperature in 40% HF.

Fission tracks were counted on a Zeiss® microscope with a computer-controlled scanning stage ("Langstage", Dumitru 1993) at magnifications of 1250x for apatite and 1600x for zircon (dry). Unless mentioned otherwise all ages given are central ages (Galbraith & Laslett 1993). Ages were calculated using the zeta calibration method (Hurford & Green 1983) with a  $\xi$  value of  $355.96 \pm 9.39$  (Durango standard, CN5) for apatite and  $141.40 \pm 6.33$  (Fish Canyon tuff standard, CN1) for zircon. Calculations were done with the aid of the windows software TrackKey (Dunkl 2002). For separation of subpopulations (i.e. the youngest population in partially annealed samples) the windows software PopShare was used (Dunkl & Székely 2002).

Lengths of confined horizontal tracks in apatite were measured at 1250x magnification. Track length distributions of confined horizontal tracks are diagnostic for different thermal histories (Crowley 1985; Gleadow et al. 1986a, b; Galbraith

& Laslett 1993) and allow for thermal modelling. Thermal modelling of fission track parameters was carried with the program AFTSolve (Ketcham et al. 2000) with the annealing model of Laslett et al. (1987).

Apart from temperature, chemical composition is known to have an effect on the annealing behaviour (Green et al. 1985, 1986; Crowley & Cameron 1987; O'Sullivan & Parrish 1995; Siddall & Hurford 1998). Thus, the long axis of etch pits on the polished surface (referred to as Dpar, Burtner et al. 1994) was measured (magnification 2000x) as an indicator of the annealing behaviour of apatite.

#### 4.3.2 Apatite (U-Th)/He dating: methodology and analytical procedure

Apatite (U-Th)/He dating records the cooling of a sample between 80 and 40°C (Wolf et al. 1998; Ehlers & Farley 2003 and references therein) and is complementary to apatite FT when reconstructing the latest exhumation stages. Apatite (U-Th)/He analyses were conducted on 4 samples: 2 from the Rodna horst and 2 from the Preluca massif. Suitability of samples for (U-Th)/He dating was mainly governed by sample quality (inclusions) and grain morphology. Between one to four apatite grains for each sample were hand-picked in ethanol at 218x magnification using a binocular microscope. While the frosted nature of the apatite grains made the identification of inclusion-free grains difficult, small zircon inclusions were only observed in one replicate of sample P4 (II). To minimize grain size variation effects (Farley 2000) grains of similar radius were selected for each aliquot. <sup>4</sup>He, U and Th analyses were conducted following the procedures of Balestrieri et al. (2005). The total analytical uncertainty of He ages of each aliquot is approximately  $\pm 10\%$  ( $2\sigma$ ), governed largely by uncertainty in blank corrections and spike concentrations. Correction for He recoil loss was made using procedures described in Farley (2002). Analyses of a Durango apatite standard aliquot (2 grains) yield  $33.1 \pm 0.7$  Ma, which is indistinguishable from mean Durango ages measured at SUERC ( $32.8 \pm 1.3$  Ma, Foeken et al. 2006) and reported Durango ages (e.g.  $32.1 \pm 1.7$  Ma, House et al. 2000).

### 4.4 Results of kinematic analyses

In the following only a summary of the Middle to Late Miocene tectonic evolution of the study area will be given (see Tischler et al. 2006

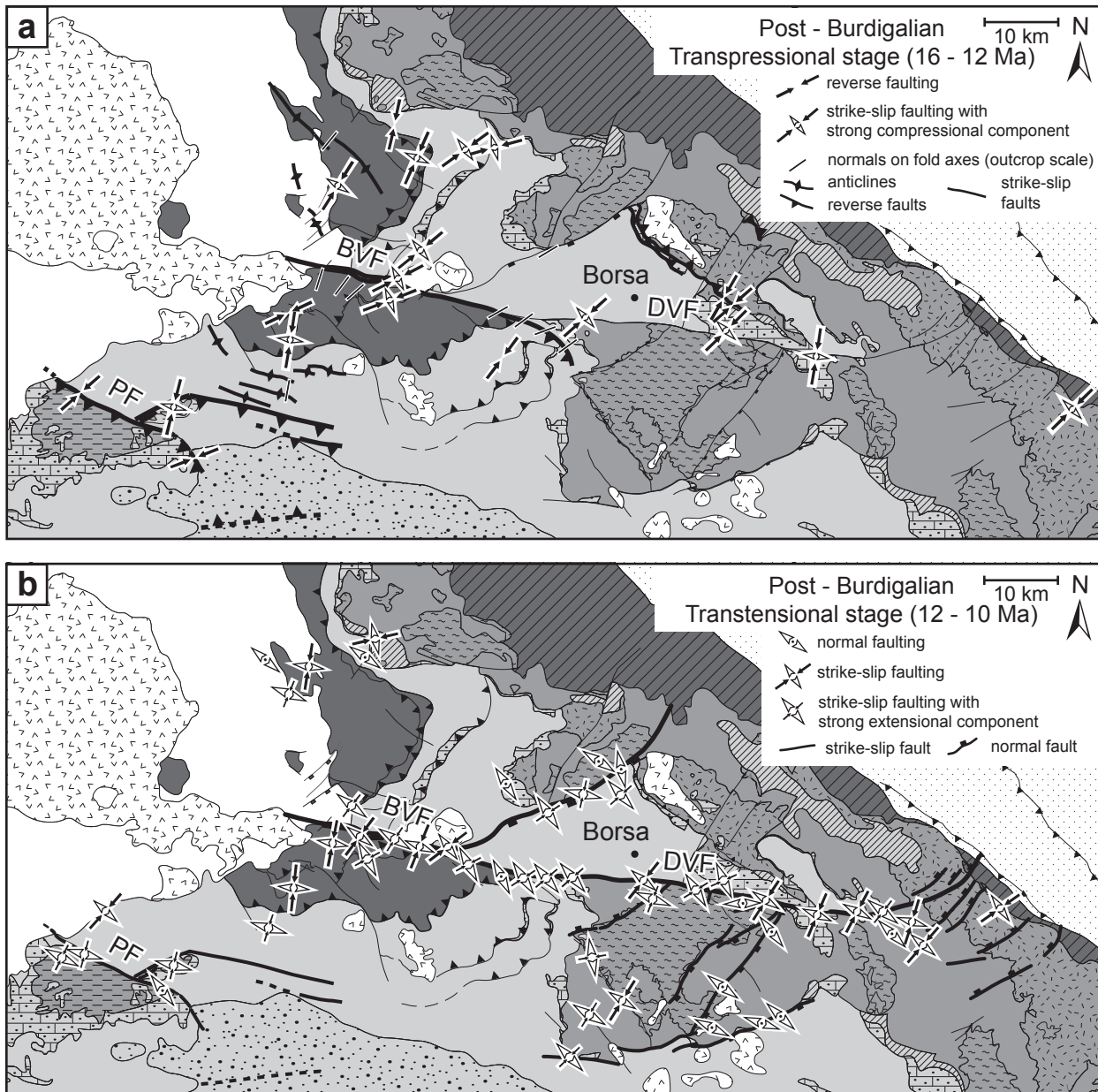


**Fig. 4.3.** Kinematics and structures related to the post-Burdigalian (16-10 Ma) tectonics in the study area (Tischler et al. 2006). The active structures are marked by thick lines (BVF = Bogdan-Voda fault, DVF = Dragos-Voda fault, PF = Preluca fault). A transpressional stage (a) precedes a transtensional stage (b), featuring constant SW-NE shortening. While the sinistral Bogdan-Voda fault is independently active during the transpressional stage (a), the Bogdan-Voda fault and Dragos-Voda fault are linked together during the transtensional stage (b).

for a detailed discussion). Two stages dominated by brittle sinistral strike-slip deformation are documented in the study area: Middle Miocene transpression (Fig. 4.3a), followed by Middle to Late Miocene transtension (Fig. 4.3b). During both stages shortening remained NE-SW oriented. The most obvious structures related to these stages are the E-W striking Bogdan-Voda fault (BVF) and the Dragos-Voda fault (DVF). The left lateral activity of the Bogdan-Voda fault is already apparent in map

view, as evidenced by the 25 km sinistral offset of the Burdigalian-age thrust contact of the Pienides (Fig. 4.3).

During the transpressional stage the Bogdan-Voda fault was active as a sinistral transpressive fault, terminating eastwards in a thrust splay geometry (Fig. 4.3a). Other major structures attributed to this first transpressional stage are NW-SE striking reverse faults (e.g. a back-thrust NE of Borsă), the Preluca fault (PF), as well as very open



NW-SE to WNW-ESE striking folds.

During the later transtensional stage (Fig. 4.3b) the Bogdan-Voda and Dragos-Voda faults both acted together as one single continuous fault. Sinistral offset along the so-called Bogdan-Dragos-Voda fault system (Tischler et al. 2006) diminishes eastwards and terminates in an extensional horsetail splay geometry. Additional features attributed to this second stage are SW-NE-striking normal faults, such as the Greben fault and numerous faults within the Rodna horst (Fig. 4.3b).

## 4.5 Results of the thermochronological analysis

### 4.5.1 Sampling approach

All sample localities are depicted in Fig. 4.4. The Preluca massif is covered by 4 samples (P1, P2,

P3, P4) while three samples are from an immediately adjacent smaller basement body located further to the NE (P5, P6, P7). The Maramures Mountains further to the NE have been sampled along two orthogonal profiles, yielding a total of 10 samples. One profile is orogen-perpendicular (samples M01, M02, M03, M04, M05); the other one crosses the Greben fault and the horsetail splay of the Bogdan-Dragos-Voda fault (samples M06, M08, M07, M09, M13, M14). In the area of the Rodna horst, located S of the Dragos-Voda fault, four vertical profiles have been sampled, each of them within a distinct fault-bounded block. Each profile comprises 5 to 6 samples (see groups of samples listed under R1, R2, R3 and R4 in Fig. 4.4). Additional samples have been collected within the central block of the Rodna horst and adjacent to the Dragos-Voda fault (sample group R5). The basement samples comprise mainly paragneisses and rarely orthogneiss.

**Table 4.1.** Zircon fission track data. All samples have been analysed using the external detector method (Gleadow 1981) with a zeta value (Hurford and Green 1983) of  $141.40 \pm 6.33$  (Fish Canyon Tuff standard, CN1).

Code	Latitude	Longitude	Alt. [m]	N Grains	Ps [ $\times 10^5 \text{ cm}^{-2}$ ]	Ns	Pi [ $\times 10^5 \text{ cm}^{-2}$ ]	Ni	Pd [ $\times 10^5 \text{ cm}^{-2}$ ]	Nd	X <sup>2</sup> [%]	Central Age $\pm 1\sigma$ [Ma]
M01	24.496670	47.729790	540	10	176.37	1291	49.32	361	3.85	3065	34	96.6 $\pm$ 7.6
M02	24.560710	47.753720	580	4	109.39	367	30.10	101	3.77	3065	13	95.7 $\pm$ 13.5
M03	24.586640	47.772540	630	20	86.88	1468	35.45	599	5.80	3605	81	99.7 $\pm$ 6.8
M04	24.628100	47.791450	680	10	70.07	436	30.54	190	5.97	3605	84	96.1 $\pm$ 9.5
M05	24.667090	47.804300	745	20	98.44	2366	37.20	894	5.86	3605	<5	107.5 $\pm$ 7.4
M06	24.698590	47.790850	790	20	129.07	2543	33.35	657	5.91	3605	<5	162.3 $\pm$ 13.0
M08	24.770543	47.690263	820	20	123.09	2703	52.32	1149	3.69	3065	<5	61.3 $\pm$ 4.7
M09	24.833619	47.647505	1660	20	126.15	2501	32.18	638	3.50	3065	22	96.2 $\pm$ 6.5
M13	25.128220	47.571246	930	14	253.89	1812	58.71	419	3.54	3065	23	107.6 $\pm$ 8.5
M14	25.279510	47.478662	850	20	137.67	2830	30.60	629	3.38	3065	<5	107.0 $\pm$ 9.1
P1	23.574760	47.430957	315	14	79.60	1010	25.22	320	3.73	3065	55	82.8 $\pm$ 6.6
P2	23.628772	47.509842	215	16	155.74	1919	47.40	584	3.42	3065	38	78.8 $\pm$ 5.6
P3	23.686807	47.488712	610	35	128.38	3336	40.87	1062	3.81	3065	<5	84.5 $\pm$ 5.5
R1-1	24.559360	47.597860	1550	17	91.73	996	31.13	338	3.46	2967	25	71.8 $\pm$ 6.1
R2-2	24.597260	47.414920	1105	20	80.41	981	32.38	395	5.74	3605	78	100.1 $\pm$ 7.6
R2-4	24.590430	47.419300	705	26	115.20	2312	34.43	691	3.52	2967	12	82.8 $\pm$ 5.9
R3-1	24.620652	47.533782	2020	20	188.30	2550	55.68	754	3.35	3065	47	79.5 $\pm$ 5.1
R3-2	24.582850	47.423290	1465	20	74.15	1642	39.02	864	6.25	3605	62	83.0 $\pm$ 5.5
R3-3	24.608990	47.528930	1310	13	76.26	842	38.77	428	6.20	3605	37	85.6 $\pm$ 6.8
R3-4	24.604450	47.526330	1155	7	94.77	607	60.11	385	6.14	3605	50	68.1 $\pm$ 5.5
R3-6	24.587980	47.518690	945	20	92.24	934	49.77	504	6.03	3605	11	78.5 $\pm$ 6.4
R4-3	24.941010	47.494710	980	2	116.94	107	37.16	34	3.62	3065	86	80.0 $\pm$ 16.2
R4-4	24.960230	47.490430	700	20	134.72	1923	45.89	655	3.69	3065	<5	77.0 $\pm$ 5.8
R5-1	24.546451	47.552021	1150	8	204.11	635	57.54	179	3.46	3065	47	86.2 $\pm$ 8.4
R5-4	24.872870	47.596160	1270	20	161.18	2517	50.33	786	3.58	3065	10	81.2 $\pm$ 5.5

**Code:** sample code; **Latitude:** Latitude in WGS84; **Longitude:** Longitude in WGS84; **Alt. [m]:** altitude above sea level; **N Grains:** number of grains counted; **Ps [ $\times 10^5 \text{ cm}^{-2}$ ]:** spontaneous track density; **Ns:** number of spontaneous tracks counted; **Pi [ $\times 10^5 \text{ cm}^{-2}$ ]:** induced track density; **Ni:** number of induced tracks counted; **Pd [ $\times 10^5 \text{ cm}^{-2}$ ]:** standard track density; **Nd:** number of standard tracks counted; **X<sup>2</sup> [%]:** Chi-square probability (Galbraith 1981). **Central Age  $\pm 1\sigma$  [Ma]:** zircon fission track central age (Galbraith and Laslett 1993).

A last group of samples has been taken from sedimentary formations. The samples S2, S4 and S5 are from sedimentary units of the Pienides while S1 and S3 are from the post-tectonic Palaeogene to Early Miocene autochthonous cover of Tisza-Dacia (Late Oligocene Borsa sandstone). Samples have been taken from fine-grained sandstone horizons.

#### 4.5.2 Zircon FT data

The zircon FT data are reported in Table 4.1. Zircon fission tracks were largely reset during the Cretaceous metamorphic overprint, associated with nappe stacking of the basements units.

The zircon fission track central ages of the Preluca massif and the Rodna horst range between 68.1 and 100.1 Ma (Fig. 4.4). Most samples pass the Chi-Square test (Table 4.1,  $\chi^2 > 5\%$ ). The zircon single grain age distributions show clusters (Fig. 4.4c,d) that indicate Late Cretaceous cooling (mainly Coniacian to Campanian) after a thermal event that led to full annealing of zircon (Fig. 4.4c,d), i.e. an event associated with temperatures exceeding 300 °C.

Some basement samples from the Maramures Mountains, however, yielded Cenomanian central ages (95.7 to 99.7 Ma; M01, M02, M03, M04, M09; Fig. 4.4b) which also pass the Chi-Square test (Table 4.1,  $\chi^2 > 5\%$ ). Hence they indicate earlier (Cenomanian) cooling after full annealing of zircon. In the most external samples (M05, M06, M13, M14) the coexistence of Late Cretaceous and Palaeozoic single grain ages (oldest single grain 310 Ma, M06, App. 4.1) indicates that annealing was only partial and was followed by Late Cenomanian cooling (Fig. 4.4b). Sample M08 with a younger Tertiary (61.3 Ma) central age forms an exception amongst this group.

No zircon FT single grain ages younger than Eocene have been found in samples from the basement units. Hence, it can be excluded that substantial heating, reaching temperatures within the ZPAZ, did result from Palaeogene to Early Miocene burial.

#### 4.5.3 Apatite FT data

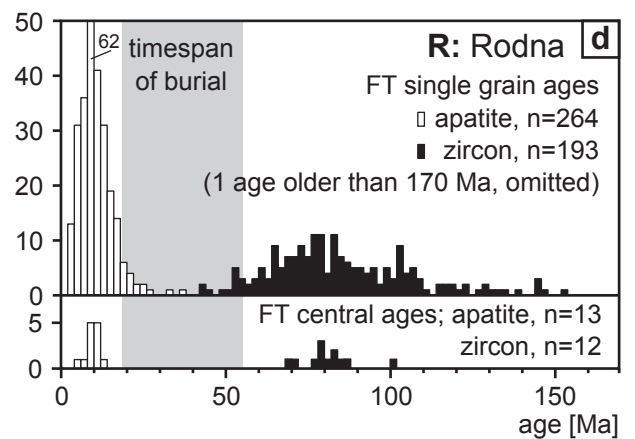
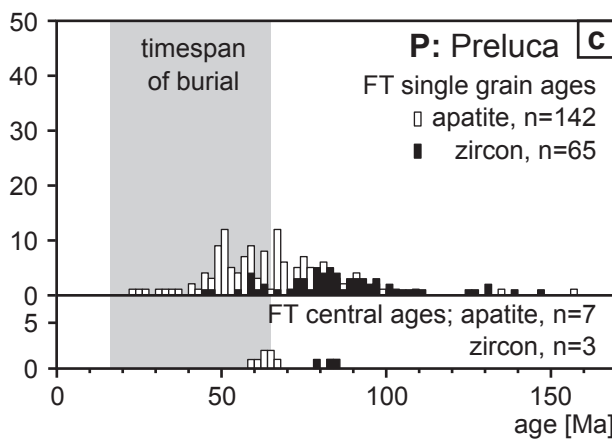
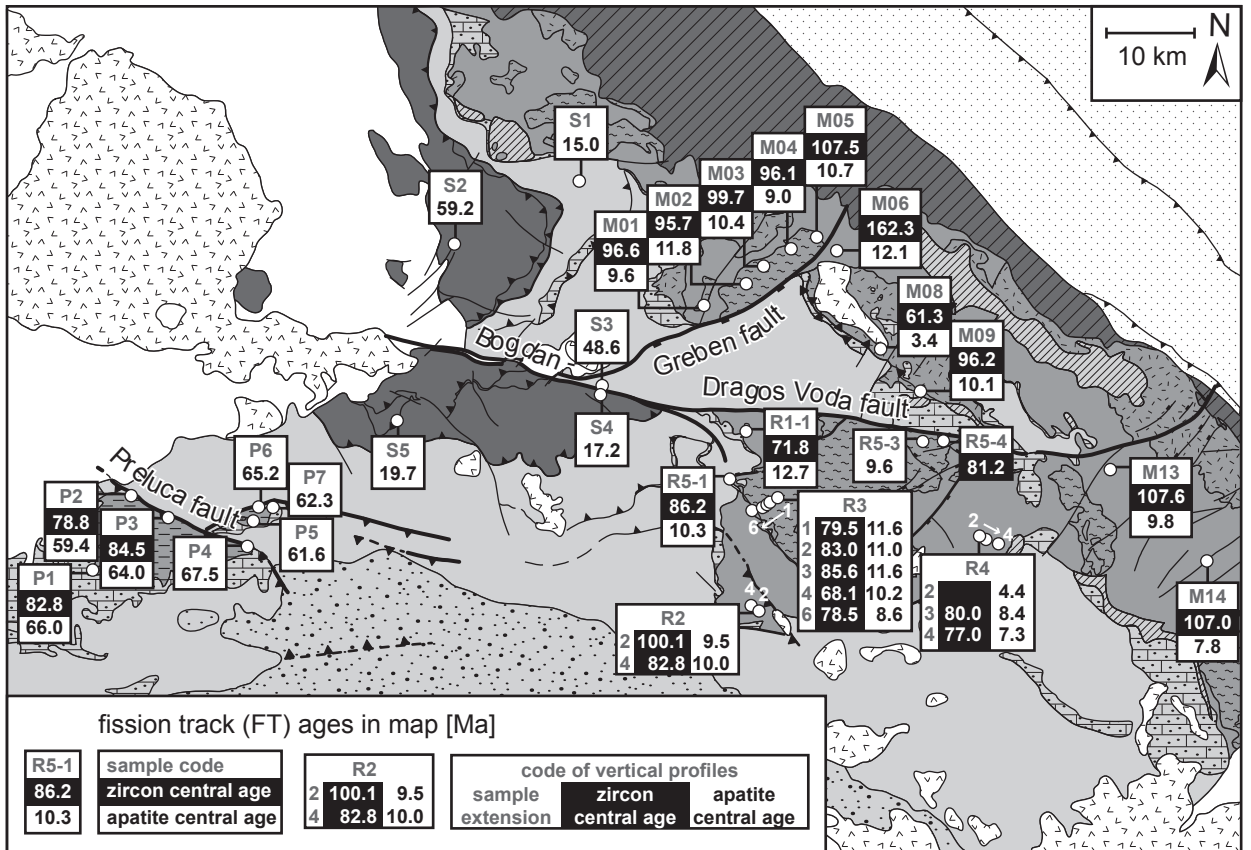
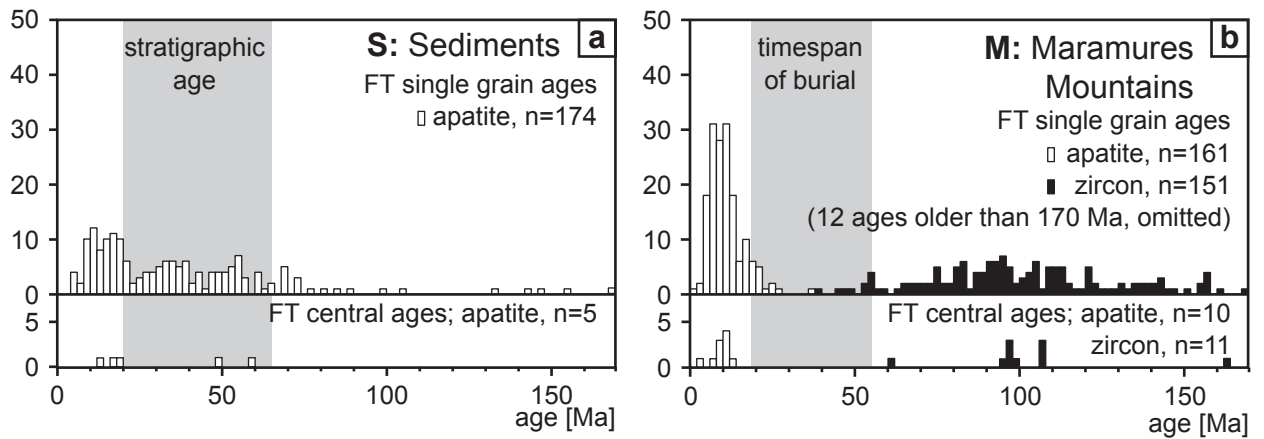
The apatite FT data are reported in Table 4.2. For the Preluca massif an overlap between zircon and apatite single grain ages is observed (Fig. 4.4c). This overlap indicates continued slow cooling from temperatures above 200 °C down to temperatures below the lower limit of the APAZ (60 °C). The apatite central ages in the Preluca massif range from 59.4 to 67.5 Ma (Fig. 4.4c). A close look at the single grain age distribution reveals weak evidence for the existence of two clusters (Fig. 4.4c). Possibly the earlier cluster is related to Late Cretaceous cooling before renewed sedimentation. The second cluster could indicate partial annealing during Palaeogene to Early Miocene burial. Although etch pit long axes in the Preluca samples spread by at least 1  $\mu\text{m}$  in each sample, suggesting compositional diversity, no clear correlation between etch pit long axis and single grain ages can be deduced (App. 4.2).

Three sedimentary samples (S1, autochthonous cover; S4 and S5, Pienides) show single grain ages that are younger than the stratigraphic age (Fig. 4.4a, App. 4.1). This indicates considerable post-depositional annealing. On the other hand samples S2 (Pienides) and S3 (autochthonous cover) show single grain ages older than the stratigraphic age (App. 4.1).

In case of the samples from the Maramures Mountains and the Rodna horst, however, Palaeogene to Early Miocene burial caused total annealing of all apatite fission tracks (Fig. 4.4b,d). Central ages range between 7.3 and 12.7 Ma and thus indicate Middle to Late Miocene cooling. Two samples even yielded younger (Pliocene) central ages (M08: 3.4 Ma; R4-2: 4 Ma), best interpreted as indicating thermal overprint during Neogene volcanic activity (Pécskay et al. 1995). This interpretation is supported by the unusually young zircon FT central age of sample M08 (Fig. 4.4).

Confined track lengths measurements (Table 4.2) were used for thermal modelling of the apatite data that will be discussed below. In case of the sedimentary samples the pre-depositional thermal history cannot be assumed to be identical for all

**Fig. 4.4. (next page)** Map indicating location of samples and results of the fission track analyses in terms of central ages, together with diagrams that summarize the single grain ages (a,b,c,d). In the sedimentary samples (a) the post-depositional thermal overprint caused strong annealing (S2, S4, S5), but also provenance ages are preserved (S1, S3). In the Bucovinian nappe stack (b,d), apatite grains have been fully reset by the Palaeogene to Early Miocene burial, while zircon remained thermally undisturbed. Overlapping single grain ages of zircon and apatite from the Preluca massif reflect continuous exhumation through the ZPAZ and APAZ during the Late Cretaceous (c).



constituent grains, hence confined track lengths were measured in dated grains only. In case of the basement samples a common thermal history of individual samples allows for length measurements also in the non-dated grains (up to a maximum of 100 lengths). Only a limited number of samples provided sufficient track length data because of the low track densities. All basement samples show unimodal track length distributions, with

mean values between 12.6 and 13.5  $\mu\text{m}$  (Table 4.2). Sedimentary samples only provided a few track lengths data, which makes a characterization of the length distribution difficult.

#### 4.5.4 Apatite (U-Th)/He data

The apatite (U-Th)/He data are reported in Table 4.3. In the Preluca massif these apatite (U-Th)/He ages scatter and do not replicate within  $2\sigma$

**Table 4.2.** Apatite fission track data. All samples have been analysed using the external detector method (Gleadow 1981) with a zeta value (Hurford and Green 1983) of  $355.96 \pm 9.39$  (Durango standard, CN5).

Code	Latitude	Longitude	Alt. [m]	N Grains	Ps [ $\times 10^5 \text{cm}^{-2}$ ]	Ns	Pi [ $\times 10^5 \text{cm}^{-2}$ ]	Ni	Pd [ $\times 10^5 \text{cm}^{-2}$ ]	Nd	X <sup>2</sup> [%]	Central Age $\pm 1\sigma$ [Ma]	N Length	Mean Length $\pm 1\sigma$ [ $\mu\text{m}$ ]
M01	24.496670	47.729790	540	25	0.49	73	112.21	16596	119.59	6511	10	9.6 $\pm$ 1.2	-	-
M02	24.560710	47.753720	580	20	0.94	114	138.73	16842	98.14	6511	32	11.8 $\pm$ 1.2	-	-
M03	24.586640	47.772540	630	15	1.12	64	148.09	8471	77.35	3606	55	10.4 $\pm$ 1.3	-	-
M04	24.628100	47.791450	680	20	1.29	129	35.66	3580	14.10	4605	58	9.0 $\pm$ 0.9	80	12.94 $\pm$ 2.21
M05	24.667090	47.804300	745	20	2.24	168	28.73	2155	7.74	4223	99	10.7 $\pm$ 0.9	100	12.98 $\pm$ 3.20
M06	24.698590	47.790850	790	3	0.51	10	87.59	1708	116.61	4196	39	12.1 $\pm$ 3.9	-	-
M08	24.770543	47.690263	820	2	0.98	4	43.90	180	8.52	4451	60	3.4 $\pm$ 1.7	-	-
M09	24.833619	47.647505	1660	16	0.53	31	90.19	5276	96.19	5773	99	10.1 $\pm$ 1.8	-	-
M13	25.128220	47.571246	930	20	0.44	64	8.57	1261	10.81	4451	99	9.8 $\pm$ 1.3	-	-
M14	25.279510	47.478662	850	20	1.34	152	32.43	3668	10.50	4451	26	7.8 $\pm$ 0.7	43	13.35 $\pm$ 2.12
P1	23.574760	47.430957	315	20	3.06	297	8.40	815	10.23	4223	65	66.0 $\pm$ 4.9	100	13.01 $\pm$ 2.54
P2	23.628772	47.509842	215	20	6.33	713	16.79	1892	8.93	4223	9	59.4 $\pm$ 3.7	100	12.98 $\pm$ 1.92
P3	23.686807	47.488712	610	20	6.93	671	18.18	1760	9.37	4223	<5	64.0 $\pm$ 4.6	100	12.86 $\pm$ 1.70
P4	23.810507	47.465312	350	22	1.09	150	26.93	3724	94.57	6511	43	67.5 $\pm$ 6.0	-	-
P5	23.817260	47.488947	390	20	18.13	2489	44.93	6169	8.50	4223	<5	61.6 $\pm$ 3.0	100	12.75 $\pm$ 1.23
P6	23.824540	47.503686	430	20	14.12	1028	37.89	2758	9.80	4223	<5	65.2 $\pm$ 4.0	100	12.62 $\pm$ 2.08
P7	23.846548	47.503894	380	20	4.84	456	15.72	1482	11.44	4451	94	62.3 $\pm$ 3.8	100	12.60 $\pm$ 1.90
R1-1	24.559360	47.597860	1550	20	0.58	41	11.86	837	14.55	4766	97	12.7 $\pm$ 2.1	-	-
R2-2	24.597260	47.414920	1105	20	0.41	63	93.25	14333	121.63	4196	92	9.5 $\pm$ 1.2	-	-
R2-4	24.590430	47.419300	705	20	0.52	51	108.36	10717	118.28	4196	88	10.0 $\pm$ 1.4	100	12.80 $\pm$ 2.65
R3-1	24.620652	47.533782	2020	24	4.41	539	65.71	8030	9.78	4451	8	11.6 $\pm$ 0.7	59	13.12 $\pm$ 2.79
R3-2	24.582850	47.423290	1465	20	2.55	357	54.69	7646	13.04	4766	10	11.0 $\pm$ 0.8	100	13.50 $\pm$ 2.20
R3-3	24.608990	47.528930	1310	20	2.48	496	48.58	9716	12.79	4766	13	11.6 $\pm$ 0.7	100	13.25 $\pm$ 2.31
R3-4	24.604450	47.526330	1155	20	0.38	50	8.30	1096	12.54	4766	99	10.2 $\pm$ 1.5	-	-
R3-6	24.587980	47.518690	945	20	0.94	111	15.89	1873	8.17	4223	79	8.6 $\pm$ 0.9	-	-
R4-2	24.931050	47.498160	1305	20	0.72	85	38.19	4499	13.00	4451	46	4.4 $\pm$ 0.5	-	-
R4-3	24.941010	47.494710	980	20	2.02	216	53.45	5730	12.48	4451	84	8.4 $\pm$ 0.6	64	12.81 $\pm$ 2.48
R4-4	24.960230	47.490430	700	20	0.89	73	26.52	2185	12.27	4451	95	7.3 $\pm$ 0.9	-	-
R5-1	24.546451	47.552021	1150	20	1.31	93	20.94	1487	9.26	4451	93	10.3 $\pm$ 1.1	-	-
R5-3	24.951870	47.550260	1400	20	3.02	218	51.72	3734	9.22	4557	8	9.6 $\pm$ 0.9	100	13.32 $\pm$ 2.45
S1	24.296360	47.854000	550	38	2.69	514	41.23	7884	12.91	4605	29	15.0 $\pm$ 0.9	15	13.68 $\pm$ 2.01
S2	24.111950	47.782210	350	39	9.25	1787	33.57	6489	10.97	4605	<5	59.2 $\pm$ 5.0	61	12.14 $\pm$ 2.09
S3	24.351650	47.641020	530	40	7.21	1500	32.93	6850	12.27	4605	<5	48.6 $\pm$ 3.0	35	12.47 $\pm$ 2.33
S4	24.348370	47.635130	555	21	1.61	174	21.52	2320	12.59	4605	12	17.2 $\pm$ 1.6	-	-
S5	24.030170	47.599060	555	36	1.48	242	129.53	21178	94.83	4196	<5	19.7 $\pm$ 2.2	19	10.08 $\pm$ 2.71

**Code:** sample code; **Latitude:** Latitude in WGS84; **Longitude:** Longitude in WGS84; **Alt. [m]:** altitude above sea level; **N grains:** number of grains counted; **Ps [ $\times 10^5 \text{cm}^{-2}$ ]:** spontaneous track density; **Ns:** number of spontaneous tracks counted; **Pi [ $\times 10^5 \text{cm}^{-2}$ ]:** induced track density; **Ni:** number of induced tracks counted; **Pd [ $\times 10^5 \text{cm}^{-2}$ ]:** standard track density; **Nd:** number of standard tracks counted; **X<sup>2</sup> [%]:** Chi-square probability (Galbraith 1981). **Central Age  $\pm 1\sigma$  [Ma]:** apatite fission track central age (Galbraith and Laslett 1993). **N length:** number of confined track lengths measured; **Mean Length  $\pm 1\sigma$  [ $\mu\text{m}$ ]:**

**Table 4.3.** Apatite (U-Th)/He data. Analyses of one Durango apatite aliquot (2 grains) yield  $33.1 \pm 0.7$ .

Code	4He [cc STP]	U238 [ng]	Th232 [ng]	Th/U	(U-Th)/He Age [Ma]	Ft	Corrected (U-Th)/He Age [Ma]	Error 2 $\sigma$	FT Central Age $\pm 1\sigma$ [Ma]
P3-I	4.29E-11	0.015	0.009	0.6	20.5	0.68	30.1	3.0	64.0 $\pm$ 4.6
P3-II	4.75E-11	0.025	0.018	0.7	13.4	0.69	19.3	1.9	
P4-I	5.79E-11	0.054	0.027	0.5	7.9	0.82	9.6	1.0	67.5 $\pm$ 6.0
P4-II	9.21E-11	0.014	0.045	3.2	30.6	0.80	38.3	3.8	
R2-4-I	1.54E-10	0.114	0.030	0.3	10.4	0.78	13.3	1.3	10.0 $\pm$ 1.4
R2-4-II	7.55E-11	0.058	0.027	0.5	9.6	0.80	12.0	1.2	
R3-2-1	8.00E-10	0.657	0.033	0.0	9.8	0.76	12.9	1.3	11.0 $\pm$ 0.8

**Code:** sample code; **4He [cc STP]:** concentration of 4He; **U238 [ng]:** concentration of U238; **Th232 [ng]:** concentration of Th232; **Th/U:** Th232/U238 ratio; **(U-Th)/He Age [Ma]:** (U-Th)/He Age [Ma]; **Ft:** correction of  $\alpha$ -recoil (Farley 2002); **Corrected (U-Th)/He Age [Ma]; Error 2 $\sigma$ ;**

**FT Central Age  $\pm 1\sigma$  [Ma]:** apatite fission track central age (Galbraith and Laslett 1993).

error. While the replicate of sample P4-II had small zircon inclusions and was therefore excluded, sample P3 and P4 both yielded apatite (U-Th)/He ages that are younger than the apatite FT single grain ages. Replicate ages from the Rodna massif yielded 12.0–13.3 Ma, which are, within 2 $\sigma$  error, indistinguishable from the accompanying apatite FT ages. This suggests fast cooling for the last stages of exhumation of the Rodna horst.

#### 4.6 Thermal modelling of the apatite FT data

Thermal modelling used the apatite single grain ages and the confined track lengths as input data (Fig. 4.5). Additionally, time-temperature (t-T)

constraints, independent from the apatite FT data, are incorporated. The t-T-paths are modelled using the software AFTSolve (version 1.3.0, Ketchum et al. 2000) with the annealing model of Laslett et al. (1987). Modelling was done inverse monotonic with 10 000 runs for each model, using a Monte Carlo modelling scheme. Initial track length was 16.3  $\mu\text{m}$  with a length reduction in age standard of 0.890. All models were run twice in order to identify reproducible trends.

In case of the basement samples such independent t-T-constraints are given by the zircon FT central ages obtained on the same sample (or samples close-by) and the age of the unconformably overlying sediments. In case of the Preluca massif the time of maximum burial can also be

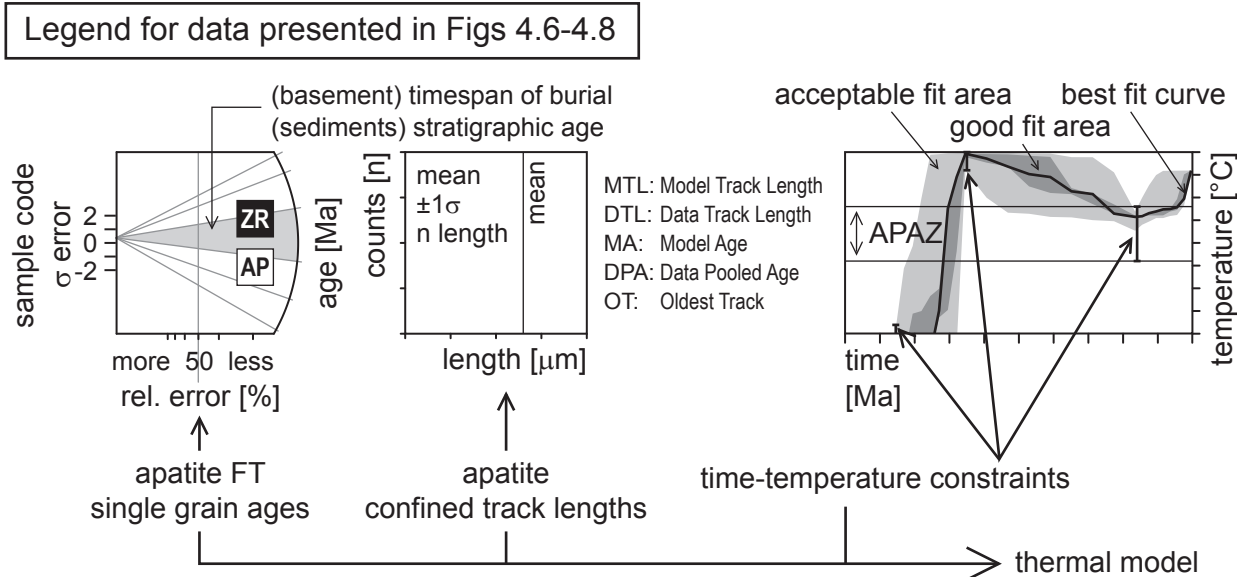


**Fig. 4.5.** Diagram explaining the thermal modelling of apatite FT data. This figure also serves as a legend for Figures 4.6-4.8. The single grain ages and the confined track lengths provide input data. Using additional independent constraints (e.g. zircon FT data, stratigraphic information), t-T-paths fitting the data are modelled.

constrained by assuming it to coincide with the end of Burdigalian sedimentation (Hida beds: 16 Ma). In the Bucovinian nappe stack maximum burial temperatures are assumed to have been reached by a combination of sedimentary and tectonic burial during imbrication of the autochthonous sediments related to thrusting of the Pienides (18.5 Ma, Tischler et al. 2006).

Regarding the sedimentary samples one t-T-constraint is given by the stratigraphic age of the dated sediment (Săndulescu & Russo-Săndulescu 1981; Săndulescu et al. 1991; Aroldi 2001). Interestingly a pre-Tertiary heating event has to be assumed in order to allow for the modelling of samples S2 and S3. The timing of maximum burial of the samples from the Pienide nappes (S2 and S5) is inferred to immediately pre-date nappe emplacement (20 Ma, Tischler et al. 2006), since erosion of the Pienides during thrusting is indicated by the deposition of a Burdigalian clastic

wedge. In case of the autochthonous cover (samples S1 and S3), the overthrusting of the Pienides is considered to have caused additional burial. Hence it was assumed that maximum temperatures were reached at the end of nappe emplacement (18.5 Ma, Tischler et al. 2006).

In case of the Preluca massif Palaeogene to Early Miocene burial caused partial annealing of apatite (Fig. 4.6). Late Cretaceous to Early Tertiary cooling is constrained by the zircon FT data and by the sedimentary unconformity. Thermal modelling suggests an increase of maximum temperatures from around 60°C (P1) in the SW to around 80°C in the NE (P5, P7), interpreted in terms of an increasing amount of burial towards the NE. The modelled maximum temperature near the Preluca fault (sample P3, 69°C) in the upper part of the apatite helium partial retention zone is in good agreement with full (P4) and partial (P3) retention of helium, as is indicated by the (U-Th)/He data.

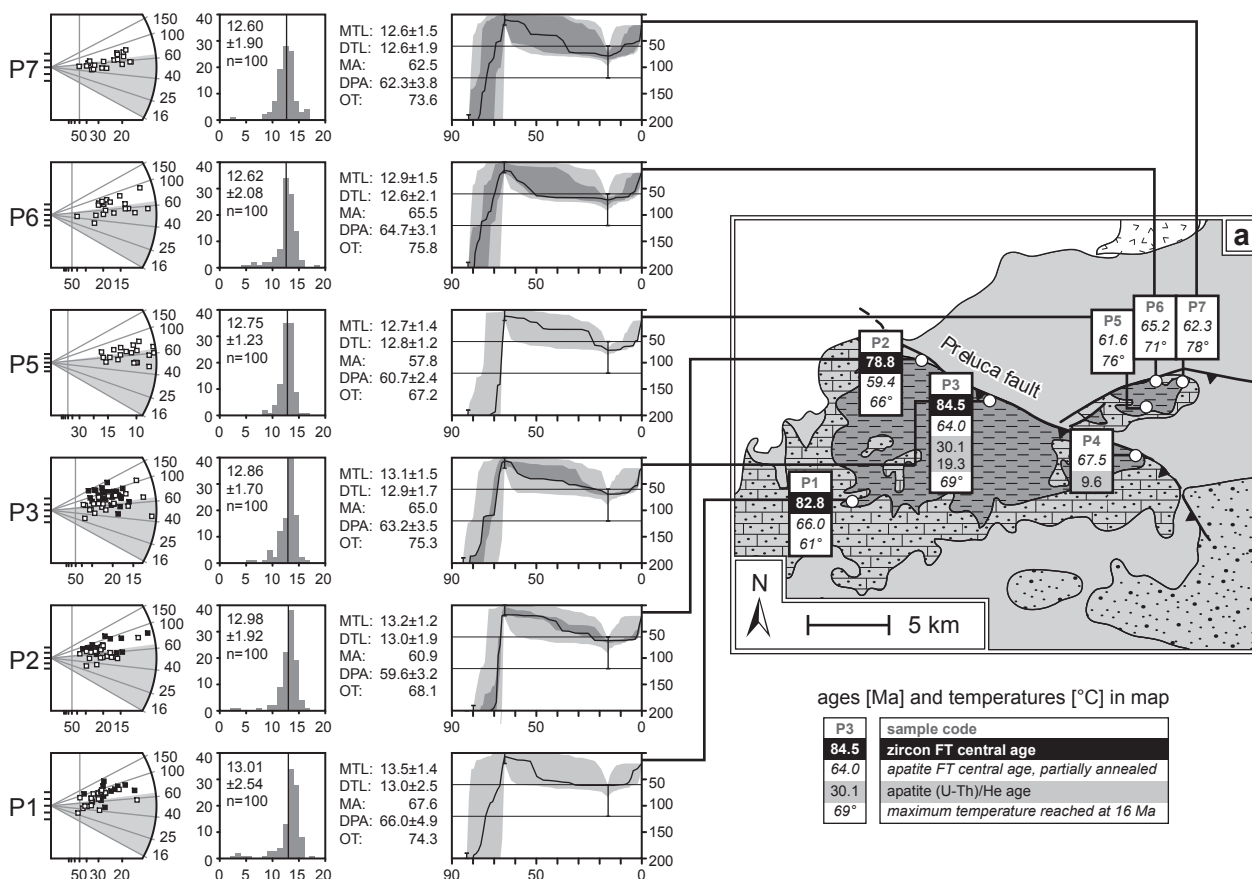


**Fig. 4.6.** Thermal modelling of apatite FT data in the Preluca massif. All radial plots (Galbraith 1990) show the same age spectrum to allow for direct comparison. Burial heating by the deposition of Palaeogene to Early Miocene sediments caused partial annealing of fission tracks in apatite. The models slightly indicate a deepening in burial by sedimentation from the SW to the NE, reflected by the increasing maximum temperatures modelled (a). The temperatures reached at the Preluca fault (69°C) are confirmed by partial (P3) and full retention (P4) of He in apatite.

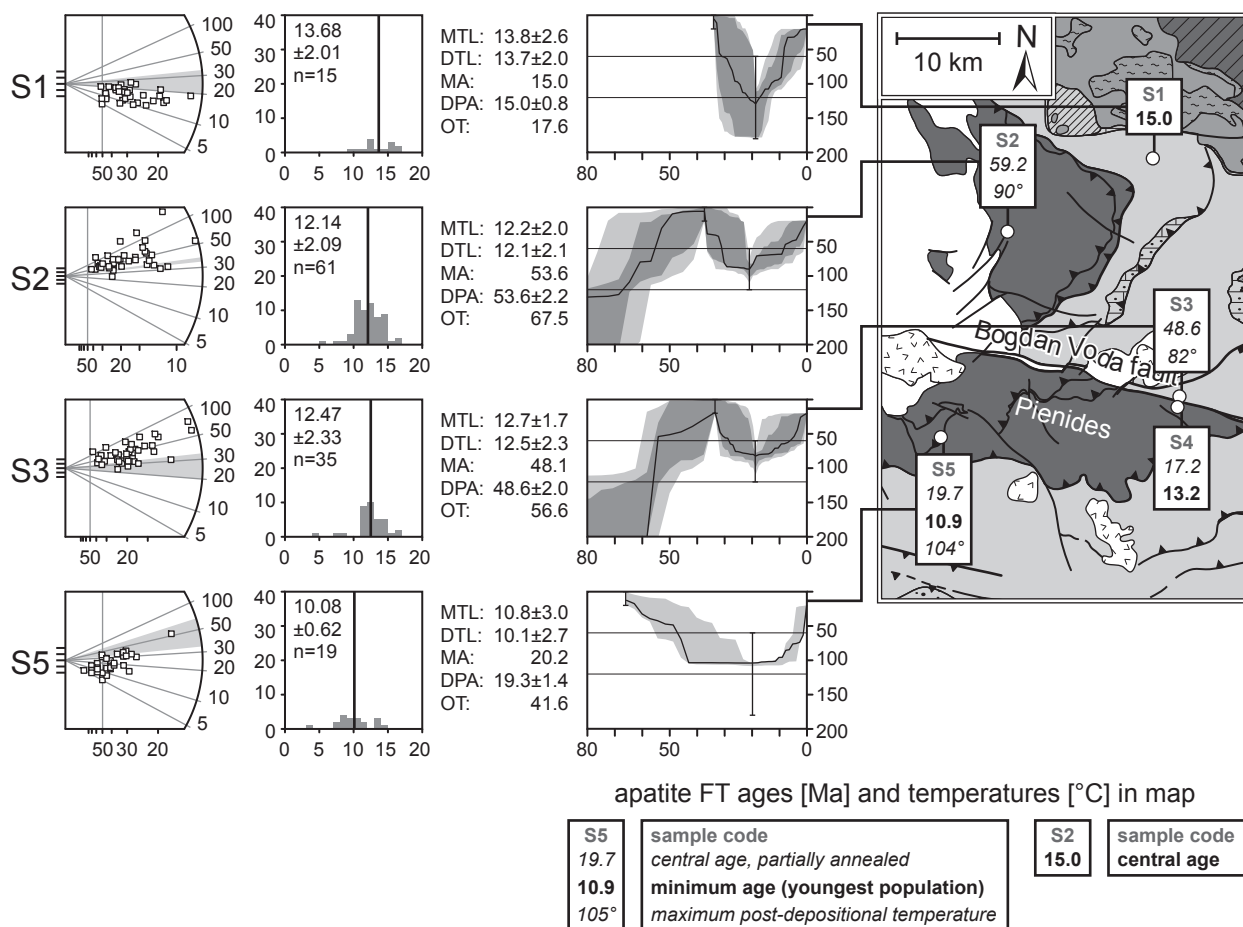


**Fig. 4.7.** Thermal modelling of apatite FT data from the sedimentary units. All radial plots (Galbraith 1990) show the same age spectrum to allow for direct comparison. All samples show at least post-depositional partial annealing of fission tracks in apatite; S1 has been fully annealed after deposition. Due to strong annealing in S4 and S5 minimum ages of the youngest populations were calculated. These minimum ages and the central age of S1 indicate Middle to Late Miocene cooling.

For samples S2 and S3 thermal modelling indicates heating to temperatures within the APAZ, followed by slow cooling (Fig. 4.7). The thermal history of S1, on the other hand, is characterized by fast heating to temperatures above the APAZ directly preceding fast cooling to temperatures within the APAZ. This short-lived thermal-pulse is most likely related to the overthrusting by the Pienides. The thermal modelling of sample S5 shows that cooling from maximum temperatures occurred after 10 Ma (Fig. 4.7). The youngest grain populations in the strongly annealed samples south of the Bogdan-Voda fault indicate cooling during the Middle (S4: 13.2 Ma) and Late Miocene (S5: 10.9 Ma).

In the case of the Bucovinian nappe stack the exhumation and burial history before 18.5 Ma was also modelled for all samples. However, due to the complete annealing of pre-Miocene apatite fission tracks, the track parameters are only sensitive

regarding the final stages of exhumation (Fig. 4.8). The complete cooling paths, including the pre-Tertiary history, are only depicted for sample M14 (exemplary for the Maramures mountains, Fig. 4.8a) and for R5-3 (exemplary for the Rodna horst, Fig. 4.8b). Both the zircon FT data and a sedimentary unconformity constrain Late Cretaceous to Eocene cooling in the Rodna horst. In the Maramures Mountains, however, the basement has already been exhumed in Cenomanian times. After maximum burial and heating at 18.5 Ma most samples enter the upper limit of the APAZ between 15 and 12 Ma before present, and enhanced cooling occurred generally between 10 and 7 Ma.

#### 4.7 Revealing the Miocene exhumation history of the Rodna horst

By integrating information provided by the available geological maps (Kräutner et al. 1978, 1982,

1983, 1989) and by constructing schematic cross sections (Fig. 4.9c,d), the progressive exhumation of a more internal part of the Bucovinian nappe stack, the Rodna horst, will now be discussed in four time slices (Fig. 4.10). The schematic cross section 1 (Fig. 4.9c) depicts reverse vertical faulting and open folding (5% profile parallel shortening) related to

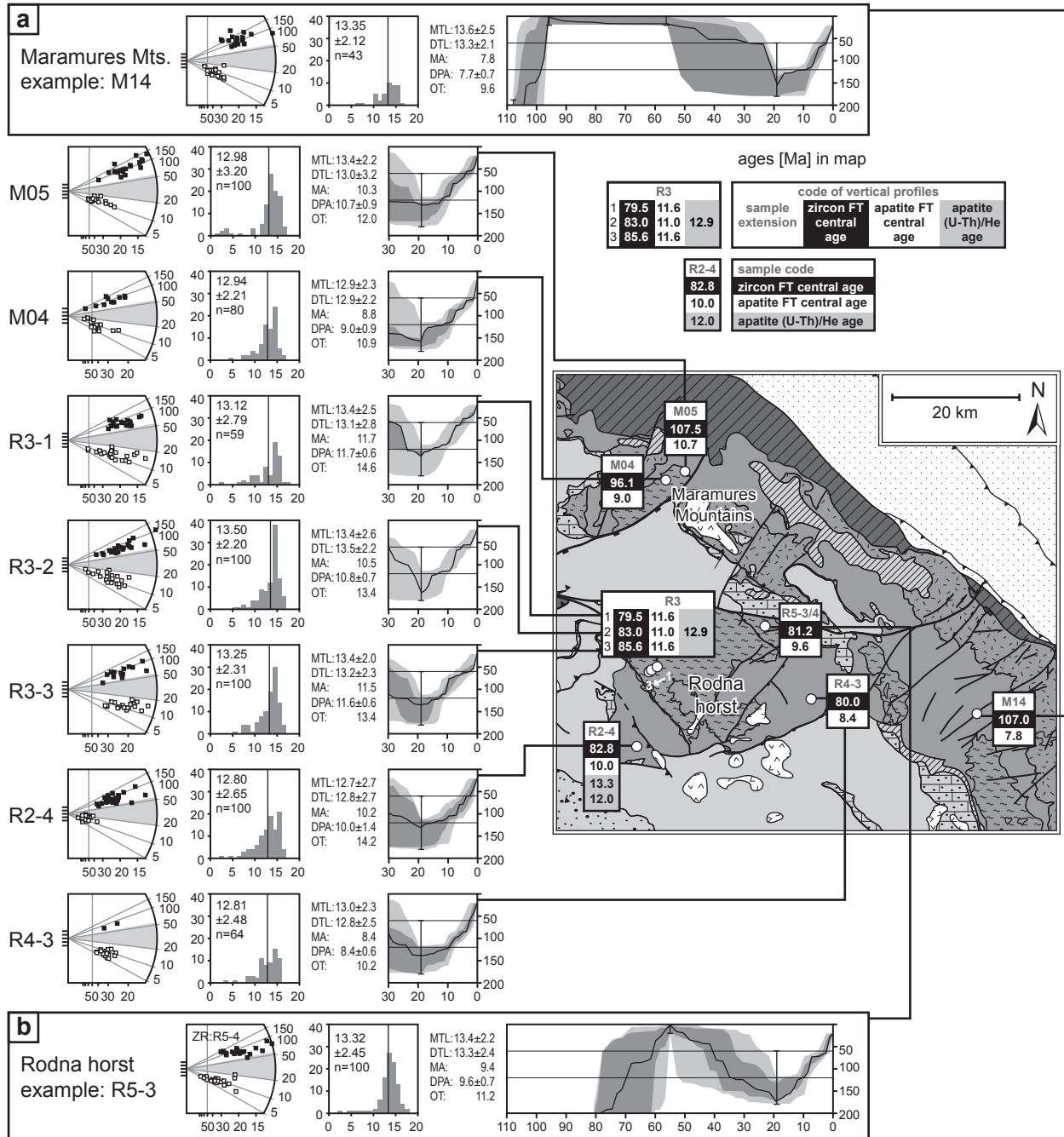
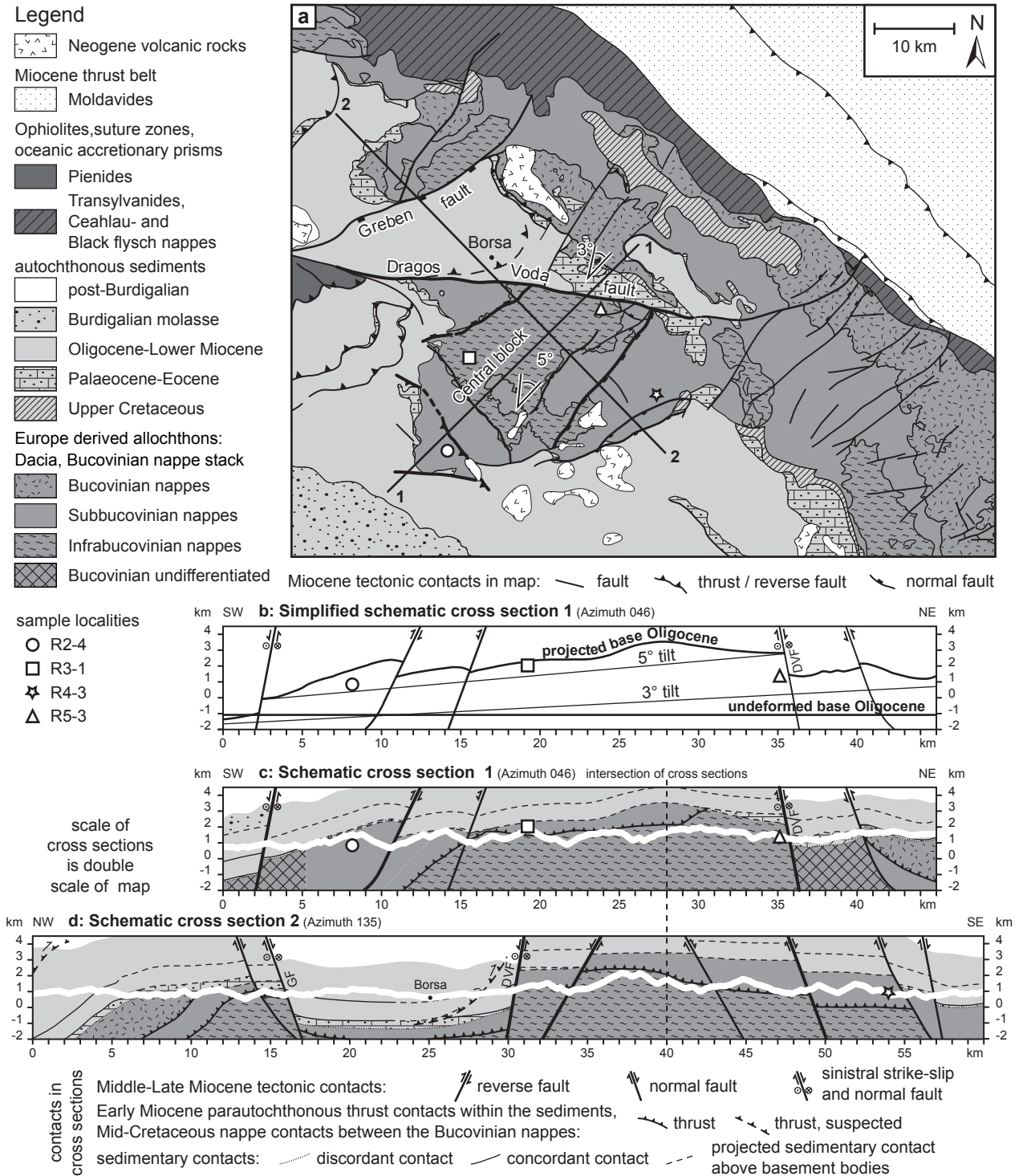


Fig. 4.8. Thermal modelling of samples from the Bucovinian nappe stack. All radial plots (Galbraith 1990) show the same age spectrum to allow for direct comparison. Because apatite has been fully annealed during Palaeogene to Early Miocene burial, the modelled  $t$ - $T$  paths are tightly constrained only for the last stages of Miocene exhumation. Therefore, the results of the complete modelling, starting in the Cretaceous, are only given for the samples M14 (a) and R5-3 (b), which serve as examples for the Maramures mountains and the Rodna horst respectively.





**Fig. 4.9.** Map (a) and schematic cross sections (b,c,d) through the Bucovinian nappe stack in the study area. Schematic cross section 1 (c) documents reverse faulting and open folding during the Middle Miocene transpressional stage, while section 2 (d) documents extension by normal faulting during the Middle to Late Miocene transtensional stage. The base of the Oligocene shows a general tilt towards the SW by approximately 3° (b). Along the central block of the Rodna horst, the tilt to the SW increases to 5°, realised along two normal faults delimiting this block by an increasing offset towards the Dragos-Voda fault (a). The suspected thrust at Borsa is drawn after Săndulescu pers. comm. 2002 ("Duplicature de Borsa").

the post-Burdigalian transpressional stage. In the perpendicular cross section 2, however, normal faulting related to the subsequent transtensional stage is more evident (Fig. 4.9d, 7% profile parallel extension). In section 1 the base Oligocene is tilted to the SW by some 3°, locally reaching up to 5° in the central block of the Rodna horst (Fig. 4.9b). Lines indicating 5° and 3° tilt are given for comparison in Fig. 4.9b. Two SW-NE striking normal faults (Fig. 4.9a), delimiting the central block, allow for this additional tilting. Offset across these normal faults increases towards the Dragos-Voda fault. This indicates that tilting occurred predominantly during the transtensional stage since deformation related to the transtensional stage dominates along the Dragos-Voda fault segment, delimiting the Rodna horst towards the north.

In the following, vertical movements predicted by structural observations are integrated with results from apatite FT thermal modelling in order to reconstruct the exhumation history of the Rodna horst. Relative uplift visible in cross sections 1 and 2 (Fig. 4.9c,d) is estimated and correlated with Middle to Late Miocene brittle tectonics which occurred between 16 and 10 Ma ago (Tischler et al. 2006). Timing and amount of these vertical movements (Fig. 4.10, column B) are then directly compared to the modelled best-fit t-T-paths inferred from apatite FT data obtained from the Rodna horst (Fig. 4.10, column C).

The undeformed base of the Oligocene deposits is used as a reference for differential tectonic uplift (Fig. 4.9b; Fig. 4.10, column B) and is defined as the null datum for the starting point at 20 Ma ago (Fig. 4.10Ba). All the subsequent time slices (Fig. 4.10Bb to Bd) show this reference plane (“undeformed base Oligocene”) for comparison.

#### *20 to 16 Ma time slice (Fig. 4.10, Row a)*

This time slice shows the relative altitudes of the samples before the onset of Miocene brittle deformations 16 Ma ago (Tischler et al. 2006). The geological cross sections (Fig. 4.9c,d) allow for an estimate of the original position of the samples relative to the base Oligocene (reference plane “undeformed base Oligocene”) at the following relative altitudes in Fig. 4.10Ba: R2-4 at -800 m, R3-1 at -200 m, R4-3 at -1000 m and R5-3 at -1400 m. The modelled t-T-paths inferred from apatite FT data show that no significant cooling occurred before 16 Ma. All samples remain at temperatures above the APAZ (Fig. 4.10Ca).

#### *16 to 12 Ma time slice: Transpressional stage (Fig. 4.10, Row b)*

During this transpressional stage, three tectonic features influencing tectonic uplift can be identified in cross section 1 (Fig. 4.9c):

1) Reverse faulting affects the SW corner of the Rodna horst. This reverse faulting influences only sample R2-4, situated in a hanging wall position.

2) Tilting is interpreted to play a subordinate role during the transpressional stage. Out of a total amount of 5°, only about 1° is assumed to have commenced between 16 and 12 Ma. The amount of relative uplift during tilting is estimated along cross section 1, and is given by the vertical distance between a horizontal line and a line tilted 1° towards the SW, intersecting at the southern boundary fault of the Rodna horst (Fig. 4.9a). This vertical distance has been measured at the respective sample locations in section 1. The projected position of sample R4-3 is at the intersection of both sections.

3) Additional relative tectonic uplift is realized by open folding in the cases of samples R3-2 and R4-3 in an anticlinal position, while R5-3 is situated in a synclinal position. The effect of open folding has been estimated by constructing the distance of the sample location to a tangent onto the synclines.

From the relative position of the specimens at the end of this stage (Fig. 4.10Bb) the following amounts of tectonically induced relative uplift can be deduced for this stage: +1300 m for R2-4, +1000 m for R3-1, +1000 m for R4-3 and +600 m for R5-3. Note that R2-4 and R3-1 are above the reference line at the end of this stage.

The uplift produced during the transpressional stage relative to the reference line base Oligocene causes a phase of slow cooling visible in the t-T-paths (16 to 11 Ma interval in Fig. 4.10Cb). R3-1 and R2-4 enter the APAZ at very low cooling rates (cooling paths with a gradient of about 2.5 °C/Ma), while R4-3 and R5-3 remain at higher temperatures.

#### *12 to 10 Ma time slice: Transtensional stage (Fig. 4.10, Row c)*

Normal and strike-slip faulting, together with 4° SW tilting led to variable amounts of relative tectonic uplift during this transtensional stage. Firstly the amount of uplift produced by this tilting (4°) is estimated. Secondly an additional uplift of the whole tilted block, as documented by an offset at its southwestern boundary fault, was applied. The amount of relative uplift for sample R4-3 is derived from its position projected into cross-

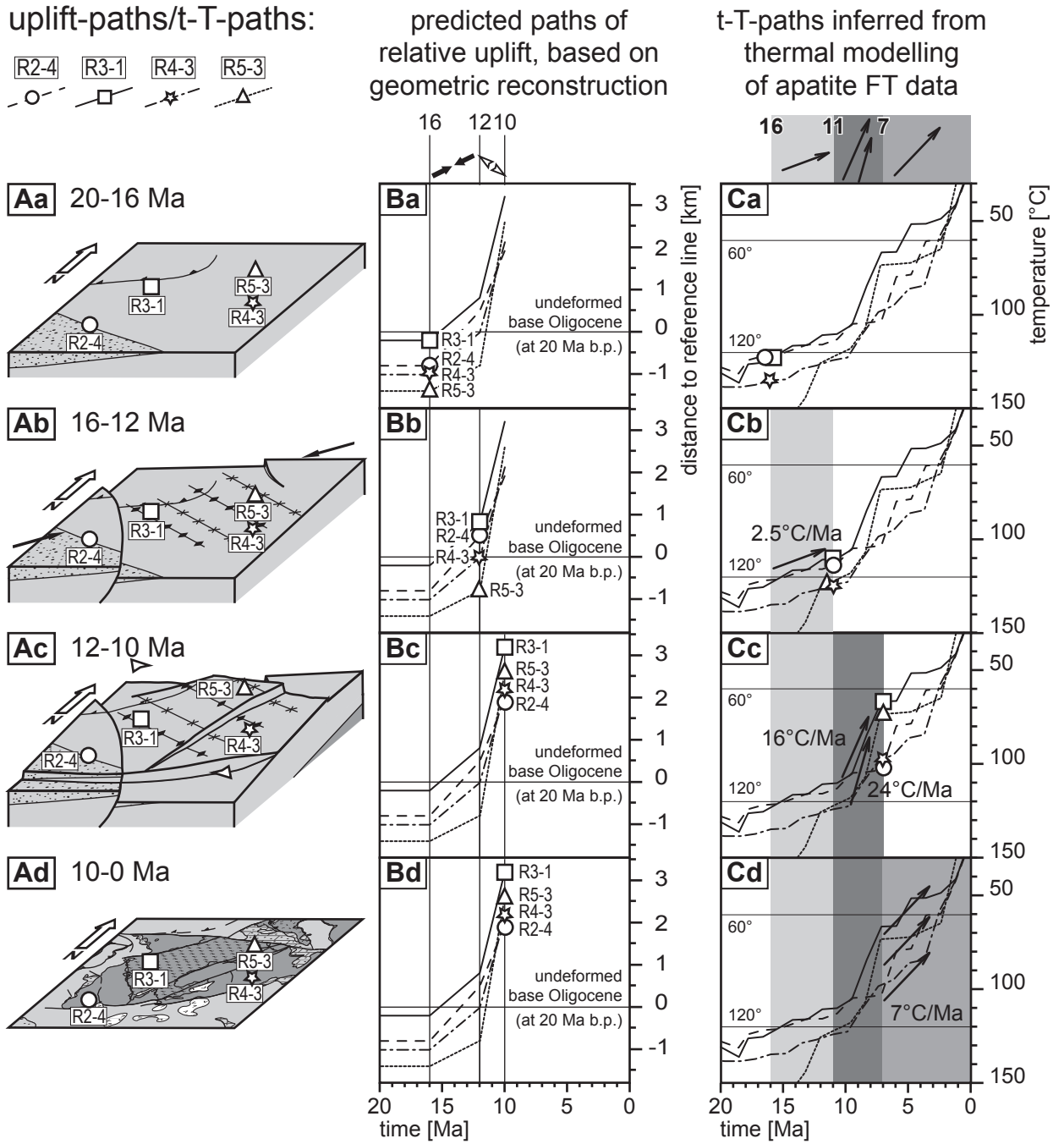


**Fig. 4.10.** Direct comparison of unscaled and schematic tectonic sketches (Column A), relative tectonic uplift paths (Column B) and cooling paths (best fit of 10000 runs) inferred from thermal modelling of apatite FT data (Column C) in the Rodna horst, from top to bottom, four subsequent time intervals (see column A). Amounts of relative tectonic uplift are estimated in respect to the undeformed base Oligocene (Fig. 4.9b). Greyscale in column C denotes time intervals and associated changes in the rate of cooling (dark = fast cooling).

section 1, corrected for normal faulting visible in cross section 2. The tectonic uplift produced during this transtensional stage relative to the reference line (Fig. 4.10Bc) amounts to: +1400 m for R2-4, +2400 m for R3-1, +2200 m for R4-3 and +3400 m for R5-3. The relatively greater uplift values deduced for R3-1 and R5-3 result in their higher position relative to R2-4 and R4-3.

Relative tectonic uplift and erosion during the transtensional stage result in a phase of enhanced exhumation and cooling visible in the t-T-paths (11 to 7 Ma interval of Fig. 4.10Cc). R5-3 enters and nearly crosses the APAZ at high cooling rates (the cooling path indicates 24 °C/Ma). At the end of this phase of enhanced cooling R3-1 and R5-3 are at the lower limit of the APAZ, while R2-4 and

R4-3 remain at higher temperatures. The relatively high cooling rates associated with this extensional stage resulted in Middle to Late Miocene apatite FT central ages in the Rodna horst.

*10 to 0 Ma time slice (Fig. 4.10, Row d):*

After cessation of the tectonic activity at 10 Ma (Tischler et al. 2006) the samples reached their present day altitude relative to the “undeformed base Oligocene” (Fig. 4.10Bd) at the following relative altitudes: +1900 m for R2-4, +2600 m for R5-3, +2200 m for R4-3 and +3200 m for R3-1. Final cooling to surface temperatures was associated with medium cooling rates of about 7 °C/Ma according to the cooling paths (Fig. 4.10Cd).

#### 4.7.1 Summary of the Miocene exhumation history deduced for the Rodna horst

The Miocene cooling and exhumation observed in the Rodna horst is the result of a combination of tectonic uplift and erosion. Relative tectonic uplift during the transpressional stage (16 to 12 Ma), together with exhumation by erosion, allowed for the observed slow cooling (16 to 11 Ma). The transtensional stage (12 to 10 Ma), however, is reflected in a phase of enhanced cooling (11 to 7 Ma) related to a combination of tectonic and erosional exhumation. Although tectonic uplift and cooling

are not contemporaneous, the tectonic stages are reflected in both relative uplift paths and cooling paths. During the transpressional stage (Fig. 4.10Ba to Bb) R3-1 and R2-4 are uplifted above the “undeformed base Oligocene” during their cooling below the upper temperature limit of the APAZ (Fig. 4.10Ca to Cb). This implies that the reference plane “undeformed base Oligocene” reflects a temperature interval close to the upper limit of the APAZ (i.e. 120 °C). Based on this observation the base of the Oligocene sediments is estimated to have been subjected to temperatures around the upper limit of the APAZ by the beginning of Middle Miocene times. This estimation is corroborated by full annealing of apatite fission tracks, as is observed in Eocene sediments located east of Borsa (Sanders 1998).

An exhumation rate for the Rodna horst can be calculated via the altitude vs. age relation, extracted from the vertical profile R3 (Fig. 4.11). Enhanced exhumation rates are deduced for the time interval 12 to 11 Ma ( $\geq 1.0$  mm/a), followed by overall slow exhumation after 10 Ma before present (the 0.1 mm/a-line is given as reference). Thus the altitude vs. age relationship corroborates the stratigraphic dating as well as the predominance of the transtensional stage along the Dragos-Voda fault.

#### 4.8 Revealing the total amount of Miocene exhumation for the entire study area

The total amount of Miocene exhumation in the study area depicted in Fig. 4.12 has been estimated on the base of the apatite FT data. The maximum palaeodepth ( $D_{max}$ ) is estimated on the basis of the maximum palaeo-temperature ( $T_{max}$ ), assuming a geothermal gradient of  $\Delta T/\Delta Z = 20^\circ\text{C}/\text{km}$  and an estimated surface temperature of  $10^\circ\text{C}$  ( $T_s$ ) on the basis of:

$$D_{max} = (T_{max} - T_s) / (\Delta T / \Delta Z)$$

A geothermal gradient of  $20^\circ\text{C}/\text{km}$  has been derived by Sanders (1998), who balanced erosion along the Carpathian and Apuseni mountains against the sedimentary infill of the Transylvanian basin.  $20^\circ\text{C}/\text{km}$  is also in accordance with present day heat flow data (Veliciu & Visarion 1984; Demetrescu & Veliciu 1991). However, a palaeo-geothermal gradient is not easy to quantify. The area is affected by volcanism, which may provide additional heat sources. Therefore the given amounts of exhumation represent maximum

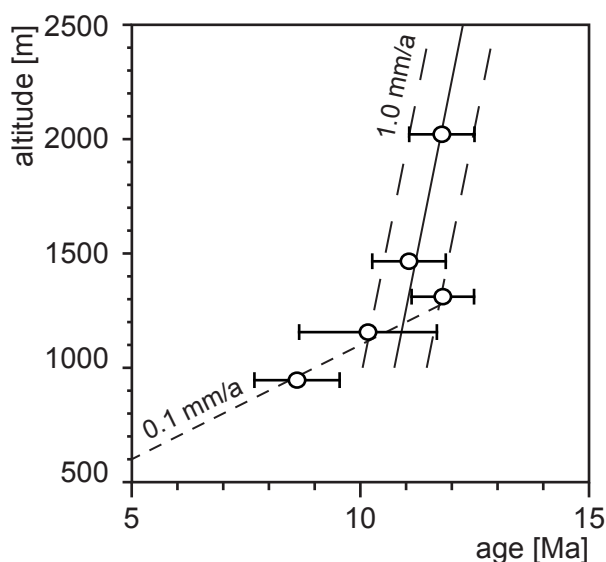


**Fig. 4.11.** Altitude vs. age plot of vertical profile R3 (Rodna horst), suggesting a two-stage exhumation history: enhanced exhumation of at least 1.0 mm/a between 12 and 11 Ma, followed by slower exhumation after 10 Ma. 1.0 mm/a and 0.1 mm/a lines are given as reference.

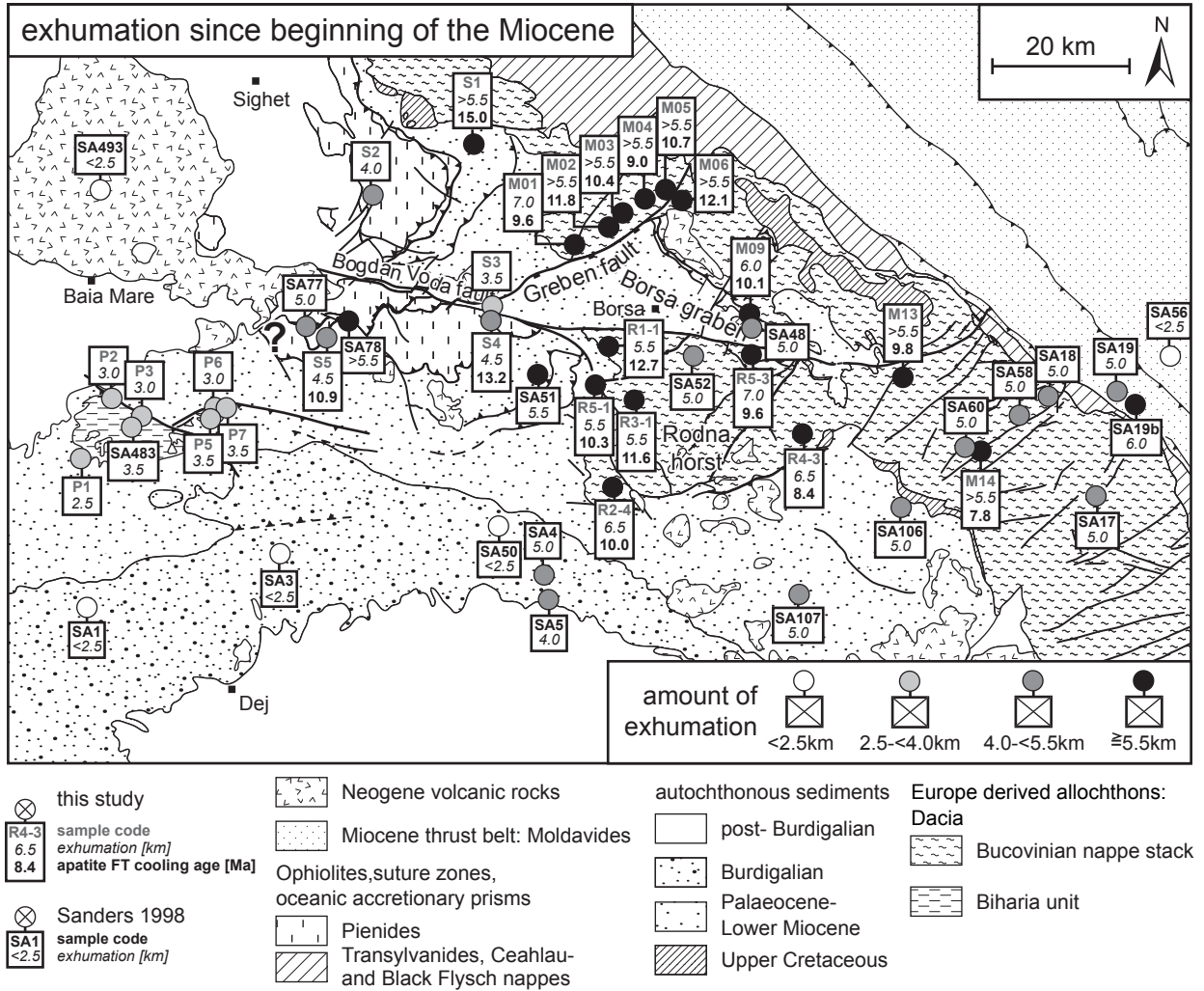


**Fig. 4.12.** Map showing the calculated amounts of Miocene exhumation in the study area. The amount of exhumation is given by the maximum palaeotemperatures inferred from apatite FT data, assuming a geothermal gradient of 20°C/km. Sample code SA refers to additional data from Sanders (1998). For most samples, the entire amount of exhumation was realised after Middle Miocene times (i.e. after 16 Ma), as indicated by Middle to Late Miocene cooling ages.

values.

In the case of samples displaying only partial annealing of apatite (samples P1, P2, P3, P5, P6, P7, S2, S3 and S5) thermal modelling indicates that Tmax was reached before the onset of Miocene exhumation. In the case of fully annealed apatite (profiles R1, R2, R3, R4, R5, samples M01, M02, M03, M04, M05, M06, M08, M09, M13, M14 and S1) Tmax has to have exceeded 120°C. Thermally undisturbed zircon in all basement samples excludes temperatures above the lower limit of the ZPAZ (Tmax <190°C) during Palaeogene to Early Miocene burial.

In the case of some samples (profiles R1, R2, R3, R4, R5, samples M01, M09) the estimation of Tmax has been improved by assuming that the base of the Oligocene approximates the upper limit of

the APAZ (120 °C, see above) before the onset of exhumation. In these cases Tmax can be derived by the vertical distance of the sample location to the base Oligocene based on maps and cross sections (Fig. 4.9) and the estimated geothermal gradient of 20 °C/km. Tmax for S4 has been estimated to 100°C, in analogy to S5 since both samples show strong, but not full annealing. All palaeo-depth, and hence also all exhumation values, given in Fig. 4.12 are rounded to 0.5 km intervals.

The Middle to Late Miocene cooling ages (central ages, youngest populations: 15.0 to 7.3 Ma) indicate that the entire amount of cooling and exhumation is the result of erosion that followed tectonic uplift during the strike-slip dominated post-Burdigalian tectonic activity in the study area. However, in the area directly north of the Bogdan-

Voda fault the total amount of exhumation (S2: 4.0 km, S3: 3.5 km) can hardly exclusively be of post-Burdigalian age, since the altitude of the base of the Middle Miocene sediments is found close to that of the collected samples. Hence north of the Bogdan-Voda fault a significant part of the total amount of exhumation seems to be due to erosion that occurred earlier, i.e. during and directly following the intra-Burdigalian thrusting of the Pienides.

The strong thermal pulse found in the westernmost area of the southern part of the Pienide nappes (marked by a question mark, Fig. 4.12) occurred relatively late, as is indicated by young cooling ages: 10.9 Ma for the youngest population (Fig. 4.12), 11 Ma and 8 Ma according to Sanders (1998). Since the base of Middle Miocene sediments is in close neighbourhood, a thermal pulse caused by burial is rather unlikely. Hence, we interpret these Late Miocene cooling ages as the result of a hydrothermal overprint. An intensive overprint of the sedimentary units of the Pienides close to the volcanic body at Baia Mare is documented by Săndulescu & Russo-Săndulescu (1981). Whether partial annealing is related to hydrothermal overprint or to heating by burial is difficult to judge.

## 4.9 Recapitulation of results

Burial by Palaeogene to Early Miocene sediments, locally combined with thrusting and frontal imbrication, caused full annealing of fission tracks in apatite in case of the samples from the Bucovinian nappe stack. Locally this is also the case for the sedimentary cover. Regarding the Preluca massif located in the southwestern part of the study area, however, the amount of burial due to the sedimentary overburden as well as the amount of exhumation were less substantial. Fission tracks in apatite from the Preluca massif remained relatively undisturbed during heating by burial, while (U-Th)/He data document considerable retention of He.

Exhumation is mainly the result of erosion triggered by uplift, accompanying and/or following post-Burdigalian strike-slip tectonic activity along the Bogdan-Drăgos-Voda fault system. Middle Miocene cooling ages (15.0 to 13.2 Ma) document exhumation during a first transpressional stage in the eastern part of the study area (Fig. 4.12). In the central part of the study area Middle to Late Miocene ages (12.7 to 7.3 Ma) indicate enhanced cooling and exhumation during and following a

second transtensional stage. The vertical profile R3 indicates enhanced exhumation of at least 1 mm/a between 12 to 11 Ma (Fig. 4.11). Enhanced final exhumation is confirmed by apatite (U-Th)/He ages which coincide with the accompanying apatite FT ages within the error limits.

## 4.10 Discussion

### 4.10.1 Hydrothermal overprint

Beyond the Miocene cooling ages also a few Pliocene apatite FT central ages were obtained in samples from the Bucovinian nappes (3.4 Ma for M08, 4.4 Ma for R4-2). Neogene volcanic activity is a likely explanation for these young ages. However, volcanism started in the Middle Miocene and activity only lasted until 9.0 Ma north of Baia Mare and 8.6 Ma in the area of the Rodna horst, respectively (Pécskay et al. 1995). Even though a second, younger phase of volcanism can be observed north of Baia Mare (8.1 to 6.9 Ma, Pécskay et al. 1995), Pliocene volcanism is only documented for areas located some 80 to 100 km south of our study area (Harghita mountains). Thus we propose that the observed late annealing of apatite is due to hydrothermal activity that postdates active volcanism. The present-day occurrence of hot springs at the southern margin of the Rodna horst also favours such an interpretation.

### 4.10.2 Burial and exhumation in the study area

The overall decrease in the amount of burial towards the SW, as deduced from the thermochronological data, is in accordance with the diminishing thickness of Oligocene sediments towards the southwest (de Brouker et al. 1998). At the southern rim of the Preluca massif apatite FT data indicate 2.5 km of burial (assuming a geothermal gradient of 20°C; Fig. 4.12). About 0.8 km of Palaeocene to Early Miocene (Aquitania) sediments are still preserved in this area (Rusu et al. 1983). Values of 2500 km for the total sedimentary overburden are in good accordance with the thickness of the Burdigalian strata which reaches about 2 km in the Transylvanian basin directly to the south, as is documented in seismic sections (de Brouker et al. 1998; Ciulavu et al. 2002; Tischler et al. this volume).

Concerning the area of the Rodna horst our apatite FT data suggest that 5.5 km of sediments accumulated above the base Oligocene. A

minimum thickness of Oligocene deposits of 2.8 km is documented in the area of Borsa (Kräutner et al. 1982). Geometric projections of the Oligocene deposits in the profiles of Fig. 4.9c and 4.9d, based on available maps (Ianovici et al. 1968; Kräutner et al. 1989; Săndulescu et al. 1991), indicate a minimum thickness which diminishes from 4.4 km NW of the Greben fault to 2.7 km SW of the Rodna horst. Higher burial depths in the NW part of the study area are directly documented by the fully annealed apatite FT sample S1 from the Oligocene deposits of this area. Yet the observed or inferred thickness of the post-Eocene deposits is still insufficient for explaining the burial depth inferred from our FT data. Excess burial can be explained by additional tectonic loading related to the emplacement of the Pienides during the Burdigalian and accompanying imbrications of the autochthonous cover (Tischler et al. 2006). Especially in the northwestern parts of the Rodna horst, additional tectonic burial appears to be indicated by tectonic considerations. In the southeastern corner of the Rodna horst, however, additional Burdigalian deposits could also allow for the necessary total overburden. However, it has to be kept in mind, that a higher geothermal gradient than the assumed 20 °C/km can also explain apparent discrepancies between palaeotemperatures and amounts of overburden. The apparent volcanic activity in the area may have increased the geothermal gradient. Therefore the mentioned values for post-Miocene exhumation (Fig. 4.12) should be considered as maximum estimates.

Although the emplacement of the Pienide nappes probably led to tectonic burial in most parts the study area, certainly in parts of the autochthonous sediments adjacent to the frontal thrust (sample S1), exhumation that accompanied or post-dated the emplacement of the Pienides is indicated by the truncation of tectonic contacts by an unconformity at the base Middle Miocene (Tischler et al. 2006). This truncation could either be explained by exhumation by erosion in the internal part of an accretionary wedge or by exhumation which post-dates nappe emplacement.

Regarding the age and the amounts of exhumation, our data are generally in good accordance with an earlier apatite FT data (Sanders 1998; Sanders et al. 1999; see Fig. 4.12). However, in contrast to Sanders (1998), our data indicate full annealing of apatite in all the basement units of the Bucovinian nappe stack. Hence we infer slightly higher values of exhumation.

#### 4.10.3 Relationships between uplift and cooling

The age vs. altitude relation (Fig. 4.11) indicates fast exhumation between 12 and 11 Ma in the Rodna horst, contemporaneous with the stratigraphically dated tectonic transtensional stage (12 to 10 Ma). On the other hand, thermal modelling of FT data indicates fast cooling between 11 and 7 Ma, i.e. slightly later. However, given high exhumation rates the observed cooling history of a sample is not only influenced by the exhumation rate alone (Brown 1991; Mancktelow & Grasemann 1997). Starting at rates exceeding 1 mm/a, advective heat transport will cause a delay of cooling with respect to exhumation (Mancktelow & Grasemann 1997). Advective heat transport not only causes a decrease in the spacing of the isotherms (i.e. an increase in geothermal gradient) but can also lead to formation of non-planar isotherms in areas with rugged relief (Stüwe & 1994; Mancktelow & Grasemann 1997; Braun 2002). Following these authors we interpret the delay between fast exhumation and fast cooling, as documented by Middle to Late Miocene cooling ages, as an effect of advective heat transport during a limited phase of fast tectonic exhumation. Sanders (1998) determined mean erosion rates of 0.5 mm/a in the East Carpathians for about the same time interval, i.e. from Middle Miocene to Pliocene times (15 to 5 Ma).

#### 4.10.4 Uplift and exhumation at a regional scale

Middle Miocene ages in the western part of the study area reflect a first stage of exhumation related to the transpressional stage of deformation. The stratigraphically dated Middle Miocene transpressional stage (16 to 12 Ma) is interpreted as a result of the NE-directed perpendicular convergence during soft collision of Tisza-Dacia with the NW-SE striking European margin.

The enhanced Middle to Late Miocene exhumation rates deduced from thermochronological analyses are contemporaneous with the transtensional stage of deformation documented in the study area. The transtensional stage of deformation is thought to be the result of oblique convergence of Tisza-Dacia with the NW-SE striking European margin, evidenced by Eward thrusting in the external Miocene thrust belt (Matenco & Bertotti 2000). Blocking of eastward movement of Tisza-Dacia in the north led to sinistral strike-slip activity along E-W trending faults and

coeval normal faulting along NE-SW directed faults (Tischler et al. 2006). This fragmentation of the crust by normal and sinistral strike-slip faulting into SW down tilted blocks led to the development of triangle shaped graben (Borsa graben) and corresponding horst structures (Rodna horst; Fig. 4.12). Exhumation of internal units during foreland propagating thrusting is also known from the westernmost Carpathians. Danišik et al. (2004) report enhanced Middle Miocene exhumation in the northern Danube basin, documented by apatite FT ages (16 to 13 Ma), contemporaneous with north directed emplacement and thrusting in the Miocene thrust belt further to the N (16 to 14 Ma, e.g. Jiricek 1979).

Although the main activity of the Bogdan-Drăgos-Voda fault system terminated at 10 Ma extensional veins within the volcanic body of Baia Mare, featuring hydrothermal ore deposits (7 to 8 Ma, Lang et al. 1994), suggest minor extensional activity after 10 Ma. Possible Late Miocene normal and strike-slip faulting may explain the extraordinarily young apatite FT ages (7.8 Ma, Fig. 4.12) in the southeastern part of the study area. Such a Late Miocene exhumation would be contemporaneous with strike-slip deformation in the external East Carpathian Miocene thrust belt, dated at 9 Ma (Matenco & Bertotti 2000).

#### 4.11 Conclusions

The basement units of the Maramures Mountains, the Rodna horst and the Preluca massif suffered a last stage of metamorphism under sub-greenschist to lowermost greenschist facies conditions during the late Early Cretaceous, followed by Late Cretaceous cooling and exhumation.

Palaeogene to Early Miocene sedimentation and thrusting caused renewed heating by burial, which led to full annealing of fission tracks in apatite in parts of the study area.

Soft collision of Tisza-Dacia with the European margin initiated a first transpressional tectonic stage (16 to 12 Ma) which caused exhumation by folding and reverse faulting in the western part of the study area. Middle Miocene cooling ages (15.0 to 13.2 Ma) are related to this tectonic stage.

Transpression was followed by transtension (12 to 10 Ma) during ongoing NE-SW shortening. The late-stage evolution of the Rodna horst is dominated by combined normal and strike-slip faulting, which led to its fragmentation into tilted and fault-bounded blocks. Fast exhumation in the central part of the Rodna area resulted in Middle to Late Miocene cooling ages (12.7 to 7.3 Ma). Exhumation rates exceeded 1 mm/a during this stage and caused advective heat transport leading to delayed cooling.

We are most grateful for the excellent introduction into the study area and its geology provided by M. Săndulescu and L. Matenco and their ongoing support. L. Matenco also critically reviewed a first version of the manuscript. Fruitful discussions with D. Badescu, M. Marin, I. Balintoni and D. Radu are also highly appreciated. H.R.G. is very grateful to F. Stuart for his introduction to the lab procedures and methods of (U-Th)/He analysis. Furthermore we thank I. Dunkl and M. Raab for their careful reviews and constructive remarks. Financial support by the Swiss National Science foundation (NF-project Nr. 21-64979.01, granted to B.F) is gratefully acknowledged.

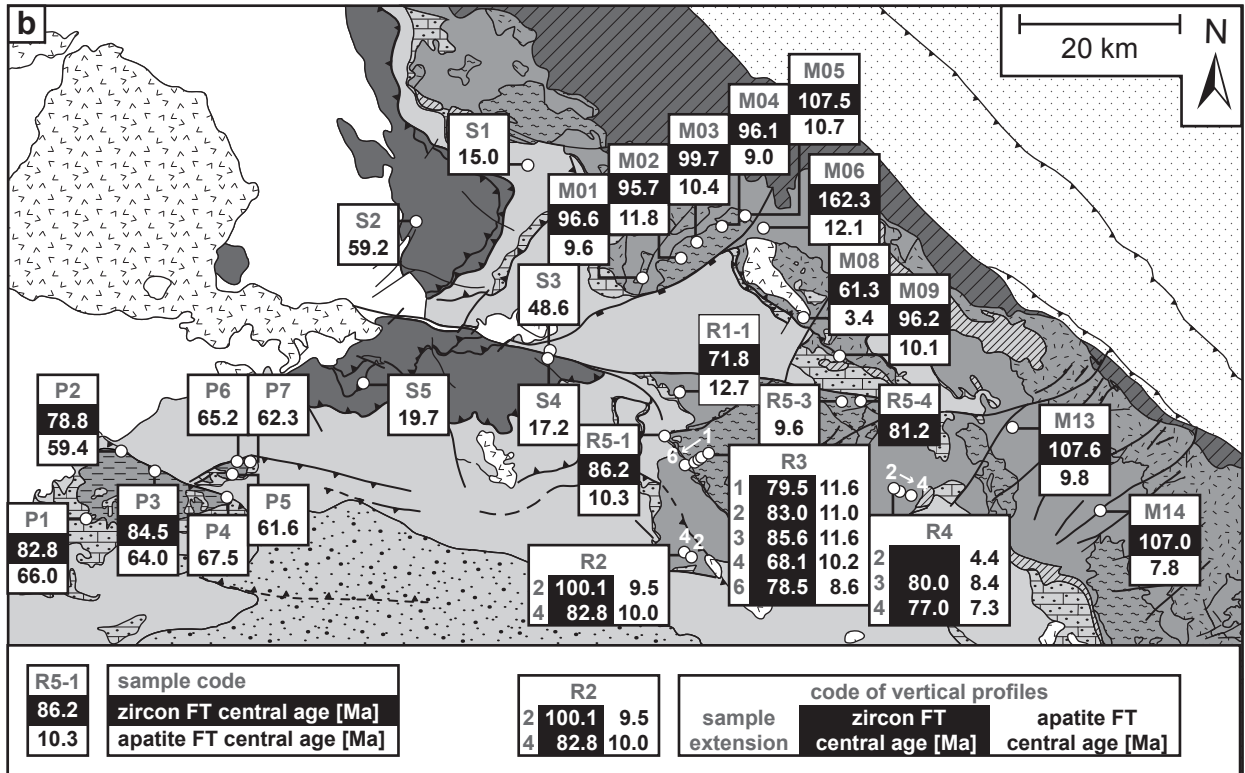


### 4.12 Appendix

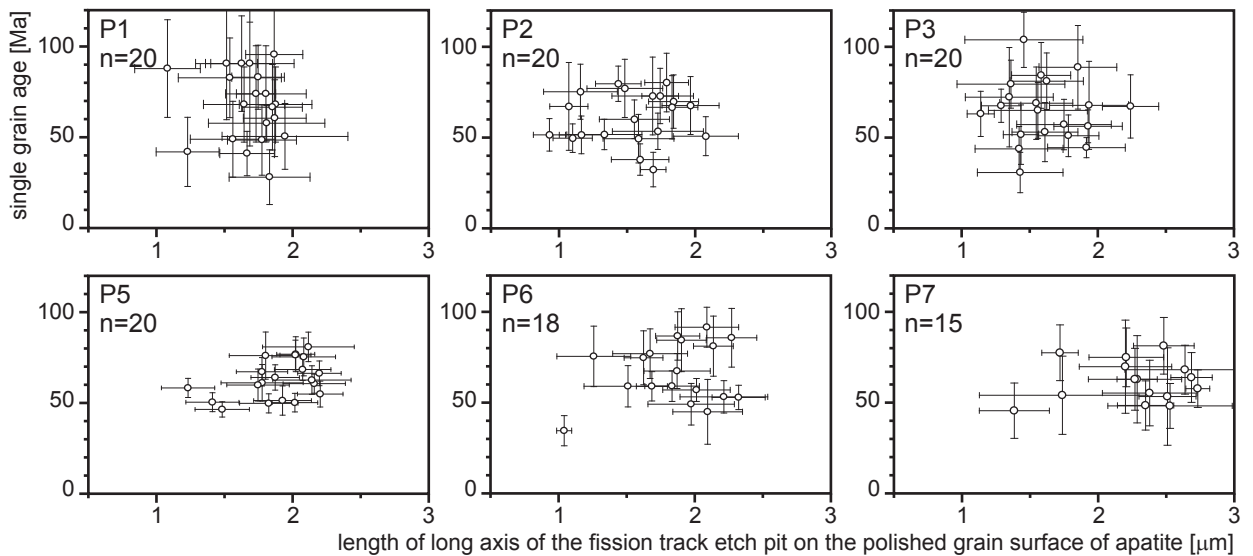
**Appendix 4.1.** Results of fission track analyses in the study area.

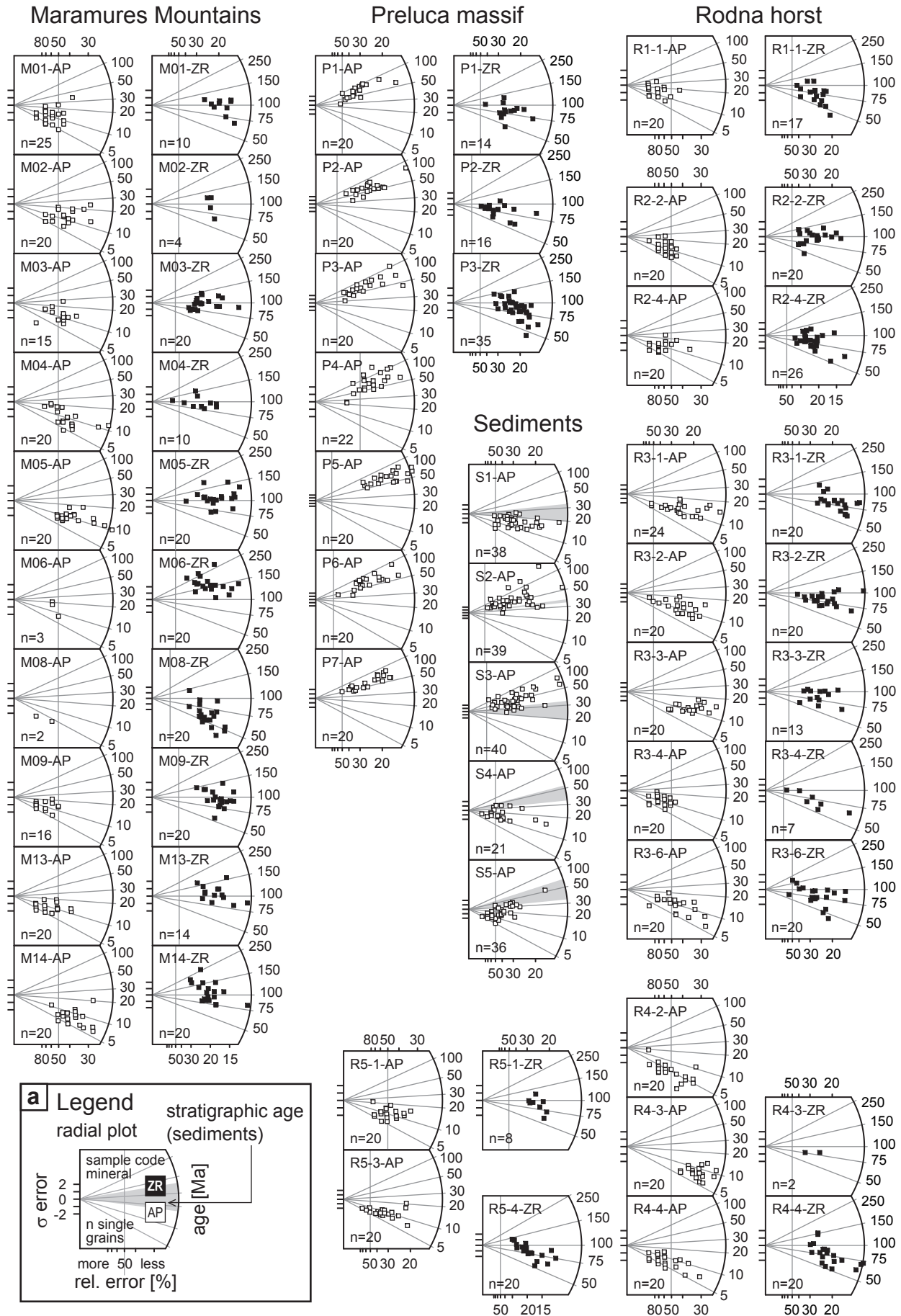
a (next page): All radial plots (Galbraith 1990) of the same data group (Ap/Zr) show the same age spektrum to allow for direct comparison.

b: All given ages in the map are central ages (Galbraith and Laslett 1993).



**Appendix 2:** Measurements of the long axis of etch pits in samples from the Preluca massif. P4 did not provide enough spontaneous tracks. Generally as many as possible etch pit long axes per grain were measured, up to a maximum of ten. The grain ages are plotted with their single grain error and the mean of the Dpar with one standard deviation.





## **Chapter 5:**

# **Paleogene burial followed by Middle Miocene exhumation during soft collision of Tisza-Dacia with the European margin**

## 5.1 Introduction

Final emplacement of the major continental blocks ALCAPA and Tisza-Dacia in the Carpathian embayment is the result of Miocene soft collision of both these blocks with the European margin (Morley 2002). During final emplacement of the ALCAPA and Tisza-Dacia blocks (Fig. 5.1) into the Carpathian embayment two main driving forces are active: a) the eastward lateral extrusion of ALCAPA (Ratschbacher et al. 1991a, 1991b) and b) the slap retreat beneath the Carpathians (Royden 1993; Nemcok et al. 1998; Wortel und Spakmann 2000; Sperner et al. 2005). This final emplacement is well documented in the external Miocene thrust belt (Jirijek 1979; Morley 1996; Zweigel et al. 1998; Matenco und Bertotti 2000).

Soft collision (Jishun et al. 1996; Morley 2002) is a mechanism during which the low amounts of compressional stress inhibited the development of typical collisional structures such as major uplift, erosion and the exposure of high-grad metamorphic rocks (Morley 2002). In the Carpathian realm soft collision is mostly interpreted to result from slab retreat, whereby the rate of plate convergence is smaller compared to the rate of subduction (e.g. Royden and Burchfiel 1989; Royden 1993, Csontos 1995; Wortel und Spakmann 2000; Sperner et al. 2002).

The highly bent shape of the Carpathian

embayment led to oblique convergence during the collision of ALCAPA (Sperner et al. 2002) and Tisza-Dacia (Zweigel et al. 1998) with the European margin at many places. Final emplacement of ALCAPA is of Early Miocene (Sperner et al. 2002) age while the final emplacement of Tisza-Dacia occurred in the Middle to Late Miocene, as documented in the main phase of thrusting in Middle Miocene in the West Carpathians (e.g. Jirijek 1979) and a main phase of thrusting in Middle to Late Miocene in the East Carpathians (e.g. Matenco and Bertotti 2000). Several studies address the emplacement mechanisms of ALCAPA (Sperner et al. 2002) and Tisza-Dacia (Decker and Peresson 1996; Linzer et al. 1998; Schmid et al. 1998; Zweigel et al. 1998). Most studies concerning the direction and timing of emplacement of Tisza-Dacia either deal with the entire East Carpathians (Linzer et al. 1998; Matenco and Bertotti 2000) or focus mainly on the southern East Carpathians (Morley 1996; Zweigel et al. 1998) and South Carpathians (Schmid et al. 1998; Fügenschuh and Schmid 2005). This study focuses on the northern East Carpathians.

On the base of structural data presented in chapter 3 this chapter aims to evaluate the burial and exhumation information obtained by the apatite fission track data discussed in chapter 4 and to compare these data to the stratigraphic record from the study area. The Tertiary burial and exhumation history is discussed based on palinspastic reconstructions from the study area

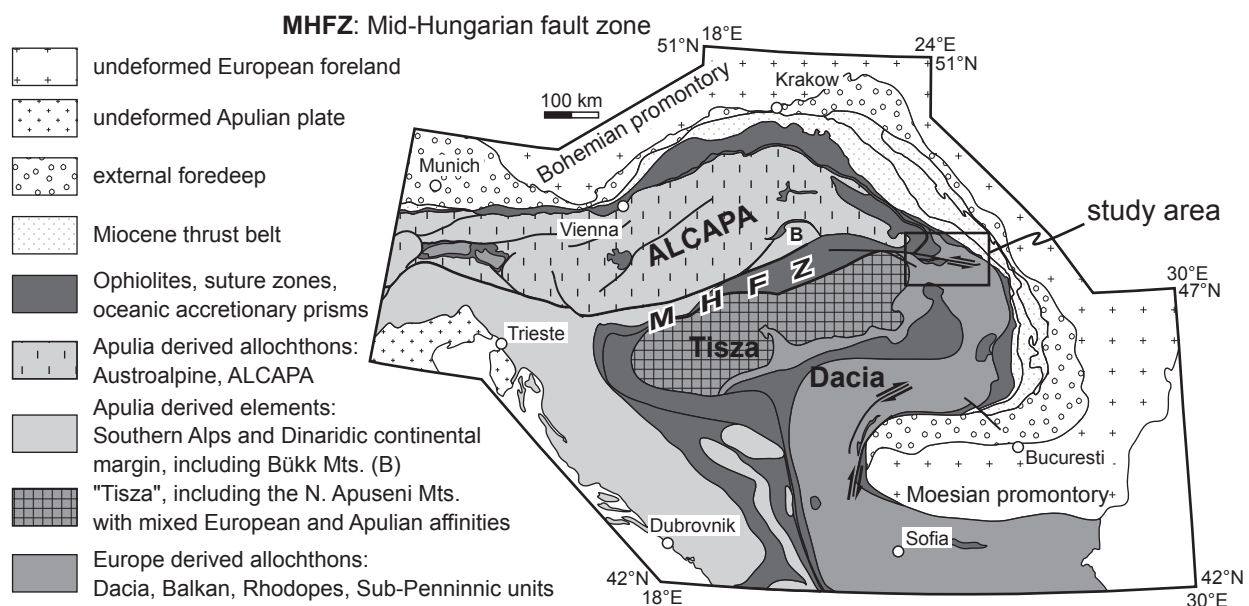


**Fig. 5.1.** Geotectonic map of the Alpine-Carpathian-Pannonian area (Schmid et al. 2008). The Miocene final emplacement of the ALCAPA and the already consolidated Tisza-Dacia block is the result of soft collision of both these blocks with the European margin.

(Tischler 2005). The mechanisms of soft collision of Tisza-Dacia along the European margin are discussed and tectonic uplift during and after emplacement is quantified.

## 5.2 Constraints of the post 16 Ma uplift

For estimating the amount of uplift since Miocene times two independent sets of constraints are available: apatite fission track data and stratigraphical observations (Fig. 5.2, Fig. 5.3). In the following the sea level is considered as constant, since eustatic sea level changes since Miocene times do not exceed 200 m (Haq et al. 1987) and are thus beyond our resolution.

A first data set is derived from the cooling and exhumation data on the base of apatite fission track analysis (details in chapter 4). The estimated maximum paleodepth ( $D_{max}$ ), i.e. amount of exhumation, is normalised to sea level ( $D_{max} +$  altitude above sea level; white dots in Fig. 5.2). This normalisation assumes that Paleogene to Early Miocene burial started at altitudes near sea level, i.e. that all of the calculated burial depth is realized below sea level. Thus the amounts of uplift given in Fig. 5.2 correspond to uplift relative to sea level. Where our own coverage of apatite fission track data is not sufficient, additional data by Sanders (1998; black dots in Fig. 5.2) are used.

The timing of exhumation as derived from apatite fission track analysis is mostly well constrained since burial led to full annealing of apatite fission tracks or at least full annealing of a (chemically distinct) population of apatites within one sample (Fig. 5.2; S4, S5). The ages observed (15.0-7.8 Ma) indicate Middle to Late Miocene cooling and exhumation by uplift and erosion. Therefore in all samples, for which an age is known (age given in Fig. 5.2), the entire amount of uplift given in Fig. 5.2 is interpreted to be realised during and following the post-Burdigalian (16 Ma) soft collision of Tisza-Dacia with the European margin. The timing of smaller amounts of exhumation as suggested by weakly to unannealed sedimentary samples (S1-S3), as well as samples from the Preluca massif, cannot be constrained in great detail.

Our fission track data suggest a  $D_{max}$  of 5.5 km for the base Oligocene (see details in chapter 4). This estimation is only valid for sections featuring the complete sedimentary column, i.e. where Oligocene sediments are in concordant contact to Eocene strata (orange line; Fig. 5.2, Fig. 5.3). Because the

thickness of Paleogene to Early Miocene sediments is not homogeneous within the study area (Fig. 5.4 and 5.5) this estimation is only valid in proximity to the Rodna horst. Hence the amount of post-16 Ma uplift can be estimated to be in the order of 5.5 km plus altitude above sea level only where the base of Oligocene is mapped (Fig. 5.2) or projected in geological schematic cross sections (Fig. 5.3 c-d).

Since most of the exhumation in the study area commenced after 16 Ma ago, the base of Mid-Miocene sedimentation (Dej Tuff; 16 Ma) provides independent constraints for post-16 Ma vertical movements (green line, Fig. 5.2 and 5.3). For simplicity the base Middle Miocene is considered as representing the sea level at 16 Ma ago. The whole amount of post Middle Miocene uplift is therefore estimated as equal to the present day elevation of the mapped (Fig. 5.2) or projected base of the Middle Miocene strata (Fig. 5.3, a,b,e). In the area of the Transylvanian basin (Fig. 5.2) the elevation of the base of Mid-Miocene sedimentation is taken from Raileanu and Radulescu (1967) and Raileanu and Saulea (1968). In the external part the present day altitude above sea level of Mid-Miocene strata in the outermost Miocene thrust belt (Ianovici and Dessila-Cordarcea, 1968) is integrated as reference points (green-black line, Fig. 5.2).

In the western part of the study area the uplift suggested by thermal modelling of apatite fission track data significantly exceeds the values evidenced by the present day elevation of the base Middle Miocene close by (Fig. 5.2; S1, S3). The most likely explanation for this discrepancy is a pre-16 Ma stage of exhumation. A phase of significant erosion between 20-16 Ma, syn- to post emplacement of the Pienides, is documented by the deposition of a Burdigalian clastic wedge (Hida beds) to the SE. This exhumation stage is also documented by the truncation of the Pienide thrust contacts by the base Middle Miocene (Fig. 5.3a). Therefore, at localities S1 and S3, only the base of the Middle Miocene strata is used to estimate the amount of post Middle Miocene uplift.

In the westernmost part of the Pienides, south of the Bogdan-Voda fault, a relatively high amount (around 6 km) of Middle to Late Miocene uplift is suggested by the apatite fission track data (cooling ages: 10.9 Ma this study; 11 Ma, 8 Ma (Sanders 1998); see Fig. 5.2). In contrast the base Middle Miocene indicates considerably lower amounts of uplift (0.9 km) in this area. Possibly the late (~ 10 Ma) heating event, reaching temperatures around 100°C, documented in the apatite fission track ages,

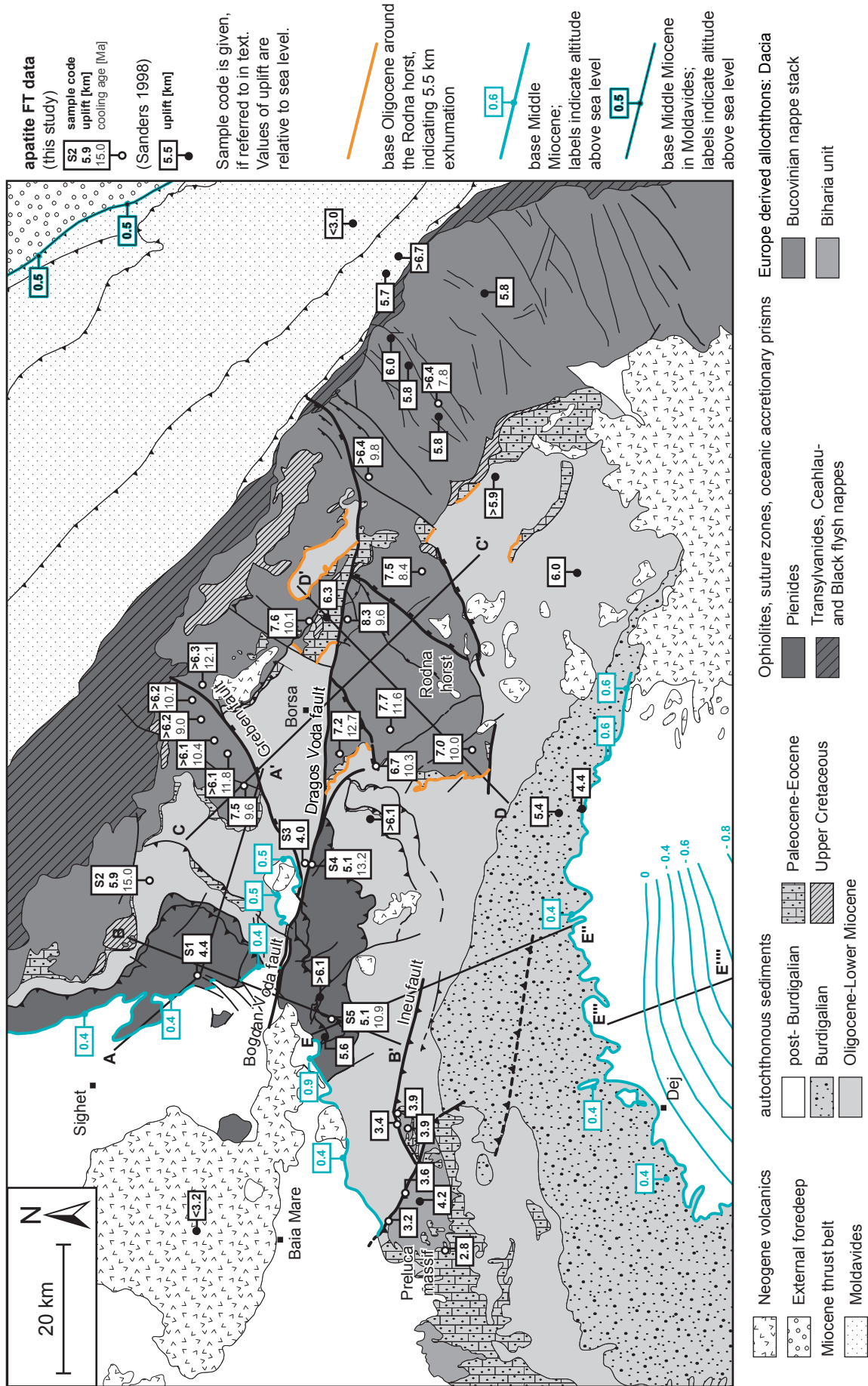


Fig. 5.2. Map showing different constraints for Miocene uplift relative to sea level in the study area. Apatite fission track ages are only given if the ages indicate cooling by post-Miocene uplift and erosion. Provenance ages or partially annealed ages are not displayed.

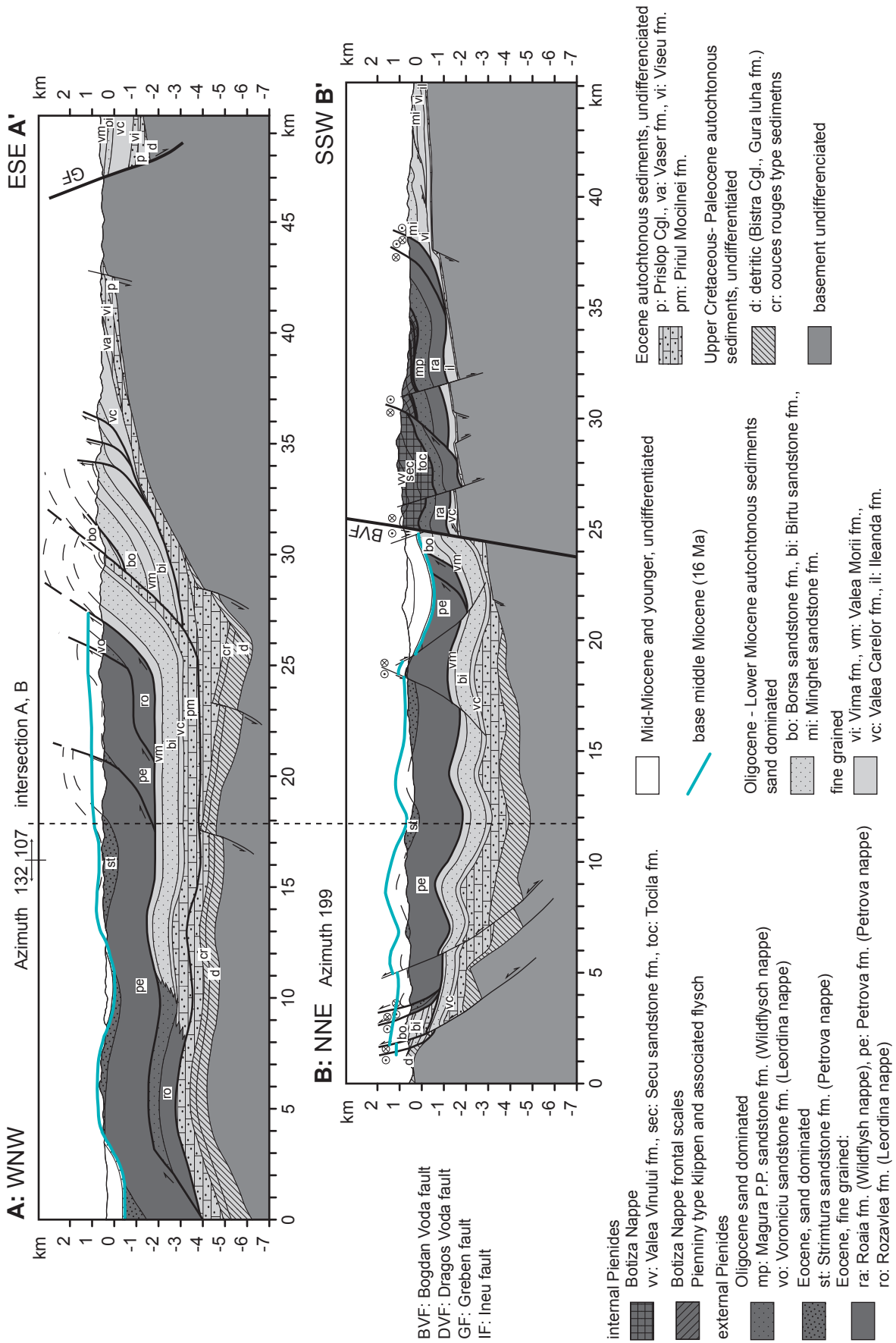


Fig. 5.3. (continued)

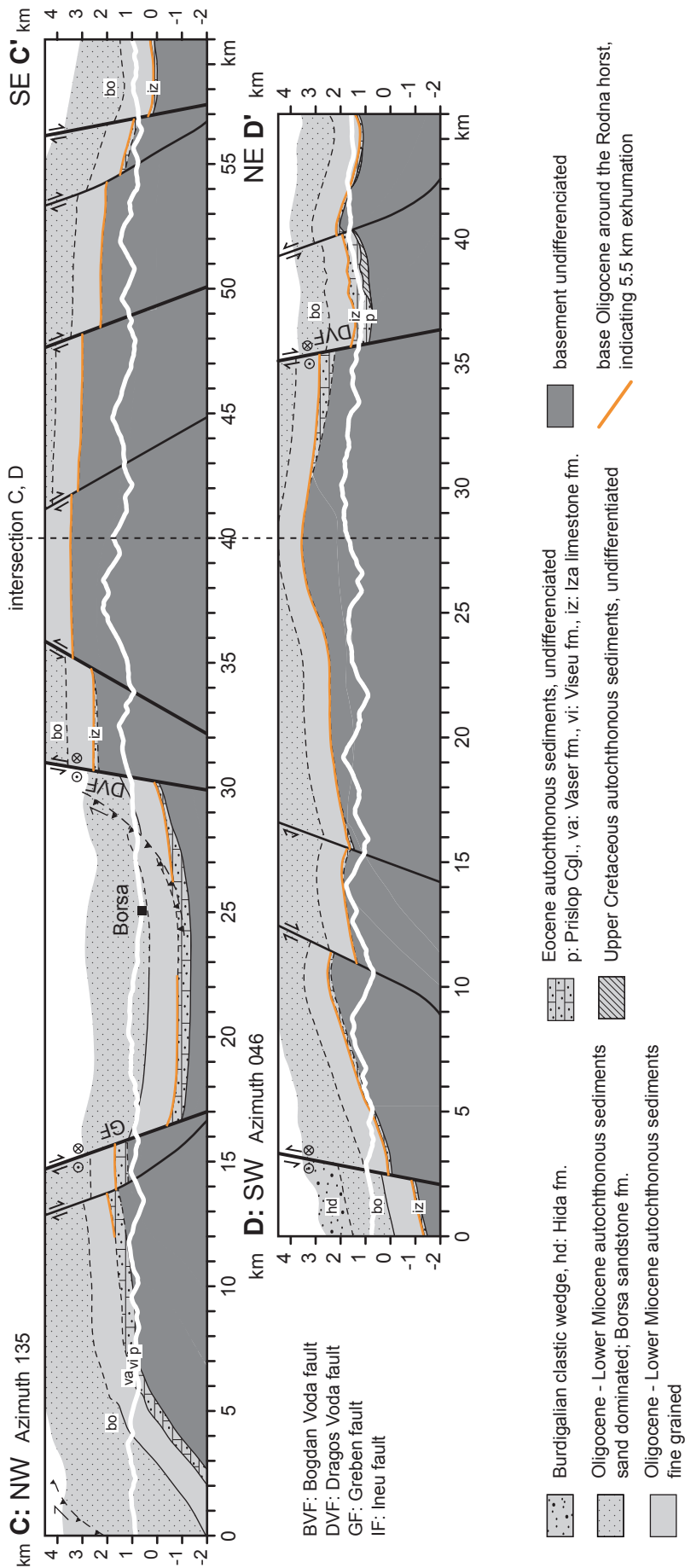


Fig. 5.3. (continued)





is the result of a hydrothermal overprint connected to the volcanic body at Baia Mare (Pecskay et al. 1994). Arguments for such a hydrothermal overprint are abundant volcanic bodies (Sandulescu and Russo-Sandulescu 1981) in this area as well as the variability of apatite fission track data (partially and fully annealed samples and age differences). Therefore apatite fission track information from around sample S5 are omitted.

### 5.3 Reconstruction of the Paleogene burial and Miocene exhumation

In the following the observed burial and exhumation data obtained from the study area will be integrated with the palinspastic reconstruction of Tischler (2005). This palinspastic reconstruction is based on a reconstruction focussing on the South Carpathians (Fügenschuh and Schmid 2005) and integrates structural data from the study area. Five time slices ranging from the Oligocene up to the present are presented. Note that the Bükk mountains are grouped to ALCAPA for the sake of simplicity.

#### 5.3.1 Paleogene to Early Miocene: Sedimentation burial (Interval 65-20 Ma)

Although sedimentation in the study area starts as early as in Paleogene times, Paleocene and Eocene strata are generally very thin (<500m) and Paleocene to Eocene sedimentation did not lead to a levelling of morphology, as is documented by the transgression of Oligocene strata onto the basement of the Rodna horst (Kräutner et al 1982). Therefore the effect of Oligocene to Early Miocene burial is considered to be the dominating factor concerning differential burial in the study area. Hence, the palinspastic reconstruction starts at the beginning of Oligocene (34 Ma, Fig. 5.4a).

The onset of Oligocene turbiditic sedimentation announces the juxtaposition of ALCAPA and Tisza-Dacia, with Tisza-Dacia in a lower plate position. The axis of the lower Oligocene basin strikes (in present day coordinates) NW-SE with sediment thicknesses diminishing towards the southwest (de Brouker et al. 1998). The upper Oligocene is characterised by massive sandstones (Borsa sandstone; Dicea et al. 1980; Sandulescu et al. 1991). Onset of coarse-grained siliciclastic sedimentation is progressively younging towards the (present day) south, finally evolving into a Burdigalian clastic wedge with a WSW-ESE striking longitudinal axis (Ciulavu

et al. 2002; Tischler 2005 and references therein). Migration of the coarse grained siliciclastic depot centres in time also leads to marked differences in thickness of these deposits. The complex temporal and spatial development of the coarse grained siliciclastic deposits might be interpreted as a result of the rotation of Tisza-Dacia during sedimentation, leading to a progressive rotation of basin axes (Tischler 2005).

Note, that the lower Oligocene basin axis depicted in Fig. 5.4c already suffered the amount of clockwise rotation of Tisza-Dacia that commenced during Oligocene times ( $13^\circ$  in Fig. 5.4a). Nevertheless the Oligocene basin axis is almost parallel to the convergence direction of ALCAPA and Tisza-Dacia. A larger amount of Oligocene clockwise rotation of Tisza-Dacia would result in an orientation of the lower Oligocene basin axis roughly perpendicular to the convergence direction of ALCAPA and Tisza-Dacia in the Oligocene. A larger amount of Oligocene rotation (about  $45^\circ$ ) of Tisza-Dacia is suggested by paleomagnetic data (Marton et al. 2007).

The complete thickness of Oligocene deposits is hard to estimate, since the top is generally truncated by erosion or tectonic contacts, respectively. North of the Rodna horst (Fig. 5.4c, log A) published stratigraphic logs (Sandulescu et al 1991) show approximately 1700m of Oligocene siliciclastic deposits. The most complete succession of Oligocene deposits is preserved directly north of the Rodna horst (2800m, Kräutner et al. 1982). Geometrical constructions of the Oligocene deposits (Fig. 5.3, Section C) based on available maps (Sandulescu et al 1991) indicate a minimum total thickness of ca. 4400m north of the Rodna horst. SW of the Rodna Horst (Fig. 5.4c, log B) published logs document a minimum thickness of 2300m for Oligocene sediments (Kräutner et al. 1989). From geometrical constructions (Fig. 5.3, Section D) of the top of the Oligocene deposits, based on available maps (Janovici et al. 1968, Kräutner et al. 1989), a total thickness of ca. 2700m can be estimated. South of the Preluca massif Oligocene to Aquitanian sedimentation reaches only thicknesses of up to 400m (Rusu et al 1983).

#### 5.3.2 Burdigalian: Syn- and post emplacement of the Pienides (Interval 20-16 Ma)

Final juxtaposition of ALCAPA and Tisza-Dacia is documented by the emplacement of the Pienides, contemporaneous to molasse sedimentation. The

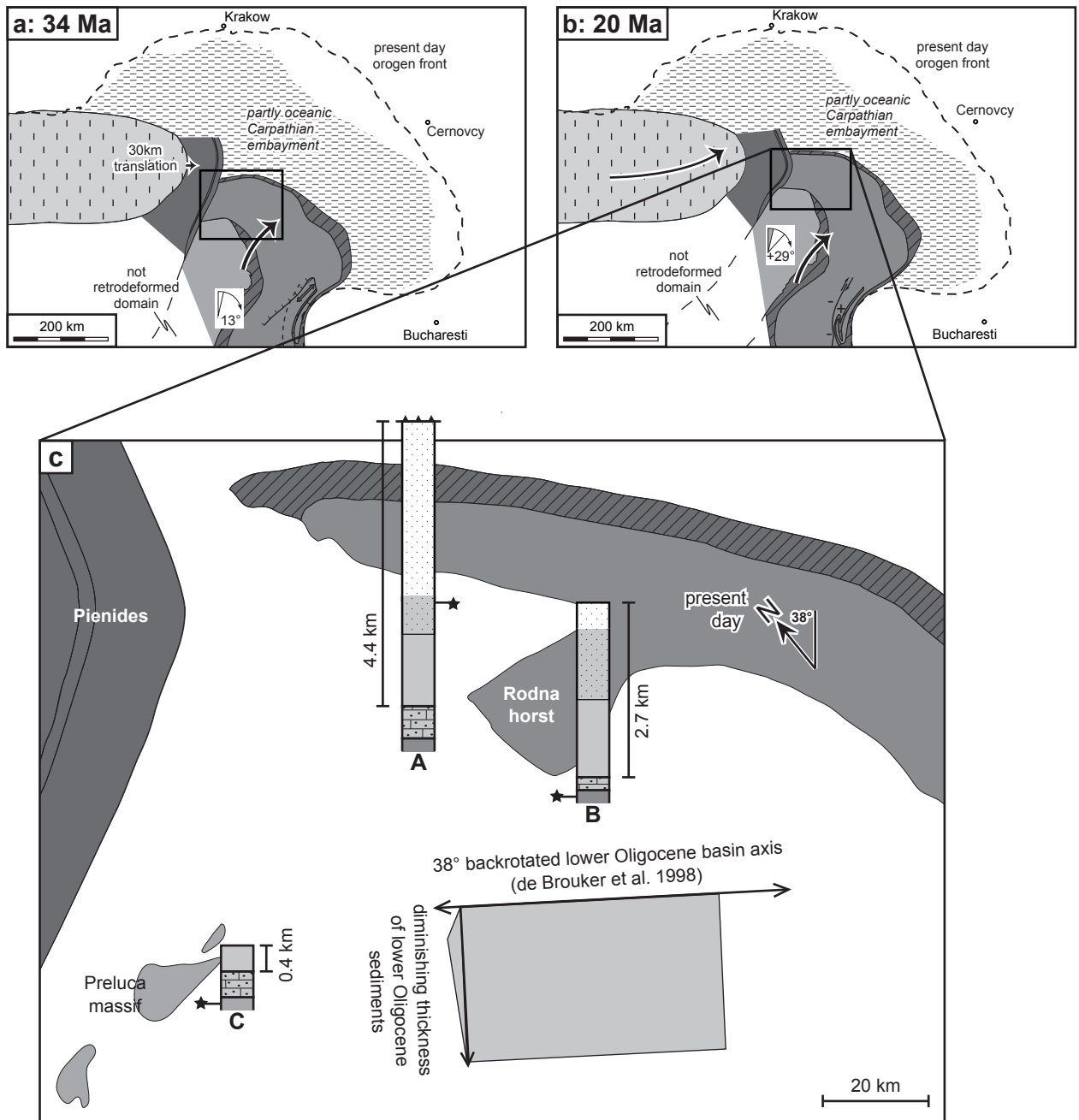


**Fig. 5.4.**

*a,b: Palinspastic reconstruction of the Oligocene to Earliest Miocene (Aquitianian) development (Tischler 2005).  
c: Palinspastic map of the restored study area, showing the retrodeformed outlines of the present day map units (20 Ma, modified after Tischler 2005). The thickness of lower Oligocene sediments diminishes towards the (present day) SW.*

(in present day coordinates) WSW-ENE striking basin axis of the Burdigalian basin is roughly perpendicular to the direction of thrusting of the Pienides (see Chapter 3). During the Burdigalian the sedimentary overburden reached its maximum throughout most of the study area.

South of the Preluca massif 2.5 km of overburden (and related temperature; a geothermal gradient of 20°C/km is used for our estimations) are

required to allow for the observed apatite FT data. The preserved Paleocene to Burdigalian sediments in this area reach a thickness of around 1200 m (400 m Paleogene, 400 m Aquitanian, 400 m Burdigalian; Rusu et al. 1983; Fig. 5.5b, log C). The thickness of the eroded Burdigalian sediments can be estimated on seismic sections (de Broucker et al. 1998; Ciulavu et al. 2002; Tischler 2005) in the Transylvanian basin. In these sections the Burdigalian clastic wedge

reaches thicknesses of up to 2 km in parts closest to the Preluca massif. Assuming this total thickness of Burdigalian deposits for the Preluca massif as well, a total burial of 2.5 km, as indicated by the apatite fission track data, is reached.

In the area of the Rodna horst some 5.5 km of post-Eocene overburden are (based on the previously outlined assumptions) needed to explain

the observed apatite fission track data. Oligocene sediments in the Rodna horst show a decrease in thickness from around 4400m (Fig. 5.5b, log A) in the north to around 2700 m (Fig. 5.5b, log B) in the south. This northward increasing burial is reflected by a sample from the Oligocene sediments (sample S2 from north of the Rodna horst, Fig. 5.2) showing full annealing of apatite fission tracks.

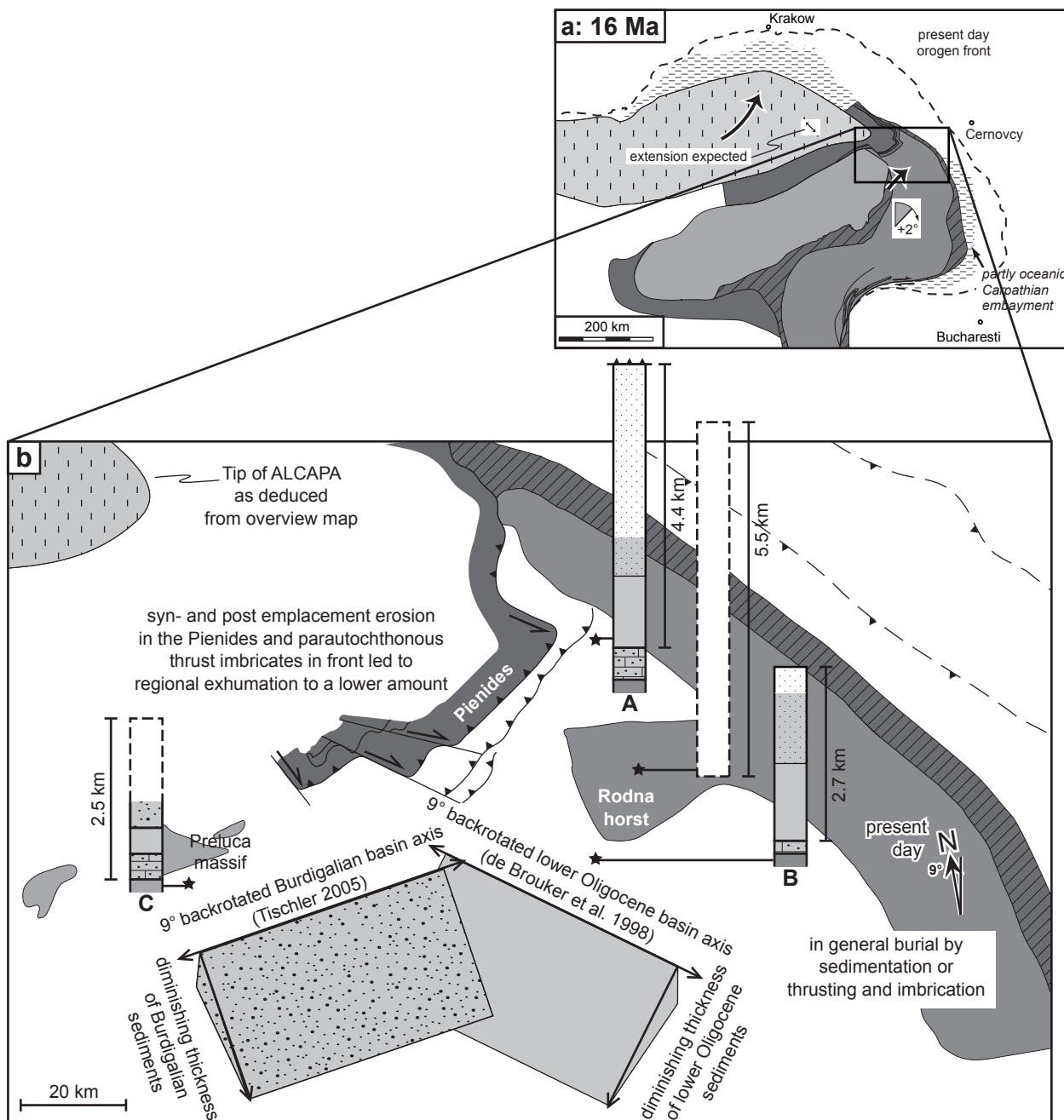


**Fig. 5.5.**

*a,b: Palinspastic reconstruction of the Burdigalian development (Tischler 2005).*

*c: Palinspastic map of the restored study area, showing the retrodeformed outlines of the present day map units (16 Ma, modified after Tischler 2005). In general the Burdigalian emplacement of the Pienides caused additional burial by thrusting and imbrication in the N and sedimentation of a Burdigalian clastic wedge in the S of the study area.*

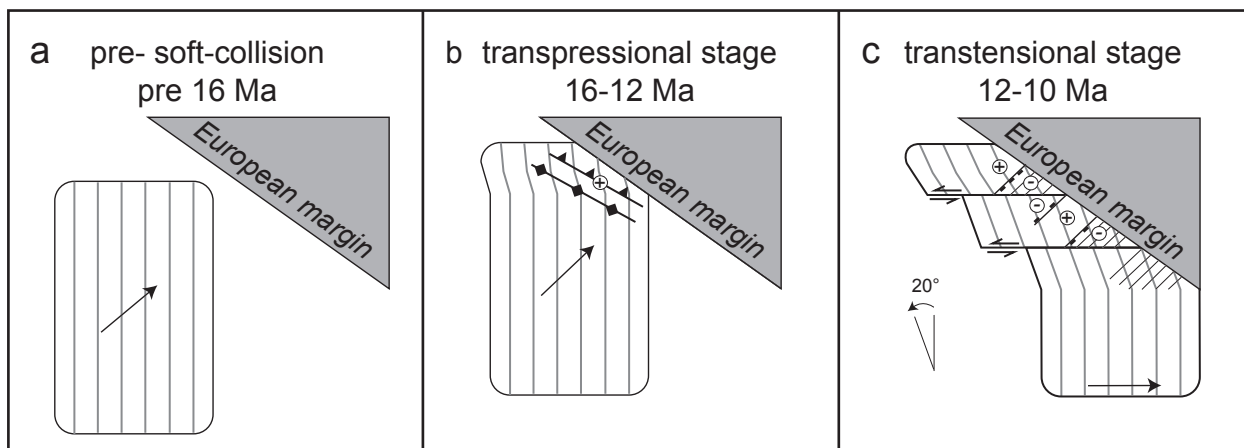


**Fig. 5.6.** General concept of the deformational processes active during soft collision of Tisza-Dacia with the European margin (Tischler 2005). The vertical lines represent "passive marker lines" (a). During the first transpressional stage (16-12 Ma) perpendicular convergence results in shortening and the formation of open folds and backthrusts (b). During the following transtensional stage (12-10 Ma) oblique convergence allowed for the fitting of Tisza-Dacia to the European margin by strike-slip and normal faulting (c).

The discrepancy between the observed thickness of the sedimentary column and the burial depth inferred from our apatite fission track data, could be explained by:

1) Additional tectonic burial caused by the emplacement of the Pienides and accompanying imbrication of the autochthonous cover (Fig. 5.3, section A). This hypothesis is most likely for the NW part of the Rodna horst.

2) An underestimation of Burdigalian deposits. This explanation is most likely for the southwestern corner of the Rodna horst, which is in close proximity to the Burdigalian clastic wedge.

Clearly a further possible reason for the discrepancy is related to the assumed geothermal gradient (20°C/km) since the fission track based estimates on burial depths are based on estimating this gradient. In the light of the strong overall evidence of magmatic activity in the whole working area (Pecskay et al. 1994, 1995) it seems likely that a geothermal gradient of 20°C/km is more an under- than an overestimate.

Although in most of the study area emplacement of the Pienides led to tectonic burial, as indicated by parts of the autochthonous sediments (S2), a syn- to post emplacement exhumation is indicated by tectonic contacts unconformably overlain by middle Miocene sediments. This could either be explained by exhumation in the internal part of an accretionary wedge, or a stage of exhumation directly following the cessation of thrusting.

### 5.3.3 Middle Miocene to present day: Soft collision (16-0 Ma)

During soft collision of Tisza-Dacia with the curved European margin (Morley 2002) two stages of strike slip dominated deformation can be discerned in the study area, a transpressional stage followed by a transtensional one (see Chapter 3). These stages are interpreted as roughly NE-SW directed compression during initial perpendicular convergence (Fig. 5.6b) followed by transtensional "fitting" to the European margin during oblique convergence (Fig. 5.6c). According to Matenco and Bertotti (2000), a change from top to NE towards top to ENE thrusting is documented in the external Miocene thrust belt between late Burdigalian and Sarmatian times. Hence the following model is put forward:

After initial NE-directed collision of the north-easternmost corner of Tisza-Dacia with the European margin (16-12 Ma, Fig. 5.7a), continued eastward migration of subduction roll-back (Sperner et al. 2005, Wortel und Spakmann 2000) is interpreted to initiate a change in the tectonic setting. Transtensional tectonics (12-10 Ma, Fig. 5.7b) allowed for the final closure of the intervening space between Tisza-Dacia and the European margin. Roughly E-W convergence oblique to the NW-SE striking European margin in the study area led to strain partitioning with contemporaneous thrusting in the outer Carpathian thrust belt and internal strike-slip deformation, as documented for the Late Cretaceous to Eocene convergence of

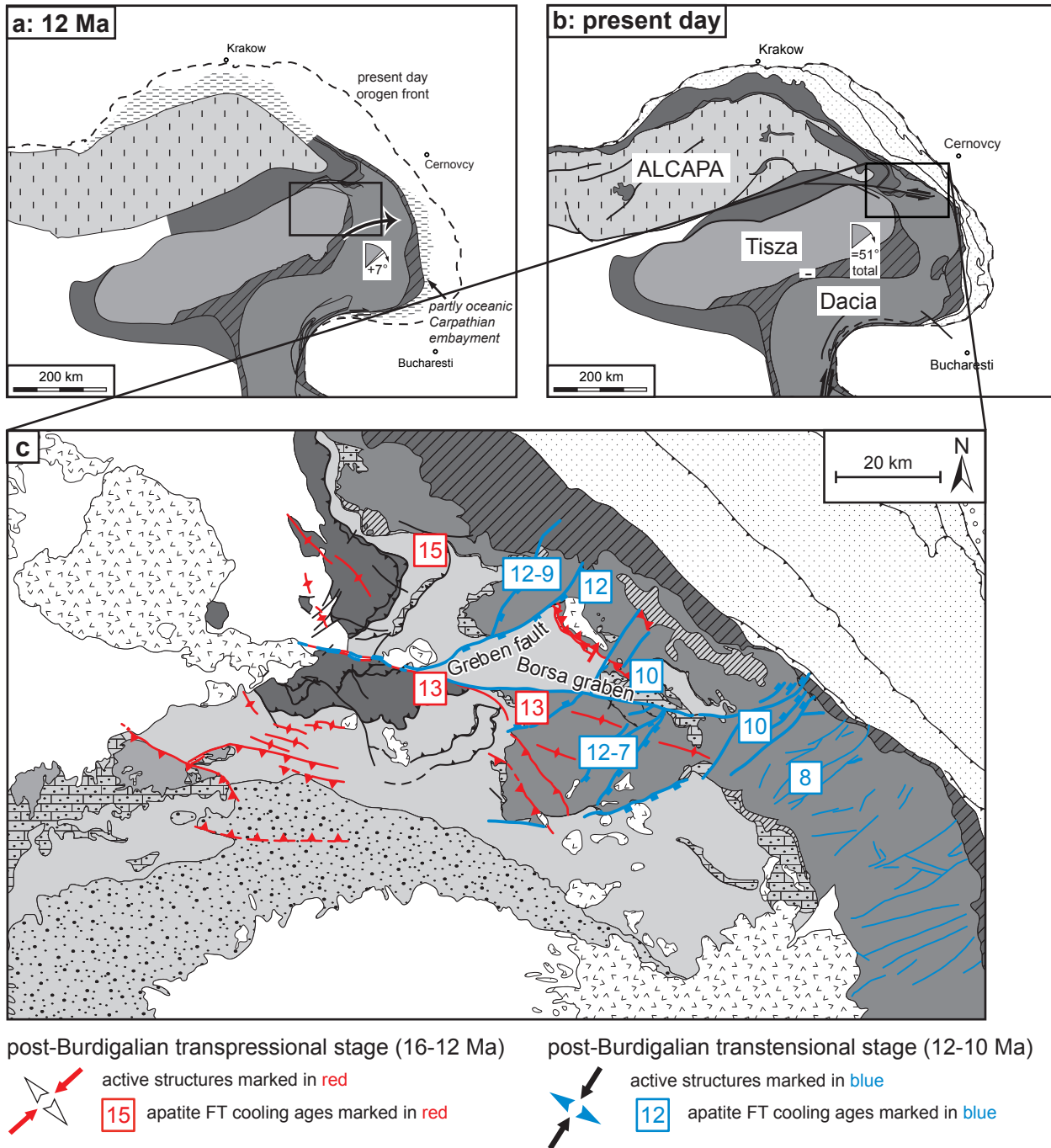


**Fig. 5.7.**

*a,b: Palinspastic reconstruction for the two post-Burdigalian tectonic stages related to soft collision of Tisza-Dacia with the European margin (Tischler 2005).*

*c: Active structures of both phases are marked by thick lines and colourcoded. Exhumation by uplift and erosion during and following both stages is documented by apatite fission track cooling ages.*

ALCAPA with Europe (Sperner et al. 2002). Thus the southern part suffered a bigger amount of eastward translation than the (already locked) northern part of the study area. These differential movements are accommodated by sinistral lateral movement along E-W striking faults in conjunction with detachment along SW-NE striking normal faults, resulting in

the formation of triangular shaped areas with less uplift. The best example for this mechanism is given by the Dragos Voda- and Greben faults delimiting the Borsa graben. This observation favours a rather distributed strike-slip and normal fault pattern ("Dragos Voda fault zone", Zweigel et al. 1998), contradicting an eastward "en bloc" extrusion of

Tisza-Dacia bounded by large strike slip faults crosscutting the external thrust belt (Decker and Peresson 1996, Linzer et al. 1998). The simple compressional “double vergent wedge”-model, as proposed by Sanders (1998) for the development of the East Carpathians may be a possible mechanism along the N-S-striking European margin to the S of the study area, but is considered unlikely for the study area itself.

Within the study area (Fig. 5.7c) the transpressional stage is expressed mainly in the western part. Apatite fission track cooling ages related to relatively minor exhumation during this stage (Fig. 5.7c) are observed in samples which have been buried only to values around the upper temperature limit of the apatite partial annealing zone (100-120°C; S2, S4). In the Bucovinian nappes enhanced exhumation during the transtensional stage led to the exhumation of levels from below the apatite partial annealing zone, obscuring the smaller amount of exhumation expected during the transpressional stage. The age differences within the Rodna horst are mainly the result of altitude differences between the samples.

#### 5.4 Uplift during and following soft collision

Based on the constraints for post-16 Ma uplift discussed above (Fig. 5.2, Fig. 5.3), a contoured uplift map is presented in Fig. 5.8. The available data points (black dots in Fig. 5.8a) have been interpolated using a minimum curvature algorithm.

In the area of the Preluca massif a region with moderate uplift (3-4 km) is visible, delimited to the north by a brittle fault. This uplifted area further extends to the east and is interpreted as a pop-up structure that formed during the transpressional stage. The two data points with 4-5 km uplift, located southwest of the Rodna horst, may suggest a possible prolongation of the pop-up structure towards the east.

The high amounts of uplift realised in the Bucovinian nappes are accompanied by a general SW-down tilting of the units towards the Transylvanian basin. This general trend is visible in all fault bounded blocks. Main structures are E-W trending sinistral strike slip faults, together with SW-NE striking normal faults. In the Rodna horst

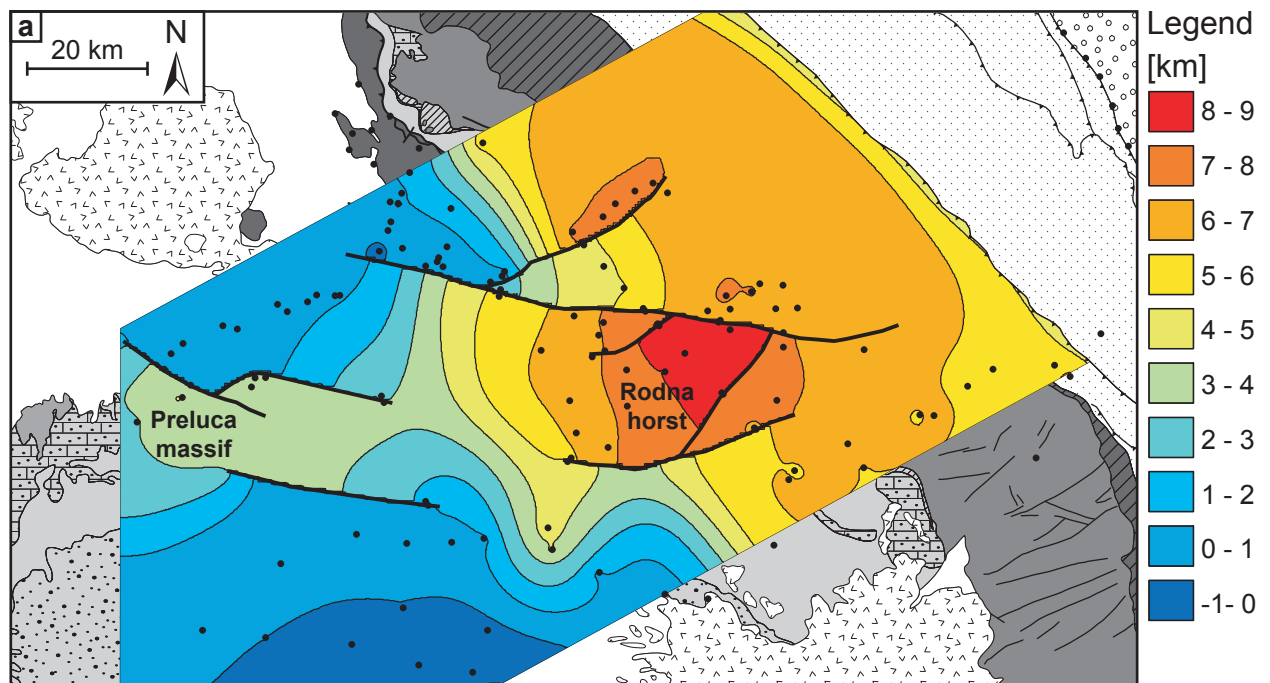
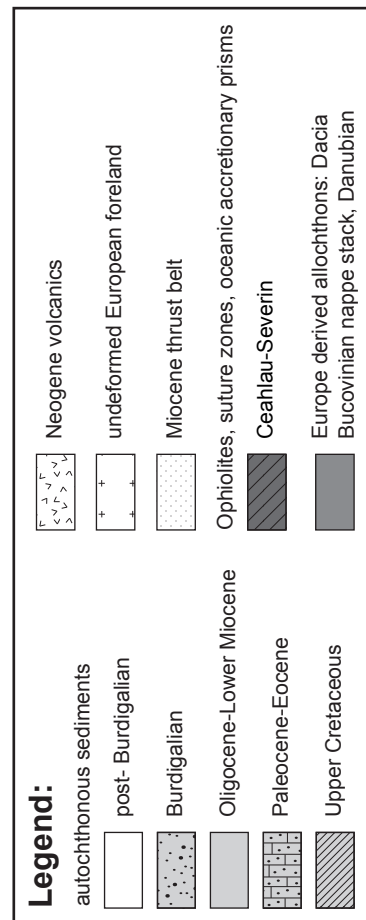
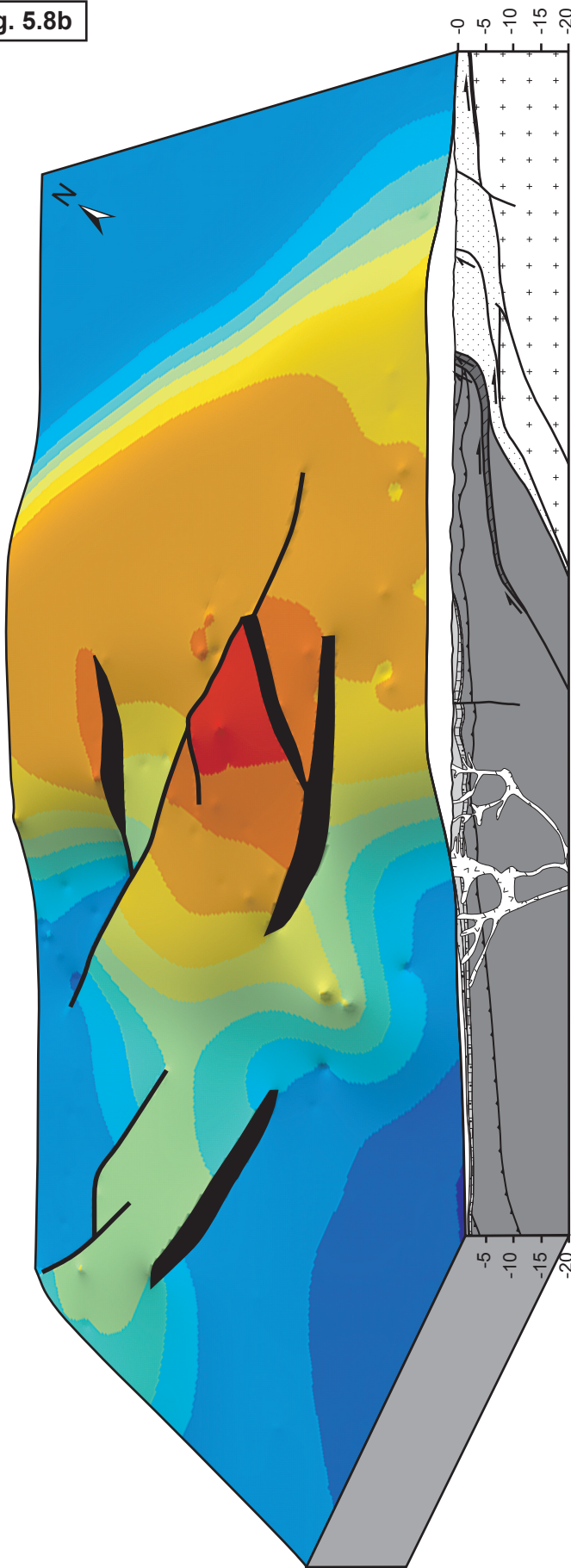


**Fig. 5.8.**

*a:* Contoured map showing the total amount uplift during and following soft collision of Tisza-Dacia with the European margin. Black dots indicate constraint input data. The amount of uplift is contoured using a minimum curvature interpolation.

*b* (next page): 3-Dimensional block model of the map. The profile given is simplified and modified after Stefanescu (1988), following largely the interpretation by Schmid et al. (2008).

Fig. 5.8b





the central block shows a stronger tilt towards the SW, allowing for by NE-ward increasing offsets along SW-NE striking normal faults. The maximum amount of post-16 Ma uplift is realised in the central block of the Rodna horst at the junction of Profiles CC' and DD' (Fig. 5.2, Fig. 5.3). There the projected base Oligocene is located at 3500 m above sea level. Together with the estimated Dmax of 5.5 km for the base Oligocene the total amount of exhumation amounts to 9 km. This observed maximum amount of uplift of 9 km is similar to values observed in the Western Carpathians during soft collision of ALCAPA (12 km, Sperner et al. 2002).

The decrease in overall offset along the Dragos-Voda fault towards the east is not only documented by the lack of lateral offset, but also by the negligible vertical offsets at its eastern termination. At the junction with the Greben fault the vertical displacement across the Bogdan-Dragos-Voda fault reaches its maximum of around 3 km. The vertical offset across the Greben fault decreases from around 2 km in the central part to negligible amounts at both tips.

## 5.5 Conclusions

In the study area Oligocene sediments accumulated in an NW-SE trending depot centre, with thicknesses diminishing towards the SW in present day coordinates. During late Early Miocene (Burdigalian, 20-16 Ma) emplacement of the Pienides (20-18.5) led to an additional tectonic burial in the NW of the study area. Syn- and post-emplacement erosion resulting in deposition of a SSE-thinning

clastic wedge caused additional sedimentary burial in the S of the study area. Burial heating caused full annealing of apatite fission tracks (i.e. >120°C) in basement units in the N and E of the study area (Bucovinian nappes). In contrast the temperatures related to Paleogene to Early Miocene burial in the SW (Preluca massif) did not exceed 80°C. Moderate exhumation by erosion is observed in parts of the Pienides and the parautochthonous imbricates.

During and following soft collision of Tisza-Dacia with the European margin, combined uplift and erosion caused exhumation of the buried rocks in two stages. Post 16-Ma uplift reached up to 9 km. During initial convergence perpendicular to the European margin NE-SW compression resulted in minor exhumation, mainly in the west of the study area.

Following oblique E-W convergence led to strain partitioning with thrusting in the external thrust belt and internal strike-slip deformation. Sinistral transtension between 12 and 10 Ma allowed for the docking and fitting of Tisza-Dacia with the NW-SE striking European margin. Differential lateral movements are distributed and deformation is accommodated by E-W striking sinistral strike slip faults and SW-NE striking normal faults, which led to fragmentation into SW-tilted blocks. Fragmentation and differential offset along the bounding faults resulted in the formation of triangular-shaped grabens and corresponding horst structures. During the transtensional stage enhanced exhumation led to the formation of observed Middle to Late Miocene cooling ages.



# Chapter 6:

# Summary

In the following the findings of this thesis are summarized, arranged in chronological order. For reference, a map of the study area is given in Fig. 6.1.

### 6.1 Cretaceous orogeny and Late Cretaceous to Paleocene exhumation

In the basement units of the northern East Carpathians (Bucovinian nappe stack) and the Preluca massif (Biharia unit) zircon fission tracks are largely reset by the last Cretaceous (Alpine) orogeny. Alpine age metamorphism in the Central East Carpathians is interpreted to have resulted from Alpine ("Austrian") top to the NE directed nappe stacking. While this Alpine metamorphic overprint only reached sub-greenschist facies in the main chain of the Central East Carpathians, temperatures up to at least 500°C (Dallmeyer et al. in prep.) are documented in the more internal Rodna horst. This temperature gradient is interpreted to have resulted from increasing tectonic overburden (up to at least 20 km) towards more internal units. Possibly this overburden was partly provided by the Transylvanian nappe stack and/or even higher tectonic units of unknown origin. Late Cretaceous cooling and exhumation is well constrained by zircon fission track data. Cenomanian cooling and exhumation in the more external Central East Carpathians is interpreted as a result of late-stage shortening related to "Austrian" nappe folding. Campanian cooling in the more internal Rodna horst is contemporaneous to cooling and exhumation in the even more internal north-easternmost outcrops of the Biharia unit (Preluca massif).

The close neighbourhood of Coniacian to Campanian zircon fission track cooling ages to Cenomanian sediments suggests tectonic exhumation. However, none of the tectonic stages so far reported for the study area can explain this stage of exhumation. The most likely process would be Late Cretaceous extensional tectonics related to orogenic collapse (Gosau type basins), but this interpretation remains to be supported by structural data. This interpretation is corroborated by the occurrence of Late Cretaceous, sediments with a syntectonic character preserved along the East Carpathian mountains. The absence of zircon fission track ages younger than Eocene excludes heating to temperatures above the zircon partial annealing zone (>300°C) during the following Tertiary development.

### 6.2 Paleogene to Early Miocene burial

Following the Cretaceous orogenies Tisza and Dacia have been amalgamated, and are considered to represent one single block during the following Tertiary development. The Tertiary history of the study area is dominated by emplacement of the continental ALCAPA and Tisza-Dacia blocks into the Carpathian embayment.

After widespread erosion during the Late Cretaceous and Paleocene, renewed sedimentation caused burial of the basement units. Sedimentation starts heterochronously in Paleocene (Preluca massif) or Eocene (Central East Carpathians) times. Onset of Oligocene turbiditic sedimentation announces the juxtaposition of ALCAPA and Tisza-Dacia, with Tisza-Dacia in a lower plate position. Oligocene sediments accumulated in an NW-SE oriented basin with thicknesses diminishing towards the SW.

During late Early Miocene (Burdigalian) the emplacement of the Pienides (20-18.5 Ma) led to additional tectonic burial in the NW of the study area. The SE-directed overthrusting of the Pienides is interpreted to express the final juxtaposition of ALCAPA against Tisza-Dacia. Syn- and post-emplacement erosion resulting in deposition of a SSE-thinning clastic wedge caused additional sedimentary burial in the S of the study area.

Burial heating caused full annealing of apatite fission tracks (i.e. >120°C) in basement units in the N and E of the study area (Central East Carpathians, Rodna horst). In contrast, temperatures related to Paleogene to Early Miocene burial did not exceed 80°C in the SW (Preluca massif). Moderate exhumation by erosion is observed in parts of the Pienides and parautochthonous imbricates.

### 6.3 Post-Burdigalian soft collision of Tisza-Dacia with the European margin

The post-Burdigalian (post-16 Ma) soft collision of Tisza-Dacia with the European margin occurred in two stages, resulting in predominantly sinistral strike-slip deformation during ongoing NE-SW shortening:

*post-Burdigalian transpressional stage (16-12 Ma)*

NE-SW compression led to the formation of open folds, most pronounced in the NE of the study area, as well as reverse faulting (e.g. Preluca fault). During this stage sinistral transpression (16 - 12

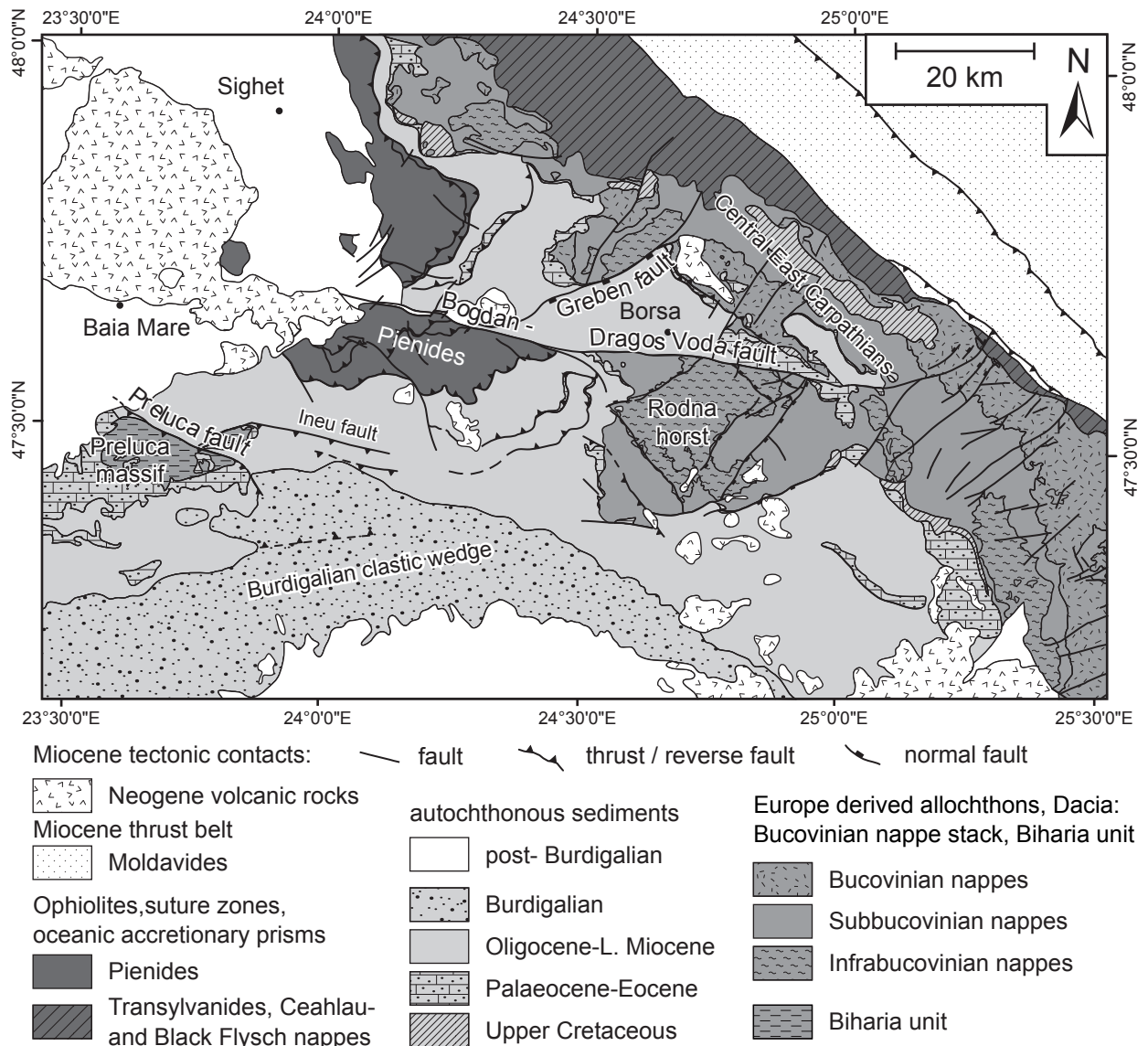


Fig. 6.1. Tectonic map of the study area

Ma) governed the activity along the Bogdan-Voda fault, which terminated eastwards in a thrust splay geometry.

#### *post-Burdigalian transtensional stage (12-10 Ma)*

The transtensional stage led to the formation of the Bogdan-Drăgos-Voda fault system. During sinistral transtension (12 – 10 Ma) the Bogdan- and Drăgos-Voda fault segments are kinematically linked and operate together with coevally active SW-NE trending normal faults. The lateral offset is reduced towards the E, the fault system terminates in an extensional horse-tail splay geometry.

During and following soft collision of Tisza-Dacia with the European margin combined uplift and erosion caused exhumation of the buried rocks, documented by apatite fission track data. Uplift

reaches up to 9 km in the Rodna horst. Apatite fission track cooling ages (15-13 Ma) related to relatively minor exhumation during the transpressional stage are observed in the sedimentary units in the western part of the study area. In the basement units of the Bucovinian nappe stack enhanced exhumation during the transtensional stage led to the exhumation of levels from below the apatite partial annealing zone, obscuring the smaller amount of exhumation expected during the transpressional stage

The late-stage evolution of the Rodna horst is dominated by combined normal and strike-slip faulting, which led to its fragmentation into tilted, fault-bounded blocks. Fast exhumation in the central part of the Rodna area resulted in Middle to Late Miocene cooling ages (13-7 Ma). Exhumation

rates exceeded 1 mm/a during this stage and caused advective heat transport and subsequently delayed enhanced cooling.

The two stages of strike-slip dominated tectonic activity are correlated to two stages of convergence of Tisza-Dacia with the European margin. Initial convergence perpendicular to the European margin led to NE-SW compression, while subsequent East-directed oblique convergence allowed for docking and fitting of Tisza-Dacia with the NW-SE striking European margin. Oblique E-W convergence led to strain partitioning with thrusting in the external thrust belt and internal strike-slip deformation. Differential lateral movements are distributed and deformation is accommodated by E-W striking sinistral strike slip faults and SW-NE striking normal faults, which led to fragmentation into SW-tilted blocks. Fragmentation and differential offset along the bounding faults resulted in the formation of triangular-shaped grabens and corresponding horst structures.

#### **6.4 Possible further fields of investigation**

A very fruitful topic for further scientific work is the role of the Late Cretaceous extensional

tectonics suggested by zircon fission track data. The similarity between the Late Cretaceous cooling ages in the internal East Carpathian basement (Rodna horst) and the more internal northern Biharia unit (Preluca massif) suggest a relation of these units during the Late Cretaceous. The Cretaceous development in the northern East Carpathians is still poorly understood and provides a large field for possible projects.

Regarding the Miocene it would be interesting to concentrate on the soft collision of Tisza-Dacia with the European margin. The interplay between the two stage development during emplacement, indicated by structural data, with uplift, suggested by thermochronological data, is constraint by the findings of this thesis and the complementary thesis in the project (Tischler 2005). As a next step analogue modelling of the suggested plate tectonic development could help to quantify and verify the results, which are based on field data. Direct comparison between tectonics observed in the field and analogue modelling have proved fruitful, for example in case of the lateral extrusion of the Eastern Alps (Ratschbacher et al. 1991a, 1991b) or soft collision of Tisza-Dacia with the European margin in the southern East Carpathians (Zweigel et al. 1998).

## References

- Andriessen PAM (1995): Fission track analysis: principles, methodology, and implications for tectono-thermal histories of sediment basins, orogenic belts and continental margins. *Geologie en Mijnbouw* 74: 1-12
- Angelier J, Mechler P (1977): Sur une méthode graphique de recherche des contraintes principales également utilisable en tectonique et enseignement: la méthode des dièdres droits. *Bull Soc Géol France VII* (19): 1309-1318
- Antonescu F, Mitrea G, Popescu A (1981): Contributii la cunoasterea stratigrafiei si tectonicii miocenului din regiunea Vadu Izei-Birsan-Botiza (Maramures). *D.S. Inst Geol Geofiz LXVI*: 5-23
- Aroldi C (2001): The Pienides in Maramures – Sedimentation, tectonics and paleogeography. PhD Thesis, Cluj: 156p
- Balestrieri ML, Stuart FM, Persano C., Abbate E, Bigazzi G (2005): Geomorphic development of the escarpment of the Eritrean margin, southern Red Sea from combined apatite fission-track and (U-Th)/He thermochronometry. *Earth Planet. Sci. Lett.* 231: 97-110
- Balintoni I (1995): Alpine structural outline of the Pannonian Carpathian realm. *Studia Universitates Babes - Bolyai, Geologia XL*(2): 3-16
- Balintoni I (1995): Alpine plate boundaries on the territory of Romania. *Studia Universitates Babes - Bolyai, Geologia XL* (1): 56-72.
- Balintoni I, Baier U (2001): Cercetari structurale în carpatii orientali. *Studia Universitates Babes - Bolyai, Geologia XLVI* (1): 3-13.
- Balintoni I, Mosonyi E, Puste A (1997): Informatii si interpretari litostratigrafice, metamorfice si structurale privitoare la masivul Rodna (Carpatii orientali). *Studia Universitates Babes - Bolyai, Geologia XLII* (2): 51-66
- Balla Z (1982): Development of the Pannonian Basin basement through the Cretaceous-Cenozoic collision; a new synthesis. *Tectonophysics* 88: 61-102
- Balla Z (1987): Tertiary paleomagnetic data for the Carpatho-Pannonian region in the light of Miocene rotation kinematics. *Tectonophysics* 139: 67-98
- Bingham C (1964): Distributions on a sphere and the projective plane. PhD. diss. Yale University, New Haven: 93p
- Blanckenburg F von, Villa IM, Baur H, Morteani G, Steiger RH (1989): Time calibration of a PT-path from the Western Tauern Window Eastern Alps: the problem of closure temperatures. *Contrib. Mineral. Petrol.* 101: 1-11
- Borcos M, Sandulescu M, Stan N, Peltz S, Marinescu F, Ticleanu N (1980): Geological Map 1:50.000 Cavnic. Bucharest, Institutul de Geologie si Geofizica
- Braun J (2002): Quantifying the effect of recent relief changes on age-elevation relationships. *Earth and Planetary Science Letters* 200: 331-343
- Broucker De G, Mellin A, Duindam P (1998): Tectonostratigraphic evolution of the Transylvanian Basin, Pre-Salt sequence, Romania, In: Dinu C (ed) BGF Special volume 1: 36-70
- Brown, RW (1991): Backstacking apatite fission track "stratigraphy": A method for resolving the erosional and isostatic rebound components of tectonic uplift histories. *Geology* 19: 74-77.
- Burchfiel BC (1980): Eastern European Alpine system and the Carpathian orocline as an example of collision tectonics. *Tectonophysics* 63: 31-61
- Burtner RL, Nigrini A, Donelick RA (1994) Thermochronology of Lower Cretaceous Source Rocks in the Idaho-Wyoming Thrust Belt. *Am Assoc Petrol Geol Bull* 78 (10): 1613-1636
- Carlson WD, Donelick RA, Ketcham, R.A. (1999): Variability of apatite fission-track annealing kinetics: I.

- Experimental results. *American Mineralogist* 84: 1213-1223
- Ciulavu D (1999): Tertiary tectonics of the Transylvanian Basin. PhD. diss. *Vrije Universiteit Amsterdam*, Amsterdam: 154p
- Ciulavu D, Dinu C, Cloetingh SAPL (2002): Late Cenozoic tectonic evolution of the Transylvanian basin and northeastern part of the Pannonian basin (Romania): Constraints from seismic profiling and numerical modeling. *EGU Stephan Mueller Special Publication Series* 3: 105-120
- Cloetingh S, Bada G, Maţenco L, Lankreijer A, Horváth F, Dinu C (2005): Thermo-mechanical modelling of the Pannonian-Carpathian system: Modes of tectonic deformation, lithospheric strength and vertical motions. *Geol. Soc. London Spec. Publ.*, (in press.)
- Crowley KD (1985): Thermal significance of fission-track length distributions. *Nuclear Tracks* 10 (3): 311-322.
- Crowley KD, Cameron M (1987): Annealing of etchable fission-track damage in apatite: Effects of anion chemistry. *Geol. Soc. Amer. Abstr. Prog.* 19: 631-632
- Crowley KD, Cameron M, Schaefer RL (1991): Experimental studies of annealing of etched fission tracks in fluorapatite. *Geochimica et Cosmochimica Acta* 55: 1449-1465
- Csontos L (1995): Tertiary tectonic evolution of the Intra-Carpathian area: a review. *Acta Vulcanologica* 7 (2): 1-13
- Csontos L, Nagymarosy A (1998): The Mid-Hungarian line: a zone of repeated tectonic inversions. *Tectonophysics* 297: 51-71
- Csontos L, Vörös A (2004): Mesozoic plate tectonic reconstruction of the Carpathian region. *Paleogeography, Paleoclimatology, Paleoecology* 210: 1-56
- Csontos L, Nagymarosy A, Horváth F, Kováč M (1992): Cenozoic evolution of the Intra-Carpathian area: a model. *Tectonophysics* 208: 221-241
- Dallmeyer RD, Neubauer F, Handler R, Fritz H, Müller W, Pana D, Putis M (1996): Tectonothermal evolution of the internal Alps and Carpathians: Evidence from  $^{40}\text{Ar}/^{39}\text{Ar}$  mineral and whole-rock data. *Eclogae Geologicae Helvetica* 89(1): 203-227
- Dallmeyer RD, Neubauer F, Krätner HG, Fritz H, Bojar AV (1998): Variscan and Alpine tectonic processes in the Eastern Carpathian orogen: Evidence from  $^{40}\text{Ar}/^{39}\text{Ar}$  mineral ages and structural analysis. *CBGA Abstract*: 113
- Dallmeyer RD, Neubauer F, Krätner HG, Fritz H, Bojar, AV: Variscan vs. Alpine tectonic processes in the Eastern Carpathian orogen: Evidence from  $^{40}\text{Ar}/^{39}\text{Ar}$  mineral ages. (in prep.)
- Danisik M, Dunkl I, Putis M, Frisch W, Kral J. (2004): Tertiary burial and exhumation history of basement highs along the NW margin of the Pannonian basin- an apatite fission track study. *Austrian Journal of Earth sciences* 95/96: 60-70
- Decker K, Peresson H (1996): Tertiary kinematics in the Alpine-Carpathian-Pannonian system: links between thrusting, transform faulting and crustal extension. In: G Wessely and W. Laebl (Eds) *Oil and Gas in Alpidic Thrustbelts and Basins of Central and Eastern Europe*. *EAGE Special Publications* 5: 69-77
- Demetrescu C, Veliciu S (1991): Heat flow and lithosphere structure in Romania. In: V Cermak and L Rybach (Eds) *Terrestrial heat flow and the lithosphere structure*. *Springer-Verlag, Berlin, New York*: 187-205
- Dicea O, Duţescu P, Antonescu F, Mitrea G, Botez R, Donos I, Lungu V, Moroşanu I (1980): Contributii la cunoasterea stratigrafiei zonei transcarpatice din maramures. *D. S. Inst geol geofiz* LXV, 4: 21- 85
- Dimitrijevic MD (2001): Dinarides and the Vardar Zone: a short review of the geology. *Acta Vulcanologica* 13: 1-8
- Duddy, IR, Green PF, Laslett GM. (1988): Thermal annealing of fission tracks in apatite 3. Variable temperature behaviour. *Chemical Geology* 73: 25-38
- Dumitru T. (1993): A new computer-automated microscope stage system for fission-track analysis. *Nuclear*



- Tracks and Radiation Measurements 21 (4): 575-580
- Dunkl I (2002): Trackkey: a Windows program for calculation and graphical presentation of fission track data. *Computers & Geosciences* 28: 3-12
- Dunkl I, Frisch W (2002): Thermochronological constraints on the Late Cenozoic exhumation along the Alpine and Western Carpathian margins of the Pannonian basin. *EGU Stephan Mueller Special Publications Series 3*: 135-147
- Dunkl I, Székely B (2002): Component analysis with visualization of fitting PopShare, a Windows program for data analysis. *Goldschmidt Conference Abstracts 2002, Geochimica et Cosmochimica Acta*, 66/15A: 201
- Ehlers TA, Farley KA (2003): Apatite (U-Th)/He thermochronometry: methods and applications to problems in tectonic and surface processes. *Earth and Planetary Science Letters* 206: 1-14.
- Farley KA (2000): Helium diffusion from apatite: General behaviour as illustrated by Durango fluorapatite. *Journal of Geophysical Research* 105: 2903-2914
- Farley KA (2002): (U/Th)/He dating: Techniques, calibrations, and applications. In: PD Porcelli, CJ Ballentine, R Wieler (Eds) *Noble Gas Geochemistry, Reviews in Mineralogy and Geochemistry* vol. 47 (2002): 819-843
- Fodor L, Jelen B, Márton M, Skaberne D, Car J, Vrabec M (1998): Miocene-Pliocene tectonic evolution of the Slovenian Periadriatic fault: Implications for Alpine-Carpathian extrusion models. *Tectonics* 17: 690-709
- Fodor L, Csontos L, Bada G, Györfi I, Benkovics L (1999): Tertiary tectonic evolution of the Pannonian basin system and neighbouring orogens: a new synthesis of paleostress data. In: Durand B, Jolivet L, Horváth F, Séranne M (Eds) *The Mediterranean basins: Tertiary Extension within the Alpine Orogen*. *Geol Soc Spec Publ* 156: 295-334
- Foeken JPT, Dunai TJ, Betotti G, Andriessen PAM (2003): Late Miocene to present exhumation in the Ligurian Alps (southwest Alps) with evidence for accelerated denudation during the Messinian salinity crisis. *Geology* 31 (9): 797-800
- Foeken JPT, Stuart FM, Dobson KJ, Persano C, Vilbert D (2006): A diode laser system for heating minerals for (U-Th)/He chronometry. DOI 10.1029/2005GC001190, *Geochem. Geophys. Geosyst* 7 (Q04015)
- Fügenschuh B, Schmid SM (2003): Late stages of deformation and exhumation of an orogen constrained by fission-track data: A case study in the Western Alps. *GSA Bulletin* 115 (11): 1425-1440
- Fügenschuh B, Schmid SM (2005): Age and significance of core complex formation in a highly bent orogen: evidence from fission track studies in the South Carpathians (Romania). *Tectonophysics* 404: 33-35
- Fügenschuh B, Mancktelow NS, Seward D (2000): Cretaceous to Neogene cooling and exhumation history of the Oetzal-Stubai basement complex, eastern Alps: A structural and fission track study. *Tectonics* 19 (5): 905-918
- Galbraith RF (1981): On Statistical Models for Fission Track Counts. *Mathematical Geology* 13 (6): 471-478.
- Galbraith RF (1990): The radial plot: Graphical assesment of spread in ages. *Nucl Tracks Radiat Meas* 17: 207-214
- Galbraith RF, Laslett GM (1993): Statistical models for mixed fission track ages. *Nucl Tracks Radiat Meas* 21: 450-470
- Gallagher K (1995): Evolving temperature histories from apatite fission-track data. *Earth and Planetary Science Letters* 136: 421-435
- Gallagher K, Brown R, Johnson C. (1998): Fission track analysis and its applications to geological problems. *Annu Rev Earth Planet Sci* 26: 519-571
- Giusca D, Radulescu D (1967): Geological map 1:200.000 No. 3 Baia Mare. Institutul de Geologie si Geofizica,

Bucharest.

- Gleadow AJW (1981): Fission track dating methods: what are the real alternatives ? *Nucl Tracks* 5: 3-14
- Gleadow AJW, Duddy IR (1981): A natural long-term track annealing experiment for apatite. *Nucl Tracks* 5 (1/2): 169-174
- Gleadow AJW, Duddy IR, Green PF, Lovering JF (1986a): Confined track lengths in apatite: a diagnostic tool for thermal history analysis. *Contributions to Mineralogy and Petrology* 94: 405-415
- Gleadow AJW, Duddy IR, Green PF, Hegarty KA (1986b): Fission track lengths in the apatite annealing zone and the interpretation of mixed ages. *Earth and Planetary Science Letters* 78: 245-254
- Gradstein F, Ogg J, Smith A (2004): *A Geologic Time Scale*. Cambridge University Press, Cambridge: 589p
- Green PF, Duddy IR, Gleadow AJW, Tingate PR (1985): Fission track annealing in apatite: Track length measurements and the form of the Arrhenius plot. *Nuclear Tracks* 10: 323-328
- Green PF, Duddy IR, Gleadow AJW, Tingate PR, Laslett GM (1986): Thermal annealing of fission tracks in apatite, 1. A qualitative description. *Chemical Geology* 59: 237-253.
- Green PF, Duddy IR, Laslett GM, Hegarty KA, Gleadow AJW, Lovering JF (1989): Thermal annealing of fission tracks in apatite, 4. Quantitative modelling techniques and extension to geological timecales. *Chemical Geology* 79: 155-182
- Gröger HR (2006): Thermal and structural evolution of the East Carpathians in northern Romania: from Cretaceous orogeny to final exhumation during Miocene collision. PhD thesis, University of Basel, Switzerland. 114p
- Gröger HR, Fügenschuh B, Tischler M, Schmid SM, Foeken J (2008): Tertiary cooling and exhumation history in the Maramures area (internal eastern Carpathians, Northern Romania): thermochronology and structural data. In: Siegesmund S, Fügenschuh B, Fritzsche N (Eds) *Tectonic Aspects of the Alpine-Dinaride-Carpathian System*. *Geol Soc Spec Publ* 298: 169-195
- Györfi I, Csontos L, Nagymarosy A (1999): Early Cenozoic structural evolution of the border zone between the Pannonian and Transylvanian basins. In: Durand B, Jolivet L, Horváth F, Séranne M (Eds) *The Mediterranean Basins: Cenozoic Extension within the Alpine Orogen*. *Geol Soc Spec Publ* 156: 251-267
- Haas J, Pero S (2004): Mesozoic evolution of the Tisza Mega-unit. *Int J Earth Sci* 93: 297-313
- Haas J, Mioč P, Pamić J, Tomljenović B, Árkai P, Bérczi-Makk A, Koroknai B, Kovács S, Rálich-Felgenhauer E (2000). Complex structural pattern of the Alpine-Dinaridic-Pannonian triple junction. *Int J Earth Sci* 89: 377-389
- Hames WE, Bowring SA (1994): An empirical evaluation of the argon diffusion geometry in muscovite. *Earth Planet. Sci. Lett.* 124: 357-367
- Haq BU, Hardenbol J, Vail PR (1987): The chronology of fluctuating sea level since the Triassic. *Science* 235: 1156-1167
- Harrison TM (1981): Diffusion of  $^{40}\text{Ar}$  in hornblende. *Contr. Minera. Petrol.* 78: 324-331
- Horváth F, Bada G, Szafián P, Tari G, Ádám A, Cloetingh S (2005): Formation and deformation of the Pannonian basin: constraints from observational data. *Geol Soc London Spec Publ*: (in press.)
- House MA, Farley KA, Stöckli DF (2000): Helium chronometry of apatite and titanite using Nd:YAG laser heating. *Earth and Planetary Science Letters* 183: 365-368
- Huismans RS, Bertotti G, Ciulavu D, Sanders CAE, Cloetingh S, Dinu C (1997): Structural evolution of the Transylvanian Basin (Romania): a sedimentary basin in the bend zone of the Carpathians. *Tectonophysics* 272: 249-268
- Hurford AJ (1986): Cooling and uplift patterns in the Lepontine Alps South Central Switzerland and an age of vertical movement on the Insubric fault line. *Contributions to Mineralogy and Petrology* 92: 413-427

- Hurford AJ, Green PF (1983): The zeta age calibration of fission track dating. *Isotope Geoscience* 1: 185-317
- Hurford AJ, Hammerschmidt, K (1985):  $^{40}\text{Ar}/^{39}\text{Ar}$  and K/Ar dating of the Bishop and Fish Canyon Tuffs: calibration ages for fission track dating standards. *Chem. Geol. (Isot. Geosci.)* 58: 23-32
- Ianovici V, Dessila-Codarcea M (1968): Geological Map 1:200000 Radauti. Bucharest, Institutul de Geologie si Geofizica
- Ianovici V, Radulescu D (1968): Geological Map 1:200000 Toplita. Bucharest, Institutul de Geologie si Geofizica
- Ianovici V, Radulescu D, Patruilus D (1968): Geological Map 1:200000 Viseu. Bucharest, Institutul de Geologie si Geofizica
- Jiricek R (1979): Tectonic development of the Carpathian arc in the Oligocene and Neogene. In: M Mahel (Editor) *Tectonic Profiles through the Western Carpathians*. Geol. Inst. Dionyz Stur, Bratislava: 205-214
- Jishun R, Baogui N, Zhiganag L (1996): Microcontinents, Soft Collision and Polycyclic Suturing. *Continental Dynamics* 1 (1): 1-9
- Kasuya M, Naeser CW (1988): The effect of  $\alpha$ -damage on fission-track annealing in zircon. *Nucl. Tracks Radiat. Meas.* 14 (4): 477-480
- Ketcham RA, Donelick RA, Carlson WD (1999): Variability of apatite fission-track annealing kinetics: III. Extrapolation to geological time scales. *American Mineralogist* 84: 1235-1255
- Ketcham RA, Donelick RA, Donelick MB (2000): AFTSolve: A program for multi-kinetic modeling of apatite fission-track data. *Geological Materials Research* 2 (1): (electronic)
- Kovács S, Haas S, Csazar G, Szederkenyi T, Buda G, Nagymarosy A (2000): Tectonostratigraphic terranes in the pre-Neogene basement of the Hungarian part of the Pannonian area. *Acta Geol Hung* 43 (3): 225-328
- Krätner T (1938): Das kristalline Massiv von Rodna (Ostkarpathen). *An. Inst. Geol. Roum. (Bucuresti)*, XIX: 164-287
- Krätner HG (1988): East Carpathians. In: V. Zoubek (Editor) *Precambrian in younger fold belts*. London, Wiley: 625-638
- Krätner HG (1991): Pre-Alpine geological evolution of the East Carpathian metamorphics. Some common trends with the West Carpathians. *Geologica Carpathica* 42: 209-217
- Krätner HG, Krätner F, Sandulescu M, Bercia HG, Bercia E, Alexandru G, Stefanescu J, Ion M (1975): Geological Map 1:50.000 No 21b Pojorita. Institutul de Geologie si Geofizica, Bucharest
- Krätner HG, Krätner F, Szasz L, Udubasa G, Istrate G (1978): Map 1:50000 Rodna Veche. Institutul de Geologie si Geofizica, Bucharest
- Krätner HG, Krätner F, Szasz L (1982): Geological Map 1:50000 Pietrosul Rodnei. Institutul de Geologie si Geofizica, Bucharest
- Krätner HG, Krätner F, Szasz L (1983): Geological Map 1:50000 Ineu. Institutul de Geologie si Geofizica, Bucharest
- Krätner HG, Krätner F, Szasz L, Seghedi I (1989): Geological Map 1:50000 Rebra. Institutul de Geologie si Geofizica, Bucharest
- Lang B, Edelstein O, Steinits G, Kovacs M, Halga S (1994): Ar-Ar dating of adularia - a tool in understanding genetic relations between volcanism and mineralization: Baia Mare (Gutii Mountains), northwestern Romania. *Economic Geology* 89: 174-180
- Laslett GM, Green PF, Duddy IR, Gleadow AJW (1987): Thermal annealing of fission tracks in apatite, 1. A quantitative analysis. *Chemical Geology* 65: 1-13
- Linzer H-G, Frisch W, Zweigel P, Girbacea R, Hann H-P, Moser F (1998): Kinematic evolution of the

- Romanian Carpathians. *Tectonophysics* 297: 133-156
- Mancktelow NS, Grasemann B (1997): Time-dependent effects of heat advection and topography on cooling histories during erosion. *Tectonophysics* 270: 167-195
- Marret R, Allmendinger RW (1990): Kinematic analysis of fault slip-data. *J Struct Geol* 12: 973-986
- Márton E (2000): The Tisza Megatectonic Unit in the light of paleomagnetic data. *Acta Geol Hung* 43 (3): 329-343
- Márton E, Fodor L (1995): Combination of palaeomagnetic and stress data - a case study from North Hungary. *Tectonophysics* 242: 99-114
- Márton E, Fodor L (2003): Tertiary paleomagnetic results and structural analysis from the Transdanubian Range (Hungary): rotational disintegration of the ALCAPA unit. *Tectonophysics* 363: 201-224
- Márton E, Fodor L, Jelen J, Marton P, Rifelj H, Kevric R (2002): Miocene to Quarternary deformation in NE Slovenia: complex paeomagnetic and structural study. *Journal of Geodynamics* 34: 627-651
- Márton E, Tischler M, Csontos L, Fügenschuh B, Schmid, SM (2007): The contact zone between the ALCAPA and Tisza-Dacia mega-tectonic units of Northern Romania in the light of new paleomagnetic data. DOI 10.1007/s00015-007-1205-5, *Swiss Journal of Geoscience* 100: 109-124
- Mason PRD, Seghedi I, Szákasc A, Downes H (1998): Magmatic constraints on geodynamic models of subduction in the Eastern Carpathians, Romania. *Tectonophysics* 297: 157-176
- Matenco L Schmid SM (1999): Exhumation of the Danubian nappes system (South Carpathians) during the Early Tertiary: inferences from kinematic and paleostress analysis at the Getic/Danubian nappes contact. *Tectonophysics* 314: 401-422
- Matenco L, Bertotti G (2000): Tertiary tectonic evolution of the external East Carpathians (Romania). *Tectonophysics* 316: 255-286
- Matenco L, Bertotti G, Cloetingh S, Dinu C (2003): Subsidence analysis and tectonic evolution of the external Carpathian-Moesian Platform during Neogene times. *Sediment Geol* 156: 71-94
- Mc Dougall I, Harrison MT (1999): *Geochronology and Thermochronology by the  $^{40}\text{Ar}/^{39}\text{Ar}$  Method*. 2nd ed. Oxford University press, Oxford: 269p
- McDowell FW, Keizer RP (1977): Timing of mid-Tertiary volcanism in the Sierra Madre Occidental between Durango City and Mazatlan, Mexico. *Geol. Soc. Amer. Bull.* 88: 1479-1487.
- Morley CK (1996): Models for relative motion of crustal blocks within the Carpathian region, based on restorations of the outer Carpathian thrust sheets. *Tectonics* 15 (4): 885-904
- Morley CK (2002): Tectonic settings of continental extensional provinces and their impact on sedimentation and hydrocarbon prospectivity. In: RW Renaut, GM Ashley (Eds) *Sedimentation in continental rifts*. Society of Sedimentary Geology special publications 73: 25-55
- Nemčok M (1993): Transition from convergence to escape: field evidence from the West Carpathians. *Tectonophysics* 217: 117-142
- Nemčok M, Pospisil, L, Lexa, J, Donelick, R.A. (1998): Tertiary subduction and slab break-off model of the Carpathian-Pannonian region. *Tectonophysics* 295: 307-340
- Neubauer F, Dallmeyer RD, Dunkl I, Schirnik D (1995): Late Cretaceous exhumation of the metamorphic Gleinalm dome, Eastern Alps: kinematics, cooling history and sedimentary response in a sinistral wrench corridor. *Tectonophysics* 242: 79-89
- O'Sullivan PB, Parrish RR (1995): The importance of apatite composition and single-grain ages when interpreting fission track data from plutonic rocks: a case study from the Coast Ranges, British Columbia. *Earth and Planetary Science Letters* 132: 213-224
- Pamic J (2000): Basic geological features of the Dinarides and South Tisia. In: J Pamic, B Tomljenovic (Eds) *Pancardi 2000 Fieldtrip Guidebook Vijesti* 37 (2): 9-18
- Paná D, Erdmer P (1994): Alpine crustal shear zones and pre-Alpine basement terranes in the Romanian

- Carpathians and Apuseni Mountains. *Geology* 22, 807-810
- Patrascu S, Panaiotu C, Seclaman M., Panaiotu CE (1994): Timing of rotational motion of Apuseni Mountains (Romania): paleomagnetic data from Tertiary magmatic rocks. *Tectonophysics* 233: 163-176
- Pécskay Z, Edelstein O, Kovacs M, Bernád A, Crihan M (1994): K/Ar age determination of Neogene volcanic rocks from the Gutai Mts. (Eastern Carpathians, Romania). *Geol Carp* 45 (6): 357-363
- Pécskay Z, Edelstein O, Seghedi I, Szakács A, Kovacs M, Crihan M, Bernád A (1995): K-Ar datings of Neogene-Quaternary calc-alkaline volcanic rocks in Romania. In: H Downes, O Vaselli (Eds) *Neogene and related magmatism in the Carpatho-Pannonian Region*. *Acta Vulcanologica* 7: 53-61
- Persano C, Stuart FM, Bishop P, Dempster TJ (2005): Deciphering continental breakup in eastern Australia using low temperature thermochronometers. *Journal of Geophysical Research* 110: 10.1029/2004JB003325
- Plasienka D, Grecula P, Mutis M, Kováč M, Hovorca D (1997a): Evolution and structure of the Western Carpathians: an overview. In: Grecula, P. et al. (eds) *Geological Evolution of the Western Carpathians*. *Mineralia Slovaca Monograph*, Bratislava: 1-24
- Plasienka D, Putis M, Kováč M, Sefara J, Hrussecky I (1997b): Zones of Alpidic subduction and crustal underthrusting in the Western Carpathians. In: Grecula, P. et al. (eds) *Geological Evolution of the Western Carpathians*, *Mineralia Slovaca Monograph*, Bratislava: 35-42
- Pfiffner OA, Burkhard M (1987): Determination of paleo-stress axes orientations from fault, twin and earthquake data. *Annales Tectonicae* 1 (1): 48-57
- Rahn MK, Brandon MT, Batt GE, Garver JL (2004): A zero-damage model for fission-track annealing in zircon. *American Mineralogist* 89: 473-484
- Raileanu G, Radulescu D (1967): Geological Map 1:200000 Bistrita. Institutul de Geologie si Geofizica, Bucharest
- Raileanu G, Saulea Z (1968): Geological Map 1:200000 Cluj. Institutul de Geologie si Geofizica, Bucharest
- Ratschbacher L, Merle O, Davy P, Cobbold P (1991a): Lateral extrusion in the Eastern Alps; Part 1, Boundary conditions and experiments scaled for gravity. *Tectonics* 10 (2): 245-256
- Ratschbacher L, Frisch W, Linzer HG, Merle O (1991b): Lateral extrusion in the Eastern Alps; Part 2, Structural analysis. *Tectonics* 10 (2): 257-271
- Ratschbacher L, Linzer HG, Moser F, Strusievicz RO, Bedeleian H, Har N, Mogos PA (1993): Cretaceous to Miocene thrusting and wrenching along the central South Carpathians due to a corner effect during collision and orocline formation. *Tectonics* 12 (4): 855-873
- Reiners PW, Ehlers TA (eds) (2005): *Low-Temperature Thermochronology: Techniques, Interpretations, and Applications*. *Reviews in Mineralogy and Geochemistry* 58: 622p
- Reiners PW, Zhou Z, Ehlers T, Xu C, Brandon MT, Donelick RA, Nicolescu S (2003): Post-orogenic evolution of the Dabie Shan, eastern China, from (U-Th)/He and fission track thermochronology. *American Journal of Science* 303: 489-518
- Roure F, Bessereau G, Kotarba M, Kusmierk J, Strzetelski W (1993): Structure and hydrocarbon habitats of the Polish Carpathian Province. *American Association of Petroleum Geologists Bulletin* 77(9): 1660
- Royden LH (1988): Late Cenozoic Tectonics of the Pannonian Basin System In: Royden LH, Horváth F (eds) *The Pannonian Basin; a study in basin evolution*. *AAPG Mem* 45: 27-48
- Royden LH (1993): The tectonic expression of slab pull at continental convergent boundaries. *Tectonics* 12 (2): 303-325
- Royden LH, Báldi T (1988): Early Cenozoic Tectonics and Paleogeography of the Pannonian and Surrounding Regions. In: Royden LH, Horváth F (eds) *The Pannonian Basin; a study in basin evolution*. *AAPG Mem* 45: 1-16
- Royden LH, Burchfiel BC (1989): Are systematic variations in thrust belt style related to plate boundary

- processes? (The Western Alps versus the Carpathians). *Tectonics* 8 (1): 51-61
- Rusu A, Balintoni I, Bombita G, Popescu G (1983): Geological Map 1:50000 Preluca. Institutul de Geologie si Geofizica, Bucharest
- Sanders C (1998): Tectonics and erosion: competitive forces in a compressive orogen. A fission track study of the Romanian Carpathians. Ph.D. thesis, Vrije Universiteit Amsterdam, Amsterdam: 204p
- Sanders CAE, Andriessen PAM, Cloetingh SAPL (1999): Life cycle of the East Carpathian orogen: Erosion history of a double vergent critical wedge assessed by fission track thermochronology. *Journal of Geophysical Research* 104 (B12): 29095-29112
- Săndulescu M (1980): Sur certain problèmes de la corrélation des Carpathes orientales Roumaines avec les Carpathes Ukrainiennes. D. S. *Inst geol geofiz LXV* (5): 163-180
- Săndulescu M (1982): Contributions à la connaissance de nappes Crétacées de Monts du Maramures (Carpathes Orientales). D. S. *Inst. geol. geofiz. LXIX* (5) *Tectonica si geologie regionala*: 83-96
- Săndulescu M (1984): *Geotectonica Romaniei*. Editura Tehnica, Bucharest: 450p
- Săndulescu M (1988): **Cenozoic Tectonic History of the Carpathians**. In: Royden LH, Horváth F (eds) *The Pannonian Basin; a study in basin evolution*. AAPG Mem 45: 17-26
- Săndulescu M (1994): Overview of Romanian Geology. In: ALCAPA II field guide book. *Romanian J of Tectonics and Reg Geol*, 75 (suppl. 2): 3-15
- Săndulescu M, Russo-Săndulescu D (1981): Geological Map 1:50000 Poiana Botizii. Institutul de Geologie si Geofizica, Bucharest
- Săndulescu M, Kräutner HG, Balintoni I, Russo-Săndulescu D, Micu M (1981): The Structure of the East Carpathians. (Guide Book B1), Carp-Balk Geol Assoc 12th Congress, Bucharest: 1-92p
- Săndulescu M, Szasz L, Balintoni I, Russo-Săndulescu D, Badescu D (1991): Geological Map 1:50.000 No 8d Viseu. Institutul de Geologie si Geofizica, Bucharest
- Săndulescu M, Visarion M, Stanica D, Stanica M, Atanasiu L (1993): Deep Structure of the inner Carpathians in the Maramures-Tisa zone (East Carpathians). *Rom J Geophysics* 16: 67-76
- Schmid SM, Berza T, Diaconescu V, Froitzheim N, Fügenschuh B (1998): Orogen-parallel extension in the South Carpathians. *Tectonophysics* 297: 209-228
- Schmid SM, Fügenschuh B, Kissling E; Schuster R (2004a): Tectonic map and overall architecture of the Alpine orogen. *Eclogae geologicae Helvetiae* 97: 93-117
- Schmid SM, Fügenschuh B, Kissling E; Schuster R (2004b): TRANSMED Transects IV, V and VI: Three lithospheric transects across the Alps and their forelands. In: W Cavazza, FM Roure, W Spakman, GM Stampfli, PA Ziegler (eds). *The TRANSMED Atlas: The Mediterranean Region from Crust to Mantle*. Springer, Berlin Heidelberg, attached CD (version of the explanatory text available from the first author as a pdf-file upon request)
- Schmid SM, Fügenschuh B, Matenco L, Schuster R, Tischler M, Ustaszewski K (2006): The Alps-Carpathians-Dinarides-connection: a compilation of tectonic units. 18th Congress of the Carpathian-Balkan Geological Association, Belgrade, Serbia, September 3-6 2006. *Conference Proceedings*: 535-538
- Schmid SM, Bernoulli D, Fügenschuh B, Matenco L, Schefer S, Schuster R, Tischler M, Ustaszewski, K (2008): The Alpine-Carpathian-Dinaridic orogenic system: correlation and evolution of tectonic units. DOI 10.1007/s00015-008-1247-3. *Swiss J Geosci*:
- Siddall R, Hurford AJ (1998): Semi-quantitative determination of apatite anion composition for fission-track analysis using infra-red microspectroscopy. *Chemical Geology* 150: 181-190
- Snedecor GW, Cochran WG. (1989): *Statistical Methods*, Eighth Edition, Iowa State University Press
- Sobel ER, Dumitru TA (1997): Thrusting and exhumation around the margins of the western Tarim basin during the India-Asia collision. *Journal of Geophysical Research* 102 (B3): 5043-5063
- Sperner B, Ratschbacher L, Nemčok M (2002): Interplay between subduction retreat and lateral extrusion:

- tectonics of the Western Carpathians. *Tectonics* 21 (6): 1051
- Sperner B, CRC 461 Team (2005): Monitoring of Slab Detachment in the Carpathians. In: Wenzel F (ed). *Perspectives in modern Seismology. Lecture Notes in Earth Sciences* 105: 187-202
- Stampfli GM, Borel G (2004): The TRANSMED transects in space and time: constraints on the paleotectonic evolution of the Mediterranean domain. In: Cavazza W, Roure FM, Spakman W, Stampfli GM, Ziegler PA (eds). *The TRANSMED Atlas: The Mediterranean Region from Crust to Mantle. Springer, Berlin and Heidelberg*: 53-80
- Stefanescu M (1988): Profiles at scale 1:200,000. Section A9. Institutul de Geologie si Geofizica, Bucharest
- Steiniger FF, Wessely G (2000): From the Thethyan Ocean to the Paratethys Sea: Oligocene to Neogene Stratigraphy, Paleogeography and Paleobiogeography of the circum-Mediterranean region and the Oligocene to Neogene Basin evolution in Austria. *Mitt Österr Geol Ges* 92: 95-116
- Stockli DF (2005): Application of low-temperature thermochronometry to extensional tectonic settings. In: PW Reiners, TA Ehlers (eds) *Low-Temperature Thermochronology: Techniques, Interpretations, and Applications. Reviews in Mineralogy and Geochemistry* 58: 411-448
- Stüwe K, White L, Brown R (1994): The influence of eroding topography on steady-state isotherms. Applications to fission-track analysis. *Earth Planet. Sci. Lett.*, 124: 63-74
- Szász L (1973): Pozitia stratigrafica a gresiilor si conglomeratelor de Prislop în estul bazinului Borsa si unele consideratii asupra neocretacicului din Maramures si Muntii Bîrgaului. *Dari de seama ale sedintelor LX (1972-2973) (5.Tectonica si Geologie Regionala)*: 143-165
- Tagami T, Shimada C (1996): Natural long-term annealing of zircon fission track system around a granitic pluton. *Journal of Geophysical Research* 101 (B4): 8245-8255
- Tagami T, Carter A, Hurford AJ (1996): Natural long-term annealing of the zircon fission-track system in Vienna Basin deep borehole samples: constraints upon the partial annealing zone closure temperature. *Chemical Geology* 130: 147-157
- Timar-Geng Z, Fügenschuh B, Schaltegger U, Wetzels A (2005): The impact of the Jurassic hydrothermal activity on zircon fission track data from the southern Upper Rhine Graben area. *Schweiz Mineral Petrogr Mitt* 84: 257-269
- Tischler M (2005): A combined structural and sedimentological study of the Inner Carpathians at the northern rim of the Transylvanian basin (N. Romania). PhD thesis, University of Basel, Switzerland. 124p
- Tischler M, Gröger HR, Fügenschuh B, Schmid SM (2006): Miocene tectonics of the Maramures area (Northern Romania): implications for the Mid-Hungarian fault zone. DOI 10.1007/s00531-006-0110-x, *International Journal of Earth Sciences*
- Tischler M, Matenco L, Filipescu S, Gröger, HR, Wetzels A, Fügenschuh B. (2008): Tectonics and sedimentation during convergence of the continental blocks ALCAPA and Tisza-Dacia: The Pienide nappe emplacement and its foredeep (N. Romania). In: Siegesmund S, Fügenschuh B, Froitzheim N (Eds) *Tectonic Aspects of the Alpine-Dinaride-Carpathian System. Geol Soc Spec Publ* 298:
- Veliciu S, Visarion M (1984): Geothermal models for the East Carpathians. *Tectonophysics* 103: 157-165
- Verseck K (2001): Rumänien. Verlag C.H. Beck (Becksche Reihe Länder): 186p
- Voda A, Balintoni I (1994): Corelari lithostratigrafice în cristalinelul Carpatilor Orientali. *Studia Universitates Babes - Bolyai, Geologia* XXXIX (1-2): 61-66
- Wagner G, Van den Haute P (1992). *Fission-track dating. Enke Verlag, Stuttgart.* 285p
- Willingshofer E, Neubauer F, Cloetingh S (1999): Significance of Gosau basins for the upper Cretaceous geodynamic history of the Alpine-Carpathian belt. *Phys. Chem. Earth Part A: Solid Earth Geodesy* 24 (8): 687-695
- Williams N, Wildmann K (2001): Romania&Moldavia. *Lonely planet publications*: 432p







## Appendix B: Fission track analysis- methodology

For an overview of the method and the most important application the reader is referred to Wagner and van den Haute (1992), Andriessen (1995), Gallagher et al. (1998) and Reiners and Ehlers (2005).

Fission track analysis is a radiometric dating procedure. Compared to other isotopic dating methods the fission damage caused in a mineral lattice by the spontaneous decay of the more abundant isotope of uranium ( $^{238}\text{U}$ ) is considered as a daughter product instead of the resulting isotopes. During the explosive fission process two approximately equal-sized fission fragments fly apart at  $180^\circ$  to each other, stripping electrons from atoms lying in their path, and creating a single fission damage trail in the enclosing atomic lattice. The fission tracks accumulate during time related to the uranium content of the grain.

### General age equation of radiometric dating methods

(Equation 1, Wagner und van den Haute 1992)

As for any radiometric dating method the age ( $t$ ) is calculated from the amount of daughter product ( $N_d$ ) and the amount of parent isotope ( $N_p$ ) on the base of the decay constant for parent isotope ( $\lambda$ ).

$$[1] N_d = N_p(e^{\lambda t} - 1)$$

The samples in this thesis are dated using the external detector method (Gleadow 1981), calculating single grain ages (Fig. B1). The content of  $^{238}\text{U}$  isotopes in the grain is calculated on the base of the natural relation of  $^{238}\text{U}$  and  $^{235}\text{U}$  isotopes. Irradiation with thermal neutrons induces the decay of  $^{235}\text{U}$  atoms and induced fission tracks are monitored in a uranium-free detector. Spontaneous fission tracks ( $N_s$ ) are counted on a defined square on the grain (Fig. B1a) and induced tracks ( $N_i$ ) are counted on the corresponding square on the detector (Fig. B1b).

To evade the direct calibration of the neutron fluence of the reactor during irradiation, the ages are calculated using the zeta- $(\xi)$ -calibration method (Hurford and Green 1983). The empirical induced, user and laboratory specific  $\xi$  value is established by counting the age of a known age standard.  $\xi$  combines all relevant constants such as the different decay constants, the natural relation of  $^{238}\text{U}$  and  $^{235}\text{U}$

and the neutron fluence, with exception of the total decay-constant of  $^{238}\text{U}$  ( $\lambda_\alpha$ ). The uranium content of the grain is deduced by comparing the induced tracks from the sample ( $N_i$ ) with the induced tracks formed by a standard glass of a defined uranium content ( $N_d$ ).

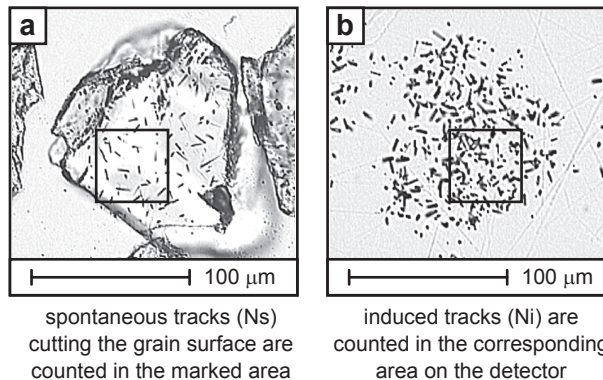


**Fig.B1.** The external detector method (e.g. apatite) A fission track single grain age is based on the ratio of spontaneous tracks ( $N_s$ ) on the grain surface (a) and induced tracks ( $N_i$ ) on a mica detector (b).

### Fission track age equation ( $\xi$ -calibration method)

(Equation 2, Wagner and van den Haute 1992)

The age of a sample ( $t$ ) is calculated from the spontaneous track density on the grain ( $\rho_s$ ), induced track density on the detector ( $\rho_i$ ) and the standard track density (uranium glass,  $\rho_d$ ) on the base of the total decay-constant of  $^{238}\text{U}$  ( $\lambda_\alpha$ ) and the described constant  $\xi$  factor.  $G$  is a geometry factor.

$$[2] t = \frac{1}{\lambda_\alpha} \ln \lambda_\alpha \frac{\rho_s}{\rho_i} \rho_d G \xi + 1$$

The fission tracks are only preserved in a cold lattice. At high temperatures the tracks disappear immediately, in a certain temperature range called partial annealing zone (PAZ) they anneal slowly and at temperatures below that PAZ the tracks are preserved. The PAZ is significant for each dated material. The applicability of fission track analysis in geological materials is restricted by the grain size, the uranium content and the age of the material (Wagner and van den Haute 1992). At a grain size of about  $100 \mu\text{m}$  spontaneous track densities between  $10^5$ - $10^7$  tracks/ $\text{cm}^2$  are required, which requires at geological time scales (1-1000 Ma) uranium contents between 1-10000 ppm. Above  $10^7$  tracks/ $\text{cm}^2$  fission tracks cannot be counted under an optical microscope.

### Thermal histories based on apatite fission track data

For apatite, which is the mineral that has been investigated in most detail for fission track analysis, the partial annealing zone (APAZZ) is relatively clearly defined between 60-120°C (Green et al. 1989; Gleadow and Duddy 1981). Because the annealing behaviour of apatite within the APAZ is well investigated (Gleadow and Duddy 1981; Green et al. 1986; Duddy et al. 1988; Carlson et al. 1999) and annealing algorithms are developed (Laslett et al. 1987; Crowley et al. 1991; Ketcham et al. 1999) it is possible to model time-temperature histories from single grain age and track length data (Green et al. 1989, Gallagher 1995, Ketcham et al. 2000). Therefore lengths of horizontal confined fission tracks were additionally measured in apatite (Fig. B2a). The confined track length distribution is diagnostic for different types of cooling histories (Crowley 1985, Gleadow et al. 1986a, b, Galbraith and Laslett 1993, Fig.B3).

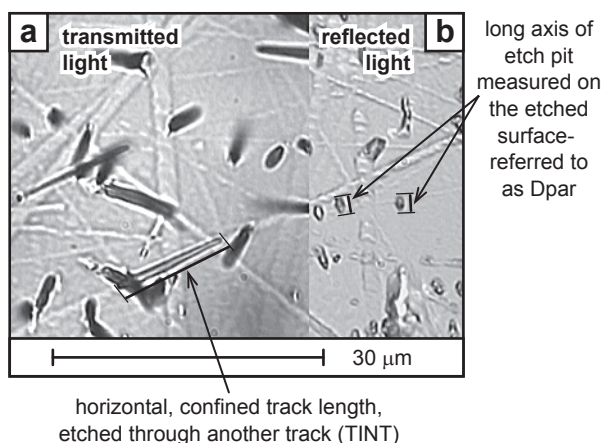


**Fig.B2.** The lengths of confined horizontal tracks (a) provide more detailed information about the thermal history and allow for thermal modelling. To estimate the chemical variation between grains of one sample the long axes of etch pits (Dpar) were measured (b).

### Chemical dependence of annealing behaviour in apatite

Track annealing of fission tracks in apatite is not only dependent on temperature, but also on chemical composition. In the chemical formula of apatite  $\text{Ca}_5[(\text{F}, \text{Cl}, \text{OH})/(\text{PO}_4)_3]$  the mixture of F, Cl and OH is variable. It is mostly agreed, that Cl-rich apatites are more resistant to annealing than F-rich apatites (Green et al. 1985, 1986; Crowley and Cameron 1987; O'Sullivan and Parrish 1995).

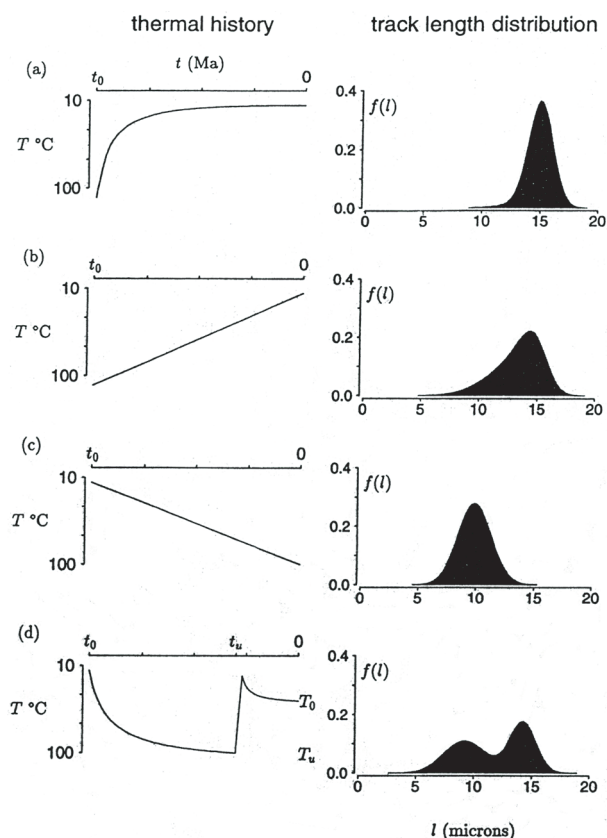


**Fig.B3.** (after Galbraith and Laslett 1993)

Some thermal histories and corresponding track length distributions : (a) rapid cooling to current temperature; (b) slow cooling to the current temperature; (c) slow heating to maximum temperature now; and (d) heating to maximum temperatures, rapid cooling and subsequent cooling.

In chemically variable samples F-apatites in general have a lower closure temperatures than, thus F-apatites show younger single grain ages than Cl-apatites. More recent publications consider rather the modifications to the crystal structure responsible for differential annealing behaviour than the content of the elements (Siddall and Hurford 1998).

An indirect indicator of these compositional dependent annealing differences is the long axis of the generally rhomb-shaped etch pit on the grain surface (referred to as Dpar, Burtner et al. 1994, see Fig. B2b). Under equal etching conditions F-rich apatites have generally a smaller Dpar length than F-Cl-OH-apatites, indicating less resistance to annealing (Burtner et al. 1994).

## Appendix C: Fission track analysis-analytical procedure

### Separation

Apart from the mineral separation described below (Fig. C1) of every sample each an egg sieced piece is left behind and a thin section is prepared.

Coarse separation:

- Smashing of the rocks in egg-sized pieces
- crushing in a jaw-crusher
- milling in a drum-mill, sieving ( $>300\ \mu\text{m}$ )
- enriching of heavy minerals on a water separating table (Wilfli-table)

Result: fraction enriched in heavy minerals

Fine separation:

- magnetic separation (three steps: 3 mAmp, 7 mAmp, 10 mAmp)
- heavy liquid separation in two steps (Bromoform:  $d=2.8\ \text{g/cm}^3$ ; Methyleniodid:  $d=3.1\ \text{g/cm}^3$ )

Result:

non magnetic zircon fraction ( $>3.1\ \text{g/cm}^3$ )

non magnetic apatite fraction ( $2.8 < x < 3.1\ \text{g/cm}^3$ )

### Zircon:

If necessary the zircon fraction has been boiled in 65%  $\text{HNO}_3$  to solve pyrite. The most suitable fraction has been enriched by panning in acetone. 2 specimens were prepared per sample and 200 grains per specimen were handpicked.

- Mounting: PFA® Teflon, heated for about 20 sec to  $300^\circ\text{C}$
- Polishing: Diamondpaste,  $\text{SiO}_2$ -solution, Aluminium-solution,
- Etching: 12-24 h in an eutectic melt of  $\text{NaOH/KOH}$  (relation: 16/23 g) at  $225^\circ\text{C}$

### Apatite:

The most suitable fraction has been enriched by panning in acetone. 2 specimens were prepared per each sample: 1. specimen: 150 apatites handpicked, 2. specimen: grains are scattered

- Mounting: epoxy resin (Araldit M)
- Polishing: Diamondpaste,  $\text{SiO}_2$ -solution, aluminium-solution
- Etching: 40 sec at room temperature ( $19\text{-}26^\circ\text{C}$ ) in 6.5 %  $\text{HNO}_3$

### External detector method

Sample specimens have been adjusted in close contact to a uranium free detector (white mica, Fig. C1). Neutron fluxes have been monitored in uranium enriched glasses CN5 (12.17 ppm U; trader:

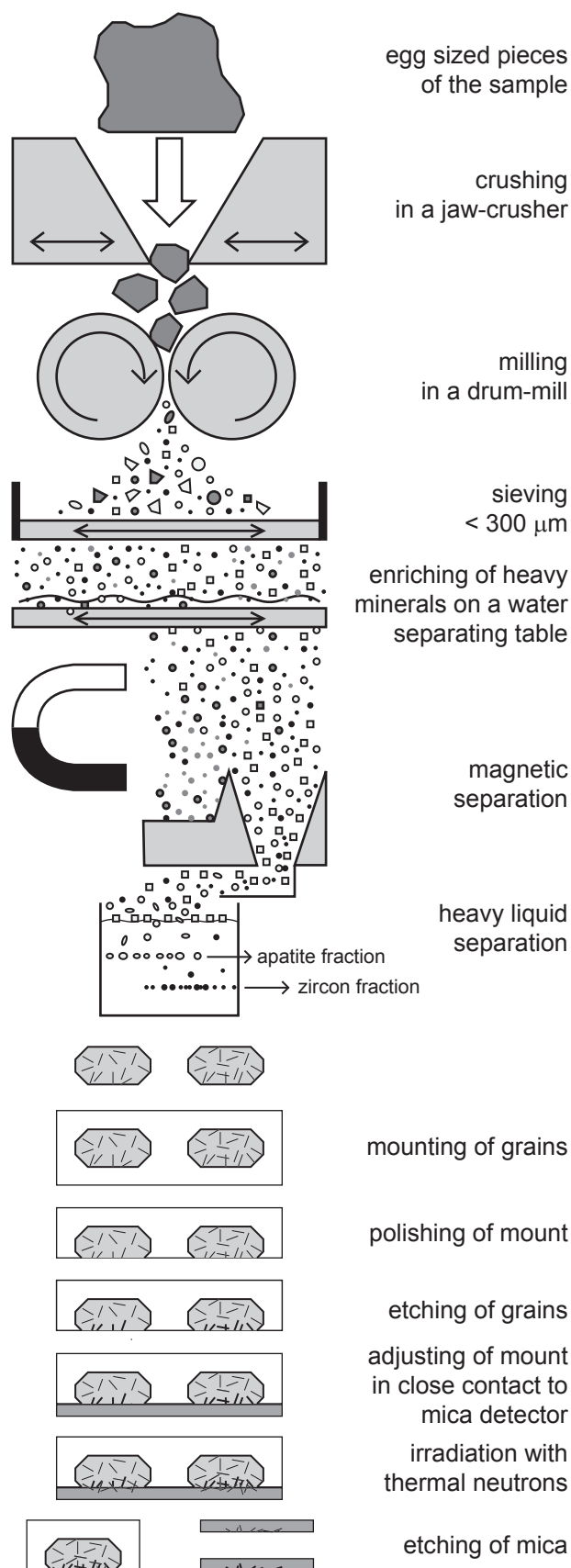


Fig. C1. Schematic picture showing the sample preparation for fission track analysis.

J. Schreurs, Corning) for apatite and CN1 (39.8 ppm U; trader: J.Schreurs, Corning) for zircon.

- Irradiation: High Flux Australian Reactor (HIFAR)
- Zircon: irradiation  $1 \times 10^{15}$  ncm<sup>-2</sup> (Fig. C2)
- Apatite (low): irradiation  $1 \times 10^{16}$  ncm<sup>-2</sup> (Fig. C3)
- Apatite (high): irradiation  $1 \times 10^{17}$  ncm<sup>-2</sup> (Fig. C4)
- Etching (mica): 40 min at room temperature in 40% HF

Sample specimens have been placed in steel or aluminium cans. A uranium glass (CN1, CN5) is placed at the bottom and the top of each can. Then for both the uranium glasses on the same area fission tracks have been counted (Nd), to define the track density representing the given uranium content (=standard track density, RhoD (Pd)). The given Nd in the data tables (Chapter 2, Chapter 3, Appendix D) is the mean of both values counted at the bottom and the top of each can. Counted values for Nd are given on CD (ExtDect.xls).

- Areas counted on uranium glasses:
- Zircon: BS24:  $40 \times 16000 \mu\text{m}^2$ , BS44, BS45:  $50 \times 16000 \mu\text{m}^2$
- Apatite(low):  $25 \times 16000 \mu\text{m}^2$
- Apatite(high): BS27:  $30 \times 640 \mu\text{m}^2$ , BS41:  $4 \times 16000 \mu\text{m}^2$ , BS43:  $10 \times 4000 \mu\text{m}^2$ , BS47:  $15 \times 4000 \mu\text{m}^2$

The standard track density for each sample given in the data tables (Chapter 2, Chapter 4, Appendix D) is calculated by a linear relation through the two counted values (Equation 3, Fig. C2-C4):

$$[3] \quad Pd(xs) = Pd(xt) + (xs - 1) \times \frac{Pd(x1) - Pd(xt)}{xt - 1}$$

- Pd: standard track density
- x1: bottom position in can
- xt: top position in can
- xs: sample position in can

#### Zeta calibration

- Age standards used:
- Zircon (Fig. C5a): Fish Canyon Tuff (Colorado)  $27.9 \pm 0.5$  Ma ( $2\sigma$ , Hurford and Hammerschmidt 1985)
- Apatite (Fig. C5b): Durango (Cerro de Mercado, Mexico)  $31.4 \pm 0.4$  Ma ( $2\sigma$ , McDowell and Keizer 1977)

To obtain a zeta value different specimens have been counted (zircon: 15; apatite: 17; CD: Zeta.xls; Fig.C5) and pooled zeta values have been calculated (zfactor.exe; <http://earth.geology.yale.edu/~brandon>). For the age calculations in this

thesis a weighted mean has been calculated from the single measurements (zetamean.exe; <http://earth.geology.yale.edu/~brandon>). Only the specimens, where the age calculation passes the Chi-Square test are considered.

- ξ Zircon:  $141.40 \pm 6.33$
- ξ Apatite:  $355.96 \pm 9.39$

#### Microscope work

Fission tracks were counted on a Zeiss® microscope with a computer-controlled scanning stage, run by the software "Langstage (3.11)" (Dumitru 1993).

Magnifications:

- CN1, CN5:  $\times 1000$  ( $1.0 \times 10 \times 100$ )
- Exception BS27 CN5:  $\times 2000$  ( $2.0 \times 10 \times 100$ )
- Zircon:  $\times 1600$  ( $1.6 \times 10 \times 100$ )
- Apatite (age):  $\times 1250$  ( $1.25 \times 10 \times 100$ )
- Apatite (length):  $\times 1250$  ( $1.25 \times 10 \times 100$ )
- Apatite (Dpar):  $\times 2000$  ( $2.0 \times 10 \times 100$ )

#### Data processing

Age data has been processed using the windows software "TrackKey (4.1)" (Dunkl 2002). For separation of subpopulations (i.e. the youngest population in partially annealed samples) the windows software PopShare was used (Dunkl and Székely 2002).

#### Chi-Square test

The evaluation of the single grain age distribution is done by the Chi-Square ( $\chi^2$ ) goodness-of-fit test. The  $\chi^2$  test (Snedecor and Cochran 1989) is a statistical method to test if a sample of data came from a population with a specific distribution. In fission track analysis the number of nuclear tracks counted have poisson distributions (Galbraith 1981).  $\chi^2$  values below 5% indicate departures from the poisson distribution, which implies more than one grain age population dated.

#### Thermal modelling

Thermal modelling of time-temperature-paths (Chapter 4) was carried out with the program "AFTSolve (1.3.0)" (Ketcham et al. 2000; annealing algorithm: Laslett et al. 1987). For thermal modelling time and temperature constraints (temperature range at a certain time) independent of apatite FT data are given and the model searches data fitting time-temperature-paths through these ranges. Input data are apatite single grain ages and confined track lengths.

BS24-48	CN1	BS44-52	CN1-01	BS45-38	CN1-08
BS24-21	ZR: R2-2	BS44-51	ZR: R3-1	BS45-37	ZR: R5-2
BS24-20	ZR: R2-2	BS44-49	ZR: M14	BS45-32	ZR: R2-5
BS24-19	ZR: M03	BS44-48	ZR: M14	BS45-28	ZR: R1-1
BS24-18	ZR: M03	BS44-47	ZR: P2	BS45-27	ZR: R2-4
BS24-16	ZR: M05	BS44-46	ZR: P2	BS45-26	ZR: R2-4
BS24-14	ZR: M06	BS44-45	ZR: R5-1	BS45-25	ZR: R2-3
BS24-12	ZR: M04	BS44-44	ZR: R5-1	BS45-24	ZR: R2-3
BS24-11	ZR: R3-6	BS44-42	ZR: M09	BS45-01	CN1-07
BS24-10	ZR: R3-6	BS44-41	ZR: M13		
BS24-09	ZR: R3-5	BS44-40	ZR: M13		
BS24-08	ZR: R3-5	BS44-38	ZR: R5-4		
BS24-07	ZR: M07	BS44-36	ZR: R4-3		
BS24-06	ZR: R3-4	BS44-35	ZR: R4-1		
BS24-05	ZR: R3-3	BS44-34	ZR: R4-1		
BS24-04	ZR: R3-3	BS44-33	ZR: M08		
BS24-03	ZR: R3-2	BS44-32	ZR: R4-4		
BS24-02	ZR: R3-2	BS44-30	ZR: P1		
BS24-01	CN1	BS44-29	ZR: M12		
		BS44-28	ZR: M02		
		BS44-27	ZR: P3		
		BS44-25	ZR: M01		
		BS44-01	CN1-06		

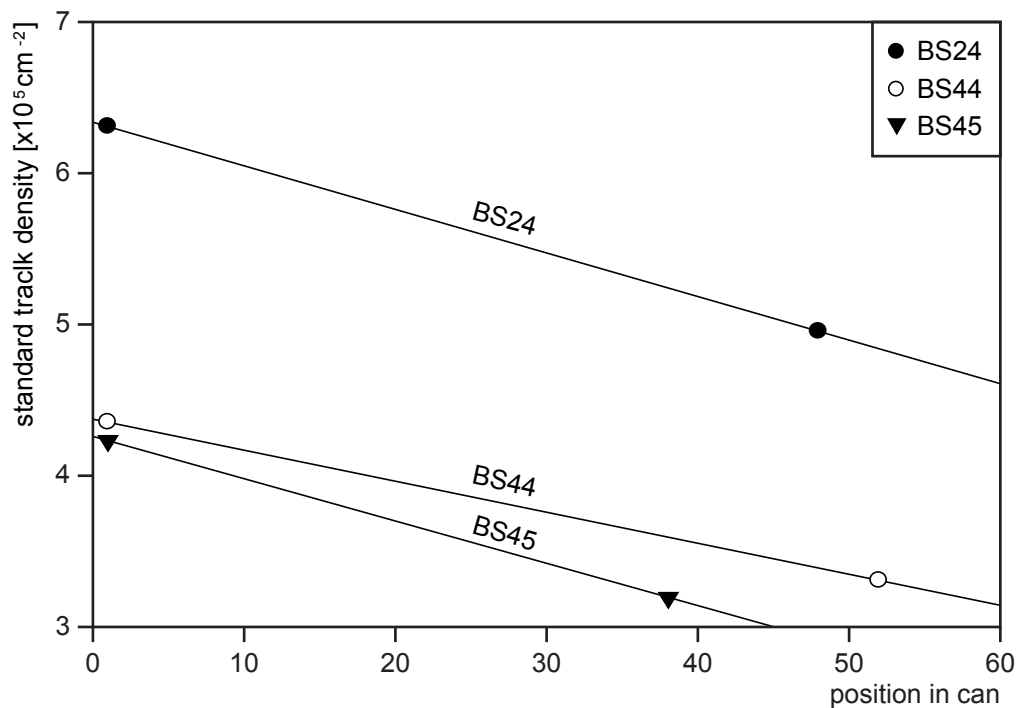
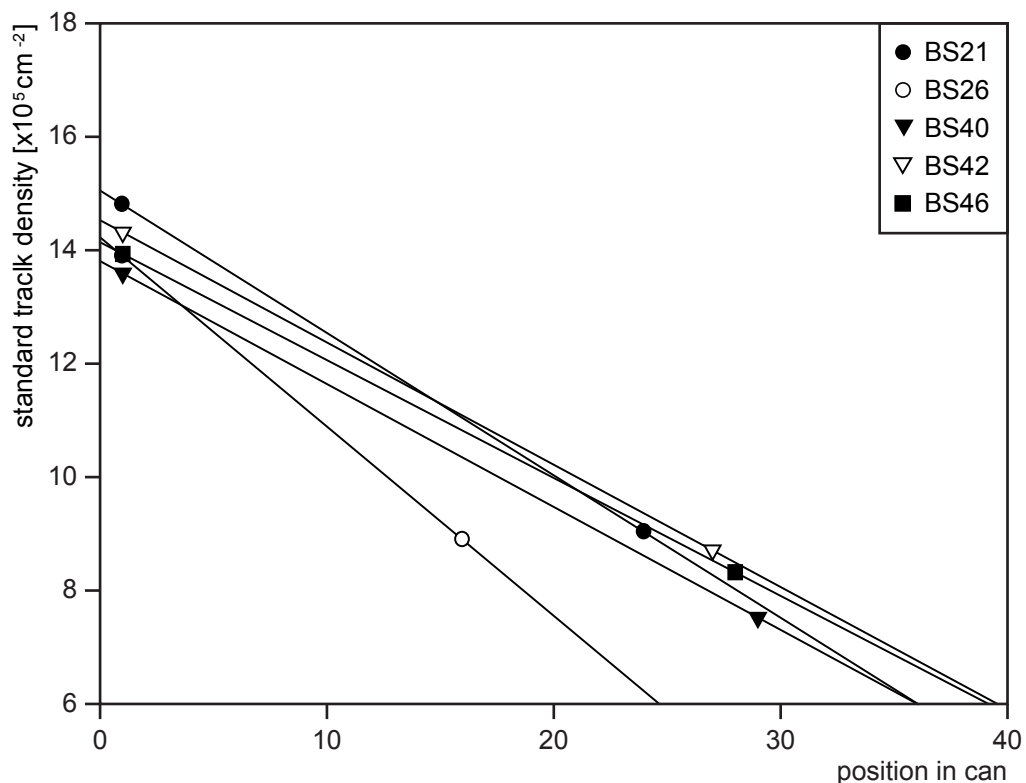


Fig. C2: Calculation of standard track densities for zircon specimens. Two standard track density values have been determined at the bottom and the top of each can (CN1). The standard track density for each sample is calculated by a straight line through both the points according to the sample position in the can. If two neighbouring specimens are counted for one sample the mean standard track density has been used.

BS21-24	CN5	BS40-29	CN5-09	BS42-27	CN5-06	BS46-28	CN5-07
BS21-11	AP: R3-5	BS40-28	AP: M05	BS42-17	AP: S1	BS46-27	AP: M08
BS21-10	AP: R3-4	BS40-26	AP: R3-6	BS42-16	AP: S1	BS46-24	AP: R5-1
BS21-09	AP: R3-3	BS40-25	AP: P5	BS42-11	AP: S3	BS46-23	AP: R5-1
BS21-08	AP: R3-2	BS40-24	AP: P5	BS42-09	AP: S4	BS46-21	AP: R3-1
BS21-04	AP: R1-3a	BS40-23	AP: P2	BS42-08	AP: S2	BS46-18	AP: M14
BS21-03	AP: R1-2a	BS40-22	AP: P2	BS42-07	AP: S2	BS46-17	AP: M14
BS21-02	AP: R1-1a	BS40-21	AP: P3	BS42-02	AP: M04	BS46-16	AP: M13
BS21-01	CN5	BS40-20	AP: P3	BS42-01	CN5-04	BS46-13	AP: P7
		BS40-19	AP: P6			BS46-09	AP: R4-4
		BS40-18	AP: P6			BS46-08	AP: R4-3
		BS40-17	AP: P1			BS46-06	AP: R4-2
		BS40-16	AP: P1			BS46-05	AP: R4-2
		BS40-01	CN5-05			BS46-01	CN5-02
BS26-16	CN5						
BS26-15	AP: R5-3						
BS26-01	CN5						



*Fig. C3: Calculation of standard track densities for apatite specimens (irradiated low). Two standard track density values have been determined at the bottom and the top of each can (CN5). The standard track density for each sample is calculated by a straight line through both the points according to the sample position in the can. If two neighbouring specimens are counted for one sample the mean standard track density has been used.*

BS27-21 <b>CN5</b>	BS41-28 <b>CN5-08</b>	BS43-29 <b>CN5-03</b>	BS47-19 <b>CN5-09</b>
BS27-20 <b>AP: M03</b>	BS41-19 <b>AP: P4</b>	BS43-21 <b>AP: S5</b>	BS47-13 <b>AP: R5-2</b>
BS27-16 <b>AP: R2-5</b>	BS41-18 <b>AP: P4</b>	BS43-08 <b>AP: M06</b>	BS47-11 <b>AP: R5-2</b>
BS27-15 <b>AP: R1-3b</b>	BS41-17 <b>AP: M02</b>	BS43-07 <b>AP: R2-4</b>	BS47-01 <b>CN5-05</b>
BS27-14 <b>AP: R1-2b</b>	BS41-16 <b>AP: M02</b>	BS43-06 <b>AP: R2-3</b>	
BS27-13 <b>AP: R1-1b</b>	BS41-05 <b>AP: M01</b>	BS43-05 <b>AP: R2-2</b>	
BS27-05 <b>AP: R1-6</b>	BS41-04 <b>AP: M01</b>	BS43-04 <b>AP: R2-1</b>	
BS27-03 <b>AP: R1-5</b>	BS41-01 <b>CN5-02</b>	BS43-03 <b>AP: R5-5</b>	
BS27-02 <b>AP: R1-4</b>		BS43-01 <b>CN5-01</b>	
BS27-01 <b>no CN5!</b>			

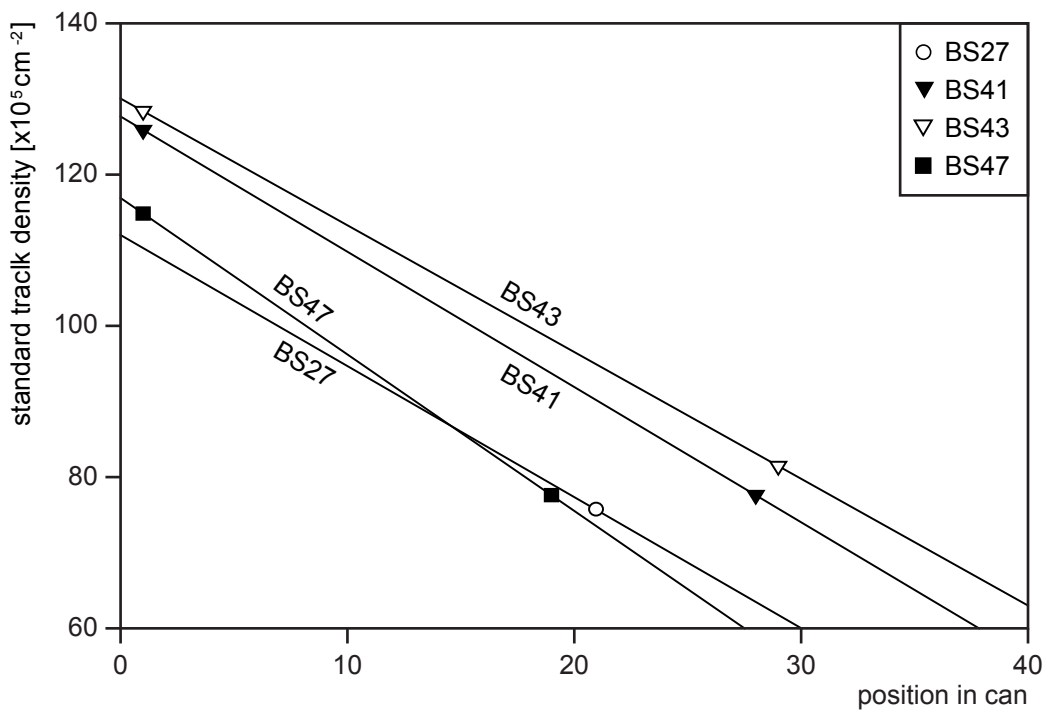


**Fig. C4:** Calculation of standard track densities for apatite specimens (irradiated high). Two standard track density values have been determined at the bottom and the top of each can (CN5). The standard track density for each sample is calculated by a straight line through both the points according to the sample position in can. If two neighbouring specimens are counted for one sample the mean standard track density has been used. In can number BS27 the CN5 at the bottom have been destroyed, hence the mean gradient of BS41 and BS43 has been used.



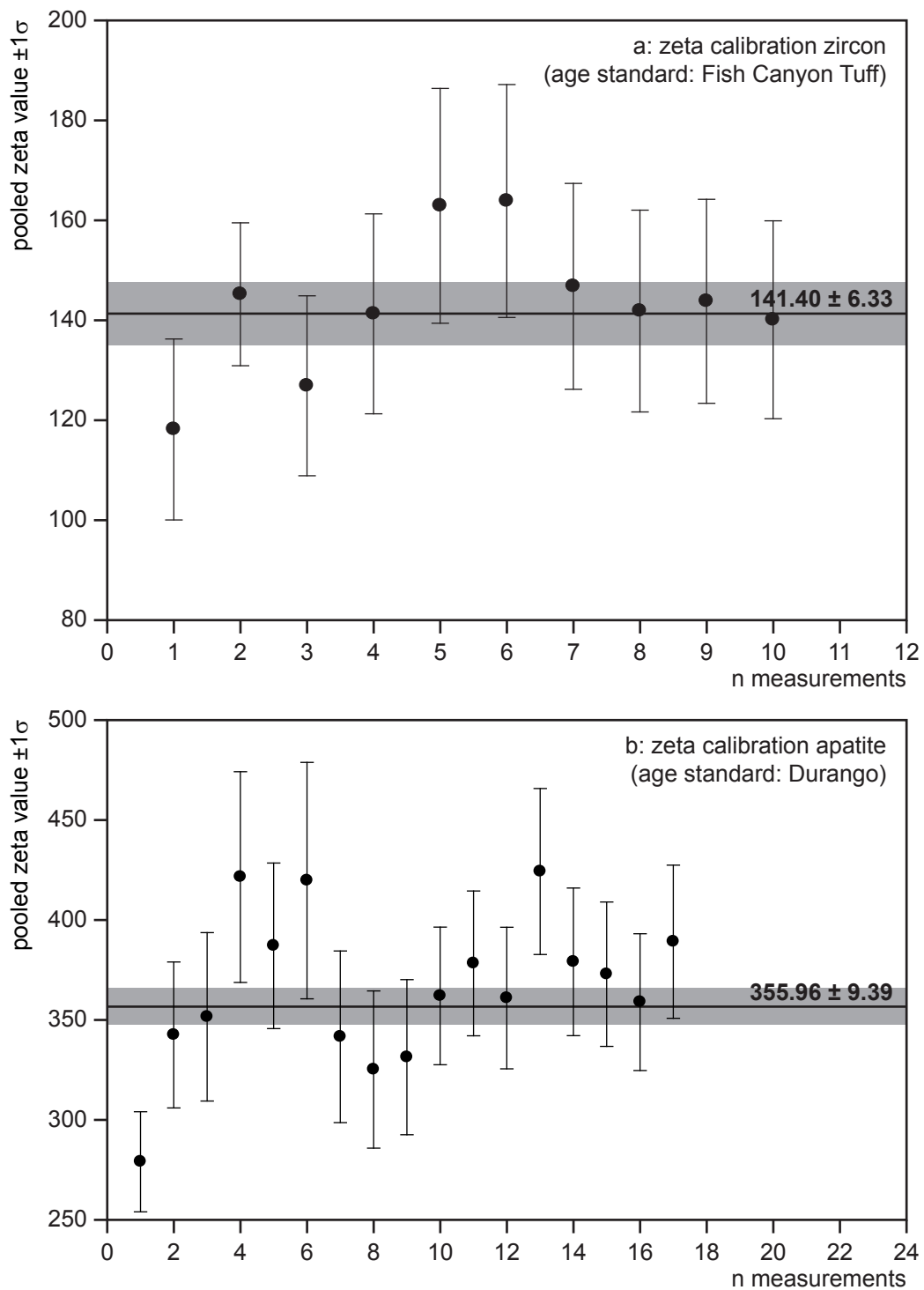


*Fig. C5. Graphs show the different pooled zeta values for zircon (a: Fish Canyon tuff) and apatite (b: Durango). For the age calculations a weighted mean of the different values has been used, indicated by the thick line and the greyscale.*

Model parameters:

- Initial track length: 16.30  $\mu\text{m}$
- Length reduction: 0.893  $\mu\text{m}$
- Dpar: 1.50
- Probabilistic approach: random Monte Carlo (10.000 paths)

Paths between the time temperature constraints are monotonic rising or falling and intersected by 4 half segments. Comparison between data and model is done by model and data age, model and data length and the Kolmogorov-Smirnov goodness-of-fit test.

**Table D1:** Apatite fission track data.

All samples have been analysed using the external detector method (Gleadow 1981) with a zeta value (Hurford and Green 1983) of  $355.96 \pm 9.3$  (Durango standard, CN5).

Code	N Grains	Ps [ $\times 10^5 \text{ cm}^{-2}$ ]	Ns	Pi [ $\times 10^5 \text{ cm}^{-2}$ ]	Ni	Pd [ $\times 10^5 \text{ cm}^{-2}$ ]	Nd	Single Grain Ages [Ma]	Age $\pm 1\sigma$ [Ma] Central (Pooled)	Loc. Z [m]	U [ppm]	Grainsize [ $\times 10^3 \mu\text{m}^2$ ]
R1-1a	20	0.58	41	11.86	837	14.55	4766	6-37	12.7 $\pm$ 2.1	1550	11.53	3.53
(R1-1b)	(40)	(0.37)	(27)	(28.17)	(2079)	(89.46)	(1452)		(10.8 $\pm$ 2.1)		(4.36)	
R1-2a	20	0.53	32	5.59	336	14.30	4766	9-84	24.2 $\pm$ 4.5	1440	5.34	3.01
(R1-2b)	(40)	(0.46)	(23)	(34.04)	(1712)	(87.73)	(1452)		(11.5 $\pm$ 2.4)		(5.28)	
R1-3a	18	0.78	32	10.71	440	14.04	4766	4-27	18.2 $\pm$ 3.4	1355	9.43	2.28
(R1-3b)	(20)	(0.45)	(15)	(35.28)	(1189)	(86.00)	(1452)		(11.2 $\pm$ 2.9)		(4.42)	
R1-4	19	0.64	33	40.54	2096	108.50	1452	7-91	30.3 $\pm$ 5.4	1215	4.77	2.72
R1-5	19	0.50	31	29.55	1820	106.77	1452	1-142	35.6 $\pm$ 7.3	1120	3.65	3.24
R1-6	16	0.40	20	25.15	1270	103.31	1452	15-79	28.9 $\pm$ 6.6	985	3.11	3.16
R2-1	16	0.34	27	27.04	2125	123.31	4196	10-145	27.8 $\pm$ 5.5	1205	2.73	4.91
R2-2	20	0.41	63	93.25	14333	121.63	4196	6-25	9.5 $\pm$ 1.2	1105	9.31	7.69
R2-3	20	0.33	40	56.94	6913	119.96	4196	5-26	12.3 $\pm$ 2.0	885	6.16	6.07
R2-4	20	0.52	51	108.36	10717	118.28	4196	4-27	10.0 $\pm$ 1.4	705	11.71	4.95
R2-5	20	0.67	46	47.24	3255	84.27	1452	6-63	21.6 $\pm$ 3.4	600	6.60	3.45
R3-1	24	4.41	539	65.71	8030	9.78	4451	7-19	11.6 $\pm$ 0.7	2020	86.51	5.09
R3-2	20	2.55	357	54.69	7646	13.04	4766	7-20	11.0 $\pm$ 0.8	1465	53.64	6.99
R3-3	20	2.48	496	48.58	9716	12.79	4766	7-18	11.6 $\pm$ 0.7	1310	46.22	10.00
R3-4	20	0.38	50	8.30	1096	12.54	4766	4-22	10.2 $\pm$ 1.5	1155	9.53	6.60
R3-5	18	0.59	77	7.47	982	12.29	4766	4-48	17.2 $\pm$ 2.2	1005	8.49	7.30
R3-6	20	0.94	111	15.89	1873	8.17	4223	3-19	8.6 $\pm$ 0.9	945	23.38	5.90
R4-2	20	0.72	85	38.19	4499	13.00	4451	2-18	4.4 $\pm$ 0.5	1305	36.51	5.89
R4-3	20	2.02	216	53.45	5730	12.48	4451	6-13	8.4 $\pm$ 0.6	980	54.45	5.36
R4-4	20	0.89	73	26.52	2185	12.27	4451	3-15	7.3 $\pm$ 0.9	700	34.70	4.12
R5-1	20	1.31	93	20.94	1487	9.26	4451	5-22	10.3 $\pm$ 1.1	1148	29.06	3.55
R5-2	10	0.26	19	18.55	1360	92.06	5773	10-71	22.9 $\pm$ 5.3	1245	2.52	7.57
R5-3	20	3.02	218	51.72	3734	9.22	4557	6-21	9.6 $\pm$ 0.9	1390	70.37	3.61
R5-5	19	0.33	24	62.76	4588	124.98	4196	5-53	11.6 $\pm$ 2.4	1455	5.89	3.85

**Code:** sample code; **N grains:** number of grains counted; **Ps [ $\times 10^5 \text{ cm}^{-2}$ ]:** spontaneous track density; **Ns:** number of spontaneous tracks counted; **Pi [ $\times 10^5 \text{ cm}^{-2}$ ]:** induced track density; **Ni:** number of induced tracks counted; **Pd [ $\times 10^5 \text{ cm}^{-2}$ ]:** standard track density; **Nd:** number of standard tracks counted; **Single Grain Ages [Ma]:** spread of single grain ages; **Age  $\pm 1\sigma$  [Ma] Central (Pooled):** apatite fission track central ages (Galbraith and Laslett 1993) or pooled ages (in brackets); **Loc. Z [m]:** altitude above sea level; **U [ppm]:** average uranium content; **Grainsize [ $\times 10^3 \mu\text{m}^2$ ]:** average grainsize counted.

## Appendix D: Statistical problems of single grain ages at low track densities

### D.1 Introduction

Out of statistical and technical reasons (Wagner and van den Haute 1992, see Appendix B), the fission track method is only applicable for a specific interval of the grain size / defined track density ratio. Since the fission track age is calculated from the ratio between spontaneous (Ns) and induced tracks (Ni), the statistical error increases with decreasing number of tracks counted. The number of uranium isotopes responsible for fission tracks is calculated from the uranium content of the grain and the area counted. The following theoretical example shows a possible dependence of the obtained age to the area counted, when dealing with low track densities.

Assuming a not-zoned grain, the induced

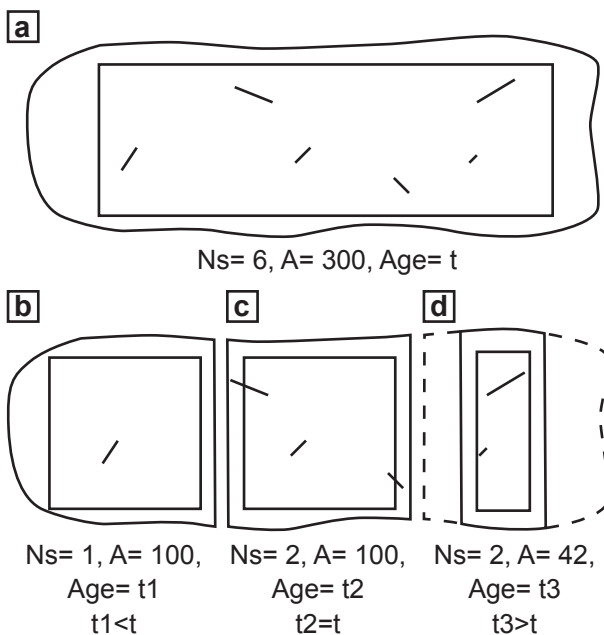


**Fig. D1.** Example to display the variability of single grain ages at low track densities.

tracks are directly proportional to the counted area. Hence, the ratio between spontaneous tracks and area counted ( $Ns/A$ ) is directly related to the ratio between spontaneous and induced tracks ( $Ns/Ni$ ). Based on this simplification  $Ns/A$  is considered to directly reflect the age in the following example (Fig. D1a). In the example shown in Fig. D1a, 6 spontaneous tracks correspond to 300 area units

( $1/50 Ns/A$ ) in the entire grain. However, the generally column-shaped apatites are usually only preserved as fragments. In our example only one of the smaller pieces reproduces the ratio of the large grain (Fig. D1c:  $1/50 Ns/A$ ). The two other fragments display lower (Fig. D1b:  $1/100 Ns/A$ ) or higher (Fig. D1d:  $1/30 Ns/A$ ) ratios, resulting in lower and higher single grain ages respectively.

In the following, the database of basement samples from a Miocene horst structure (Rodna horst), is used to test if this theoretically expected error source can be confirmed by actual data, and if an influence of grain size and uranium content on single grain ages can be discerned.

### D.2 Results

#### D.2.1 Apatite fission track data

In the Rodna horst 24 samples have been dated (Table D1, Fig. D2). Four vertical profiles (R1, R2, R3, R4) in four blocks, separated by brittle faults were sampled. The samples were taken along natural slopes with inclinations between 20-30°. Four additional samples were taken from the central block (R5).

The central ages show two groups, spreading between Late Eocene to Early Miocene (17.2-35.6 Ma) and between Middle to Late Miocene (7.3-12.7 Ma), respectively. An outlier is sample R4-2, with a Pliocene age (4.4 Ma). This young age is possibly the result of a hydrothermal overprint and is therefore excluded from the following discussion.

In the study area (Rodna horst), the geological frame indicates Paleogene to Early Miocene burial and following exhumation (Chapter 4). Therefore the Middle to Late Miocene central ages are interpreted as cooling ages after full annealing of apatite.

The most obvious explanation for the Late Eocene to Early Miocene central ages would be only partial annealing of these samples during Paleogene to Early Miocene burial. Therefore these central ages are discussed in more detail below.

#### D.2.2 Evaluation of the apatite fission track data

The most likely explanation for an increasing degree of annealing is increasing temperature. At temperatures around the upper limit of the apatite partial annealing zone (120°C) small differences in burial depth (i.e. sample elevation) can cause substantial differences from partial to full annealing.

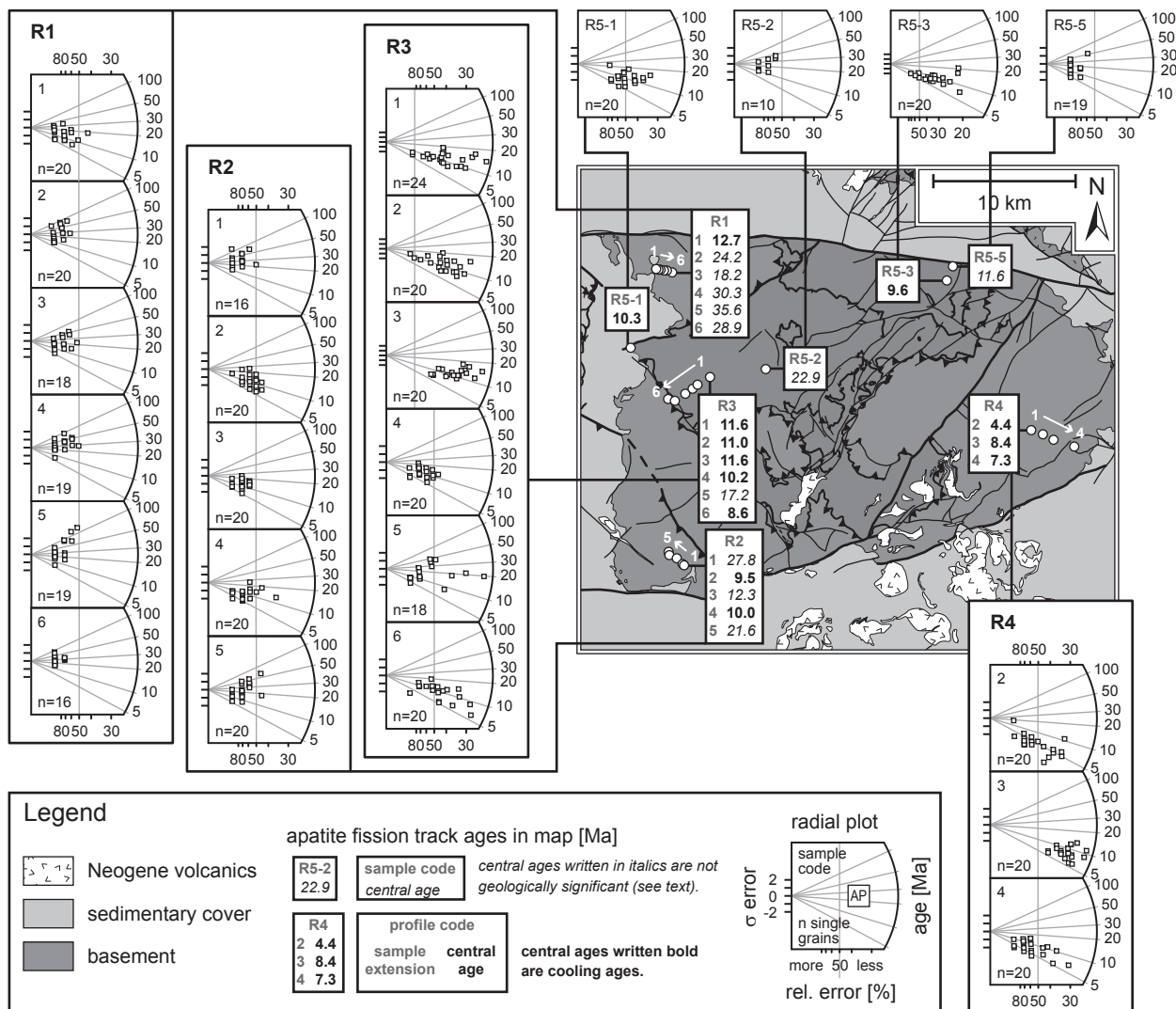


**Fig. D2.** Results of apatite fission track analyses from the Rodna horst. The same scale is used in all radial plots (Galbraith 1990) to allow for direct comparison. All given ages in the map are central ages (Galbraith and Laslett 1993), which is a weighted mean of the single grains. Only the ages printed regular bold are cooling ages. Ages written in italics are central ages, which are not geologically significant.

Yet the vertical profiles R2 and R3 do not allow this interpretation (Table D1, Fig. D2) as Early Miocene to Eocene ages occur at the top and the bottom of the vertical profiles (R2) and in between fully annealed samples (R3).

Another possible parameter causing different annealing behaviour is the chemical composition of the grains. Profile R3 is selected as an example (Fig. D3) to check possible chemical reasons for partial annealing. Within profile R3 there is one sample of an Early Miocene age (R3-5) between samples of Middle to Late Miocene central ages. Within the profile different lithologies are dated. Samples R3-1, R3-5 and R3-6 are metasedimentary micaschists (Fig. D4a), while R3-3 and R3-4 derive from an orthogneiss (Fig. D4b). Apatites from the micaschists show a greater variety in annealing

behaviour (Fig. D3a,d,e) in comparison to the orthogneisses (Fig. D3b,c), as inferred by a larger spread in Dpar lengths. The relatively short Dpar lengths in the orthogneiss (1.0-1.8  $\mu\text{m}$ ) indicate less resistance to annealing, which is in accordance with the observed full annealing of these samples. In the three micaschists also long Dpar lengths (>2 mm) occur, indicating apatites with more resistant to annealing, but nevertheless R3-1 and R3-6 are fully annealed.

Since a lower degree of annealing (temperature as well as chemical variation) can be excluded as reason for the Early Miocene to Eocene ages, another parameter has to influence the obtained ages. When plotting the single grain ages of R3-5 against their uranium content (Fig. D5) it can be observed, that Oligocene to Eocene single grain

ages (23.8-54.8 Ma) only occur in grains containing less than 5 ppm uranium.

This relationship is also obvious in the uranium content vs. age plot for all ages (Fig. D6a,b). The Eocene and Early Miocene central ages occur only in samples with less than 12 ppm average uranium, while all samples above 20 ppm uranium show Middle to Late Miocene central ages (Fig. D6a). The corresponding single grain age plot (Fig. D6b), however, shows that single grains of low Uranium content show a large spread in age. Hence, low Uranium content can not be the only reason for extraordinarily old single grain ages.

Profile R1 is a good example for a more detailed discussion, since 5 of 6 samples of R1 show Eocene to Early Miocene central ages (Fig. D6c-e). The single grain ages are grouped in accordance to the number of spontaneous tracks per grain ( $N_s$ ; given on data point symbol), the uranium content is indicated by greyshade. Within the grains of one group (equal  $N_s$ , similar U content) the single grain

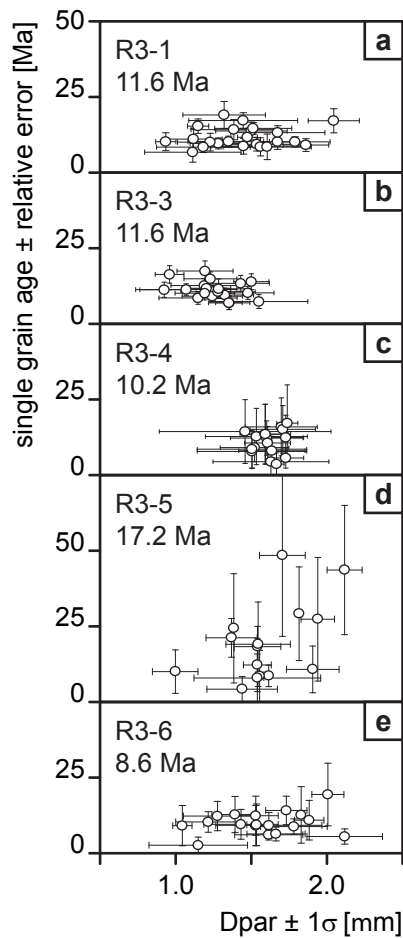


Fig. D3. Single grain age against  $D_{par}$  plots of samples from profile R3. The central age is given below the sample code.

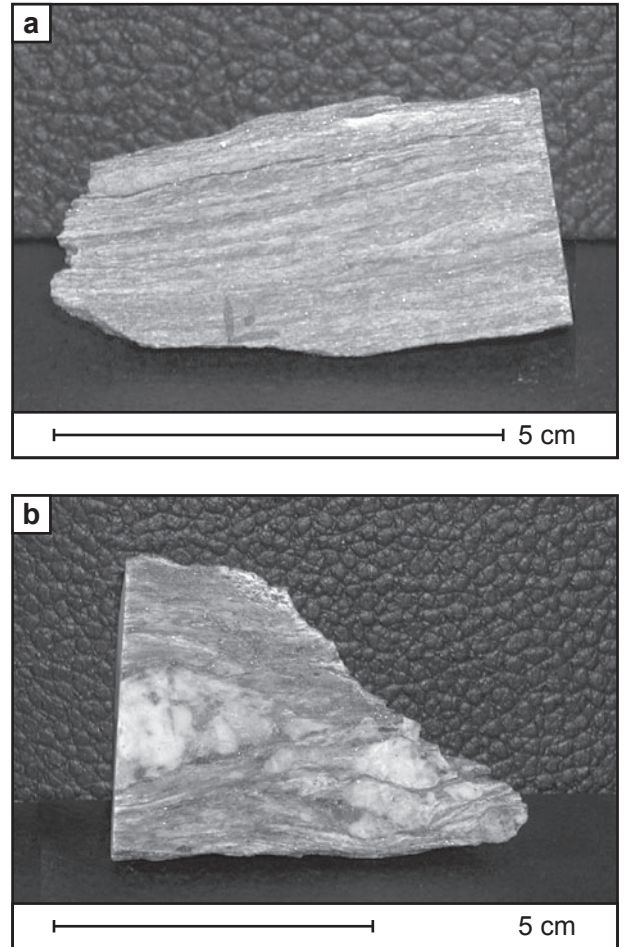


Fig. D4. Examples of the sampled lithologies. Most samples derive from metasediments (a). Rarely orthogneiss have been sampled (b).

age is exponentially related to the area counted. The area / age dependence is strongest for grains below 5 ppm uranium, while only weak above 10 ppm. Considering the large amount of small grains of

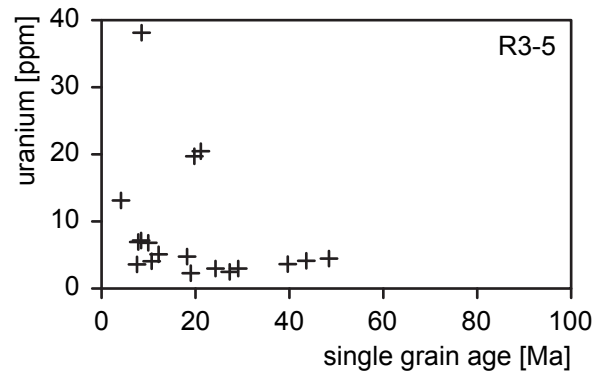
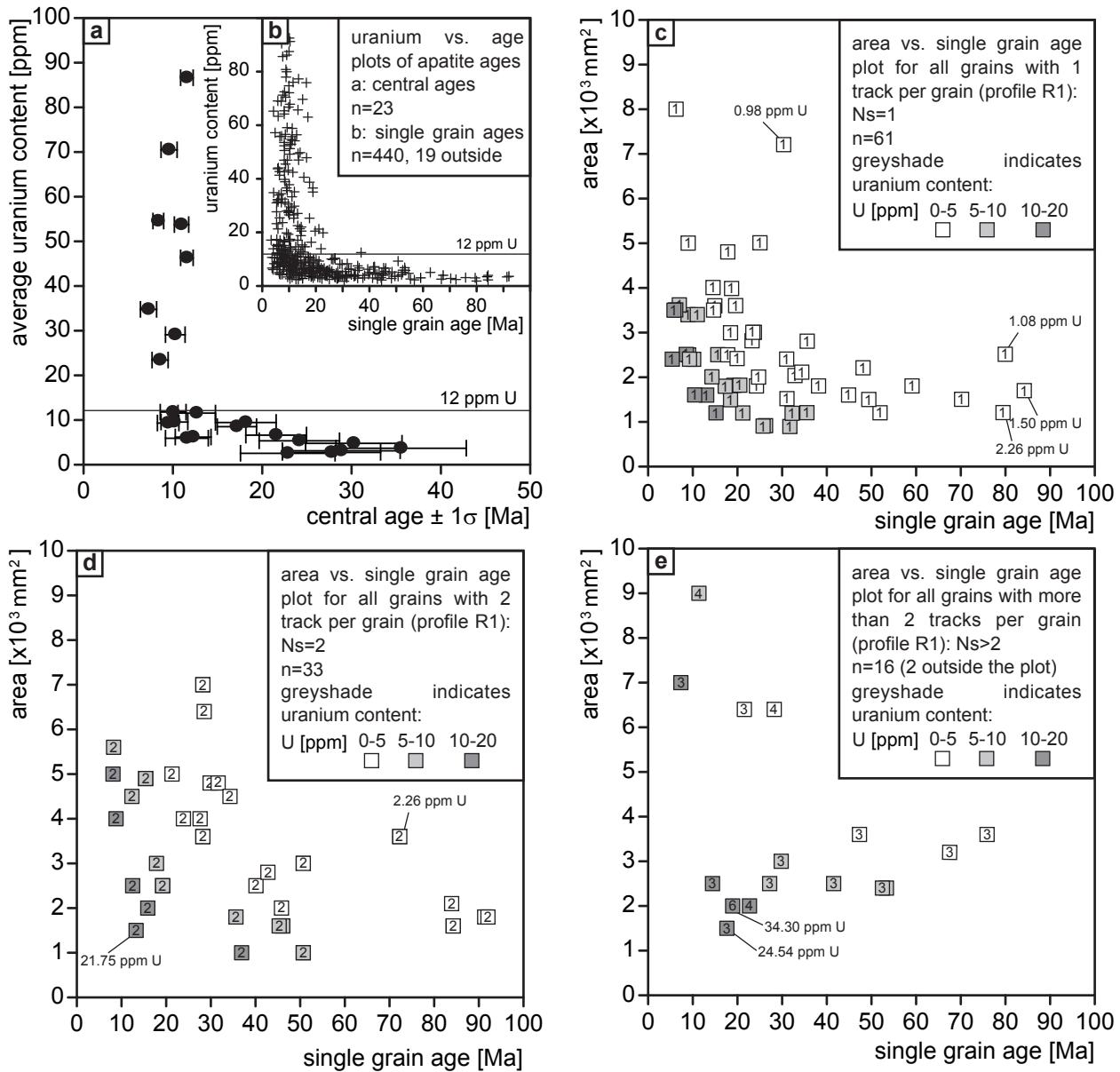


Fig. D5. Uranium vs. single grain age plot of sample R3-5. Single grain ages older than Miocene (>23 Ma) only occur in grains of less than 5 ppm uranium.



**Fig. D6.**

a-b: The uranium vs. age plots show that central ages above 13 Ma (a) and single grain ages above 23 Ma (b) respectively only occur in grains containing less than 12 ppm uranium.

c-e: The area vs. single grain age plots of profile R1 are grouped by the number of spontaneous tracks counted per grain (c: Ns=1, d: Ns=2, e: Ns>2). The value of Ns is given on data point symbol by number, while greyshade indicates uranium content. The age/area relation is strongest in grains of 0-5 ppm uranium and negligible above 10 ppm uranium.

very low uranium content in the samples of R1, the ages in profile R1 seem to be rather of geometrical than of geological significance.

To evade geometrical and statistical effects due to low tracks numbers, the samples R1-1, R1-2 and R1-3 were counted a second time, also considering grains without tracks (Ns=0). The resulting pooled ages (Fig. D7; TableD1, written in brackets) are Middle to Late Miocene (10.8-11.5 Ma). The central age of R1-1 (12.7 $\pm$ 2.1 Ma) is confirmed by the pooled

age (10.8 $\pm$ 2.0 Ma) within the error bars (Fig. D7), indicating, that an average counted area of 3530  $\mu\text{m}^2$  results in a reliable central age at 11.53 ppm uranium. The central age of R1-3 (18.2 $\pm$ 3.4 Ma) is not confirmed by the pooled age (11.2 $\pm$ 2.9 Ma; Fig. D7), indicating that at 9.43 ppm uranium an average area counted of 2200  $\mu\text{m}^2$  does not result in geologically significant central ages. Below 6 ppm uranium (R1-2) an average counted area of even 3005  $\mu\text{m}^2$  does not result in a geologically significant central age.

Due to this observation central ages of samples around 10 ppm average uranium content are only accepted to be of geological significance, if the grainsize is high enough (above  $3500 \mu\text{m}^2$ ). Samples of an average uranium content below 9 ppm are not considered. Due to these constraints central ages of R1-2 to R1-6, R2-1, R2-3, R2-5, R3-5, R5-2 and R5-5 are not considered as cooling ages and are not included in the geological interpretation.

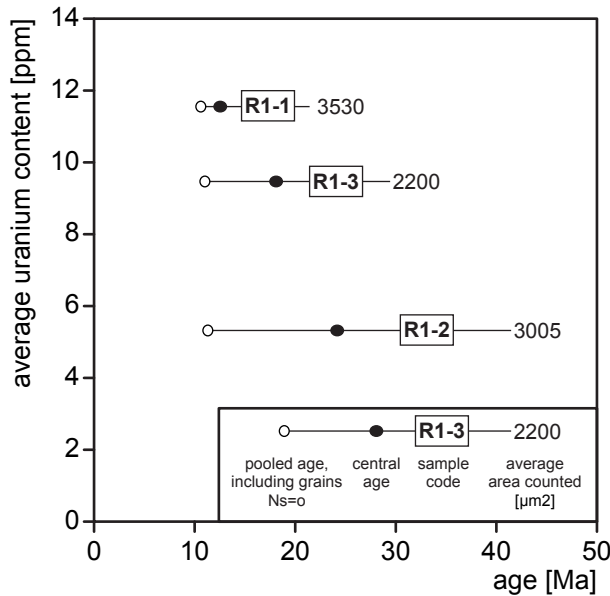


Fig. D7. Uranium vs. age plot of the samples R1-1, R1-2 and R1-3. Pooled ages (white symbol) include grains without tracks ( $N_s=0$ ).

### D.3 Conclusions

At very low track densities (average  $N_s < 2$  per grain) the interpretation of single grain ages is highly dangerous, because small grains of only very few tracks may appear significantly older than they actually are. At such low track densities the external detector method (Gleadow 1981), which is based on single grain ages, can only be used, if grains without tracks are included ( $N_s=0$ ) and a pooled age is calculated. An alternative at very low track densities is the grain population method, which averages across the entire sample, not considering single grains (Gleadow 1981).





# Curriculum vitae Heike R. Gröger

Office address:  
StatoilHydro ASA  
Forusbeen 50  
4035 Stavanger  
Telephone: +47 91753553  
e-mail: heigr@statoilhydro.com



## Personal Details

---

Date of birth: 06.08.1974  
Place of Birth: Northeim  
Citizenship: German  
Marital Status: Single

## School and Studies

---

### University leaving qualification: PhD in Geology

**08.06.2006** University of Basel (Switzerland)

Thesis: *"Thermal and structural evolution of the East Carpathians in northern Romania: from Cretaceous orogeny to final exhumation during Miocene collision"*

Supervisors: Prof. Bernhard Fügenschuh, Prof. Stefan Schmid, Prof. Andreas Wetzel

Methods used:

structural field work (brittle structures), zircon/apatite fission track analysis, apatite (U-Th)/He analysis

Degree: "summa cum laude"

**10.2001-09.2006** postgraduate studying Geology in Basel (Switzerland)

### University-leaving qualification: Diplom in Geology

**11.05.2001** Georg-August-Universität Göttingen (Germany)

Thesis: *"Gefüge- und Texturentwicklung amphibolitfazieller Gesteine an der „Windy Pass“-Überschiebung in den nördlichen Cascade-Mountains, Washington, USA"*

Mapping: *"Geologische Kartierung des Chiwaukum Schist Fensters an der „Windy Pass“-Überschiebung im Cascades Crystalline core, Washington, USA"*

Supervisors: Dr. Bernd Leiss, Dr. Axel Vollbrecht, Prof. Siegfried Siegesmund

Methods used:

Structural field work (ductile structures), texture analysis using neutron diffraction

Degree: "very good"

**10.1995-09.2001** studying Geology in Göttingen (Germany)

### School-leaving qualification: Abitur ("Allgemeine Deutsche Hochschulreife")

**15.06.1994** Otto-Hahn-Gymnasium Göttingen (Germany); Grade: 1.6

**08.1981-06.1994** School education in Hardegsen and Göttingen (Germany)

## Work experience and technical skills

---

03.1993-09.1995      Various full and half time jobs (e.g. Kitchen help, Groom, Tool grinder); 3 month development aid in Bolivia.

### Practicals/Internships:

#### "Instituto Costarricense de Electricidad" (04.01.-05.03.1999)

- Detailed description of the pyroclastic deposits of the Cerro Chopo cinder cone (Costa Rica)
- Checking of ash samples and seismic stations

#### Exploration companies (Costa Rica, Bolivia): 05./12.1998

- Short experiences in (metal) exploration field work

#### Assistance at the Geological Institute of Göttingen (1997 – 2001)

##### Teaching:

- Assistant during short course "Texture Analysis"

##### Technical duties:

- X-ray/Neutron diffraction texture analysis: sample preparation, measurement, processing of data, including introduction for new assistants
- Creation of user-manuals for the analytical software (Texture analysis)
- 10.1999: organising assistance during the International Conference on Textures and Physical properties of rocks

#### Assistance at the Geological Institute of Basel (2001 – 2005)

##### Teaching:

- Assistant during various undergraduate-level courses (geology and geodynamics, structural geology, construction of sections)
- Assistant during field excursions in Switzerland

##### Technical duties:

- Administration of the institutional address list
- Introduction of student assistants in the fission track laboratory
- 11.2003: organising assistance during the first Swiss Geoscience Meeting in Basel

### Analytical methods:

- Sound experience in sample preparation (texture analysis, fission track analysis, U/Pb analysis, heavy mineral analysis, microfossil extraction)
- Sound experience in microscope work: handpicking (binocular), fabric analysis in thin section, fission track analysis
- Sound experience in texture analysis using X-ray/Neutron diffraction: sample preparation, measuring, processing of data
- Basic experience in mass spectrometry: measuring procedures

### Field Work (excluding excursions)

- Volcanological field work in the Cerro Chopo cinder cone, Costa Rica (4 weeks)
- Mapping in the Cascades Crystalline Core, Washington, USA (6 weeks)
- Structural and sedimentological field work in northern Romania (~20 weeks)

## Miscellaneous

---

**Languages:** German (native speaker)  
English (good written and spoken skills)  
Spanish/Romanian (basic spoken/understood)

**Driving Licence:** yes

### **Computer skills:**

Operating systems: Microsoft Windows family

Applications: experienced computer user, most important applications listed below:

- Microsoft Office package
- GIS Software: MapInfo, ArcGIS
- Graphics: Adobe Illustrator, Adobe Photoshop, CorelDraw, Micrographics Designer

### **Organisational and administrative activities:**

- Organization of a petition for the Geological Institute in Basel, including co-organization of a departmental open day for the general public (01-03.2004)
- Organization of a number of social events at the Earth Sciences department (such as PhD parties, annual dinner parties), including planification and preparation of dinner buffets for around 50 people (2001-2006)

### **Voluntary work in a Christian youth organisation (BDKJ): 1990-2000**

- Organization of youth group journeys (e.g. to Norway)
- Planification of weekend courses for confirmation candidates
- development aid in collaboration with local youth organisations (Bolivia)

### **Teaching:**

- Extra coaching in Math and English up to secondary school levels (1 student)
- Riding lessons (1 student)

